IDENTIFICATION OF CRACK PARAMETERS FROM VIBRATION SIGNATURE OF BEAM USING DIFFERENT OPTIMIZATION TECHNIQUES

Thesis submitted by

AMIT BANERJEE

Doctor of Philosophy

(Engineering)

DEPARTMENT OF MECHANICAL ENGINEERING

FACULTY OF ENGINEERING &TECHNOLOGY

JADAVPUR UNIVERSITY, KOLKATA 700 032

2018

JADAVPUR UNIVERSITY

KOLKATA-700032, INDIA

INDEX NO. 268/14/E

1. Title of Thesis:

Identification of Crack Parameters from Vibration Signature of Beam Using Different Optimization Techniques

2. Name, Designation & Institution of the Supervisor:

Prof. Goutam Pohit

Professor, Department of Mechanical Engineering

Jadavpur University, Kolkata 700032

3. List of Publications (Referred Journals):

I. **Banerjee, A. and Pohit, G.,** Comparison study of crack detection of cantilever beam using artificial neural network and wavelet transform, Journal of Mechatronics and Intelligent Manufacturing, (2013), 2 (3/4), 161-176.

II. **Banerjee, A. and Pohit, G.,** Crack detection in rotating cantilever beam by continuous wavelet transform, Applied Mechanics and Materials, (2014), 592-594, 2021-2025.

III. **Banerjee, A. and Pohit, G.,** Crack investigation of rotating cantilever beam by fractal dimension analysis, Procedia Technology, (2014), 14. 188-195.

IV. **Banerjee, A., Panigrahi, B. and Pohit, G.,** Crack modelling and detection in Timoshenko FGM beam under transverse vibration using frequency contour and response surface model with GA, Nondestructive Testing and Evaluation, (2016), 31 (2), 142-164.

V. **Banerjee, A., Pohit, G. and Panigrahi, B.,** Vibration Analysis and Prediction Natural Frequencies of Cracked Timoshenko Beam by Two Optimization Techniques – Cascade ANN and ANFIS, Materials Today: Proceedings, (2017), 4, 9909–9913.

4. List of Patents: Nil

5. List of Presentations in International Conferences:

I. **Banerjee, A. and Pohit, G.**, Comparison study of crack detection of cantilever beam using artificial neural network and wavelet transform, 2nd International Conference on Advanced Manufacturing and Automation, Kalasalingam University, Tamil Nadu, 28 – 30th March, 2013 (Paper. ID AS- 13)

II. **Banerjee, A. and Pohit, G.**, Crack investigation of rotating cantilever beam by fractal dimension analysis, 2nd International Conference on Innovations in Automation and Mechatronics Engineering – 2014 organized by G H Patel College of Engineering & Technology, Gujarat, 7 – 8th March, 2014 (Paper ID 26)

III. **Banerjee, A. and Pohit, G.**, Crack detection in rotating cantilever beam by continuous wavelet transform, International Mechanical Engineering Congress, NIT Tiruchirappally, Tamil Nadu, 13-15th June, 2014 (Paper. ID C – 017)

IV. **Banerjee, A., Pohit, G. and Panigrahi, B.**, Vibration analysis and prediction natural frequencies of cracked Timoshenko beam by two optimization techniques - cascade ANN and ANFIS, International Congress on Resent Trend in Engineering and Material Science, Jaipur National University, Jaipur , India, 17-19th March2016 (Paper. ID 2-IC-1206)

V. **Banerjee, A. and Pohit, G.**, Vibrational Analysis and Detection Crack Parameter in Clamped-Clamped Beam Using Cascade Artificial Neural Network, 6th International Congress on Computational Mechanics And Simulation -2016, IIT Bombay, Mumbai, India, 27th June -1st July 2016. (Paper ID-903).

VI. **Banerjee, A. and Pohit, G.**, Crack Detection by Vibration Experiment Data Using Cascade Neuro-GA Hybrid Technique, 1st International Conference on Mechanical Engineering-2018, Jadavpur University, Kolkata, India, 4th January -6th January 2018. (Paper ID -101).

CERTIFICATE FROM THE SUPERVISOR/S

*This is to certify that the thesis entitled "**Identification of crack parameters from vibration signature of beam using different optimization techniques**" submitted by Shri AMIT BANERJEE who got his name registered on 13.02.2014 for the award of Ph.D. (Engineering) degree of Jadavpur University is absolutely based upon his own work under my supervision and neither his thesis nor any part of the thesis has been submitted for any degree/ diploma or any other academic award anywhere before.*

(Goutam Pohit)

Signature of the Supervisor
and date with Office Seal

“This page is intentionally left blank”

About the Author

The author, Sri ***AMIT BANERJEE*** was born at Halisahar in North 24 Parganas district of West Bengal. He did his diploma in Mechanical Engineering from North Calcutta Polytechnic, Kolkata in 2001. He graduated in Mechanical Engineering (Sec B) in 2009 from The Institution of Engineers (India). In 2012, he completed Master of Mechanical Engineering in Machine Design specialization from Jadavpur University. He has been awarded the Senior Research Fellowship by State Government scheme for pursuing PhD work in the Department of Mechanical Engineering at Jadavpur University.

"This page is intentionally left blank"

Acknowledgement

This thesis would not have been possible without the help of so many people in so many assorted ways. So I would like to take this opportunity to express my heartfelt gratitude to them for supporting me of this thesis.

Last five years in this thesis outcome of my research work carried out at Jadavpur University. Thank you Jadavpur University for given me this kind of rear opportunity.

I am as grateful of Prof. Goutam Pohit as my honourable supervisor. He had support me through my thesis with his patience and knowledge. It is his endless guidance and constant encouragement. It will cherish every moment of his wise company.

I would like to thank Jadavpur University for awarding me the Senior Research Fellowship (SRF), under State Government Fellowship Scheme. The financial assistance provided by State Government was not only very encouraging but also kept the underlying thesis work smoothly running.

In the last few years on my thesis I work on machine element laboratory. Thanks you all of past and present members of Machine Elements Laboratory, research scholars and post graduate students. Their valuable suggestions and input have certainly helped to improve the overall content of the thesis. Special thanks go to my friends Brajesh Panigrahi, Priyambada Nayak, for their involvement. I would also express my thanks to all the members of Machine Element Laboratory, Vijay Barethiye, Arkadeb Mukhopadhyay, Tamanas Jana, Sushanta Ghuku, Santanu Duari, Sanjib Kundu, Bikash Panja, Abhijit Biswas, Smrutiranjan Pradhan, Ajay Wagmare, Prasanna Gadhari, for their support. Their very presence and the lighter moments that we shared definitely brought solace in the days of hardship. I also thanks to my friend Kushal Bhattacharyya for his association.

I take this opportunity to avow my sincere appreciation to Prof. Partha Bhattacharya, who actively encouraged and provided experimental setup of my Ph.D. work at Structural Laboratory in Civil Engineering Department, Jadavpur University.

I would like to convey my thanks to the Head of the Department and all the academic and technical staffs of Mechanical Engineering Department, Jadavpur University, Kolkata.

In this respect, I would also like to grab this opportunity to express my heart-felt gratitude to my relative and friends whose support, suggestions and helping attitude helped my

way out to the completion of the thesis. Special mention of my friend Mita Sen is called for her continued support and encouragement.

Thank you Maa, without this person never be complete this thesis. She always support me, her contribution always encourage me lots.

Amit Banerjee

TO

MAA

"This page is intentionally left blank"

Table of Contents

			Page No
List of Publications and Presentations from the Thesis			i
Certificate of supervisor			iii
About the Author			v
Acknowledgement			vii
Dedication			ix
Table of contents			xi
List of Figures			xv
List of Tables			xxiii
Abstract			xxv
Chapter 1	**INTRODUCTION**		**1-30**
1.1	Background and Importance		1
1.2	Motivation of Thesis		5
1.3	Literature Review		7
	1.3.1	Principle of Virtual Work Literatures on Crack Theory, Model and Analysis of Beam like Structure by Classical Methods**.**	8
	1.3.2	Literatures on Crack Model and Analysis of Beam like Structure by Finite Element Method**.**	12
	1.3.3	Literatures on Experimental Work of Crack Detection	16
	1.3.4	Literatures on Damage Detection of Structure Based on Frequency Changes	18
		1.3.4.1 Forward Problem	18
		1.3.4.2 Inverse Problem	19
	1.3.5	Literatures on Crack Detection of Structure Based on Direct Comparison Mode Shape	23
	1.3.6	Literatures on Crack Detection of Structure Based on Curvature Mode Shape	24
	1.3.7	Summary of the Literature Review	27
1.4	Objective of the thesis		27

1.5	Contribution of the thesis	28
1.6	Layout of the thesis	28
1.7	Summary	29
Chapter 2	**DYNAMIC ANALYSIS OF ISOTROPIC AND FGM CRACKED BEAM USING NUMERICAL METHOD AND FEM.**	**31-48**
2.1	Introduction	31
2.2	Model Description and numerical analysis	31
2.3	Finite element analysis	35
2.4	Results and Discussion	41
2.4.1	Comparison study of Numerical method with FEM method	41
2.4.2	Vibration analysis of FEM result of cracked FGM beams	42
2.4.3	Vibration response of cracked and un-cracked rotating cantilever beam using FEM	45
2.5	Summary	47
Chapter 3	**EXPERIMENTAL INVESTIGATION OF DYNAMIC BEHAVIOR OF CRACKED BEAM STUCTURE**	**49-60**
3.1	Introduction	49
3.2	Experimental Study on Cracked Beam by FFT analysis using oscilloscope	49
3.2.1	Experimental Set Up	49
3.2.2	Test Procedure	51
3.3	Experimentation Description by Data Acquisition System	52
3.3.1	Experimental Set Up	52
3.3.2	Test Procedure	53
3.4	Results and Discussion	53
3.5	Summary	59
Chapter 4	**CRACK IDENTIFICATION AND DIAGNOSIS BY OPTIMIZATION TECHNIQUE**	**61-84**
4.1	Introduction	61
4.2	Crack detection by Cascade Artificial Neuron Network (CANN)	62
4.2.1	Design and architecture of Cascade Artificial Neuron Network	64

4.3	Crack detection by Response Surface Methodology (RSM)	68
	4.3.1 Design and architecture of Response Surface Methodology	69
4.4	Crack detection by Genetic Algorithm (GA)	72
	4.4.1 Design and architecture of Genetic Algorithm	74
4.5	Crack detection by Contour Plot Intersection Method	76
4.6	Crack detection by Adaptive Neuro-Fuzzy Interference system (ANFIS)	78
	4.6.1 Design and architecture of Adaptive Neuro-Fuzzy System	79
4.7	Analysis of Hybrid Technique for Crack Detection	81
	4.7.1 Cascade Neuro-GA Hybrid Technique	81
	4.7.2 Response Surface Methodology with GA	83
4.8.	Summary	83
Chapter 5	**RESULTS AND DISCUSSION OF CRACK PARAMETER IDENTIFICATION BY OPTIMIZATION TECHNIQUES**	**85-118**
5.1	Introduction	85
5.2	Forward Problem	85
	5.2.1 Crack identification of beam using cascade ANN	86
	5.2.2 Crack identification of beam using ANFIS	88
5.3	Inverse Problem	91
	5.3.1 Crack parameter identification of isometric beam	92
	5.3.1.1 Crack parameter identification from first three natural frequencies using CANN	92
	5.3.1.2 Crack parameter identification from first three natural frequencies using ANFIS	96
	5.3.2 Crack parameter identification of FGM beam	100
	5.3.2.1 Crack parameter identification from first three natural frequencies using Frequency Contour plot	100
	5.3.2.2 Crack parameter identification from first three natural frequencies using RSM	106
	5.3.2.3 Crack parameter identification from first three natural frequencies using RSM with GA.	110
	5.3.3 Crack parameter identification from experiment result	113
	5.3.3.1 Crack parameter identification from first four natural frequencies using CANN	113

5.3.3.2 Crack parameter identification from first four natural frequencies using GA 114
5.3.3.3 Crack parameter identification from first four natural frequencies using Neuro-GA hybrid technique, 116
5.4 Summary 117
Chapter 6 CRACK IDENTIFICATION BY PORFILE ANALYSIS OF MODE SHAPE 119-160
6.1 Introduction 119
6.2 Wavelet Transform Method 120
6.2.1 Introduction of Wavelet Transform 120
6.2.2 Design of Wavelet Transform for Crack Identification 122
6.3 Fractal Dimension (FD) method 123
6.3.1 Introduction of FD method 123
6.3.2 Design of FD method for Crack Identification 124
6.4 Curvature Method 125
6.4.1 Design of Curvature Method for Crack Identification 125
6.5 Irregularity extracted method 126
6.5.1 Design of Irregularity extracted method 126
6.6 Result and Discussion 128
6.6.1 Identification of Crack Rotating Cantilever Beam by Continuous Wavelet Transform 138
6.6.2 Identification of Crack Rotating Cantilever Beam by FD Method 136
6.6.3 Identification of Crack Rotating Cantilever Beam by Curvature Method 144
6.6.4 Identification of Crack Cantilever Beam by Irregularity Extracted Method 150
6.6.5 Identification of Crack Cantilever Beam from Experimental Results by Irregularity Extracted Method 154
6.7 Summary 160
Chapter 7 CONCLUSION AND FUTURE SCOPE OF WORK 161-164
7.1 Introduction 161
7.2 Conclusion from Crack Detection Optimization Technique 162
7.3 Conclusion from Crack Detection Profile Analysis of Mode Shapes 163
7.4 Future scope of work 164

References **165-177**

List of Figures

		Page No
Figure 2.1	(a) Cracked beam (b) Cracked beam modelled with a rotational spring	32
Figure 2.2	Mesh model with singular element	39
Figure 2.3	Mesh model with nonsingular element	39
Figure 2.4	Model of Crack with singular element, a = crack depth	39
Figure 2.5	FGM beam with an open edge crack	39
Figure 2.6	(a) First natural frequencies of FGM (k = 5) clamped–clamped cracked beam (crack depth ratio = 0.2 at mid-length of beam) against number of material layer, (b) second natural frequencies of FGM (k = 5) clamped–clamped cracked beam (crack depth ratio = 0.2 at mid-length of beam) against number of material layer and (c) third natural frequencies of FGM (k = 5) clamped–clamped cracked beam (crack depth ratio = 0.2 at mid-length of beam) against number of material layer	40
Figure 2.7	Rotating cantilever beam	40
Figure 2.8	(a) First natural frequency ratios of FGM cantilever beams with an edge crack at varying locations for a crack depth ratio of 0.3, (b) second natural frequency ratios of FGM cantilever beams with an edge crack at varying locations for a crack depth ratio of 0.3 and (c) third natural frequency ratios of FGM cantilever beams with an edge crack at varying locations for a crack depth ratio of 0.3.	42
Figure 2.9	(a) First natural frequency ratios of FGM clamped–clamped beams with an edge crack at varying locations for a crack depth ratio of 0.3, (b) second natural frequency ratios of FGM clamped–clamped beams with an edge crack at varying locations for a crack depth ratio of 0.3 and (c) third natural frequency ratios of FGM clamped–clamped beams with an edge crack at varying locations for a crack depth ratio of 0.3.	43
Figure 2.10	(a) First natural frequencies of FGM cantilever beams with an edge crack at varying locations for a crack depth ratio of 0.3, (b) Second natural frequencies of FGM cantilever beams with an edge crack at varying locations for a crack depth ratio of 0.3 and (c) Third natural frequencies of FGM cantilever beams with	44

an edge crack at varying locations for a crack depth ratio of 0.3.

Figure 2.11 (a) First natural frequency ratios of rotating cantilever beams with an edge crack at varying locations for a crack depth ratio of 0.3, (b) second natural frequency ratios of rotating cantilever beams with an edge crack at varying locations for a crack depth ratio of 0.3 and (c) third natural frequency ratios of rotating cantilever beams with an edge crack at varying locations for a crack depth ratio of 0.3. 45

Figure 2.12 First three mode shape of rotating cracked beam at rotational speed 100rad/sec (a) first mode (b) second mode and (c) third mode 46

Figure 3.1 Different Crack Position of Samples Test 50

Figure 3.2 Photograph of the experimental set up with oscilloscope 51

Figure 3.3 Schematic diagram of experimental setup with oscilloscope 52

Figure 3.4 Photograph of the experimental set up with data acquisition system 54

Figure 3.5 Schematic diagram of experimental setup with data acquisition system 55

Figure 3.6 Natural frequency ratios of clamped–clamped beams for (a) second mode with crack depth ratio of 0.2, (b) third mode with crack depth ratio of 0.4 and (c) first mode with crack depth ratio of 0.6 and natural frequency ratios of cantilever beams for (d) first mode with crack depth ratio of 0.2, (e) third mode with depth ratio of 0.4 and (f) second mode with crack depth ratio of 0.6. 57

Figure 3.7 Mode shape of the cracked beam with one open edge crack obtain from experimentation and FEM analysis (a) first mode shape crack location (l_c/l=0.1765) with size (d_c/h=0.4), (b)second mode shape crack location (l_c/l=0.1765) with size (d_c/h=0.4), (c) third mode shape crack location (l_c/l=0.1765) with size (d_c/h=0.4), (d) forth mode shape crack location (l_c/l=0.4118) with size (d_c/h=0.4), (e) third mode shape crack location (l_c/l=0.4118) with size (d_c/h=0.6) and (f) forth mode shape crack location (l_c/l=0.5294) with size (d_c/h=0.2) 58

Figure 3.8 Mode shape of the double cracked beam(crack location (l_c/l=0.1765) with size (d_c/h=0.4)) and (crack location (l_c/l=0.7647) with size (d_c/h=0.6)) obtain from experimentation and FEM (a) second mode and (b) third mode 59

Figure 4.1 Schematic Diagram of (a) biological neuron network and (b) artificial neuron network 63

Figure 4.2	Schematic diagram of artificial neural network with activation function	65
Figure 4.3	Schematic diagram of cascade forward back propagation neural network	66
Figure 4.4	Block diagram of cascade forward artificial neural network for crack detection	67
Figure 4.5	Central Composite Design for two variable	71
Figure 4.6	Encoding the chromosomes into bit strings	74
Figure 4.7	Crossover of bit strings	74
Figure 4.8	Mutation of bit strings (a) Before Mutation (b) After Mutation	75
Figure 4.9	Block diagram of ANFIS	78
Figure 4.10	Block diagram of Neuro-GA technique	82
Figure 4.11	Block diagram of RSM with GA technique	83
Figure 5.1	(a) First natural frequencies of clamped-clamped beams with an edge crack at varying locations for a crack size 0.04 m, (b) Second natural frequencies of clamped-clamped beams with an edge crack at varying locations for a crack depth ratio of 0.5 m and (c) Third natural frequencies of clamped-clamped beams with an edge crack at varying locations for a crack depth ratio of 0.3 m	91
Figure 5.2	Regression plot of CANN for natural frequencies and crack parameter network	92
Figure 5.3	ANFIS model structure	97
Figure 5.4	First natural frequency contour plots for clamped–clamped FGM beam (k = 0.2) with single transverse crack, (b) second natural frequency contour plots for clamped–clamped FGM beam (k = 0.2) with single transverse crack and (c) third natural frequency contour plots for clamped–clamped FGM beam (k = 0.2) with single transverse crack.	101
Figure 5.5	First natural frequency contour plots for cantilever FGM beam (k = 5) with single transverse crack, (b) second natural frequency contour plots for cantilever FGM beam (k = 5) with single transverse crack and (c) third natural frequency contour plots for cantilever FGM beam (k = 5) with single transverse crack.	102

Figure 5.6 a) Crack prediction using frequency contours of first natural frequencies in clamped-clamped beam (first —, second -----, third——): case 1,(b) Crack prediction using frequency contours of first natural frequencies in clamped-clamped beam (frist —, second -----, third ——): case 2,(c) Crack prediction using frequency contours of first natural frequencies in clamped-clamped beam (frist —, second -----, third ——): case 3,(d) Crack prediction using frequency contours of first natural frequencies in clamped-clamped beam (frist —, second -----, third ——): case 4,(e) Crack prediction using frequency contours of first natural frequencies in cantilever beam (first —, second -----, third — —): case 5, (f) Crack prediction using frequency contours of first natural frequencies in cantilever beam (first —, second -----, third — —): case 6. 103

Figure 5.7 (a) Crack prediction using frequency contours of first natural frequencies in cantilever beam (frist —, second -----, third ——): case 1,(b) Crack prediction using frequency contours of first natural frequencies in cantilever beam (frist —, second -----, third ——): case 2,(c) Crack prediction using frequency contours of first natural frequencies in cantilever beam (frist —, second -----, third ——): case 3,(d) Crack prediction using frequency contours of first natural frequencies in cantilever beam (frist —, second -----, third ——): case 4,(e) Crack prediction using frequency contours of first natural frequencies in cantilever beam (frist —, second -----, third ——): case 5,(f) Crack prediction using frequency contours of first natural frequencies in cantilever beam (frist —, second -----, third ——): case 6 104

Figure 5.8 Predicted frequencies vs. Frequency obtained by numerical analysis 107

Figure 5.9 Residual vs. Observation Order 107

Figure 5.10 (a) Fitness function value as a function of generation number: case number 1 of FGM (k = 0.2) clamped–clamped beam, (b) fitness function value as a function of generation number: case number 6of FGM (k = 5) cantilever beam. 111

Figure 6.1 Bi orthogonal 6.8 wavelet (a) decomposition scaling function (b) decomposition of wavelet function 123

Figure 6.2 Extracting irregularity from total mode shape (a) Total Profile, (b) Waviness Profile (c) Roughness Profile 127

Figure 6.3 Wavelet coefficient for (a) Scale 2, (b) Scale 8 and (c) Scale 64 129

Figure 6.4	Wavelet coefficient plot for (a) resolution, r = 1, (b) resolution, r = 5 and (c) resolution, r = 20	130
Figure 6.5	Wavelet coefficient plot for (a) second mode shape and (b) third mode shape	131
Figure 6.6	CWT plot for (a) location 250 mm from fixed end and (b) location 450 mm from fixed end	131
Figure 6.7	CWT plot for crack depth (a) 1mm, (b) 2 mm, (c) 3 mm, (d) 4 mm and (e) 5mm	132
Figure 6.8	Wavelet coefficients vs. Depth	133
Figure 6.9	CWT plot for different rotating speed (a) 50 rad/s, (b) 100 rad/s, (c) 150 rad/s and (d) 200 rad/s	133
Figure 6.10	CWT plot of double cracked beam with 1 mm and 5mm crack depth at location50 mm and 450 mm from fixed end respectively (a) first mode, (b) second mode and (c) third mode and CWT plot of double cracked beam with 5 mm and 1mm crack depth at location50 mm and 450 mm from fixed end respectively (d) first mode, (e) second mode and (f) third mode	134
Figure 6.11	CWT plot of triple cracked beam with for second mode shape	136
Figure 6.12	CWT plot of triple cracked beam with for third mode shape	136
Figure 6.13	FD plot (a) r=1, (b) r=2, (c) r=5 and (d) r=20	137
Figure 6.14	FD plot (a) at crack location 250 mm from fixed end and (b) at crack location 450 mm from fixed end	138
Figure 6.15	FD plot at crack location 450 mm for (a) second mode and (b) third mode	138
Figure 6.16	FD plot at crack location 450 mm with s=2 (a) second mode and (b) third mode	139
Figure 6.17	FD plot at crack location 450 mm with s=5 (a) second mode and (b) third mode	139
Figure 6.18	FD plot at crack location 450 mm with s=10 (a) second mode and (b) third mode	139
Figure 6.19	FD plot for crack depth (a) 1mm, (b) 2 mm, (c) 3mm, (d) 4 mm and (e) 5 mm	140
Figure 6.20	Square root of neat estimated FD vs. Depth	141
Figure 6.21	FD plot for rotating speed (a)50 rad/s, (b) 100 rad/s, (c) 150 rad/s and (d) 200 rad/s	142

Figure 6.22	FD plot of double cracked beam with5 mm and 1mm crack depth at location 50 mm and 450 mm from fixed end respectively for (a) second mode and (b) third mode	143
Figure 6.23	FD plot of double cracked beam with 1 mm and 5 mm crack depth at location 50 mm and 450 mm from fixed end respectively for (a) second mode and (b) third mode	143
Figure 6.24	FD plot of triple cracked beam with for second mode shape	143
Figure 6.25	FD plot of triple cracked beam with for third mode shape	143
Figure 6.26	Curvature plot for (a) r=1, (b) r=5, (c) r=20	144
Figure 6.27	Curvature plot for first mode at crack location (a) 250 mm and (b) 450 mm from fixed end	145
Figure 6.28	Curvature plots for second mode at crack location (a) 250 mm and (b) 450 mm from fixed end	145
Figure 6.29	Curvature plots for second mode at crack location (a) 250 mm and (b) 450 mm from fixed end	145
Figure 6.30	Curvature plot for crack depth (a) 1mm, (b) 2 mm, (c) 3 mm, (d) 4 mm and (e) 5 mm	146
Figure 6.31	Curvature vs. Crack Depth	147
Figure 6.32	Curvature plot for rotating speed (a) 50 rad/s, (b) 100 rad/s, (c) 150 rad/s and (d) 200 rad/s	148
Figure 6.33	Curvature plot of double cracked beam with 5 mm and 1mm crack depth at location 50 mm and 450 mm from fixed end respectively for (a) second mode and (b) third mode	149
Figure 6.34	Curvature plot of double cracked beam with 1 mm and 5mm crack depth at location 50 mm and 450 mm from fixed end respectively for (a) second mode and (b) third mode	149
Figure 6.35	Curvature plot of triple cracked beam with for second mode shape	150
Figure 6.36	Curvature plot of triple cracked beam with for third mode shape	150
Figure 6.37	Filtration result of the single cracked beam (crack location at l_c/L = 0.1765) based on triangular filtration (a) First mode, (b) Second mode, (c) Third mode, (d) Forth mode	151
Figure 6.38	Filtration result of the single cracked beam (crack location at l_c/L = 0.7059) based on triangular filtration (a) First mode, (b) Second mode, (c) Third mode, (d) Forth mode	152

Figure 6.39 Filtration result of third mode of single cracked beam (crack location at l_c/L= 0.7647) based on triangular filtration (a) r=200, (b) r=40, (c) r=20 153

Figure 6.40 Filtration result of forth mode of single cracked beam (crack location at l_c/L= 0.1765) based on triangular filtration with different crack sizes 154

Figure 6.41 Roughness for crack vs. crack size 154

Figure 6.42 Filtration result of second mode shape of single cracked cantilever beam four different crack scenario (a) $d_c/h = 0.2$ at $l_c = 0.412L$, (b) $d_c/h = 0.2$ at $l_c = 0.647$ L (c) $d_c/h = 0.6$ at $l_c = 0.1765L$ and (d) $d_c/h = 0.6$ at $l_c = 0.765L$ based on triangular filtration 155

Figure 6.43 Filtration result of third mode shape of single cracked cantilever beam four different crack scenario (a) $d_c/h = 0.2$ at $l_c = 0.412L$, (b) $d_c/h = 0.2$ at $l_c = 0.647$ L (c) $d_c/h = 0.6$ at $l_c = 0.1765L$ and (d) $d_c/h = 0.6$ at $l_c = 0.765L$ based on triangular filtration 156

Figure 6.44 Filtration result of forth mode shape of single cracked cantilever beam four different crack scenario (a) d_c/h = 0.2 at l_c = 0.412L, (b) $d_c/h = 0.2$ at $l_c = 0.647$ L (c) $d_c/h = 0.6$ at $l_c = 0.1765L$ and (d) $d_c/h = 0.6$ at $l_c = 0.765L$ based on triangular filtration 157

Figure 6.45 Filtration result of third mode shape of single cracked cantilever beam with two different crack scenario (a) d_c/h = 0.4 at x_0=0.2941 L, (b) d_c/h= 0.4 at l_c= 0.5294 L and forth mode shape of single cracked cantilever beam with two different crack scenario (c) d_c/h= 0.4 at l_c=0.2941L and (d) d_c/h= 0.6 at l_c= 0.5294L based on triangular filtration 158

Figure 6.46 Filtration result of third mode shape of double cracked cantilever beam (a) d_c/h =0.4 at l_c/L = 0.1765 and d_c/h =0.6 at l_c/L = 0.7647, (b) d_c/h =0.6 at l_c/L =0.1765 and d_c/h =0.4 at l_c/L = 0.7647, (c) d_c/h=0.6 at l_c/L =0.2941 and d_c/h=0.4 at l_c/L = 0.4118 159

Figure 6.47 Filtration result of forth mode shape of double cracked cantilever beam (a) d_c/h =0.4 at l_c/L = 0.1765 and d_c/h =0.6 at l_c/L = 0.7647, (b) d_c/h =0.6 at l_c/L =0.1765 and d_c/h =0.4 at l_c/L = 0.7647, (c) d_c/h=0.6 at l_c/L =0.2941 and d_c/h=0.4 at l_c/L = 0.4118 160

“This page is intentionally left blank”

List of Tables

		Page No
Table 2.1	Comparison of the first three natural frequencies of cracked FGM beam	41
Table 2.2	Rotational cantilever beam characteristics	46
Table 3.1	Geometric and physical properties of cantilever beam and clamped-clamped beam	54
Table 3.2	Comparison of natural frequencies (Hz) of a crack cantilever beam obtained through experimental and FEM analysis	56
Table 5.1	CANN result (Forward Problem)	86-88
Table 5.2	ANFIS result (Forward Problem)	88-90
Table 5.3	Percentage errors of natural frequencies using CFBP and ANFIS method	91
Table 5.4	CANN result (Inverse Problem)	93-94
Table 5.5	Actual and predicted results of cracked clamped-clamped beams using CANN	95
Table 5.6	ANFIS result (Inverse Problem)	97-99
Table 5.7	Actual and predicted results of cracked clamped-clamped beams using ANFIS	100
Table 5.8	Actual and predicted results of cracked clamped-clamped beam using Frequency Contours method	105
Table 5.9	Actual and predicted results of cracked cantilever beams using Frequency Contours method	106

Table 5.10	Comparison of contour plot crack detection of cracked beam by first three natural frequencies	106
Table 5.11	Actual and predicted results of cracked clamped-clamped beam using RSM	109
Table 5.12	Actual and predicted results of cracked cantilever beam using RSM	110
Table 5.13	Actual and predicted results of cracked clamped-clamped beams using RSM with GA	112
Table 5.14	Actual and predicted results of cracked cantilever beams using RSM with GA	112
Table 5.15	CANN optimization results of cantilever beam with error	114
Table 5.16	GA optimization of cantilever beam with error	115
Table 5.17	Neuro GA optimization of cantilever beam with error	117

Abstract

The present thesis deals with identification of crack in beam like structure using the dynamic response of the system. Changes in the loading patterns, weakening or degeneration of structures with the time may cause development or extension of existing cracks in the structure, especially in engineering beam structures which are designed for prolonged life. Hence the prediction of the location and depth of a crack in beam type structures is an important aspect of structural health monitoring for ensuring their safety. There are significant changes in the vibration response of cracked structures when the crack depth is significant in comparison to the depth of the structure. A crack in beam changes dynamics characteristics, such as natural frequencies and mode shapes. Such changes depend on crack size and location. However when the crack is relatively small, it is difficult to identify the presence of the crack by a mere observation of the vibration response data. From this, it is clear that by utilizing vibration parameters, the position and depth of the crack of cracked beam can be predicted. Actual crack model develop in a structure is very difficult. So damage zone can be quantified into a concept known as equivalent crack size. To estimate the equivalent crack length, the vibration characteristics of the damaged specimen is matched with the vibration characteristics of those specimen. It is found through literature review that although many studies have been conducted on damage diagnosis of different structural element. However damage detection procedure can be develop with different methodology. Hence this has motivated to study the detection of crack in beam like structure under different boundary condition.

In the present work, vibration parameters are obtained using (1) a numerical technique using Ritz approximation, (2) finite element analysis and (3) experimental measurement for intact intact and cracked isometric and FGM beams. Vibration parameter natural frequencies are calculated through numerical techniques and finite element analysis. Comparisons of numerical method and finite element method with experimental results are made. Different mode shapes obtained from finite element analysis is also compared with experimental results.

A large number of cracked beam specimens are modelled and evaluated their natural frequencies. These data are used to generate five different optimization technique namely cascade artificial neural network, response surface measurement, genetic algorithm, contour plot

intersection and adaptive neuro-fuzzy to design an online predicting tool for diagnosis of crack location and its depth. After using these homogeneous techniques two hybrid techniques Neuro-GA and response surface measurement with genetic algorithm are employed. The improved optimization technique results are compared with other methods especially with numerical results to obtain authenticity of proposed design. It is found that the compared results are in good agreement. These methods can be used as an alternative to health monitoring systems.

In this thesis, local damage detection procedure profile analysis is also performed. Four profile analyses are Wavelet analysis, Fractal Dimension method, curvature method and irregularity extracted method. In order to produce better result some modification is carried out on those profile analysis techniques. All profile analyses are compared with their merits and demerits. It is also shown that all these methods can produce satisfactory results with some limitation based on profile.

Chapter 1

INTRODUCTION

Outline of the Chapter: *1.1 Background and Importance, 1.2 Motivation of Thesis, 1.3 Literature Review, 1.3.1 Crack Beam Model by Finite Element Analysis, 1.3.2 Damage Detection of Structure Based on Frequency Changes, 1.3.2.1 Forward Problem, 1.3.2.2 Inverse Problem, 1.3.3 Damage Detection of Beam Based on Mode Shape Variation, 1.3.4 Damage Detection of Beam Based on Curvature Mode Shape, 1.3.5 Literatures on Experimental Work of Crack Detection, 1.3.6 Summary of the Literature Review, 1.4 Objective of the Thesis, 1.5 Contribution of the Thesis, 1.6 Layout of the Thesis, 1.7 Summary.*

1.1 Background and Importance

Damage in engineering systems is defined as intentional or unintentional changes to the material and geometric properties of these systems. It adversely affects the current and future performance of these systems. Therefore one of the most important aspects of evaluation of structural systems and ensuring their lifetime safety is structural damage detection.

From early 1970s, the dynamic response of cracked beams and rotors has been investigated increasingly because damages in rotating shaft of various power transmissions occurred quite often. Cracks may be caused by fatigue under service conditions as a result of the limited fatigue strength. They may also occur due to mechanical defects. Another group of cracks are initiated during the manufacturing processes. Generally, they are small in sizes. Such small cracks are known to propagate due to fluctuating stress conditions. If these propagating cracks remain undetected and reach their critical size, then a sudden structural failure may occur.

During operation, all structures are subjected to degenerative effects that may cause initiation of structural defects such as cracks which, as time progresses, lead to the catastrophic failure or breakdown of the structure. Thus, the importance of inspection in the quality assurance of manufactured products is well understood. Cracks or other defects in a structural element influence its dynamical behaviour and change its stiffness and damping properties. Consequently, the natural frequencies of the structure contain information about the location and dimensions of the damage (Krawczuk, 1995).

Structural damage detection has gained increasing attention by the scientific community since unpredicted major hazards, in conjunction with human losses, have been reported. Aircraft crashes and the catastrophic bridge failures are some of the examples. Development of an early damage detection method for structural failure is one of the most important keys in maintaining the integrity and safety of structures. The cracks can be present in structures due to their limited fatigue strengths or due to the manufacturing processes. These cracks open for a part of the cycle and close when the vibration reverses its direction. These cracks will grow over time, as the load reversals continue, and may reach a point where they pose a threat to the integrity of the structure. As a result, all such structures must be carefully maintained.

Engineering structures deteriorate due to its regular usage over time. This process can be initiated or even accelerated due to environmental effects and adverse load configurations. The safety of a deteriorated structure can be ensured with structural health monitoring (SHM). SHM denotes a reliable system with the ability to detect and interpret adverse "change" in a structure due to damage or normal operation (Ramanamurthy and Chandrasekaran 2008). With the methods of SHM, the performance of a structure is controlled. Usually, deterministic threshold values are taken as performance criteria for the monitoring process. The exceeding from these values during the monitoring process indicates a further increase of damage or deterioration and should lead to immediate measures. The highest safety could be achieved if the monitoring strategy covers the complete structure. Usually, this is not possible due to the related costs. Therefore optimal and cost effective maintenance strategies are required.

A large portion of the costly maintenance required for the space shuttle is examination of the structural integrity. Fatigue, foreign object debris (FOD), and operational vibrations cause damage that is not always visible at the surface. These methods of locating damage are costly and time-consuming. The present study investigates a possible simpler, less expensive method. If the self-monitoring systems in satellites could detect structural damage, they could possibly repair the damage before operational ability was impaired.

The need for an advanced structural health monitoring system can be found in several industries. The continual rise in air traffic has burdened the aerospace industry with demands for lower aircraft production and maintenance costs coupled with operational efficiency and environmentally friendly operations, while maintaining the level of safety. Health monitoring systems hold the possibility of reducing structural weight and minimizing structural

inspection requirements. These effects in turn reduce operation and maintenance costs significantly.

The demand for advancement of structural health monitoring is also growing in the space industry, as spacecraft size, complexity, and lifetime continue to increase. Damage is likely to occur due to exposure to the space environment, orbital manoeuvring loads, spacecraft docking operations, and collisions with space debris. The common visual inspection is impractical and impossible in many space applications, such as unmanned spacecraft and spacecraft in high-altitude orbits. A reliable method of in-orbit damage detection of both location and extent is critical to schedule necessary repairs and/or mission changes.

All structures are prone to damage, may be due to over-stressing in operation or due to extreme environmental conditions or due to any accidental event. Crack present in the component may grow during service and may result in the component failure once they grow beyond a critical limit. It is desirable to investigate the damage occurred in the structure at the early stage to protect the structure from possible catastrophic failures. There are various non-destructive techniques (NDTs) available for the detection of the discontinuities in the structural components and the mechanical components. They are efficient but time consuming, expensive and laborious, particularly for slender beam like components. The crack present in the component imparts local flexibility to the component and reduces the natural frequency of free vibration of the component. The local damage also affects the mode shapes of the vibration of the component. Thus, Vibration Based Inspection (VBI) can be a potential method for crack detection. Though, there has been an intense study on crack detection through vibration based inspection, there is a need to develop an effective and economically appropriate approach.

Among many SHM techniques, the dynamic response-based damage detection method attracts most attention due to its simplicity for implementation. This technique makes use of the dynamic response of structures which offers unique information on the defects contained with these structures. Changes in the physical properties of the structures due to damage can alter the dynamic response, such as the natural frequency and mode shape. These parameter changes can be extracted to predict damage detection information, such as the presence, location, and severity of damage in a structure. The natural frequency provides the simplest damage detection method since damage tends to reduce the stiffness of the structure. Therefore, a reduction of natural frequency may indicate the existence of damage in a

structure. However, the natural frequency is a global feature of the structure, from which the location of the damage is difficult to determine. The modal parameters (e.g., the mode shape and flexibility), which can capture the local perturbation due to damage are used in order to locate damage.

Vibration-based global monitoring not only allows immediate evaluations, but can also be used for continuous long-term monitoring. The goal would be to extract information about the structure's remaining lifetime, time intervals to the next maintenance and immediate shutdown. This information would benefit many fields, including civil engineering structures, railway systems, wind power stations, and others. Global methods require a coarse sensor network since they monitor the whole system, but they are less sensitive and have a lower spatial resolution than the local methods. However, these problems can be resolved by using a computational model.

The fundamental idea for vibration-based damage identification is that the damage-induced changes in the physical properties (mass, damping, and stiffness) will cause detectable changes in modal properties (natural frequencies, modal damping and mode shapes). For instance, reductions in stiffness result from the onset of cracks. Therefore, it is intuitive that damage can be identified by analyzing the changes in vibration features of the structure (Doebling *et al*., 1998).

Although in vibration test, the excitation and response are always measured and recorded in the form of time history, it is usually difficult to examine the time domain data for damage identification. A more popular method is to examine the modal domain data through modal analysis technique, in which the time domain data is transformed into the frequency domain, and then the modal domain data can be further extracted from the frequency domain data. During the past three decades, great effort has been put forward in the researches of all three domains namely, time, frequency, and modal domains. It seems that this effort will continue since no single existing method can solve all the damage identification problems from various types of damages and structures. However, the modal domain methods attract more attention and play a dominant role in the state-of-the-art of structural damage identification. The modal domain methods evolve along with the rapid development of experimental modal analysis technique, and they gain their popularity because the modal properties (i.e., natural frequencies, modal damping, modal shapes, etc.) have their physical meanings and are thus easier to be interpreted or interrogate than those of abstract mathematical features extracted from the time or frequency domain. During the last

three decades, extensive research has been conducted in vibration-based damage identification, and significant progress has been achieved in this area.

Flaws in structures in the form of cracks produce local change in stiffness altering their dynamic response (Chondros and Dimarogonas, 1980). It may also alter mass distribution and damping properties of the structure. If a structure is defective, there is a change in the stiffness and damping of the structure in the region of the defect. Usually, stiffness decreases and damping increases if the defect appears in the form of a micro or macro crack. A reduction in stiffness implies a reduction in the natural frequencies of vibration. A crack on a structural member introduces a local flexibility which is a function of the crack depth.

Materials were studied traditionally consisting of self-similar crack growth ahead of the existing cracks. In plastic materials, a plastic zone is formed ahead of the crack tip whereas in composites a damage zone is developed. In the above cases, the exact length of the crack cannot be measured. However, the effect of the damage can be estimated by studying the vibration characteristics before and after the development of damage zone. The damage zone can be quantified into a concept known as 'equivalent crack length'. In order to estimate the equivalent crack length, the vibration characteristics of the damaged specimen is matched with the vibration characteristics of various crack lengths specimen.

Major characteristics of structures, which undergo change due to presence of crack, are mentioned below

- The natural frequency
- The amplitude response due to vibration
- Mode shape
- Modal Damping

Hence it is possible to use change in natural frequency and its mode shape to detect the presence of crack in a structure.

1.2 Motivation of Thesis

Structural damage identification using dynamic parameters of the structure has become an important research area. The standard procedure of performing routine maintenance and replacing parts before they have actually used up their life is inefficient and

costly. For example currently 27 % of an average aircraft's life cycle cost is spent on inspection and repair (Hall, 1999). The strong need to develop effective damage identification techniques for structural health monitoring and damage detection at the earliest possible stage is of paramount importance to the civil, mechanical, and aerospace engineering industries.

Beams are one of the most commonly used structural elements. Beams are a major part of many different types of construction projects, be they residential, commercial or public like buildings, bridges and factories. Damages may occur in beam-like structures due to different type of loads. It has also been observed that the presence of cracks in machine elements like structures also lead to operational problem as well as premature failure. Any type of failure in one, such as fatigue cracks, causes serious damage to the system. The damage may lead to plant shutdown leading to great economical loss. Thus, many attempts in recent years have been made to deal with crack detection methods. For this reason, methods allowing early detection and localization of cracks have been the subject of intensive investigation during the last two decades. As a result, a variety of analytical, numerical and experimental investigations now exist.

The general interest in timely assessment of damage in structures and with the advent of modern computing techniques, the health monitoring has received a considerable attention since last two decades. The process of damage detection consists of mainly three stages, (1) detecting, (2) locating and (3) quantifying the extent of damage. Most researchers have proposed methods for the detection of existence of structural damage via monitoring the structural responses. However, it is difficult to find the location and extent of damage.

The dynamic response of structures can offer unique information on defects due to its presence in the structures. Changes in the physical properties of the structures owing to damage will alter the dynamic responses such as natural frequencies, damping and mode shapes. These physical parameter changes can be extracted to estimate damage information. In the past 20 years, a lot of work has been published in the area of damage detection, where various methods had been proposed. The modal parameters such as natural frequencies and mode shapes can be used to detect the initiation and development of cracks.

The basic idea behind this technology is that modal parameters (notably frequencies, mode shapes, and modal damping) are functions of the physical properties of the structure (mass, damping, and stiffness). Therefore, changes in the physical properties will cause detectable changes in the modal properties. The motivation for the development of this

technology is presented. Different methods can be used to forecast the position and severity of different structures. The methods are categorized according to various criteria such as the level of damage detection provided, model-based vs. non-model-based methods and linear vs. nonlinear methods. The methods are also described in general terms including difficulties associated with their implementation and their fidelity. Future-planned applications of those methods to actual engineering systems can be summarized.

1.3 Literature Review

The effects of damage on a structure can be classified as linear or nonlinear. A linear damage situation is defined as the case when the initially linear-elastic structure remains linear-elastic after damage. The changes in modal properties are a result of changes in the geometry and/or the material properties of the structure, but the structural response can still be modelled using linear equations of motion. Linear methods can be further classified as model-based and signal based. Model-based methods assume that the monitored structure responds in some predetermined manner that can be accurately discredited by finite element analysis, such as the response described by Euler-Bernoulli beam theory.

Nonlinear damage is defined as the case when the initially linear-elastic structure behaves in a nonlinear manner after the damage has been introduced. One example of nonlinear damage is the formation of a fatigue crack that subsequently opens and closes under the normal operating vibration environment. Other examples include loose connections that rattle and nonlinear material behaviour such as that exhibited by polymers. The majority of the studies reported in the literature address only the problem of linear damage detection.

Another classification system for damage-identification methods defines three levels of damage identification, as follows (Rytter, 1993):

• Level 1: Determination that damage is present in the structure

• Level 2: Level 1 plus determination of the geometric location and severity of the damage

• Level 3: Level 2 plus prediction of the remaining service life of the structure

To date, vibration-based damage identification methods that do not make use of some structural model primarily provide Level 1 damage identification. When vibration-based methods are coupled with a structural model, Level 2 damage identification can be obtained in some cases. Level 3 prediction is generally associated with the fields of fracture

mechanics, fatigue-life analysis, or structural design assessment and, as such, is not addressed in this thesis.

Dynamic response of linear and nonlinear beams having cracks is investigated by number of authors using different techniques in last few decades. The following sections briefly describe various literatures available related to research work on the crack detection in structures.

1.3.1 Literatures on Crack Theory, Model and Analysis of Beam like Structure by Classical Methods.

Saw cuts are used to model crack in a structure. But no matter how thin a cut is, it will not behave as a crack. A thin cut results in a local flexibility substantially less than the local flexibility associated with a fatigue crack. So theories were developed by some previous literatures. Dimarogonas (1996) published a review of the state of the art of vibration based methods for testing cracked structures. Erdogan and Wu (1997) analyzed the plane elasticity problem for a no homogeneous layer containing a crack perpendicular to the boundaries. Their problem was solved under three different loading conditions, namely fixed grip, membrane loading and bending applied to the layer away from the crack region. They presented mode I stress intensity factors for embedded as well as edge cracks for various values of dimensionless parameters representing the size and location of the crack and the material no homogeneity. Some sample results can also be given for the crack opening displacement and the stress distribution. Chondros *et al.* (1998) developed a continuous cracked beam vibration theory for the lateral vibration of cracked Euler Bernoulli beams with single edge or double edge open cracks. Yokoyama and Chen (1998) studied free vibration of uniform Euler- Bernoulli beam with single edge crack using a modified line spring model. Natural frequencies and mode shapes are obtained for various crack parameters. Pohit *et al.* (1999) investigated free out of plane vibration of a rotating beam with a nonlinear elastomeric constraint. They presented a parametric study revealing the influence of the nonlinear constraint. The linear analysis is performed by two techniques one based on a power series expansion and the other based on the Rayleigh Ritz principle. A numerical perturbation technique is applied to determine the frequency amplitude relationship. Pugno *et al*. (2000) presented a technique capable of evaluating the dynamic response of a beam with several breathing cracks perpendicular to its axis and subjected to harmonic excitation. They analyzed the vibrational response to harmonic force of a cantilever beam with cracks of

different size and location using harmonic balance approach and the results are compared with those obtained through numerical integration. Dharmaraju *et al.* (2004) presented identification of an open crack model in a beam based on force–response measurements. They presented a general identification algorithm to estimate crack flexibility coefficients and the crack depth based on the force–response information. The general identification algorithm was extended to overcome practical limitations of measuring number of degrees of freedom. Marur and Prathap (2005) employed three simplifications, which are not consistent with the governing variational principles. First one is equivalent quasilinearization technique, which is shown to have a reduced non-linear stiffness. The second, where 'neglect of inplane displacements' takes place, is seen to register an excessive non-linear stiffness. Thirdly, when both these simplifications are introduced together, they produce results closer to those of variationally correct ones. They highlighted the necessity of formulating this class of problems in variationally correct and consistent manner. Douka and Hadjileontiadis (2005) studied time frequency analysis of the free vibration response of a beam with a breathing crack. The primary aim in their study was to reveal the nonlinear behaviour of the system by using time frequency methods as an alternative to Fourier analysis methodology. They analyzed simulated and experimental response data by applying empirical mode decomposition and Hilbert transform and the instantaneous frequency. Binici (2005) proposed a method the Eigen frequencies and mode shapes of beams containing multiple cracks and subjected to axial force. Cracks were assumed to introduce local flexibility changes and were modelled as rotational springs. Chasalevris and Papadopoulos (2006) studied the dynamic behaviour of a cracked beam with two transverse surface cracks. Each crack was characterized by its depth, position and relative angle. A local compliance matrix of two degrees of freedom, bending in the horizontal and the vertical planes is used to model the rotating transverse crack in the shaft. Dynamic response was calculated based on the available expressions of the stress intensity factors strain energy release rates. Ramezani *et al.* (2006) had shown effect of rotary inertia and shear deformation on vibration characteristics of a micro beam without any crack. Extended Hamilton's principle is used to develop equation of motion and then solved it by multiple scale method. Loya *et al.* (2006) developed a model for cracked beam with a rotational and an extensional spring and solved for natural frequencies by a perturbation technique. Bikri *et al.* (2006) investigated the geometrically non-linear free vibrations of a clamped–clamped beam containing an open crack. Their semi-analytical model was based on an extension of the Rayleigh–Ritz method to non-linear vibrations, which was mainly influenced by the choice of the admissible functions. Aydogdu

and Taskin (2007) investigated free vibration of simply supported FG beam. Young's modulus of beam varied in the thickness direction according to power law and exponential law. Governing equations were found by applying Hamilton's principle. Navier type solution method was used to obtain frequencies. Different higher order shear deformation theories and classical beam theories were used in the analysis. Yan *et al.* (2007) presented a general summary and review of state-of-the-art and development of vibration-based structural damage detection. Viola *et al.* (2007) investigated the changes in the magnitude of natural frequencies and modal response introduced by the presence of a crack on an axially loaded uniform Timoshenko beam using a particular member theory. A new and convenient procedure based on the coupling of dynamic stiffness matrix and line-spring element was introduced to model the cracked beam. The application of the theory was demonstrated by two illustrative examples of bending–torsion coupled beams with different end conditions, for which the influence of axial force, shear deformation and rotary inertia on the natural frequencies were studied. Behzad *et al.* (2008) presented continuous model for vibration analysis of a beam with an open edge crack. A quasi-linear displacement field was suggested for the beam and the strain and stress fields were calculated. Sina *et al.* (2009) proposed a new beam theory different from the traditional first-order shear deformation beam theory to analyze free vibration of functionally graded beams. The beam properties were assumed to be varied through the thickness following a simple power law distribution in terms of volume fraction of material constituents. The governing equations of motion were derived using Hamilton's principle. Different boundary conditions were considered and comparisons were made among different beam theories. Also, the effects of boundary conditions, volume fraction and shear deformation on natural frequencies and mode shapes were investigated. Ariaei *et al.* (2009) presented an analytical approach, as well as a calculation method for determining the dynamic response of the undamped Euler–Bernoulli beams with breathing cracks under a point moving mass using the so-called discrete element technique and the finite element method. Kitipornchai *et al.* (2009) modelled the functionally graded Timoshenko beam as two sub beam connected by a rotational mass less spring. Using Ritz method followed by a direct iterative process fundamental nonlinear frequencies were obtained. Effect of bending extensional coupling for functionally graded material was shown which might not have significant effect on isotropic materials. Rezaee and Hassannejad (2010) investigated a new analytical method for vibration analysis using perturbation method of a cracked simply supported beam. They presented a governing equation which revealed the super harmonics of the fundamental frequency due to the nonlinear effects in the dynamic

response of the cracked beam. The solution of the governing equation also derived for the system damping changes due to the changes in the crack parameters, geometric dimensions and mechanical properties of the cracked beam. Simsek (2010) investigated vibration of a functionally graded simply supported beam due to a moving mass by using Euler–Bernoulli, Timoshenko and the third order shear deformation beam theories The system of equations of motion was derived by using Lagrange's equations. Trial functions denoting the transverse, the axial deflections and the rotation of the cross-sections of the beam were expressed in polynomial forms. The constraint conditions of supports were taken into account by using Lagrange multipliers. Mazanoglu and Sabuncu (2010) investigated bending vibration of non-uniform rectangular beams with multiple edge cracks along the beam's height. They used energy based method for defining the vibration of height-edge cracked beams. The opening form of the height edge crack was determined when the external moment was assumed to be applied for stretching the beam's width. Strain energy increase was obtained by calculating the strain change at the stretched surface by taking into account the effect of angular displacement of the beam due to the bending. They used Rayleigh-Ritz approximation method in the analysis. Eftekhari *et al*. (2011) presented an analytical model of cracked cantilevered beams made of functionally graded materials. They modelled open edge crack as a massless elastic rotational spring. Wei *et al*. (2012) introduced an analytical method for solving the free vibration of cracked FGM beams with axial loading using rotational beam model. Based on the transfer matrix method, then the recurrence formula was developed to get the Eigen value equations of free vibration of FGM beams. Due to the decrease in the determinant order, the developed method was simpler and more convenient to analytically solve the free vibration problem of cracked FGM beams. Attar (2012) provided an analytical approach to investigating natural frequencies and mode shapes of a stepped beam with an arbitrary number of transverse cracks and general form of boundary conditions. They modelled stepped cracked beam as an assembly of uniform sub-segments connected by massless rotational springs representing local flexibility induced by the non-propagating edge cracks. A simple transfer matrix method was utilized to obtain the general form of characteristic equation for the cracked beam, which was a function of frequency, the locations and sizes of the cracks, boundary conditions, geometrical and physical parameters of the beam. The proposed method was then used to form a system of 2N equations in order to identify N cracks exploiting 2N measured natural frequencies of the damaged beam.

1.3.2 Literatures on Crack Model and Analysis of Beam like Structure by Finite Element Method.

A variety of analytical, numerical and experimental crack beam model was developed by different researcher. Finite element methods had been widely employed to analyze cracked structures since they could deal with engineering structures of complex geometry in an efficient manner, Some of the relevant works on cracked beam modelling by finite element analysis are reviewed in the following paragraphs.

Sekhar and Prabhu (1992) presented a method to calculate the vibration character by applying models based finite element analysis. Saavedra and Cuitino (2001) introduced a cracked finite element stiffness matrix for FEM analysis of crack systems. The proposed element used to evaluate the dynamic response of a cracked free-free beam and a U frame when a harmonic force was applied. Krawczuk (2002) presented the use of the wave propagation approach combined with a genetic algorithm and the gradient technique for damage detection in beam-like structures. For modelling the beam structures, a new type of beam spectral finite element with a transverse open and non-propagating crack was applied. Sinha and Friswell (2002) studied experimental vibration behaviour of a free–free beam with a breathing crack under sinusoidal input force using a simple finite element model for a crack in beam. This method was used finite element (FE) modelling with standard two node Euler–Bernoulli beam elements, except for those elements containing a crack. For the crack element, FE stiffness matrix was obtained by generating the flexibility matrix of a beam element with a crack using the strain energy density function given by linear fracture mechanics theory. Cacciola *et al*. (2003) presented Monte Carlo method to evaluate in time domain the higher order statistics of the non-linear beam model by finite elements. The numerical application was performed on a cantilever beam showed high sensitivity of the skewness coefficient of the rotational degrees of freedom to the non-linear behaviour of the system. Zheng and Kessissoglou (2004) presented the natural frequencies and mode shapes of a cracked beam using the finite element method. In their study, an ‘overall additional flexibility matrix’, instead of the ‘local additional flexibility matrix’, was added to the flexibility matrix of the corresponding intact beam element to obtain the total flexibility matrix, and therefore the stiffness matrix. Cam *et al.* (2005) studied on the location and depth of cracks in cracked beams using impact echo method. Here three dimensional V shaped edge cracked beam was modelled by solid element. Chondros and Labeas (2007) studied torsional vibration of a circumferentially cracked cylindrical shaft through an ‘‘exact’’ analytical

solution and a numerical finite element analysis. The FE formulation was developed based on Euler–Bernoulli cracked beam using 3-D non-singular 8-node brick element solid 45. The circumferential crack is modelled by assuming the corresponding nodes of the two crack surfaces to deform independently. Karthikeyan *et al.* (2007) developed a method of the crack localisation and sizing in a beam from the free and forced response measurements. That method was given flexibility coefficient as a by-product. Timoshenko beam theory was used in the beam modelling for transverse vibrations. The finite element method was used for the cracked beam free and forced vibration analysis. Orhan (2007) studied the free and forced vibration analysis of a cracked beam in order to indentify the crack in a cantilever beam. Single and two edge cracks were evaluated. Same kind of cracked beam was modelled with discretized into 1510 elements with 2300 nodes. Al-Said (2007) proposed a simple crack identification technique based on a suggested mathematical model to identify crack position and depth in a stepped cantilever beam carrying a rigid disk at its tip. In FEA, 10-node tetrahedral element type was used to model clamped-free stepped beam carrying a rigid disk; the crack is represented by sharp V-notch. A non-uniform mesh with very fine mesh in the vicinity of the crack is used in FE modelling. Jose *et al.* (2009) presented physics based 3D model of new machine damage simulator equipment, which had built up by ANSYS considering the Timoshenko beam hypothesis. They had taken in accounts, various types of damages, for example, transverse cracks, imbalance, misalignment, bent shafts and their combinations. They carried out both off-line and on-line experiment verifications. Various kinds of external exciters through piezoelectric actuator have employed in their model, and the dynamic responses had measured. Buezas *et al.* (2011) presented 2D elasticity finite element model to study a clamped-free beam. Wu (2011) developed two dimensional beam structure using plane 42 element. A high meshing density was applied around the crack area such that the stress/strain singularity at the crack position was able to be accurately revealed. Zhong and Oyadiji (2011) modelled crack simple supported beam using 20 node 3D brick element which is denoted in the ABAQUS FE package as C3D20R. Cheng *et al*. (2011) investigated vibration characteristics of cracked rotating tapered beam by p-version finite element method. In their formulation, the shape functions enriched with the shifted Legendre orthogonal polynomials were employed to represent the transverse displacement field within the rotating tapered beam element. The crack element stiffness matrix and the p-version finite element model of the structural system were obtained by using fracture mechanics and the Lagrange equation, respectively. Another cracked beam model was proposed by Mazanoglu and Sabuncu (2012). Cracks were modelled as slots formed by subtracting thin transverse

blocks from the simulated beam. Widths of the slots were chosen as 0.0004 m. Element type referred to as 'Solid95' was employed. Al-Ansari (2012) employed finite elements model of stepped cantilever beam using solid tetrahedral element. Nematollahi *et al*. (2012) presented an open-edge crack beam model by divided beam in different segment along the length for meshing. High density meshing was applied crack segment. They used Four-node quadrilateral element to mesh structure. Stojanovic *et al*. (2013) suggested non-linear vibration of Timoshenko damaged beams by p-version finite element method. Torabi *et al*. (2014) used differential quadrature element method (DQEM) to analyze the free transverse vibration of a multiple cracked non-uniform Timoshenko blade rotating with a constant angular velocity.

Due to the presence of the crack there is a singularity in the stress field at the crack tip. Usually quarter- point elements are used to model the singular behaviour in the stress field. Chati *et al*. (1997) presented comparison study in natural frequencies when the singular elements were used and when they were not used. Nandwana and Maiti (1997) presented for detection of the location and size of a crack in a stepped cantilever beam. During crack model around the crack tip, quarter point singularity elements were used. Behzad *et al*. (2005) was investigated finite element analysis for a rectangular beam with an open edge crack. In this analysis singular elements were used for meshing process and the natural frequencies had been obtained. Lee (2009) provided a method to identify multiple cracks in a beam using the vibration amplitudes. A finite element analysis was carried out using two dimensional finite elements with singular element. In this analysis the singular elements with high density mesh were used for meshing process.

Composites materials are intended to be used more extensively now a day. There are several techniques for composite modelling crack structure such as microscopic modelling, macroscopic modelling, mixed modelling, discrete reinforcement modelling and sub modelling. However, the most common use in finite element simulations of composite material are layered shells, layered-solids, stacked solid elements and stacked or layered continuum shells. One of the important types of composite material is functionally graded material (FGM) having great application potential in many high-temperature engineering fields such as aerospace vehicles, nuclear reactors, power generators, automobile industries. The concept is to make a composite material by varying the microstructure from one material to another material with a specific gradient. Rousseau and Tippur (2000) studied the effect of different elastic gradient profiles on the fracture behaviour of dynamically loaded

functionally graded materials having crack parallel to the elastic gradient. This study simulated dynamic analysis on glass filled epoxy FGMs. Kumar *et al*. (2004) developed finite element model and applied on a transverse crack locale of a composite cracked beam. They assumed a small number of inner elements modelled of one-dimensional wave direct and applied 1st-order shear deformation kinematics in each of this wave direct. They concluded the advantages of their planned approach, limits of the element and future scope of enhanced analytic study of cracked beam. Palacz *et al*. (2005) worked on a multilayer laminated composite beam by using spectral finite element analysis. They studied about flexure-shear coupled wave transmission of a composite laminated beam and calculated stiffness matrix of the beam. They stated that the waves propagate faster in one direction material than the multi-layer composite material. Hu *et al*. (2006) presented an approach to detect surface cracks in composite laminates using modal analysis and strain energy method. Plate was discretized into layered-solid elements. To simulate a surface crack, the nodes at location of surface crack were replaced by separated nodes. Ayhan (2007) presented stress intensity factors for three dimensional cracks contained in functionally graded materials. A 3D finite-element based fracture analysis program, FRAC3D, was developed. Aloulou *et al*. (2009) studied study the influence of material non homogeneity on the buckling resistance of the graded layer for various crack positions, coating thicknesses and different orthotropic FGMs. They used triangular plane elements for discretized the structure. Material properties were assigned according to centroidal coordinate of each element and were constant within each element. Rosales *et al*. (2009) presented two crack detection inverse problem approaches with a power series technique and artificial neural network. Yu and Chu (2009) presented a methodology to estimate the crack location and size in FGM beams by p-version of finite element method. Beam was discretized with 8-node quadrilateral plane stress element. The edge crack was modelled by generating two independent sets of nodes along the crack surfaces. Ramanamurthy and Chandrasekaran (2011) studied damage detection method in a composite cantilever beam with an edge crack using finite element method. They modelled the composite beam with the layered element (Shell 99). The FE analysis software ANSYS was used in the modal analysis to obtain mode shapes. Katunin (2011) *et al.* developed of cracked composite plate model using eight-node composite type hexagonal elements. Khan (2014) *et al.* studied fault diagnosis of cracked cantilever composite beam by vibration measurement and radial basis function neural network. They selected and used solid shell 190 for meshing the composite beam.

Crack is not always fully open some cases. Some crack is open and closes alternatively in every cycle of loading. This type of phenomenon present in a crack is called breathing crack. Last few years breathing crack models were developed by some researcher. Andreaus *et al*. (2007) developed breathing crack model of beam using two-dimensional finite elements. The behaviour of the breathing crack was simulated as a frictionless contact problem. Chatterjee *et al*. (2011) presented a breathing crack in cantilever beam using contact model dynamic analysis**.** They applied constraints between the surfaces to prevent penetration of nodes of one crack face into the other crack face. Waheed *et al*. (2011) presented breathing crack model of simple blade by finite element program using contact element. Liong and Proppe (2013) presented breathing crack model in a rotor. Shaft is discretized with 4108 plane strains and 8 node quadrilateral elements. The fracture process zone was modelled by 8 node rectangular cohesive elements having zero thickness. One face of cohesive elements was connected to continuum elements with 4 nodes, while the other face was given symmetric displacement boundary conditions. Thus, an artificial interface was created along the fracture process zone.

1.3.3 Literatures on Experimental Work of Crack Detection

Experiments are devised as a methodical procedure to recreate the conditions of actual working environment of a structural component in order to predict its behaviour under such conditions. Experiments may also be performed with an objective to verifying or establishing the validity of a theoretical simulation study. In recent years, increase in computational capabilities of computers has meant that simulation studies have taken precedence in investigating of crack of various structural elements. However, this has not diminished the significance of experimental studies, which are now used to substantiate the findings of theoretical analysis. Experimental analyses of different aspects of dynamic behaviour of various structural elements have been conducted by different researchers. In the following paragraph a concise description of some experimental crack investigations available in literature is provided.

Patil and Maiti (2005) presented experimental studies to verify the accuracy and effectiveness of their numerical method. The beam response of cantilever beam with multiple cracks was analyzed by the FFT analyzer. Nahvi and Jabbari (2005) presented an analytical as well as experimental approach to the crack detection in open cracked cantilever beam by vibration analysis. Beam was excited by a hammer and the response is obtained using an accelerometer attached to the beam. Yoon *et al.* (2007) studied an experimental analysis on

double crack simply supported beam. Machorro-Lopez *et al.* (2009) presented a numerical and experimental study detecting damaged non-rotating and damaged rotating shafts by analyzing the coupled vibratory response obtained by implementing different kinds of external excitations. Experiments and simulations performed using a piezoelectric actuator on one bearing housing to stimulate responses that were then measured using triaxial accelerometers on the other bearing housing. Wang and Wu (2011) studied for the location detection of a delamination in a beam structure under a static displacement with a spatial wavelet transform. In that research, two delaminated cantilever beams with different dimension and materials subjected to a static displacement at their free ends were investigated experimentally. The static profiles of the delaminated beams acquired by a high-precision laser profile sensor were analyzed with the Gabor wavelet to identify the delamination location. Al-Ansari *et al.* (2012) a comparison study were performed between experimental result and ANSYS program results of cracked simple supported beam. Universal vibration approaches was employed in that study. Mazanoglu and Sabuncu (2012) presented an algorithm for detecting cracks on the beams and a statistical process for minimizing the measurement errors. Data acquisition was achieved by exciting the beam using an impact hammer and by taking the vibration response using a miniature accelerometer. 30000 samples were collected with sampling rate 6000 Hz to observe the first four peaks of the natural frequencies in the spectrum.

1.3.4 Literatures on Damage Detection of Structure Based on Frequency Changes

A crack location and a crack size model are formulated by relating fractional changes in modal energy to changes in natural frequencies due to damage such as cracks. These methods are generally based on the inspection frequency changes. The amount of literature related to damage detection using shifts in resonant frequencies is quite large. Few significant literatures are reviewed in the following paragraphs.

Salawu (1997) presented a review on the use of modal frequency changes for damage diagnostics. The observation that changes in structural properties cause changes in vibration frequencies was the motivation for using modal methods for damage identification and health monitoring. A more thorough reviewed and reference list could be found in Doebling (1998). An effort had been made to include the early work on the subject, some papers representative of the different types of work done in this area, and papers that were considered by the

authors to be significant contributions in this area. Chondros *et al.*(1998) presented cracked elements behaviour based on the continuous crack flexibility vibration theory were correlated with numerical solutions, the lumped crack beam vibration analysis and experimental results obtained on aluminium and steel beams with open cracks.

1.3.4.1 Forward Problem

The forward problem (i.e. to gain accurate natural frequencies of the beam-like structures knowing the cracks' characteristics), which usually falls into the category of Level 1 damage identification, consists of calculating frequency shifts from a known type of damage. Typically, the damage is modelled and then the measured frequencies are compared to the predicted frequencies to determine the damage. Forward problem is also known as direct method. Friswell (1994) presented the results of an attempt to identify damage based on a known catalog of likely damage scenarios. The authors presumed that an existing model of the structure was highly accurate. Using this model, they computed frequency shifts of the first several modes for both the undamaged structure and all the postulated damage scenarios. Then ratios of all the frequency shifts were calculated. Juneja, *et al*. (1997) presented a forward technique called contrast maximization to match the response of the damaged structure to a database of structural responses to locate the damage. Masoud *et al*. (1998) studied the effect of crack depth on the transverse vibrational characteristics. They investigated the effect of prestress on the natural frequencies of a symmetrically cracked fixed-fixed beam with a stress on the coupling between the crack depth and the axial load. Gounaris and Papadopoulas (2002) presented a method for crack identification in rotating shafts by coupled response measurement. Patil and Maiti (2003) presented a method for detection of multiple open cracks in slender Euler-Bernoulli beams based on frequency measurements. Their method was based on the transverse vibration modelling through transfer matrix method and representation of a crack by rotational spring. The procedure was given a linear relationship explicitly between the changes frequencies of the beam and the damage parameters. Those parameters were determined from the knowledge of changes in the natural frequencies. Lin (2004) presented both direct and inverse methods on free vibration analysis of simply supported beams with a crack. In the forward problem he applied Timoshenko beam theory on two separate beams with compatibility requirements of the crack. Douka *et al*. (2004) studied influence of two transverse open cracks on the anti-resonances of a double cracked cantilever beam for crack investigation by both analytically and experimentally. Kisa and Gurel (2006) proposed a numerical model that combines the

finite element and component mode synthesis methods for the modal analysis of beams with circular cross section and containing multiple non-propagating open cracks. Sahoo and Maity (2007) presented an inverse problems damage assessment of structures using hybrid neuro-genetic algorithm. Chasalevris and Papadopoulos (2008) investigated the coupled bending vibrations of a stationary shaft with two cracks. They also studied about effect of vibration of cracked shaft on the relative crack orientations. Sekhar (2008) presented the different studies on double or multi-cracks and noted the influences and identification methods in vibration structures such as beams, rotors, pipes, etc. Wang *et al*. (2011) studied both forward and inverse problems of pipe transverse crack detection. First, Rayleigh beam elements of Daubechies wavelet were constructed to solve the forward problem. Then in the inverse problem a genetic algorithm was used to identify the pipe crack location and size, solving the smallest sample points of the difference between the outputs of structural vibration and the pipe crack model. Tlaisi *et al*. (2012) employed a crack detection method in shaft using lateral and torsional vibration measurements and analysis. Their experimental and finite element results were indicated that the use of the rate of change of frequencies, modal amplitudes as a function of crack depth ratio. Djidrov *et al*. (2014) presented vibration analysis and frequency response analysis of cantilever aluminium beam with bonded piezoelectric transducer by using finite element method. Gillich and Praisach (2014) presented a method, based on natural frequency changes, to detect damages in beam-like structures and to assess their location and severity, considering the particular manner in which the natural frequencies of the weak-axis bending vibration modes change due to the occurrence of discontinuities. Both power spectrum and time–frequency analysis was applied for modal identification and damage detection.

1.3.4.2 Inverse Problem

The inverse problem, which is typically Level 2 damage identification, consists of calculating the damage parameters, e.g., crack length and/or location, from the frequency shifts. Soft computing is required for inverse problem. Inverse problem is also known as indirect method.

Dado (1997) proposed a direct mathematical model for the prediction and identification of transverse cracks in beams with different end conditions. The input data for this algorithm were the natural frequencies of the first two bending modes of vibrations of the damaged beam. Using these two input values and with the availability of accurate frequency measurements and ideal end conditions, the crack location and depth were identified in term

of known beam parameters. Khan *et al*. (2000) used a scanning laser Doppler vibrometer to measure mode shapes in a steel cantilever beam, a steel cantilever plate and concrete beams. Cracks were located in the test specimens from localised mode shape discontinuities. Yang *et al.* (2001) investigated the influence of cracks on structural dynamic characteristics during the vibration of a beam with open crack using energy base method. To identify the crack, the frequency contours with respect to crack depth and location were defined and plotted. Viola *et al*. (2001) developed a non-destructive procedure for the determination of location and size of a crack in structure. A global minimization approach was employed for identify the crack element in discretized structure. Chinchalkar (2001) described a numerical method for determining the location of a crack in a beam of varying depth when the lowest three natural frequencies of the cracked beam were known. The crack was modelled as a rotational spring and graphs of spring stiffness versus crack location were plotted for each natural frequency. The point of intersection of the three curves defined the location of the crack. Kim *et al*. (2003) presented crack detection in beam-type structures using frequency data. A crack location model and a crack size model were formulated by relating fractional changes in modal energy to change in natural frequencies due to damage such as cracks or other geometrical changes. Next, the feasibility and practicality of the crack detection scheme were evaluated for several damage scenarios by locating and sizing cracks in test beams for which a few natural frequencies were available. An attempt had been made to detect the presence of a crack in beams, and determined its location and size, based on experimental modal analysis results. A crack detection methodology changes in natural frequencies and frequency response function amplitudes based on experimental modal analysis results as a function of crack depths and locations were used by Owolabi *et al*. (2003). Loutridis *et al*. (2005) proposed a method for crack detection in beams based on instantaneous frequency and empirical mode decomposition. To estimate the size of the crack, a simple relation was established, which relates the mean variation of the instantaneous frequency to the depth of the crack. The variation of the instantaneous frequency increases with crack depth following a second-order polynomial law and used as an indicator for crack size. Horibe and Watanabe (2006) carried out a method for identifying of a crack in a plate that uses a genetic algorithm based on changes in natural frequencies. Choubey *et al*. (2006) presented crack detection of pressure vessel by artificial neural networks. Natural frequencies corresponding to different crack sizes for a particular location were used as input patterns to an artificial neural network. Buezas *et al.* (2008) presented a damage detection method in structural elements taking into account a crack contact model. A generic algorithm optimization method was applied for

crack detection in structural elements. Xiang *et al*. (2008) proposed a method on crack detection in a shaft by combination of wavelet-based elements and genetic algorithm. Baghmisheh *et al*. (2008) proposed a fault diagnosis method based on genetic algorithms and a model of damaged structure. The identification of the crack location and depth in the cantilever beam was formulated as an optimization problem, and binary and continuous genetic algorithms were used to find the optimal location and depth by minimizing the fitness function which is based on the difference of measured and calculated natural frequencies. Saridakis *et al*. (2008) presented a model for the coupling effect of bending vibrations on the cracked shaft. Three optimizations techniques neural networks, genetic algorithms and fuzzy logic were applied for identification of crack. Yu *et al*. (2009) presented a contour plot method for identification of crack in functionally graded material beams. They applied a random from uniform distribution for error calculation in their crack identification result. Fang and Perera (2009) used a response surface methodology based damage identification technique. The proposed method was implementation of inverse problems by model updating in which the response surface models substitute the finite element models. Perk *et al*. (2009) proposed sequential approaches for damage detection in beams using time-modal features and artificial neural networks. Their scheme of the sequential approaches mainly consisted of two phases: time-domain damage monitoring and modal-domain damage estimation. In the first phase, an acceleration-based neural networks algorithm was designed to monitor the occurrence of damage in a structure by using cross-covariance functions of acceleration signals measured from two different sensors. By using the acceleration feature, the ABNN was trained for potential damage scenarios and loading patterns which are unknown. In the second phase, a modal feature-based neural networks algorithm was designed to estimate the location and severity of damage in the structure by using mode shapes and modal strain energies. Begambre and Laier (2009) proposed a particle swarm optimization simplex algorithm model based damage identification procedure using frequency domain data. The formulation of the objective function for the minimization problem is based on the frequency response functions of the system. They presented hybrid method performs better in different benchmark functions than the Simulated Annealing (SA) and the basic PSO. Singh and Tiwari (2010) developed a two-step multi-crack identification algorithm based on forced responses from a non-rotating shaft. The size and the accurate location of cracks were obtained by using multi-objective genetic algorithms. Nazari *et al*. (2011) presented a method for crack location and depth detection in symmetric beams using artificial neural network and finite element method. Buezas *et al*. (2011) determined crack depth and crack location

detection with genetic algorithms taking into account a crack contact model. Fang *et al*. (2011) presented response surface based model updating using D-optimal design for damage identification of a beam. Moradi *et al*. (2011) investigated the application of bees algorithm with the accuracy of the algorithm verified through both numerical and experimental studies on the cracked cantilever beams. The results (i.e., the predicted location and size of the cracks) obtained through bees algorithm were compared with those of particle swarm optimization, a popular and robust swarm-based optimization method, to investigate the robustness of the proposed method. Parhi and Choudhury (2011) developed a smart crack detection of a cracked cantilever beam using fuzzy logic technology with hybrid membership functions. Saeed *et al*. (2011) utilised single and multiple artificial neural networks and multiple adaptive neuro-fuzzy inference systems artificial intelligence (AI) techniques for crack identification in curvilinear beams based on changes in vibration characteristics. Vibration analysis had been performed by applying the finite element method to compute natural frequencies and frequency response functions (FRFs) for intact and damaged beams. Mazanoglu *et al*. (2012) proposed an algorithm by contour plot for detection of cracks in beams and a process which minimizes the errors in experimental results. Nanda *et al*. (2012) obtained the location and amount of crack in beam like structures based on the incremental particle swarm optimization technique. Barad *et al*. (2013) carried out crack detection in cantilever beam by contour diagram. Yang *et al*. (2013) studied damage identification approach for plate structures based on frequency measurements. They presented plate damage detection method using frequency contour lines. Mohan *et al*. (2013) used the use of frequency response function with the help of particle swarm optimization technique, for structural damage detection and quantification. Garg *et al*. (2014) developed a hybrid approach based on response surface methodology and genetic algorithm to detect crack in cantilever beam type structures. In this paper, a numerical as well as an experimental study was designed to predict a single open crack in cantilever beams. The crack was modelled using response surface methodology. The weighted sum of the squared errors between the measured and computed natural frequencies was used as the objective function. This objective function was minimized using genetic algorithm optimization technique. Majumdar *et al*. (2014) presented structural damage detection based on modal parameters using continuous ant colony optimization.

1.3.5 Literatures on Crack Detection of Structure Based on Direct Comparison Mode Shape

The position of the crack can be predicted by comparing the fundamental mode shapes of the structure with and without a crack. Furthermore the depth of the crack can be obtained by the change of mode shape of the structure with and without a crack. In the following paragraphs a brief account of some of the relevant research works available in literature is provided.

Tsai and Wang (1996) studied vibration analysis and diagnosis of a cracked shaft. The position of the crack was predicted by comparing the fundamental mode shapes of the shaft with and without a crack. Ratcliffe (1997) presented a technique for locating damage in a beam that uses a finite difference approximation of a Laplacian operator on mode shape data. Kim *et al*. (2003) put forward a comparison study on damage identification frequency-based method and mode shape-based method in beam-type structures. For mode shape- based damage detection (MBDD) method damage index algorithm to localize and estimate severity of damage from monitoring changes in modal strain energy was formulated. Bakhary *et al*. (2007) proposed a statistical approach for damage detection using artificial neural network with consideration of uncertainties. Parhi and Das (2008) proposed an approach on structural damage detection by fuzzy-Gaussian technique. They used fuzzy logic controller with six input parameters and two output parameters. The input parameters to the fuzzy-Gaussian controller were relative deviation of first three natural frequencies and relative value of first three mode-shapes percentage deviation. The output parameters of the fuzzy inference system were relative crack depth and relative crack location. Fayyadh and Razak (2011) used of mode shape deviations for the identification of damage location. The residual values from curve fitting procedure on mode shape vectors with Chebyshev standard rational series were used to detect the damage along the beam length. Parhi and Dash (2011) analysed the dynamic behaviour of a beam structure containing multiple transverse cracks using neural network controller. The first three natural frequencies and mode shapes had been calculated using theoretical, finite-element and experimental analysis for the cracked and un-cracked beam. The calculated relative natural frequencies and mode shape difference were used to train the feed-forward multi-layered neural network controller with back-propagation technique for the prediction of crack. Relative crack locations and relative crack depths are the output of the neural controller. Rao *et al*. (2012) presented vibration analysis of a cracked cantilever beams with open transverse crack. A fuzzy logic inference system was used to

analyze the crack in cantilever beam. The relative deviation of first three natural frequencies and relative value of first three mode shape difference were the input parameters to fuzzy logic inference system and relative crack depth and relative crack location are the output parameters of the fuzzy inference system. Thatoi *et al.* (2014) presents a novel hybrid fuzzy logic based artificial intelligence (AI) technique applicable to diagnosis of the crack parameters in a fixed beam by using the vibration signatures as input. Deviations in the vibration signatures for the first three mode shapes had been taken as input parameters for a fuzzy logic based controller for calculation of crack location and its severity as output parameters.

1.3.6 Literatures on Crack Detection of Structure Based on Curvature Mode Shape

Damage induces changes to the dynamic properties of a structure, consequentially causing irregularity of local mode shape; moreover, this irregularity can be characterized by an abrupt peak with the position and magnitude of the peak indicating the location and severity of the damage in a quantitative fashion. The curvature mode shape is directly related with the local information of a structure. Therefore, it is more sensitive to local damage of a structure. In order to locate and size identify the damage, some local damage detection had been developed by different researcher. A brief overview of some of the relevant and recently published works is provided in the following paragraph.

Wang and Deng (1999) presented a structural damage detection technique based on wavelet analysis of spatially distributed structural response measurements. The detection or displacement response was analyzed with the wavelet transform and the presence of the crack was detected by a sudden change in the spatial variation of the transformed response. Okafor and Dutta (2000) presented investigation of the detection and quantification of damage in beams. The research incorporated a new method for automated sensing with a laser-based optical system and information processing with wavelet transforms. A simple method for crack identification in beam structures based on wavelet analysis is carried out by Douka *et al.* (2003). The fundamental vibration mode of a cracked cantilever beam was analyzed using continuous wavelet transform and both the location and size of the crack were estimated. Ovanesova and Suarez (2004) applied wavelet transform to detect cracks in frame structures, such as beams and plane frames. Loutridis *et al.* (2004) proposed crack identification in double-cracked beams based on wavelet analysis. The proposed technique was validated both

analytically and experimentally in case of a double cracked cantilever beam having cracks of varying depth at different positions. Chang and Chen (2004) used a technique for thick rotating blade damage detection based on spatial wavelet analysis. Hadjileontiadis *et al*. (2005a) employed crack identification in beam structures based on fractal dimension analysis. The fundamental vibration mode of a cracked cantilever beam was analyzed and both the location and size of the crack were estimated. The location of the crack was determined by the sudden changes in the spatial variation of the analyzed response, while the size of the crack was related to the fractal dimension measure. Hadjileontiadis *et al*. (2005b) investigated crack detection in beams using kurtosis. Wang (2006) studied damage detection technique using the roughness profile of structural mode shape. Hadjileontiadis and. Douka (2007) detected cracks in plate structures based on fractal dimension analysis. Zhong and Oyadiji (2007) proposed method of crack detection in simply supported beams without baseline modal parameters by stationary wavelet transform. Qiao *et al*. (2007) carried out dynamic response based damage detection techniques for composite laminated plates using smart piezoelectric materials and modern instrumentation like scanning laser vibrometer. The experimental and numerical curvature mode shapes were primarily used to detect the presence, location, and size of the delamination. Three relatively new damage detection algorithms, simplified gapped smoothing method, generalized fractal dimension, and strain energy method were employed to analyze the experimental and numerical curvature mode shape data and uniform load surface curvatures. Messina (2008) presented refinements of damage detection methods based on wavelet analysis of beams, plates and shells. The refinements were in regard to of wavelet-algorithms which were aimed at significantly reducing those border distortions normally arising during a wavelet-damage detection procedure. Ramanamurthy and Chandrasekaran (2008) depicted different damage algorithms namely curvature mode shape method, damage index method, curvature damage factor, gapped smoothing method and strain energy method to locate the crack in a cantilever composite beam. Wang and Qiao (2008) proposed damage detection technique using irregularity profile of a structural mode shape of E-glass/epoxy laminated composite beam. Irregularity profile was extracted from the mode shape by two types of numerical filters, i.e., triangular and Gaussian. Srinivasarao *et al*. (2010) presented crack identification in beam structures by analyzing the fundamental mode of cracked cantilever beam using continuous wavelet transform. “Symmetrical 4” wavelet was used for crack detection on cracked cantilever beam. Shi *et al*. (2010) studied feasibility of using computer vision technique to automatically collect static deformation profile, and analyzed the profile to detect and locate

the damages using several popular signal processing methods. The profiles were then processed to reveal the existence and location of the irregularities on the deformation profiles by applying fractal dimension, wavelet transform and roughness methods, respectively. Liu *et al.* (2010) presented a crack detection method for fibre reinforced composite beams based on the continuous wavelet transform. The Gabor and Morlet wavelets were chosen for wave signal processing owing to their good time-frequency characteristics. Ramanamurthy and Chandrasekaran (2011) studied vibration analysis of a cantilever beam with two open transverse cracks and also studied the response characteristics with damage identification is based on the damage index method. Vallabhaneni and Maity (2011) developed a computer code to assess structural damages from curvature damage factor using radial basis neural network. Wang and Wu (2011) studied delamination location using spatial wavelet analysis through finite element model and experimental studies. Zhong and Oyadiji (2011) proposed detection of cracks in simply-supported beams by continuous wavelet transform of reconstructed modal data. This new approach was based on finding the difference of the CWTs of the two sets of mode shape data. Those two modal data sets, which constitute two new signal series, were obtained and reconstructed from the modal displacement data of a cracked simply supported beam. Li *et al.* (2011) put forward a fractal dimension-based damage detection method for beams with a uniform cross-section. An FD-based index for damage localization was proposed using the difference of the angle between two successive points. The relationship between the angle expressed in FD and the modal strain energy was established and an FD-based index for estimation of damage extent was then presented and predicted the severity of the damage. Lonkar and Srivastava (2011) an algorithm based on curvature, Wavelet Transform and surface fitting technique was proposed for damage detection. Jiang *et al.* (2012) proposed a method for crack detection from the slope of the mode shape using complex continuous wavelet transform. Through complex continuous wavelet transform of the slope of the mode shape using Complex Gaus1 wavelet the locations of cracks were detected from the modulus line and the angle line of wavelet coefficients. Bai *et al.* (2012) demonstrated fractal dimension method on multiple cracks identification in numerically simulated damage scenarios. The effectiveness of the method was experimentally validated by using a scanning laser vibrometer to acquire higher-order mode shapes of a cracked cantilever beam. Li *et al.* (2013) explained how to locate multi-crack in a damaged structure using FEA with three-step-meshing. Xiang *et al.* (2013) presented a method for identification of damage locations based on operating deflection shape (ODS). The ODS of a damaged plate-like structure excited by a harmonic force was calculated using

wavelet numerical method. The performance of wavelet numerical method was verified to analyze eigenvalue problem.

1.3.7 Summary of the Literature Review

Various discussions had been made on different methods of identification of fault due to the presence of a crack in beams, their locations and sizes. These methodologies can be used for crack detection of various structural systems. Hence it is concluded that the future work on the problem of fault recognition of rotating and non-rotating isotropic and FGM beam can be carried out by using more advanced optimization and profile analysis techniques using vibration signature of the system.

1.4 Objective of the thesis

Primary objective of the present thesis is to predict the location and size of a crack in different types of beam structures using their vibration signature. The objectives of this thesis can be enumerated as below:

1. Vibrational analysis is carried out of isotropic and FGM cracked beam by a numerical technique using Ritz approximation. Followed by three-dimensional FEM modal analysis is performed on both rotating and non-rotating cracked beam using ANSYS. In order to verify the applicability and performance of the formulation, a comparison study is performed between Numerical and FEM.

2. Extensive experiment on vibration analysis of different types of isotropic beams are carried out to validate the results obtained by finite element and numerical analysis method.

3 Various types of homogeneous optimization techniques such as, artificial neural network, response surface methodology (RSM), genetic algorithm (GA), contour plot intersection and adaptive neuro-fuzzy with hybrid optimization techniques RSM-GA, Neuro-GA are applied to identify its size and location of the crack from the response data obtained from the numerical result, finite element modelling results and experimental data of the intact and cracked beam.

4. Profile analysis techniques namely wavelet analysis, fractal dimension, curvature analysis and irregularity extraction method are applied to identify the size and location of the crack from the mode shape obtained from finite element modelling and experimental of the intact and cracked beam.

5. Comparison studies are performed between all crack detection techniques.

1.5 Contribution of the thesis

The main contribution of this thesis is that three dimension cracked beam model developed in ANSYS environment with different boundary condition followed by different crack detection technique applied on finite element results. Both isotropic and FGM cracked beam are performed. However most of the earlier studies crack detection of FGM beams are based on two dimensional models. Vibration analyses are also performed for finding crack size and location of rotating cantilever beam. From the literature review, it is evident much work has not been carried out for crack detection of rotating beams.

Different non-destructive crack detection techniques are introduced as novelty of the present analysis to forecast crack location and its depth in beam like structure. Considerable improvements have been observed after modification of those techniques. Some hybrid optimization model has been designed in this thesis to reduce prediction error for detection of crack size and location. However hybrid crack detection model has been developed in recent years.

Further investigations are carried out to observe of vibration parameters from experimental procedures FFT analyser. The vibration of modal data obtain from experimental analysis is compared with finite element analysis. All the data obtained from various discussed methods are validated.

1.6 Layout of the thesis

The current thesis organized in following chapters.

In chapter 1, described importance and motivation of the thesis, review of the available literature objective on present study and contribution of thesis.

In chapter 2, model Description and numerical analysis with MATLAB code followed by finite element analysis (FEA) in ANSYS environment are carried out and to study the vibration parameters of the intact and cracked isotropic and FGM beams with different boundary conditions. Results of Numerical method with FEM method are compared. Finite element method is also performed on rotating cracked cantilever beam.

In chapter 3, the details of experiment setup for experimental validations are presented. Experiments are conducted on intact and cracked beams and measurements of dynamic parameters of beams are compared with those obtained from FEM analysis.

In chapter 4, methodology of different crack detection optimization technique namely, artificial neural network, response surface measurement, genetic algorithm, contour plot intersection and adaptive neuro-fuzzy and hybrid techniques as a combination two methods are described.

In chapter 5, application of crack investigation by homogeneous and hybrid optimization techniques from numerical, FEM and experimental data are presented. Comparison study of those techniques with merit and demerit are also included.

In chapter 6, explains the methodology of profile analysis of mode shapes of natural frequencies by wavelet analysis, fractal dimension, curvature analysis and irregularity extraction method for crack identification. Merit and demerit of those techniques are discussed.

In chapter 7, includes the conclusion of the present thesis work and provides the future scope of the different aspects of the study presented in the thesis work.

1.7 Summary

The chapter briefly introduces importance of crack detection of structure by vibrational analysis. Detail literature survey is furnished on damage detection of different structures. Brief description about what is the objective of the present thesis is given. An insight into various crack detection techniques utilized in the thesis work is presented. Finally, the contributions of the present research work followed by chapter-wise lay out of the thesis are described.

"*This page is intentionally left blank*"

DYNAMIC ANALYSIS OF ISOTROPIC AND FGM CRACKED BEAM USING NUMERICAL METHOD AND FEM.

Outline of the Chapter: *2.1 Introduction, 2.2 Model Descriptionand numerical analysis, 2.3 Finite element analysis, 2.4 Results and Discussion, 2.4.1 Comparison study of Numerical method with FEM method, 2.4.2 Vibration analysis of FEM result of cracked FGM beams, 2.4.3 Vibration analysis of FEM result of rotating cantilever beams, 2.5 Summary*

2.1 Introduction

The present approach can make it easier to find out the position and crack size of cracked beam structure from the data accumulated through the vibration signature. The crack grew in the structure produces flexibility at the locale of the crack which results in a reduction of natural frequency and the change in the mode shape. In this chapter, anumerical technique is proposed based on the Timoshenko beam theory followed by the Ritz approximation to capture the dynamic response of a cracked isotropic and FGM beam under transverse vibration. Then finite element model of beam with different boundary condition with single and multiple open and breathing transverse cracks is developed in ANSYS environment. Both rotating and non-rotating structures are taken into account. Material properties are changed along the height of the beam in case of functionally gradation material (FGM). Modal analysis is obtained for different cracked beam to obtain their frequencies and mode shape. In order to ascertain the accuracy of the proposed method, a comparison study is performed between numerical and finite element method.

2.2 Model Descriptionand numerical analysis

In this section, modelling of the cracked FGM beam is described first. Numerical technique is proposed based on Timoshenko beam theory followed by the Ritz approximation to capture the dynamic response of a cracked FGM beam under transverse vibration.

Figure 2.1 shows a beam having a transverse open crack of depth d_c at a distance l_c from one of the end. Beam length and depth are taken as L and h, respectively.The mid plane of the beam corresponds to z = 0 and downward direction from the mid plane is assumed to be positive.

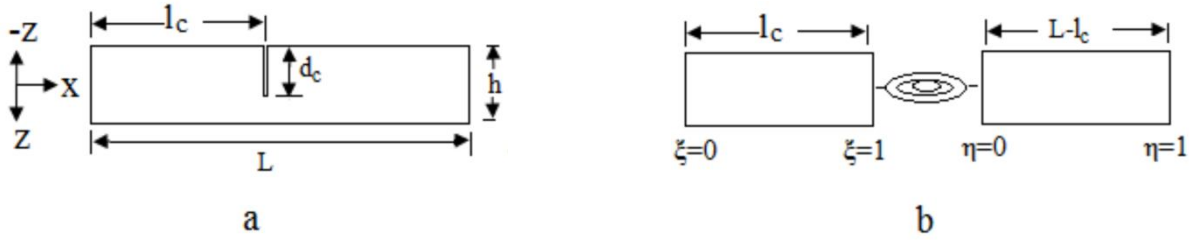

Figure 2.1(a) Cracked beam (b) Cracked beam modelled with a rotational spring

In order to find out dynamic response of the cracked beam, Timoshenko beam theory is adopted. In order to model the crack, a mass less rotational spring is considered in place of crack in such a manner that bending stiffness of the rotational spring matches with the stiffness induced due to crack. Properties of beam, namely, Young's modulus *E* (z) and mass density ρ (z) are assumed to vary exponentially in thickness direction z as given in the Equation. 2.1.

$$E(z) = E_1 \sqrt{k} e^{\left(\frac{z}{h}\ln(k)\right)}, \qquad \rho(z) = \rho_1 \sqrt{k} e^{\left(\frac{z}{h}\ln(k)\right)} \tag{2.1}$$

Here E_1 and E_2 elastic modulus of the top (z=-(h/2)) and bottom surface of the beam, respectively. ρ_1 represents mass density and k represents the gradation relation ($k=E_2/E_1$) of the FGM material of the beam. Using fracture mechanics theory bending stiffness of the rotational spring (K_t) is derived as

$$K_t = \frac{1}{G} \tag{2.2}$$

Here G is the flexibility induced due to crack andcan be derived as [F. Erdogan and B.H. Wu (1997)]

$$G = \int_0^{\varsigma} \frac{72\pi\left(1-\upsilon^2\right)\varsigma F^2(\varsigma)}{E(d_c)h^2} d\varsigma \tag{2.3}$$

In equation 2.3 $E(d_c)$ is the elastic modulus at crack tip, υ is the Poisson's ratioand F (ς) is the function of crack depth ratio ($\varsigma=d_c$/h). Expression given by Kitipornchai et al. (2009) is used to represent the crack correction functions for FGM beams *F* (ς) (for ς< 0.7) and given by

$$F(\varsigma) = 1.150 - 1.662\,\varsigma + 21.667\,\varsigma^2 - 192.451\,\varsigma^3 + 909.375\,\varsigma^4 - 2124.310\,\varsigma^5 + 2395.83\,\varsigma^6 - 1031.750\,\varsigma^7 \quad \text{for } k=1$$

$$F(\varsigma) = 1.762 + 0.3\,\varsigma - 24.225\,\varsigma^2 + 170.387\,\varsigma^3 - 554.549\,\varsigma^4 + 1009.567\,\varsigma^5 - 971.767\,\varsigma^6 + 395.919\,\varsigma^7 \quad \text{for } k=0.2 \tag{2.4}$$

$$F(\varsigma) = 0.650 - 0.859\,\varsigma + 12.511\,\varsigma^2 - 72.627\,\varsigma^3 + 267.910\,\varsigma^4 - 535.236\,\varsigma^5 + 545.139\,\varsigma^6 - 211.706\,\varsigma^7 \quad \text{for } k=5$$

Displacement fields in space and time coordinates of Timoshenko beam can be given by

$$U(x,z,t) = U(x,t) + z\{\Psi(x,t)\}, \tag{2.5a}$$

$$W(x,z,t) = W(x,t). \tag{2.5b}$$

Here $U(x, t)$, $W(x, t)$ and $\Psi(x, t)$ represent longitudinal stretching, transverse and rotational displacement of neutral plane in space and time coordinates, respectively.

Strain and stress fields can be expressed as

$$\varepsilon_x = \frac{\partial U}{\partial x} + z\frac{\partial \Psi}{\partial x},\ \gamma_{xz} = \frac{\partial W}{\partial x} + \Psi,\ \ \sigma_{xx} = \frac{E(z)}{1-\upsilon^2}\left[\frac{\partial U}{\partial x} + z\frac{\partial \Psi}{\partial x}\right],\ \sigma_{xz} = \frac{E(z)}{2(1+\upsilon)}\left(\frac{\partial W}{\partial x} + \Psi\right) \tag{2.6}$$

Here, ε_x, γ_{xz}, σ_{xx} and σ_{xz} are normal strain, shear strain, normal and shear stress, respectively

While deriving the energy equations it is assumed that a part of the strain energy is associated due to crack and is proportional to the square of rotational discontinuity at the crack section. Thus kinetic and potential energy functional of the cracked beams are given by

$$\begin{aligned}
KE &= \frac{1}{2}\int_0^{l_c}\int_{(-h/2)}^{h/2} \rho(z)\left\{\left[\frac{\partial U_1}{\partial t} + z\frac{\partial \Psi_1}{\partial t}\right]^2 + \left(\frac{\partial W_1}{\partial t}\right)^2\right\} dzdx + \frac{1}{2}\int_{l_c}^{L}\int_{(-h/2)}^{h/2} \rho(z)\left\{\left[\frac{\partial U_2}{\partial t} + z\frac{\partial \Psi_2}{\partial t}\right]^2 + \left(\frac{\partial W_2}{\partial t}\right)^2\right\} dzdx \\
PE &= \frac{1}{2}\int_0^{l_c}\int_{(-h/2)}^{h/2} \frac{E(z)}{1-\upsilon^2}\left\{\left[\frac{\partial U_1}{\partial x} + z\frac{\partial \Psi_1}{\partial x}\right]^2 + \frac{E(z)}{2(1+\upsilon)}\left(\frac{\partial W_1}{\partial x} + \Psi_1\right)^2\right\} dzdx + \\
&\frac{1}{2}\int_{l_c}^{L}\int_{(-h/2)}^{h/2} \frac{E(z)}{1-\upsilon^2}\left\{\left[\frac{\partial U_2}{\partial x} + z\frac{\partial \Psi_2}{\partial x}\right]^2 + \frac{E(z)}{2(1+\upsilon)}\left(\frac{\partial W_2}{\partial x} + \Psi_2\right)^2\right\} dzdx + \frac{1}{2}K_t(\Delta\Psi)^2.
\end{aligned} \tag{2.7}$$

In the equation (2.7), subscripts 1and 2 stand for left and right sub beams, respectively. $\Delta\Psi$ is rotational discontinuity and is given by $\Psi_2 - \Psi_1$. In order to simplify equation (2.7), harmonic motion is assumed and stiffness and inertial parameters are taken as given below

$$\{K_1, K_2, K_3\} = \int_{(-h/2)}^{h/2} \frac{E(z)}{1-\upsilon^2}\{1, z, z^2\} dz,\ K_4 = \int_{(-h/2)}^{h/2} \iota\frac{E(z)}{2(1+\upsilon)} dz, \{M_1, M_2, M_3\} = \int_{(-h/2)}^{h/2} \rho(z)\{1, z, z^2\} dz \tag{2.8}$$

Using equation (2.8) energy expressions can be rewritten for maximum potential and kinetic energy and is given by

$$KE_{\max} = \frac{\Omega^2}{2}\int_0^{l_c}\left(M_1U_1^2 + M_3\Psi_1^2 + M_1W_1^2\right)dx + \frac{\Omega^2}{2}\int_{l_c}^{L}\left(M_1U_2^2 + M_3\Psi_2^2 + M_1W_2^2\right)dx$$

$$PE_{\max} = \frac{1}{2}\int_0^{l_c}\left(K_1\left(\frac{\partial U_1}{\partial x}\right)^2 + K_3\left(\frac{\partial \Psi_1}{\partial x}\right)^2 + K_4\left(\frac{\partial W_1}{\partial x} + \Psi_1\right)^2\right)dx + \frac{1}{2}\int_{l_c}^{L}\left(K_1\left(\frac{\partial U_2}{\partial x}\right)^2 + K_3\left(\frac{\partial \Psi_2}{\partial x}\right)^2 + K_4\left(\frac{\partial W_2}{\partial x} + \Psi_2\right)^2\right)dx + \frac{1}{2}K_t\left(\Delta\Psi\right)^2 \quad (2.9)$$

Different normalized coordinate system ξ and η are assigned to represent longitudinal direction of left and right sub beams, respectively as shown in Figure 2.1 (b). Both the sub beams are solved individually using the following non-dimensional scheme

$$\xi = \frac{x}{l_c} \text{ and } \eta = \frac{x - l_c}{L - l_c} \quad (2.10)$$

$$u = \frac{U}{h}, w = \frac{W}{h}, \psi = \Psi, \alpha = \frac{l_c}{h}, \alpha_1 = \frac{L - l_c}{h}, \omega = \Omega\sqrt{l_c\left(L - l_c\right)\frac{M_1}{K_1}}, \beta = \frac{L - l_c}{l_c}$$
$$\left\{m_3, k_3, k_4\right\} = \left\{\frac{M_3}{M_1h^2}, \frac{K_3}{K_1h^2}, \frac{K_4}{K_1}\right\}. \quad (2.11)$$

Using equations (2.10) and (2.11) and multiplying each expression by $(L\text{-}l_c)/ (K_1h^2)$, the expressions of maximum kinetic energy and potential energy in dimensionless form are given as follows.

$$KE^* = \frac{\omega^2}{2}\left[\int_0^1\left(u_1^2 + m_3\psi_1^2 + w_1^2\right)d\xi + \beta\int_0^1\left(u_2^2 + m_3\psi_2^2 + w_2^2\right)d\eta\right] \quad (2.12)$$

$$PE^* = \frac{\beta}{2}\int_0^1\left\{\left(\frac{\partial u_1}{\partial \xi}\right)^2 + k_3\left(\frac{\partial \psi_1}{\partial \xi}\right)^2 + k_4\left(\frac{\partial w_1}{\partial \xi}\right)^2 + k_4\alpha^2\psi_1^2 + k_4\alpha\frac{\partial w_1}{\partial \xi}\psi_1\right\}d\xi$$
$$+ \frac{1}{2}\int_0^1\left\{\left(\frac{\partial u_2}{\partial \eta}\right)^2 + k_3\left(\frac{\partial \psi_2}{\partial \eta}\right)^2 + k_4\left(\frac{\partial w_2}{\partial \eta}\right)^2 + k_4{\alpha_1}^2\psi_2^2 + k_4\alpha_1\frac{\partial w_2}{\partial \eta}\psi_2\right\}d\eta + \frac{1}{2}k_t^*\left(\Delta\psi\right)^2$$

Energy functional of the beam can be obtained as

$$\Pi = PE^* - KE^* \quad (2.13)$$

Trial functions are chosen as the admissible functions which satisfy the natural boundary conditions at the ends and compatibility conditions at the crack section. In case of a clamped-clamped beam transverse, longitudinal and rotational displacement and slope may be assumed to be zero at both ends, namely, at $\xi = 0$ and $\eta = 1$. At the crack location, continuity is assumed in transverse and longitudinal displacement. Discontinuity is allowed only in rotation at crack location.

Thus, $Moment_{\text{at crcaked section}} = k_t^*(\psi_2 - \psi_1) = k_3 \frac{\partial \psi_2}{\partial \eta}$

In order to satisfy the conditions mentioned above, following admissible functions are chosen

$$\begin{aligned} u_1 &= \sum_{j=1}^{j=N} A_j \xi^j (1-\xi) + \xi \sum_{j=1}^{j=N} a_j,\ u_2 = \sum_{j=1}^{j=N} a_j (1-\eta)^j \\ w_1 &= \sum_{j=1}^{j=N} B_j \xi^j (1-\xi) + \xi \sum_{j=1}^{j=N} b_j,\ w_2 = \sum_{j=1}^{j=N} b_j (1-\eta)^j \\ \psi_1 &= \sum_{j=1}^{j=N} C_j \xi^j (1-\xi) + \xi \sum_{j=1}^{j=N} \left\{ 1 + (j) \frac{k_3}{k_t^*} \right\} c_j,\ \psi_2 = \sum_{j=1}^{j=N} c_j (1-\eta)^j \end{aligned} \tag{2.14}$$

Similarly for clamped-free beam admissible functions are taken as

$$\begin{aligned} u_1 &= \sum_{j=1}^{j=N} A_j \xi^j (1-\xi) + \xi \sum_{j=1}^{j=N} a_j,\ u_2 = \sum_{j=1}^{j=N} a_j (1+\eta)^j \\ w_1 &= \sum_{j=1}^{j=N} B_j \xi^j (1-\xi) + \xi \sum_{j=1}^{j=N} b_j,\ w_2 = \sum_{j=1}^{j=N} b_j (1+\eta)^j \\ \psi_1 &= \sum_{j=1}^{j=N} C_j \xi^j (1-\xi) + \xi \sum_{j=1}^{j=N} \left\{ 1 - (j) \frac{k_3}{k_t^*} \right\} c_j,\ \psi_2 = \sum_{j=1}^{j=N} c_j (1+\eta)^j \end{aligned} \tag{2.15}$$

Substituting equations (2.14) or (2.15) into Eq. (2.12) and minimizing the energy functional by taking derivative with respect to six unknown parameters one may obtain a set of linear governing equations of cracked beam, which is given below

$$[K]\{V\} = \lambda [M]\{V\} \tag{2.16}$$

In the above equation, [K_{linear}], {V}, [M] and λ, are stiffness matrix, unknown coefficients, mass matrix and frequency parameter (ω^2), respectively. Solving as the eigenvalue problem equation (2.16) gives the desired vibrational response i.e. natural frequencies and mode shapes.

Above beam model is solved numerically by MATLAB code using gauss quadrature integration technique. Twenty four numbers of Gauss points are generated for each part of the beam in normalized co-ordinates (ξ and η).

2.3 Finite element analysis

Vibration analysis of different cracked beams is carried out using ANSYS 13.

In order to perform numerical experiment, modal and harmonic analysis of the beam is performed following the steps outlines below.

Define Materials

- Set preferences (Structural).
- Define constant material properties.
- Beam divided with some layer along its height and material parameters are constant in each layer (FGM beam).

Model the Geometry

- Create the beam geometry with crack.

Generate Mesh

- Define element type of beam.
- Define element type at crack surface (Breathing crack).
- Mesh the volume.
- Refine the mesh at crack position.
- Singular elements apply around the crack tip (Special case).

Apply Constraint

- Apply different boundary condition for both end fixed beam, cantilever beam, hinged beam.
- Apply angular velocity about global origin parallel to height of the beam(Rotating beam).
- Apply forcing term for forced vibration analysis.

Obtain Solution

- Specify analysis type modal.
- Solve.

Brick SOLID 186 elements are used for the analysis. These elements have 20 nodes with one node at each corner and another node at middle of each edge. Material properties are

constant within each element. Convergence check is carefully performed and the number of elements is determined such that increasing the number of elements does not change the significant digits of the results. This implies that element refinement is sufficient to capture the correct material property gradation and accurate results. In order to reduce modelling time, ANSYS Parametric Design Language (APDL) is used. APDL is a scripting language that one can use to automate common tasks and build a model in terms of parameters. In particular, the definition of graded orthotropic material properties can only be accomplished with APDL.

The most important region in a fracture model is the region around the edge of the crack. In linear elastic problems, it has been shown that the displacements near the crack tip (or crack front) vary as a function of $\sqrt{r}$, where r is the distance from the crack tip. The stresses and strains are singular at the crack tip, varying as a function of $1/\sqrt{r}$. To pick up the singularity in the strain, the crack faces should be coincident, and the elements around the crack tip (or crack front) should be quadratic, with the midside nodes placed at the quarter points. Such elements are called singular elements. However for vibration analysis, global changes in the dynamics of the beam are desired, rather than the local variation in the stress field due to presence of crack. As a result natural frequency especially in transverse direction do not affected by singular element. But it is more effective in case of curvature mode shape analysis. Figure 2.2 and 2.3 shows three dimensional mesh model with singular element and without singular element. Figure 2.4 shows model of crack with singular element

The material properties of the FGM change throughout the thickness of beam. Volume of the beam has been divided into various equal parts along the thickness in order to make the changes in properties. Each part has the finite portion of the thickness and treated like isotropic material. In order to ensure thickness volume parts to represent the gradation relation without affecting the accuracy a convergence study is performed. Material properties have been calculated at the midplane of each of this layer by using gradation power law

$$E(z) = (E_2 - E_1)\left(\frac{2z+h}{2h}\right)^n + E_1 \tag{2.17}$$

$$\rho(z) = (\rho_2 - \rho_1)\left(\frac{2z+h}{2h}\right)^n + \rho_1 \tag{2.18}$$

and exponential gradation,

$$E(z) = E_0 e^{\beta z}, \quad \rho(z) = \rho_0 e^{\beta z} \tag{2.19}$$

where the subscripts 0, 1 and 2 denote midplane *(z = 0)*, the top surface *(z = −h/2)* and bottom surface *(z = h/2)*, respectively; β and *n* are the constants characterizing the distributions of material properties. $n = 0$ or $\beta = 0$ correspond to an isotropic homogeneous beam. Poisson's ratio *v (z)* is assumed to be a constant.

An FGM beam is considered with an edge crack parallel to the direction of the material gradient undergoing transverse bending vibration, as shown Figure 2.5. 3-D 20-node SOLID186 element is used for analysis. The element is defined by 20 nodes having three degrees of freedom per node: translations in the nodal *x*, *y*, and *z* directions. The element supports large deflection, and large strain capabilities. In order to achieve the material properties of the FGM beams thickness direction of the beam model has been divided into various layers.In this approach a high meshing density is applied around the crack area such that the stress/strain singularity at the crack position can be accurately revealed. Block Lanczos method is used for the eigenvalue extraction. In order to insure the minimum number of layers required to represent the gradation relation as mentioned in equation 1 without affecting the accuracy. Results for first three natural frequencies with the different layer numbers are shown in Figure 2.6. It is observed that the converged results are obtained when the numbers of layers are more than 40. Therefore numbers of layers are taken as 40 for all subsequent analysis.

Rotational conditions are modeled in ANSYS by applying angular velocity about Y-axis at global origin as shown in Figure. 2.7. One end of the beam is fixed a certain distance (*r*) from global origin in X direction.

The first, second and third mode shapes of cracked beam corresponding to various crack locations and depths are obtained. Due to the presence of cracks, vibration characteristic such as natural frequencies, mode shape, amplitude changes. These changing properties are applied for prediction of crack by different optimization techniques such as ANN, RSM, GA, and Contour plot intersection. The first three mode shapes for transverse vibration of cracked beams are plotted for crack detection through subsequent application of wavelet analysis, fractal dimension and curvature technique.

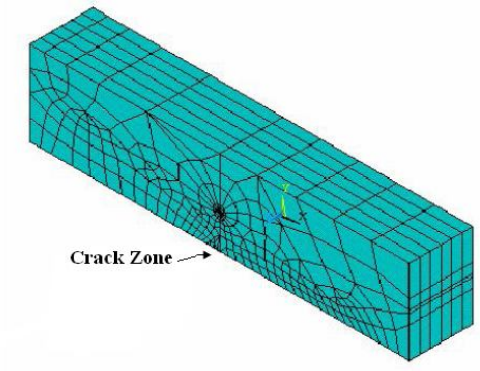

Figure 2.2 Mesh model with singular element

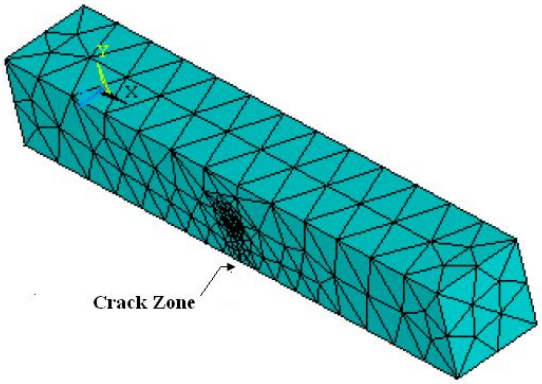

Figure 2.3 Mesh model with nonsingular element

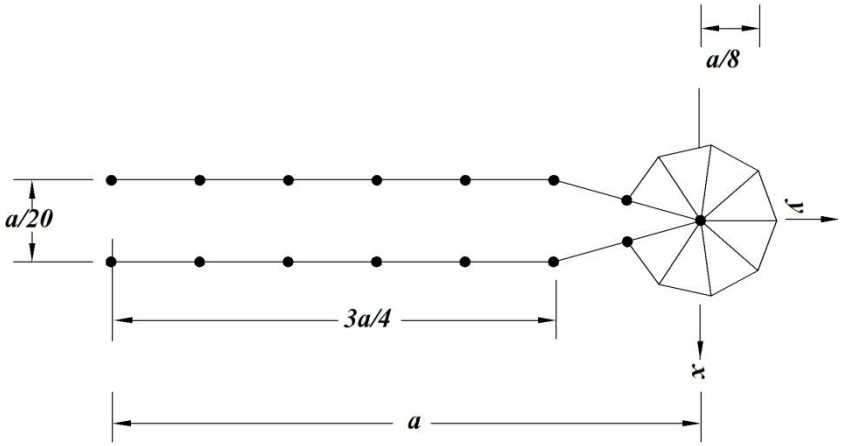

Figure 2.4 Model of Crack with singular element, *a*= crack depth

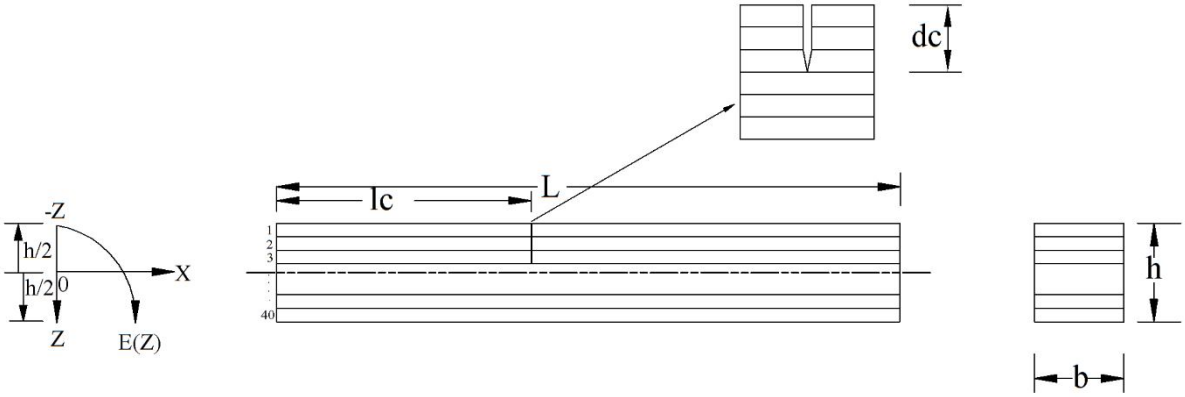

Figure 2.5 FGM beam with an open edge crack.

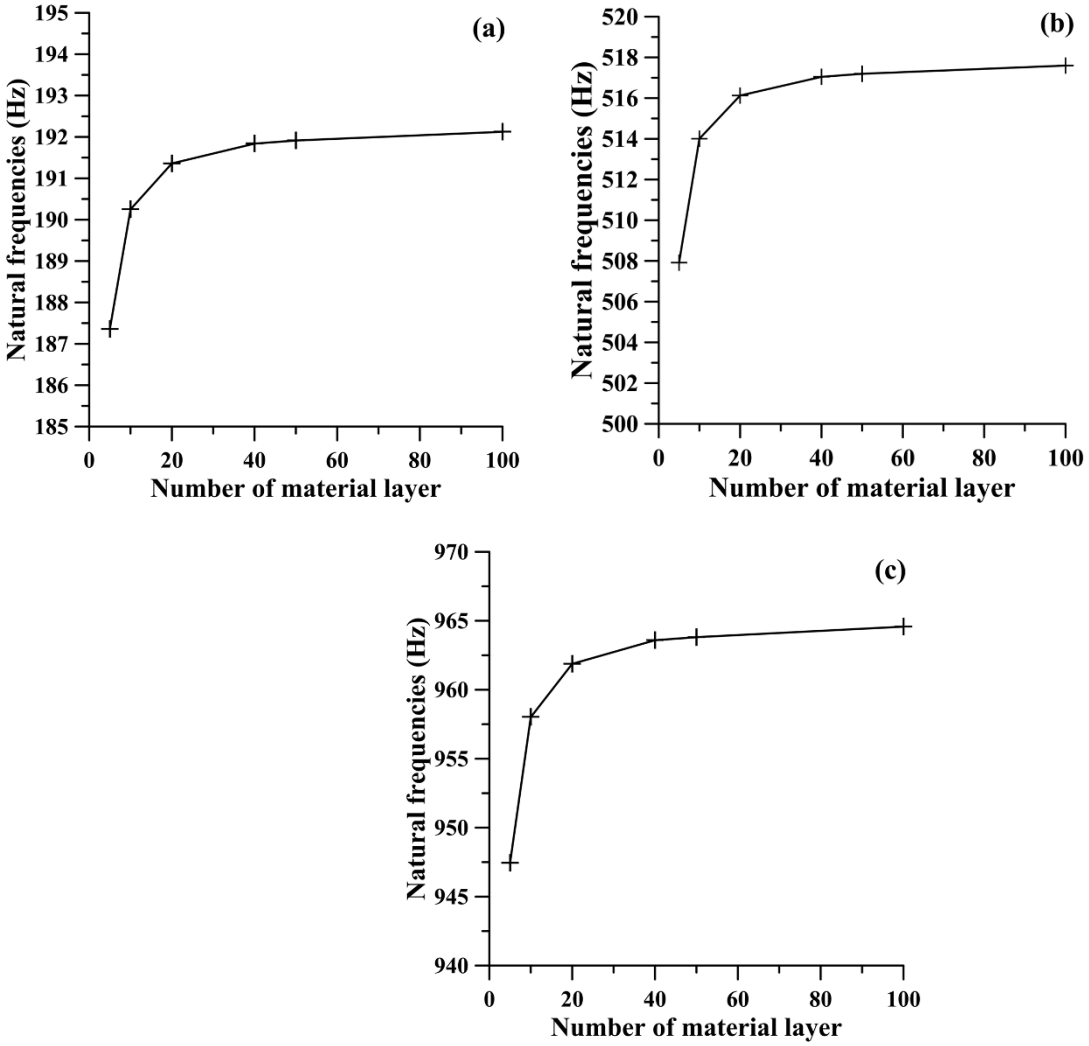

Figure 2.6 (a) First natural frequencies of FGM (k = 5) clamped–clamped cracked beam (crack depth ratio = 0.2 at mid-length of beam) against number of material layer, (b) second natural frequencies of FGM(k = 5) clamped–clamped cracked beam (crack depth ratio = 0.2 at mid-length of beam) against number of material layer and (c) third natural frequencies of FGM (k = 5) clamped–clamped cracked beam (crack depth ratio = 0.2 at mid-length of beam) against number of material layer.

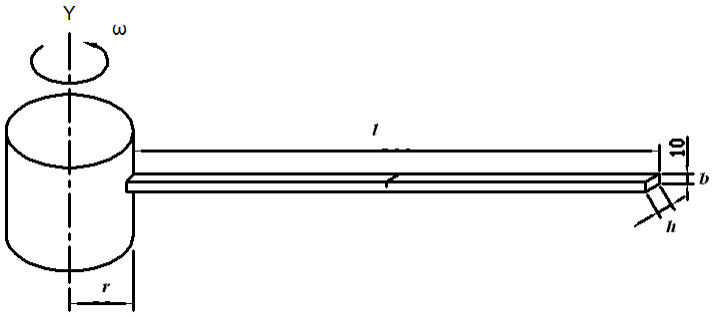

Figure 2.7 Rotating cantilever beam

2.4 Results and Discussion

Free vibration modal analysis is carried out for a series of different type cracked beams using ANSYS. The crack depth ratio (a/h) is varied from 0.1 to 0.5. Normalized crack location (l_c/l) is varied from 0.1 to 0.9. Two type FGM beam with $k=E_2/E_1=\rho_2/\rho_1=$ 0.2 and 5.0 are considered for analysis. For rotating beam different rotational speed 50 rad/s, 100 rad/s, 150 rad/s and 200 rad/s of beam is considered for analysis.

The relative frequencies and average mode shape deviation for different cracked depth and location are obtained from Equation (29) and (30).

$$Relative\ Natural\ Frequency = \frac{Natural\ frequency\ of\ crack\ beam}{Natural\ frequecy\ of\ cracked\ free\ beam} \tag{2.20}$$

$$Average\ Mode\ Shape\ Deviation = \frac{Total\ mode\ shape\ deviation\ all\ inspection\ point}{number\ of\ inspection\ point} \tag{2.21}$$

2.4.1 Comparison study of Numerical method with FEM method

Table 2.1 Comparison of the first three natural frequencies of cracked FGM beams

Cracked Beam		First Mode			Second Mode			Third Mode		
	l_c/L	Numerical	ANSYS	Error %	Numerical	ANSYS	Error %	Numerical	ANSYS	Error %
Clamped-Clamped d_c/h=0.2 k=5	0.062	191.86	191.4	0.21	516.75	514.1	0.5	979.04	973.24	0.6
	0.18	194.94	193.6	0.69	518.95	515.33	0.7	970.7	966.91	0.39
	0.28	194.85	193.5	0.69	514.06	512.2	0.35	974.59	970.18	0.45
	0.37	193.72	192.7	0.52	515.63	513.4	0.43	974.94	974.85	0.01
	0.5	192.79	192.0	0.38	520.65	517.0	0.7	965.01	963.51	0.16
Cantilever d_c/h=0.2 k=5	0.06	30.54	30.19	1.16	190.66	187.9	1.44	524.01	517.87	1.19
	0.31	31.07	30.6	1.54	192.83	189.7	1.64	520.66	515.51	1
	0.5	31.39	30.79	1.95	190.2	187.7	1.3	527.27	521.16	1.17
	0.68	31.41	30.87	1.75	191.32	188.7	1.35	517.39	513.56	0.75
	0.93	31.43	30.9	1.72	193.37	190.3	1.57	526.5	521.05	1.05
Clamped-Clamped d_c/h=0.4 k=5	0.06	184.24	184.2	0.02	508.17	505.3	0.56	974	967.22	0.7
	0.18	194.53	192.9	0.83	513.36	510.4	0.58	941.16	940.5	0.07
	0.28	193.99	192.8	0.61	495.1	495.2	0.04	957.91	954.85	0.32
	0.37	189.46	189.0	0.23	501.58	500.7	0.16	977.97	972.99	0.51
	0.5	185.95	185.9	0.01	520.65	516.9	0.72	927.37	929.01	0.18
dc/h=0.2- k=0.2	0.06	189.36	189.3	0.01	513.84	511.5	0.44	977.31	971.99	0.55
	0.18	194.82	193.5	0.65	517.27	514.6	0.52	961.50	959.82	0.18
	0.28	194.59	193.4	0.59	508.24	507.5	0.13	969.23	966.04	0.33
	0.37	192.45	191.7	0.35	511.28	509.8	0.28	979.51	974.68	0.5
	0.5	190.73	190.4	0.16	520.65	517.2	0.66	954.13	954.14	0.0

Geometric and material properties of beam are taken as E_1 = 70 GPa, ν = 0.33, ρ_1 = 2780 kg/ m3, L/h = 16, h = 0.1 m, d_c/h = 0.2 & 0.4, ι = 5/6. ι represents correlation factor between two layers. For subsequent analysis, these properties will remain unchanged until and unless mentioned otherwise. First three natural frequencies of cracked clamped–clamped beam and cantilever beam with two crack sizes (crack depth ratio 0.2 and 0.4) and two material gradient k = 5 and k = 0.2 are obtained by numerical analysis and FEM analysis. A comparison result is shown in Table 2.1. It can be seen that results obtained from numerical analysis and FEM analysis matched fairly well.

2.4.2 Vibration analysis of FEM result of cracked FGM beams

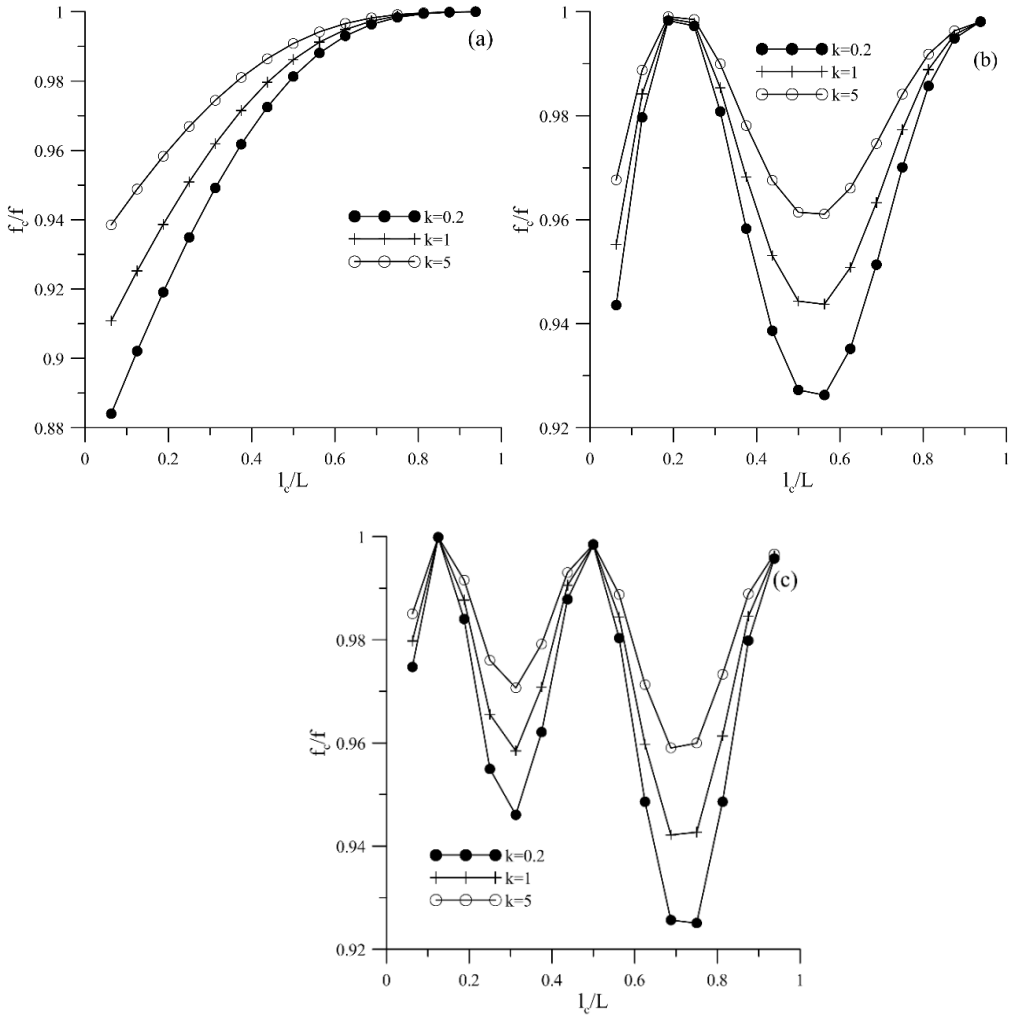

Figure 2.8 (a) First natural frequency ratios of FGM cantilever beams with an edge crack at varying locations for a crack depth ratio of 0.3, (b) second natural frequency ratios of FGM cantilever beams with an edge crack at varying locations for a crack depth ratio of 0.3 and (c) third natural frequency ratios of FGM cantilever beams with an edge crack at varying locations for a crack depth ratio of 0.3.

The first three natural frequency ratios as functions of crack location for a particular crack depth ratio (*d*c/h = 0.3) with different material gradients for cantilever beam are shown in Figure 2.4. It can be observed that the first natural frequency increases monotonically with decreasing slope as the crack location moves from the fixed end to the free end (Figure 2.8(a)). On the other hand, the second and third relative frequencies oscillate under the same situation (Figure 2.8(b) and (c)). It can also be observed that for all three modes, frequencies are higher when the crack is near to free end. This is due to the fact that bending moment vanishes at the free end.

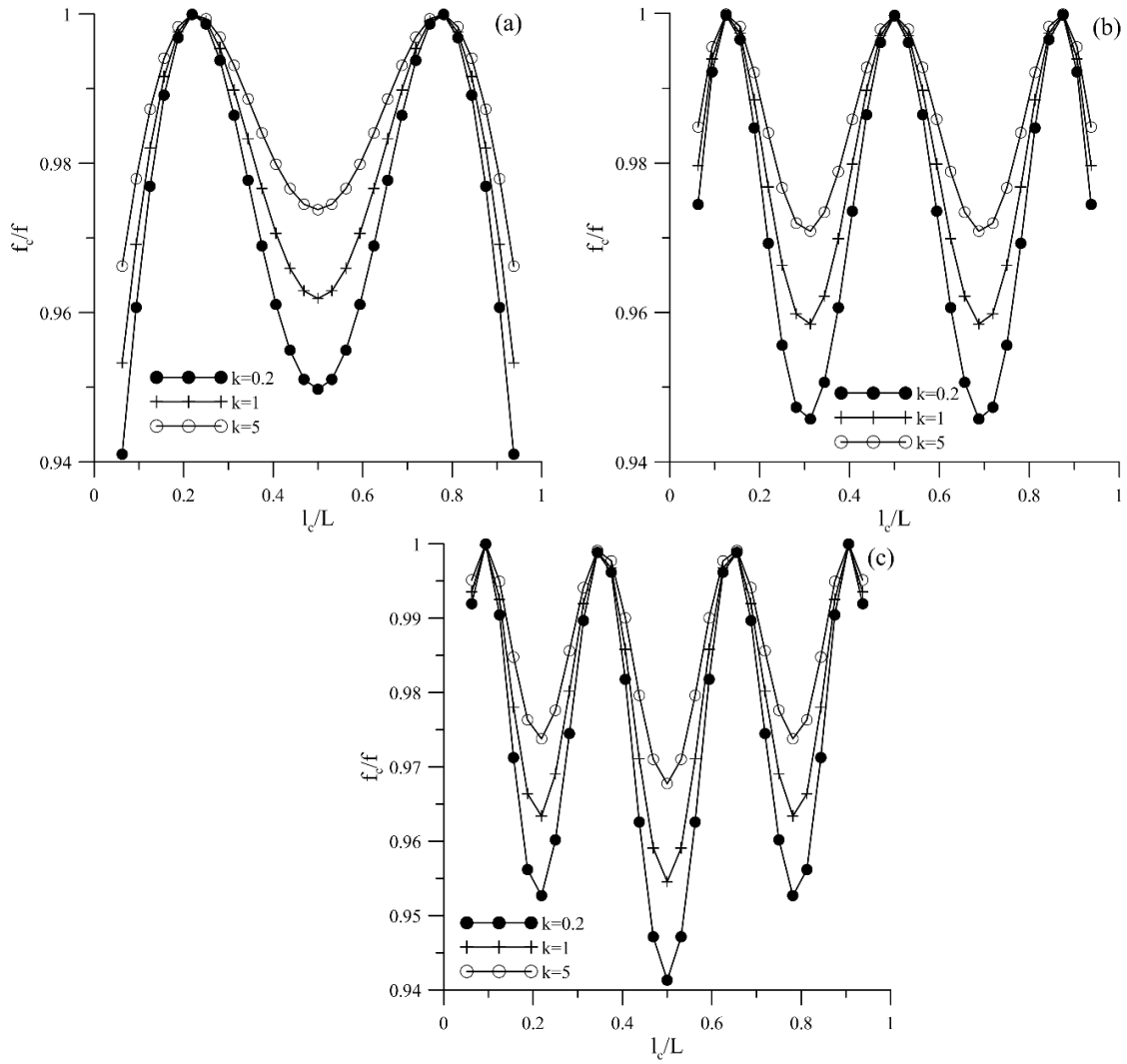

Figure 2.9 (a) First natural frequency ratios of FGM clamped–clamped beams with an edge crack at varying locations for a crack depth ratio of 0.3, (b) second natural frequency ratios of FGM clamped–clamped beams with an edge crack at varying locations for a crack depth ratio of 0.3 and (c) third natural frequency ratios of FGM clamped–clamped beams with an edge crack at varying locations for a crack depth ratio of 0.3.

Same set of results for clamped–clamped condition are shown in Figure 2.9. It is observed that all three natural frequencies oscillate with position of crack. It can be observed from the Figures 2.8 and 2.9 that the crack effect on the vibrational response is not significant when crack is either located at any of the nodes of vibration or at the point of inflection. Effect of crack on natural frequencies tends to become prominent if crack location shifts away from either of these points. An additional fact can be highlighted from Figure 2.8 that frequency ratio decreases as material gradient decreases. It can be concluded that crack produces more effect on natural frequency if it is at the stiff side of the beam.

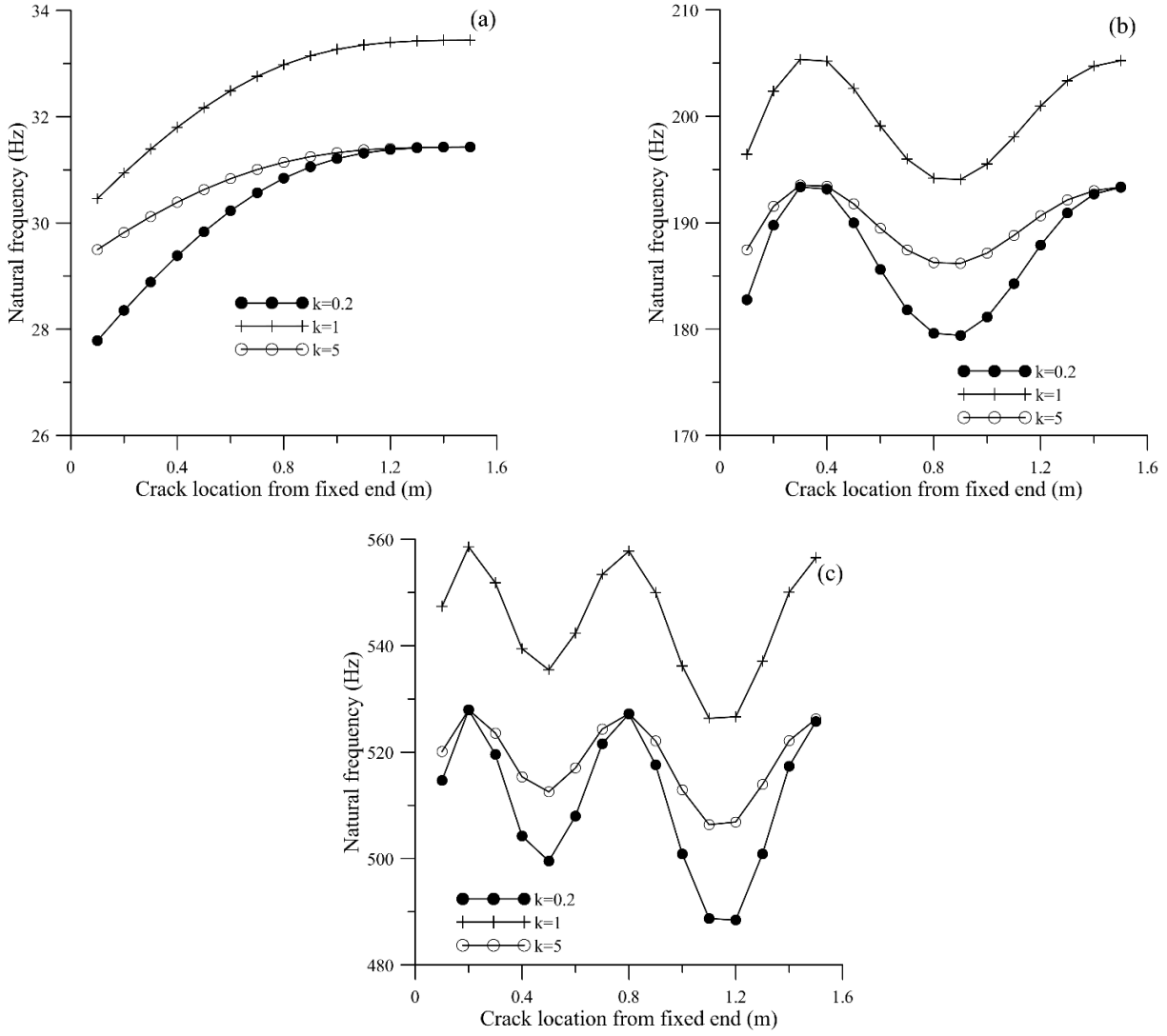

Figure 2.10. (a) First natural frequencies of FGM cantilever beams with an edge crack at varying locations for a crack depth ratio of 0.3, (b) Second natural frequencies of FGM cantilever beams with an edge crack at varying locations for a crack depth ratio of 0.3 and (c) Third natural frequencies of FGM cantilever beams with an edge crack at varying locations for a crack depth ratio of 0.3.

Figure 2.10 illustrates the effect of crack location on natural frequencies. It can be observed that values of natural frequencies of FGM beams are much smaller than isotropic beam. An interesting phenomenon can be observed that natural frequencies are nearly equal for both k = 0.2 and k = 5 when the crack location is either at any of the node of the vibration or at the point where bending moment vanishes.

2.4.3 Vibration response of cracked and un-cracked rotating cantilever beam using FEM

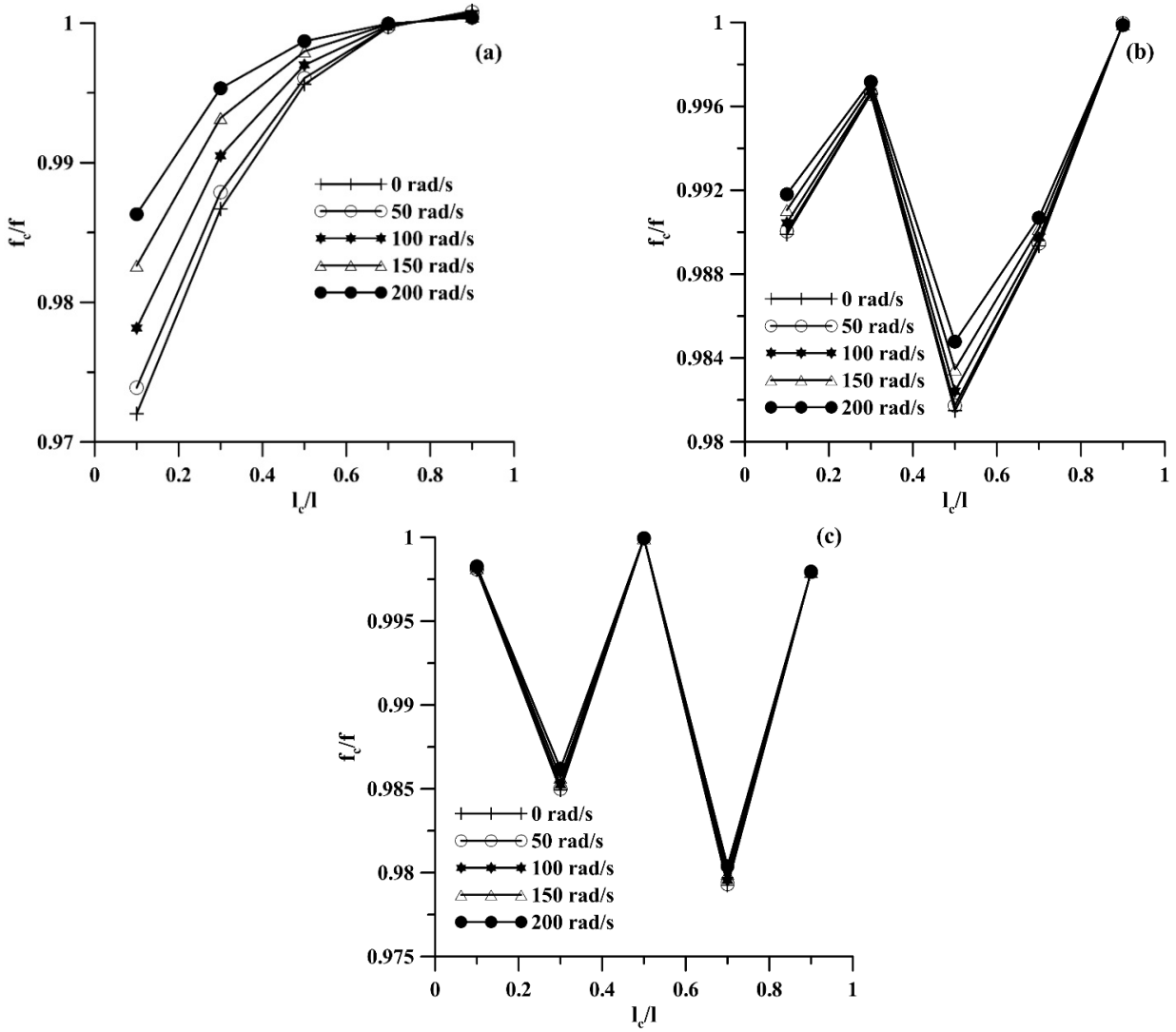

Figure 2.11 (a) First natural frequency ratios of rotating cantilever beams with an edge crack at varying locations for a crack depth ratio of 0.3, (b) second natural frequency ratios of rotating cantilever beams with an edge crack at varying locations for a crack depth ratio of 0.3 and (c) third natural frequency ratios of rotating cantilever beams with an edge crack at varying locations for a crack depth ratio of 0.3.

Free vibration finite element analysis is carried out on a series of rotating cracked beams. Cantilever beam properties are given Table 2.2. The crack depth ratio (a/h) is varied from 0.1 to 0.5. Normalized crack location (l_c/l) is varied from 0.1 to 0.9.

Table 2.2 Rotational cantilever beam characteristics

Density (kg/m^3)	**Poisson Ratio**	**Elasticity Modulus(GPa)**	**Length (l) (mm)**	**Thickness (mm)**	**Depth (h) (mm)**	**Distance of fixed end from rotational axis (mm)**
2700	0.33	69	500	15	10	50

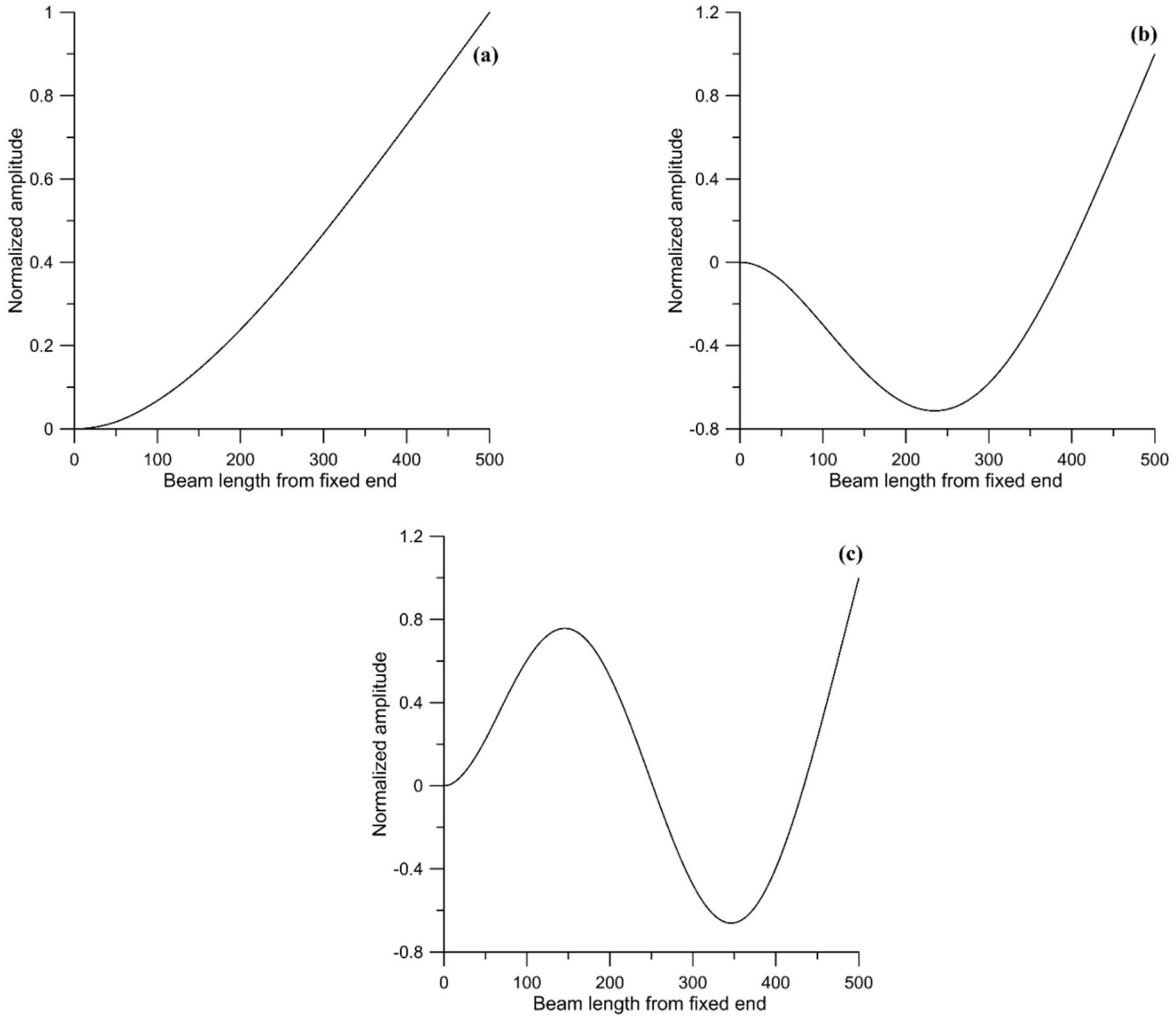

Figure 2.12 First three mode shape of rotating cracked beam at rotational speed 100 rad/sec (a) first mode (b) second mode and (c) third mode

The first three natural frequency ratios as functions of crack location for a particular crack depth ratio (d_c/h = 0.3) with different rotational speed for rotating cantilever beam are shown in Figure 2.11. It can be observed that natural frequency increases with rotational speed at a particular location of crack on the beam. This is due to the fact that rotational inertia reduces bending moment. It can also be observed that rotational speed has less effect on natural frequency ratios for higher (third) natural frequency as seen from Figure 2.11 (c).

The simulation result of a rotating cracked beam (crack location 50 mm from fixed end with 3 mm depth and rotational speed 100 rad/sec) obtained by ANSYS software. Graphical presentations of transverse vibration mode shapes of the same beam are shown in Figure 2.12 (a), (b) and (c). However by observing the mode shape it is difficult to detect the existence and location of the damage.

2.5 Summary

In this chapter first numerical analysis is performed on intact and cracked beam. Both cantilever and clamped-clamped beam are considered for numerical model. Isotropic as well as FGM beam are taking for analysis. All analysis is done by with help of MATLAB software. Then three dimensional FEM analyses are performed with the help of ANSYS software. Results of natural frequencies are compared both cases. Lastly dynamic analysis is performed on rotating intact and cracked cantilever beam the help of ANSYS software. First, second and third natural frequencies are evaluated and their mode shapes are captured.

"*This page is intentionally left blank*"

EXPERIMENTAL STUDY OF CRACKED BEAM

Outline of the Chapter: *3.1 Introduction, 3.2 Experimental Study on Cracked Beam with Help of Oscilloscope, 3.2.1 Experimental Setup, 3.2.2. Test Procedure, 3.3 ExperimentalStudy on Cracked Beam by Data Acquisition System, 3.3.1 Experimental Setup, 3.3.2. Test Procedure, 3.4 Results and Discussion, 3.5 Summary.*

3.1 Introduction

Theoretical studies of dynamic behaviors of cracked beam have been dealt in the prior chapter. Free vibration analysis of intact and cracked beam is performed in chapter 2.In this context, it is necessary to conduct experimental investigations of these aspects of the study. It is felt that the experimentations would offer completeness to the theoretical simulations, as well as provide further independent validation to the theoretical results. However, the objective of the actual experiments is not only to validate theoretical result, but also to use the experimental observations for remodeling the mathematical formulation of the theoretical analysis, if necessary.

In the present study, dynamic behavior such as natural frequencies and mode shape of intact and cracked beams with different boundary conditions are determined experimentally. All experimentation is done with two different experimental setup. First natural frequencies of beam with different boundary condition are determined with the help of oscilloscope. The second experimentation is conducted with data acquisition system. Mode shape of cantilever beam is determined by this data acquisition experimentation setup.

3.2 Experimental Study on Cracked Beam by FFT analysis using oscilloscope.

The details of the experimental procedure are mentioned below.

Specimens are made out of an aluminum metal having cracks of different sizes and at different locations along the length of the beam. The cracks are made by EDM wire cut machining. The width of wire cut is 0.6 mm. Some specimens are shown in Figure 3.1

3.2.1 Experimental Set Up

The experimental setup is shown in Figure. 3.2. The figures also indicate the major components, hydraulic fixture, pressure gauge, accelerometer, coupler for accelerometer,

oscilloscope. The free vibration experimentation is carried out by exciting the system at its deflected configuration with the blow of a soft rubber hammer. Figure 3.3 shows the schematic diagram of the set up.

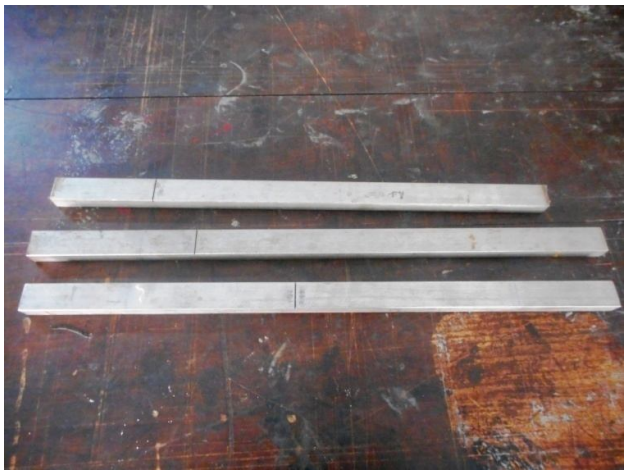

Figure 3.1 Different Crack Position of Samples Test

An accelerometer ((Manufacturer: Kistler Instrument Corporation, Type: 8728A500, acceleration range: ± 500g (g = 9.80665 m/s2), frequency range: 1 Hz–10 kHz (± 5%))) with a mass of 1.6 gm is fixed at a suitable position on the top edge of the beam using Petro-Wax adhesive material.Since the dynamic mass of the accelerometer is significantly less than the test specimen, it can be assumed that the response is not affected by the mass loading. The location of the accelerometer is chosen carefully to avoid any nodal points and it is approximately placed near the point of maximum displacement amplitude. The accelerometer senses motion perpendicular to the base and it has two components - a sensing assembly and an impedance converter. The sensing assembly, which does not require any external power source to operate, consists of a seismic mass and a piezoelectric crystal. The impedance converter is a miniature electronic circuit which converts the high impedance charge signal generated by the piezoelectric element into a low impedance voltage output signal. The circuit is powered by an external power source or coupler.

The accelerometer is connected to a coupler (Manufacturer: Kistler Instrument Corporation, Type: 5114, Frequency response: 0.07 Hz – 60 kHz (± 5%)), which provides the constant current power supply to the impedance converter of the accelerometer and decouples the DC bias voltage from the output signal. The coupler itself is externally powered by an AC-DC power adapter. The instrument also decouples the DC bias voltage from the output signal. It operates as the electrical interface between low-impedance, voltage mode

piezoelectric sensor and display or recording device, which in the present scenario is a digital oscilloscope. The connection between the accelerometer and the coupler is through a two-wire cable, which carries both the signal and power.

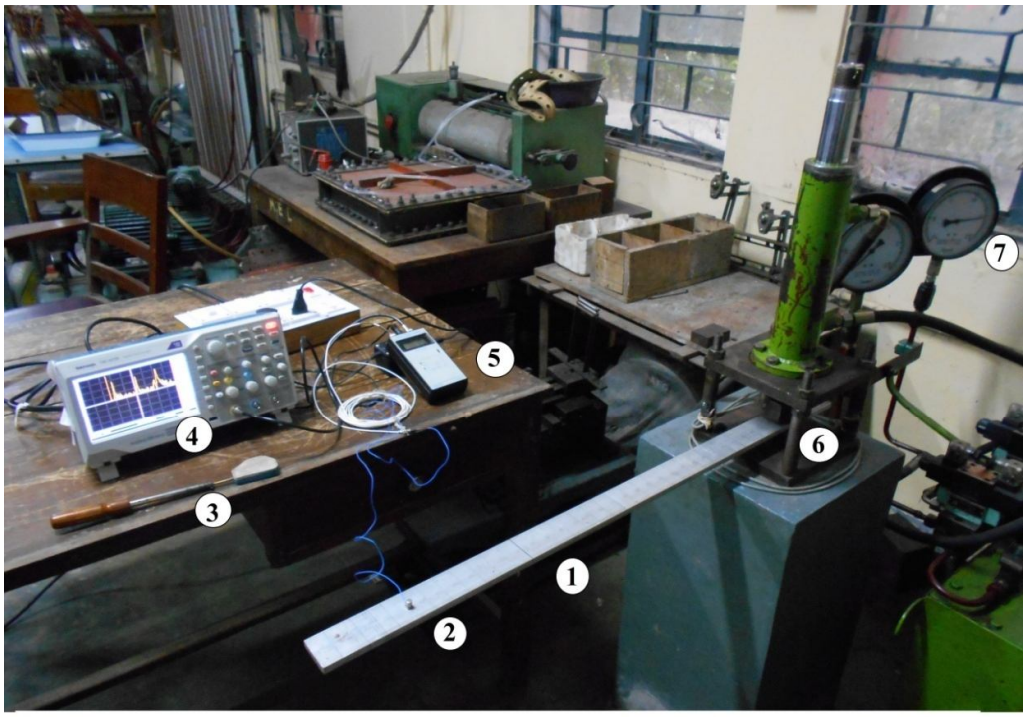

Figure 3.2 Photograph of the experimental set up with oscilloscope

The coupler output is connected to a display device two channel digital real time oscilloscope (Tektronix TBS 1072B) with the following specifications: peak detect bandwidth: 70MHz, sample rate range: 50 samples/s–1Gigasamples/s, record length: 2500 samples and lower frequency limit: 10 Hz. It has the capability to transform a time domain signal into frequency domain through a Fast Fourier Transform (FFT) module. The analyzer has a digital readout for the peaks.

3.2.2 Test Procedure

Experiments are carried out to determine the free vibration characteristics of the cracked and crack free cantilever beam. For cantilever beam one end and for clamped-clamped beam both are clamped by hydraulic fixture with 2 tonne load with ram diameter 44 mm. The oscilloscope is set to ‘math’ mode and ‘auto’ trigger mode is kept on. It is then kept ready by pressing the ‘RUN’ button as the system is hammered to provide disturbance and it

captures the signal from the vibrating beams and plots the signal in frequency domain. The oscilloscope captures and plots the signal from the vibrating system in frequency-amplitude plane. Using horizontal and vertical cursors the amplitude (in dB) and frequency (in Hz) of the signal are read from the display and collect the first four pick value.The whole experimental procedure is replicated for different crack beam specimens.

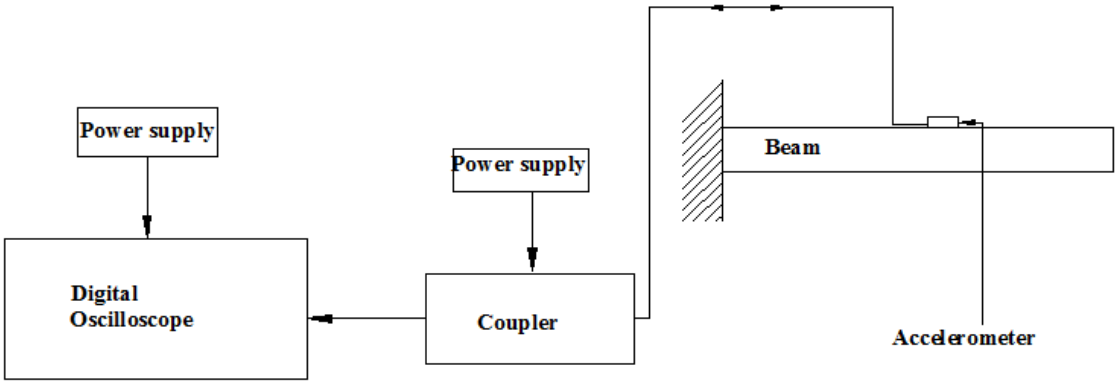

Figure 3.3 Schematic diagram of experimental setup with oscilloscope

3.3 Experimentation Description by Data Acquisition System

The following section provides a brief description of theset up and test procedure.

3.3.1 Experimental Set Up

An experimental set up, as shown in Figure 3.4, is prepared to carry out free vibration experiments on the cantilever beam. Figure 3.5 shows the schematic diagram of the free vibration set up with indications of the major components. The free vibration experimentation is carried out by exciting the system with the blow of a hammer. The beam is discretized 34 equal segments which produced total 35 exciting location from fixed end to free end along the length of the beam.

One end of beam is bolted firmly so as to simulate clamped boundary condition. The accelerometer (Manufacturer: Bruel and Kjear, Type: 4507, acceleration range: ± 500g (g = 9.80665 m/s^2), frequency range: 0.3 – 6000 Hz (± 5%)) is a shear mode piezoelectric sensor and accelerometer housing has slots that allow the use of mounting clips. The mounting clip is mounted on the beam at a suitable position using Petro-Wax adhesive material. The locations of the accelerometer are carefully selected to avoid any nodal points. The mass of the accelerometer (4.8 grams) is significantly less than the mass of the beam and hence it can be assumed that system response is not significantly affected by the effect of mass loading of

the accelerometer. The accelerometer is connected to Data Acquisition System (Manufacturer: Bruel and Kjear (B & K), Type: 3050, 6 channels, Frequency range 0 – 51.2 kHz). An impact hammer (Type – PCB - 086C01, Sensitivity 11.2 mv/N, Measurement range ± 444 N pk, Resonance frequency > 15 kHz) is also connected to Data Acquisition System. Data Acquisition System is linked to a computer. In order to evaluate frequency response B & K Pulse Labshop software (Version 14.1.1) is connected to computer at the time of excitation.

3.3.2 Test Procedure

Experiments are carried out to determine the free vibration characteristic of cantilever beam. The setup is made ready by making the electrical connections for computer, Data Acquisition System. The accelerometer is mounted on the test specimen at predefined location using petro wax adhesive material. In order to get best results, hammer test is applied all 35 excitation location and test is repeated 5 times for each excitation location. The input and output data are stored using a Data Acquisition System. In real time experiment, the data are generally captured after a finite interval of time. Exponential Window is used for the response measurements. Frequency Response Function (FRF) (dB/1.00g/N) is evaluated of each excitation using Labshop software. All frequency response data is stored in the computer for offline post processing. In order to reduce random experimental error whole test procedure is repeated 5 times.

After getting the frequency response curve ME'scopeVES software (Version 5.1.2009.1113) is connected. The modal properties are evaluated using this software. Modal parameters (Frequency, Damping and Mode Shape) are extracted for first four modes in transverse direction of a structure from a set of FRFs by Modal curve fitting. Curve fitting is a data reduction process that converts the dynamic information from a set of FRFs into a set of modal parameters.

3.4 Results and Discussion

Free vibration experimentation is carried out on series of cracked beams. The geometric and physical properties of the beam are shown in Table 3.1.First four natural frequencies of cracked beams are determined by oscilloscope. Natural frequencies are obtained for three crack depth ratio (a/h) with various locations (l_c) along the length of the beam. Amplitude of transverse vibration of cracked cantilever beam at various locations along the length of the beam is recorded.

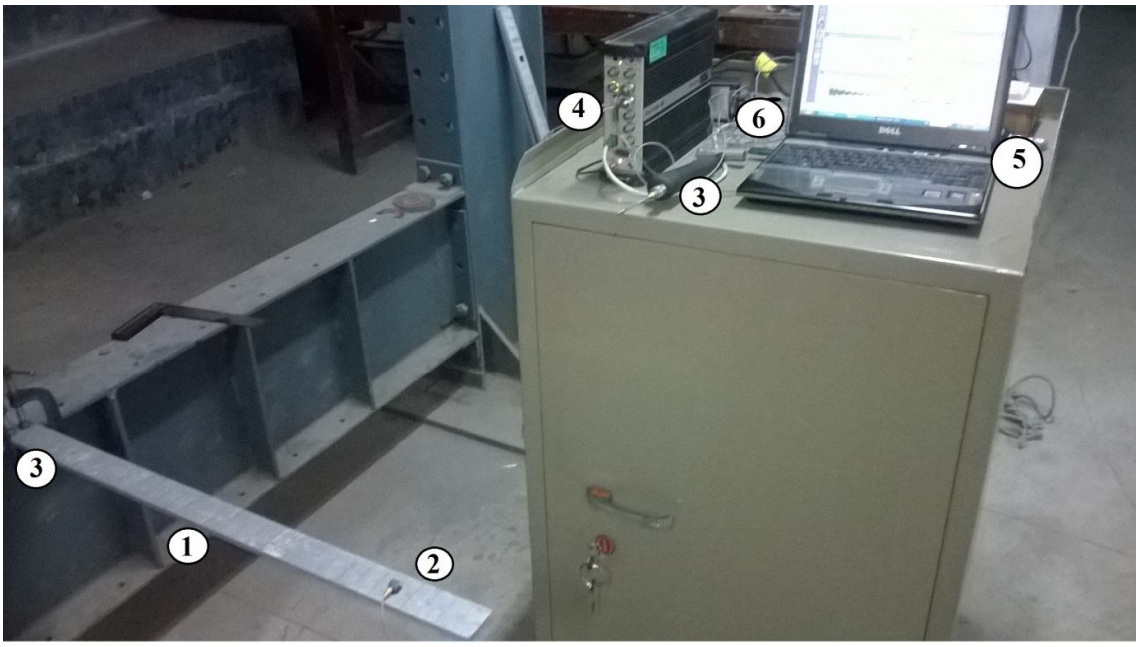

1. Beam 2. Accelerometer 3. Hammer 4. Data Acquisition System
5. Computer 6. Dongle 7. Clamp

Figure3.4 Photograph of the experimental set up with data acquisition system

First three natural frequencies of cracked clamped-clamped and cantilever aluminum beams at different location are measured and compared with FEM result. Some of the results obtained from FEM analysis and experimental are shown in Table 3.2. Values of frequency obtained from experiment results are less than FEM result. The difference can be attributed to some damping loss and replicating boundary conditions of the system. The first three natural frequency ratios as functions of crack location for a crack depth ratio for clamped-clamped and cantilever beam are shown in Figure 3.6. It can also be observed that curves obtained from FEM analysis and experimentation matched fairly well.

Table 3.1 Geometric and physical properties of cantilever beam and clamped-clamped beam

Beam	**Density (kg/m^3)**	**Poisson Ratio**	**Elasticity Modulus (GPa)**	**Length (L) (mm)**	**Thickness (W) (mm)**	**Depth (h) (mm)**
Cantilever	2780	0.33	69	600	50	10
Clamped-clamped	2780	0.33	69	838	50	10

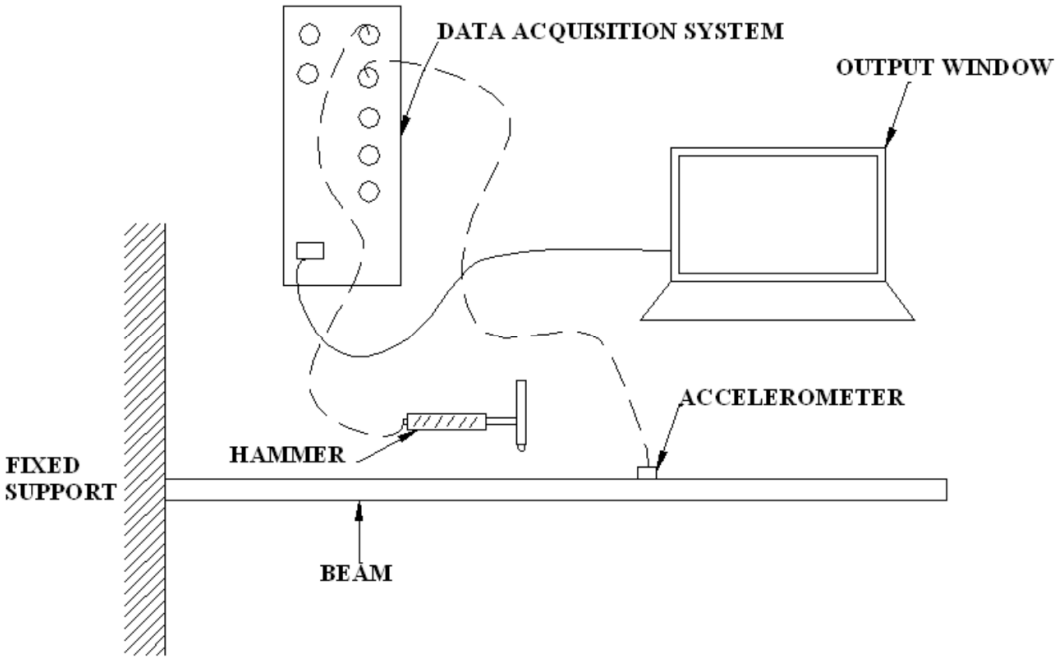

Figure 3.5 Schematic diagram of experimental setup with data acquisition system

In order to evaluate mode shape of cantilever beam a vibration analysis is performed with the help of data acquisition system on cracked beam with seven different crack locations (l_c/L=0.0588, 0.1765, 0.2941, 0.4118, 0.5294, 0.6471and 0.7647). Here length of beam is taken as 850 mm whereas beam width and thickness are same as mention in table 3.1.Crack size ratios vary from 0.2 to 0.6 (d_c/h) In case of double cracked beam, three cracked beams with different crack scenarios (d_c/h =0.4 at l_c/L= 0.1765 and d_c/h =0.6 at l_c/L = 0.7647,d_c/h =0.6 at l_c/L=0.1765 and d_c/h =0.4 at l_c/L = 0.7647 and d_c/h=0.6 at l_c/L =0.2941 and d_c/h=0.4 at l_c/L = 0.4118) are taken for experimentation.

First four mode shapes is evaluated from experimentation of series cracked beam. Normalized mode shapes of experimental results are compared with FEM results and are shown in Figure 3.7. It can be observed that incase of first mode shape [Figure 3.7(a)], some irregular roughness is found on experimental results but this irregularly is completely absent in case of second, third and fourth mode shape. It can also be observed that experimental results are slightly deviating from FEM results near the clamping end. This is due to the fact that experimental beam is not completely fixed at clamping end. However both mode shapes obtain from experimentation and FEM analysis are very closely matches with one other. In this case similar observation is found as Figure 3.7. But in all cases, crack cannot be visualized from these curves without any modification. Figure 3.8 shows mode shape of double crack beam.

Table 3.2 Comparison of natural frequencies (Hz) of a crack cantilever beam obtained through experimental and FEM analysis

Cracked Beam		**First Mode**			**Second Mode**			**Third Mode**		
	l_c/L	**Exp**	**FEM**	**Error %**	**Exp**	**FEM**	**Error %**	**Exp**	**FEM**	**Error %**
Clamped-Clamped d_c/h=0.2	0.1408	70.7	73.32	3.71	196	202.25	3.19	386	394.77	2.27
	0.2589	70.8	73.46	3.76	195	200.83	2.99	383	393.57	2.76
	0.3759	70	73.17	4.53	196	201.04	2.57	385	395.95	2.85
	0.5	69.8	72.95	4.513	196	202.25	3.19	381	392.39	2.99
Cantilever d_c/h=0.2	0.165	21.2	22.12	4.34	136.5	140.57	2.99	380	392.99	3.42
	0.3367	21.3	22.3	4.694	136.5	140.1	2.64	377	389.45	3.3
	0.5	21.5	22.41	4.234	135	138.88	2.87	382	393.38	2.98
	0.6817	21.6	22.48	4.074	135.5	139.58	3.01	376	387.87	3.16
Clamped-Clamped d_c/h=0.4	0.1408	70	73.08	4.4	196	202.26	3.19	384	393.79	2.55
	0.2589	70.6	73.43	4.01	193	199.3	3.26	380	390.54	2.78
	0.3759	68.8	72.81	5.83	194	199.7	2.94	385	395.58	2.75
	0.5	67.8	72.37	6.74	195	202.25	3.71	377	388.02	2.93
Cantilever d_c/h=0.4	0.165	20.6	22.48	9.13	136	140.27	3.14	380	392.61	3.32
	0.3367	21.2	21.688	2.30	134.5	139.26	3.54	370	384.55	3.93
	0.5	21.4	22.083	3.19	131	136.66	4.32	382	393.35	2.97
	0.6817	21.6	22.328	3.37	133.5	138.04	3.44	366	381.35	4.19
Clamped-Clamped d_c/h=0.6	0.1408	68.6	72.36	5.48	195	202.23	3.71	379	389.45	2.76
	0.2589	70.4	73.33	4.16	186	193.56	4.06	370	381.21	3.03
	0.3759	67	71.44	6.63	190	194.82	2.54	384	394.86	2.83
	0.5	65	70.19	7.98	195	202.25	3.72	364	373.74	2.68
Cantilever d_c/h=0.6	0.165	22	22.48	2.18	135	139.43	3.28	378	390.91	3.42
	0.3367	19.7	20.076	1.91	130.5	136.12	4.31	348	367.81	5.69
	0.5	21.2	21.185	-0.07	123.5	128.28	3.87	382	393.32	2.96
	0.6817	21.5	21.951	2.1	125.5	131.88	5.08	329	358.49	8.96

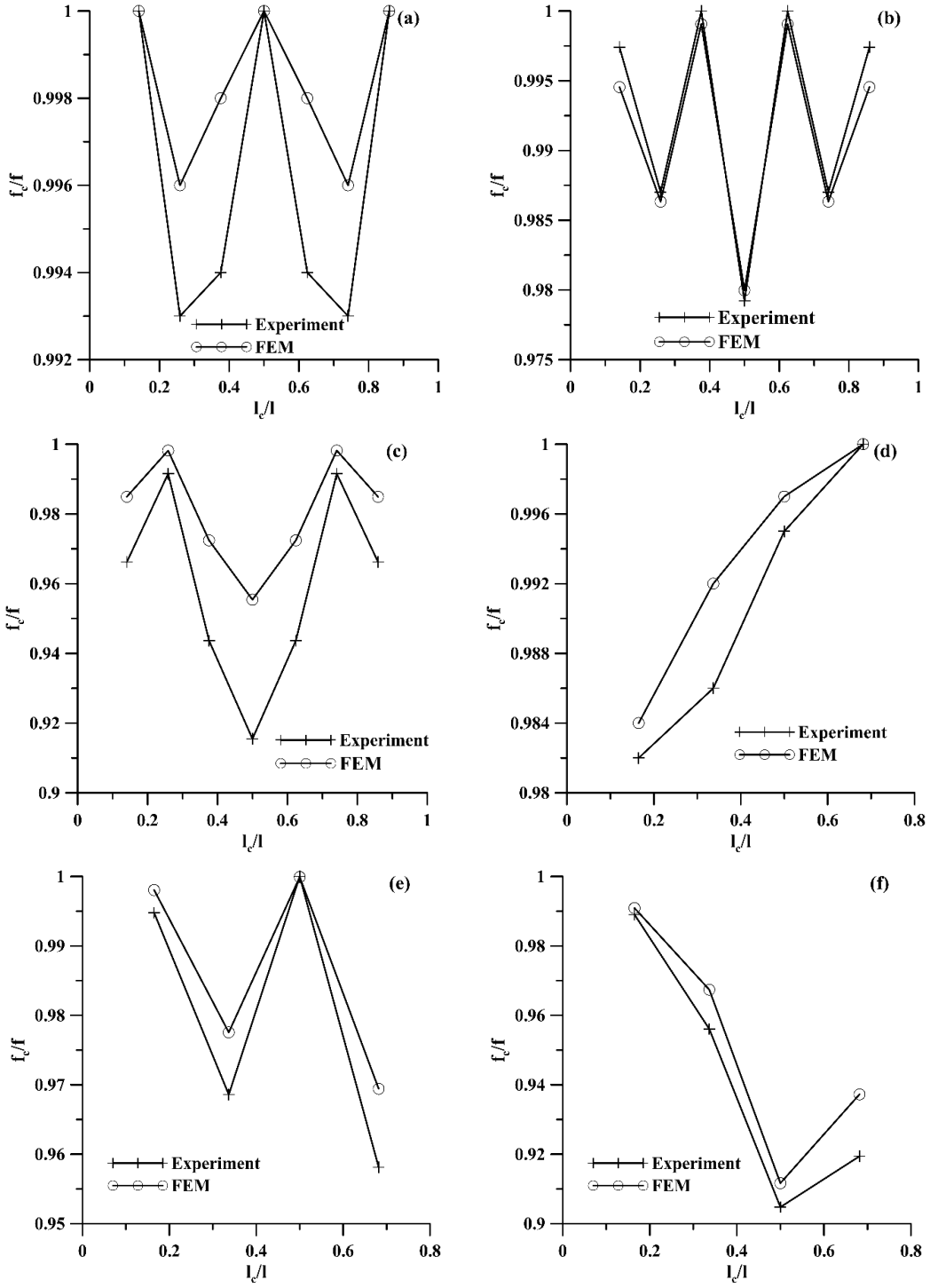

Figure 3.6 Natural frequency ratios of clamped–clamped beams for (a) second mode with crack depth ratio of 0.2, (b) third mode with crack depth ratio of 0.4 and (c) first mode with crack depth ratio of 0.6 and natural frequency ratios of cantilever beams for (d) first mode with crack depth ratio of 0.2, (e) third mode with depth ratio of 0.4 and (f) second mode with crack depth ratio of 0.6.

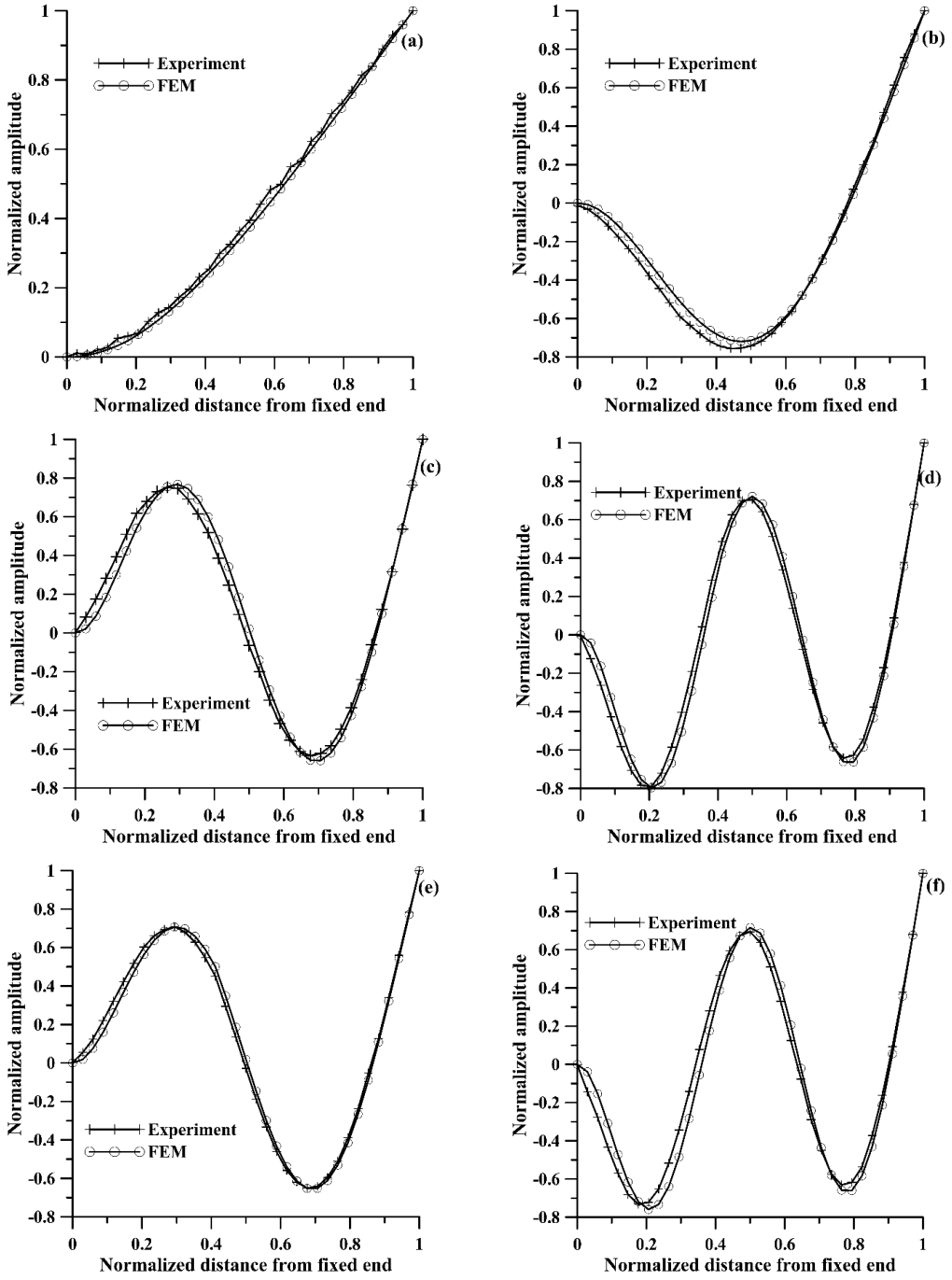

Figure 3.7 Mode shape of the cracked beam with one open edge crack obtain from experimentation and FEM analysis (a) first mode shape crack location (l_c/l=0.1765) with size (d_c/h=0.4), (b)second mode shape crack location (l_c/l=0.1765) with size (d_c/h=0.4), (c) third mode shape crack location (l_c/l=0.1765) with size (d_c/h=0.4), (d) forth mode shape crack location (l_c/l=0.4118) with size (d_c/h=0.4), (e) third mode shape crack location (l_c/l=0.4118) with size (d_c/h=0.6) and (f)) forth mode shape crack location (l_c/l=0.5294) with size (d_c/h=0.2)

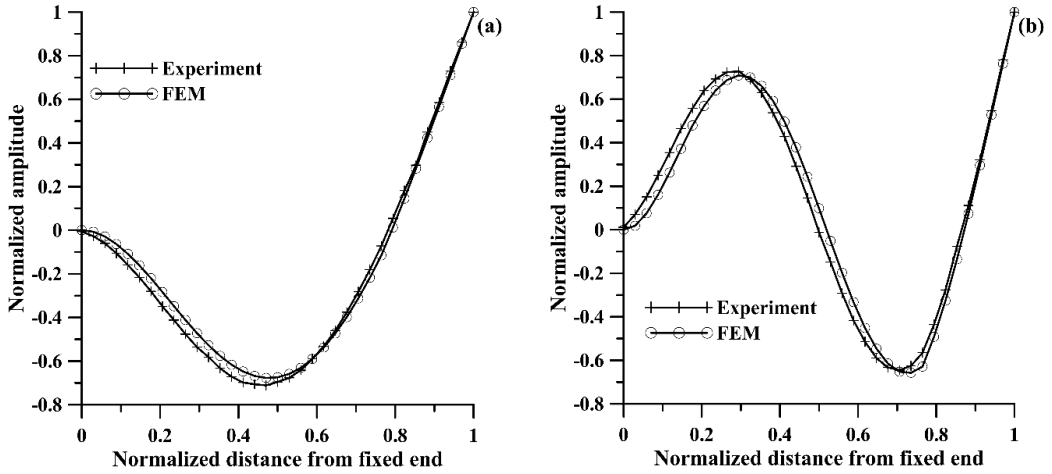

Figure 3.8 Mode shape of the double cracked beam (crack location (l_c/l=0.1765) with size (d_c/h=0.4)) and (crack location (l_c/l=0.7647) with size (d_c/h=0.6)) obtain from experimentation and FEM (a) second mode and (b) third mode

3.5 Summary

At first, natural frequencies of intact and cracked beams are determined. One end and both end clamped both are consider for analysis. Natural frequencies are measure by FFT analysis of oscilloscope. A comparison study is performed with FEM results. Then experimental study is undertaken for two kind single and double cantilever beam system with the help of data acquisition system. A set up simulating clamped boundary conditions is developed and experimentations are carried out for series of cracked beams.The objective of these experiments is to determine mode shape of natural frequencies. Mode shape obtained from experimentation is plotted with FEM results. Although the experimental results exhibit similar nature as those generated by FEM analyses, the actual values are found to be less than finite element results. This may be due to insufficiency replicating boundary conditions of the system and damping loss.

"*This page is intentionally left blank*"

Chapter 4

METHODOLOGY OF DIFFERENT OPTIMIZATION TECHNIQUES FOR CRACK IDENTIFICATION

Outline of the Chapter**:** *4.1 Introduction, 4.2 Analysis of Artificial Neural Network for crack detection,4.2.1Introduction of Cascade Artificial Neural Network, 4.2.2 Design and architecture of Cascade Artificial Neuron Network, 4.3 Analysis of Response Surface Methodology for Crack Detection, 4.3.1 Introduction of Response Surface Methodology, 4.3.2 Design and architecture of Response Surface Methodology, 4.4 Analysis of Genetic Algorithm for Crack Detection, 4.4.1 Introduction of Genetic Algorithm, 4.4.2 Design and architecture of Genetic Algorithm, 4.5 Analysis of Contour Plot Intersection for Crack Detection, 4.6 Analysis of Adaptive Neuro-Fuzzy for Crack Detection, 4.7 Analysis of Hybrid Technique for Crack Detection, 4.7.1 Cascade Neuro-GA Hybrid Technique, 4.7.2 Response Surface Methodology with GA, 4.8 Summary*

4.1 Introduction

Crack initiation and its propagation or extension of pre-existing cracks during the service condition can be a cause of severe hazard. Mostly the failures occur due to the fatigue of the material and pre-crack present in beam type structures. Crack detection in structures at the work site e.g. away from the laboratory has posed a challenge. Condition monitoring technique is a big relief for the field engineers to identify and estimate the length of the crack which can be fatal for the component. Optimization techniques have been used for the solution that minimizes the error norm. Proper regularization optimization techniques may be used for ill-poseinverse problems. These techniques are very importantfor obtaining stable solutions of the ill-posed inverse problems. An inverse problem can be formulated as a minimizationproblem to detect crack parameters. Different optimization technique for crack detection is discussed in great detail in this chapter. First, dynamic response of the beam is obtained by numerical, FEM, and experiment analyses. Then different optimization techniques are applied to determine crack locations and sizes.

This present chapter is comprises of five different sections. Section 4.2 speaks about the introduction to Artificial Neural Network and details of the steps which is to be pursued to design and develop Artificial Neural Network system. The analysis of the response surface measurement is employed for single transverse crack recognition which has been explained in Section 4.3. The section 4.4 highlights on the crack detection by genetic algorithm

optimization technique. The section 4.5 gives details analysis contour plot intersection. The section 4.6 explains adaptive neuro-fuzzy on crack detection of beam. The analysis hybrid techniques have been explained in section 4.7.

4.2 Crack detection by Cascade Artificial Neuron Network (CANN).

Cascade Artificial Neural Networks (CANN) has emerged as a promising tool for monitoring and classification of fault in machine and equipment. This technique is well prepared for solving inverse vibrational problems in the context of monitoring and fault detection because of their pattern recognition and interpolation capabilities. ANN also successfully approach and classify the problems associated with nonlinearities, provided they are well represented by input patterns, and also can avoid the complexity introduced by conventional computational methods. It consists of a given set of inputs for which desired outputs are determined by establishing proper and desired relationship between the inputs and their outputs. The mapping between the input and the output is not given but has to be learned and once the mapping is learned or trained the desired outputs can be obtained. It helps to increase the efficiency of design process.

Studies on neural networks have been motivated to imitate the way that the brain operates.The schematic model of biological neuron network and artificial neuron network is shown in Figure 4.1. It is well complex and interrelated sets of armour (dendrite, axon, terminals, soma, and nucleus), provides for a variety of sensory actions for example smell, test, touch, vision, hearing, etc. Normally the biological neurons are understood to accumulate the neural stipule and processing in the memory and learn the neural structure eases of the creation of fresh linking in the neurons. The NNT collects a huge quantity of well interrelated handling out neurons acting inside analogous to work out for the exact request, such as learning model identification or statistical data sorting, throughout the learning course. Learning within organic structure engages for linking with the synaptic weights which live inside the neurons. The neural network, by its extraordinary talent, it can collect the sense from vague or complicated data. Mcculloch and Pitts, (1943) have presented a replica of the neural network through numerous hypothesis regarding how neurons work. The simplest definition of a neural network, more properly referred to as an artificial neuralnetwork (ANN), is provided by the inventor of one of the first neurocomputers (Robert Hecht-Nielsen, 1988). He defines a neural network as “computing system made up of a

number of simple, highlyinterconnected processing elements, which process information by their dynamic state response toexternal inputs."

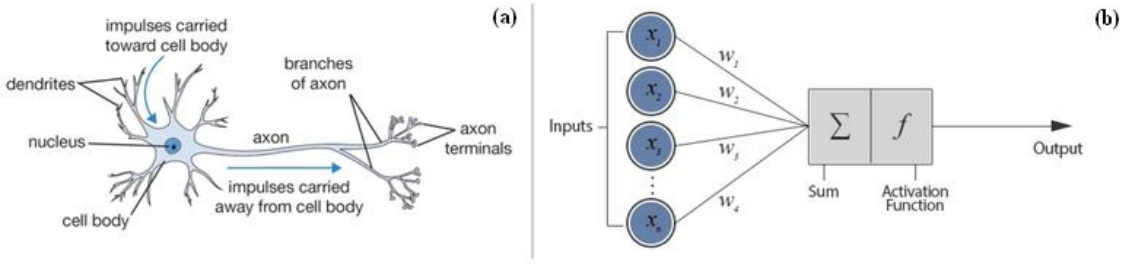

Figure 4.1 Schematic Diagram of (a) biological neuron network and (b) artificial neuron network

Depending on the nature of the application and the strength of the internal data patterns it cangenerally expect a network to train quite well. This applies to problems where the relationships maybe quite dynamics or non linear. ANNs provide an analytical alternative to conventional techniques which are often limited by strict assumption of normality, linearity, variable independence etc. Because an ANN can capture many kinds of relationships it allows the user to quickly and relatively easily model phenomena which otherwise may have been very difficult or impossible to explain otherwise.

Some advantages of ANN are described as:

- ANNs have the ability to learn and model non-linear and complex relationships, which is really important because in real-life, many of the relationships between inputs and outputs are non-linear as well as complex.
- The NNT maps use the surroundings for weights of the neuron. Further, they execute as per the circumstances.
- ANNs can generalize—after learning from the initial inputs and their relationships, it can infer unseen relationships on unseen data as well, thus making the model generalizes and predict on unseen data.
- Neural network models have the ability to detect all possibleinteractions between predictor variables
- Neural networks can be developed using multiple different training algorithms
- Unlike many other prediction techniques, ANN does not impose any restrictions on the input variables (like how they should be distributed). Additionally, many studies have shown that ANNs can better model data with high volatility and non-constant

variance, given its ability to learn hidden relationships in the data without imposing any fixed relationships in the data. This is something very useful in financial time series forecasting (e.g. stock prices) where data volatility is very high.

- The network of NNT is composed of a huge quantity of interrelated neurons running paralleled to the answer of particular output. The neurons of NNT learn via illustration. For this purpose, unique trainers are modelled and produced of these kinds of aptitudes.

The most important features [Haykin, (2006)] of the ANN are:

- The inputs to the neuron are allocated by means of neuron weight, which in sequence; influence the judgment building aptitude of the NNT. In this way, the neuron inputs are named as weighted input.
- The weighted neuron input is followed by means of collectively hidden neurons as an additional value. If the addition value goes beyond the prefixed limit value then only neuron starts firing; otherwise the neuron does not fire.
- For restraining the neuron output range, usually the standardized output array is specified in range as [0, 1] or [-1, 1].

The abilities of different networks can be related to their structure**,** dynamics and learning methods. Neural Networks offer improved performance over conventional technologies in areas which includes: Machine Vision**,** Robust Pattern Detection**,** Signal Filtering**,** Virtual Reality, Data Segmentation**,** Data Compression**,** Data Mining**,** Text Mining, Artificial Life**,** Adaptive Control**,** Optimization and Scheduling**,** Complex Mapping and more.

4.2.1 Design and architecture of Cascade Artificial Neuron Network

In this present chapter an artificial neuron is presented in the context of vibration phenomenon. The transfer function net input n, a scalar quantity, is the sum of the weighted input w_p and the bias b. This sum is the argument of the transfer function. Here f is a transfer function, typically a step function or a sigmoid function, that takes the argument n and produces the output a. w and b are both adjustable scalar parameters of the neuron. The central idea of neural networks is that such parameters can be adjusted so that the network exhibits some desired or interesting behaviour. Thus, you can train the network to do a particular job by adjusting the weight or bias parameters, or perhaps the network itself will adjust these parameters to achieve some desired end. A neuron with a single R-element input

vector is shown below. Here the individual element input p_1, p_2 ... p_R are multiplied by weights $w_{1,1}$, $w_{1,2}$...$w_{1,R}$ and the weighted values are fed to the summing junction. Their sum is simply Wp, the dot product of the (single row) matrix W and the vector p. The neuron has a bias b, which is summed with the weighted inputs to form the net input n. The perception internal sum, n of the inputs is passed through a transfer or activationfunction, f which can be any monotonic function.

So,

$$n = w_{1,1}p_1 + w_{1,2}p_2 + ... + w_{1,R}p_R + b \tag{4.1}$$

$$\text{or, } n = W * p + b$$

Neuron with vector input is shown in Figure 4.2.

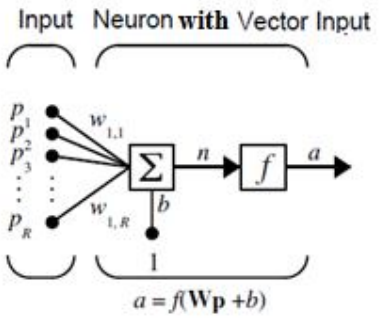

Figure 4.2 Schematic diagram of artificial neural network with activation function

A non-linear transformation defeats the purpose of using a neural filter implementation. A function that limits the amplitude range and limits the output strength of each perception of a layered network to a defined range in a non-linear manner will contribute to a nonlinear transformation. There are many forms of activation functions, which are selected according to the specific problem. All the neural network architectures employ the activation function which defines as the output of a neuron in terms of the activity level at its input (ranges from -1 to 1 or 0 to 1). In this present approach activation functions are the sigmoid functions (equation 4.1). This is because they are differentiable and probabilistic interpretation which simplifies the classification task.

$$f(x) = \frac{1}{1 + e^{-\alpha x}}, \ \alpha > 0 \tag{2.1}$$

A learning rule defines as a procedure for modifying the weights and biases of a network. There are three major learning paradigms, each corresponding to a particular abstract learning task. These are unsupervised learning, supervised learning and

reinforcement learning. Unsupervised Learning neural network is only given a set of inputs and it's the neural network's responsibility to find some kind of pattern within the inputs provided without any external aid. Supervised Learning is taught by a set of input-output pairs. The aim is to train the network to recognize the applied input with the desired output. Reinforcement learning is similar to supervised learning in that some feedback is given, however instead of providing a target output a score is given based on how well the system performed. Supervised learning is applied for crack detection due to this learning process more supervised and learning than other learning process.

The Cascade forward back propagation algorithm of Artificial Neural Network (ANN) models performed better than Feed forward back propagation algorithm models, especially in reducing the scatter of predictions. In this thesis cascade forward back propagation is applied for crack detection. A weight connection is connected from the input to each layer and from each layer to the successive layers. The input-output relationship of cascade forward artificial neural network with transfer function is shown in Figure 4.3. A simple block diagram of cascade forward artificial neural networkfor crack detection is Figure 4.4.

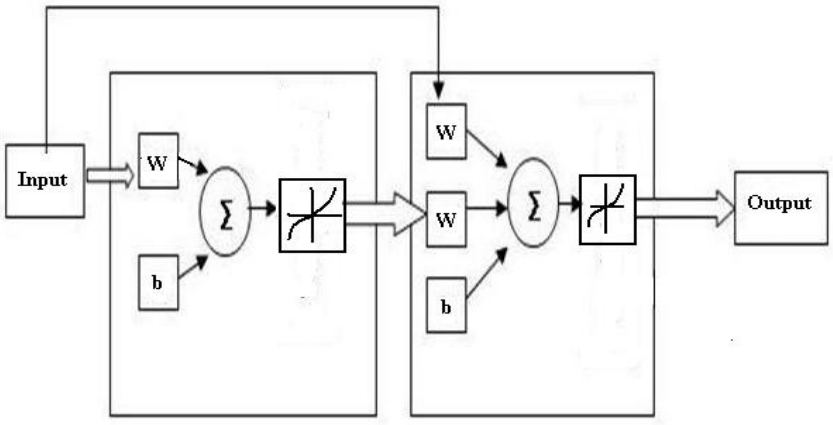

Figure 4.3 Schematic diagram of cascade forward back propagation neural network

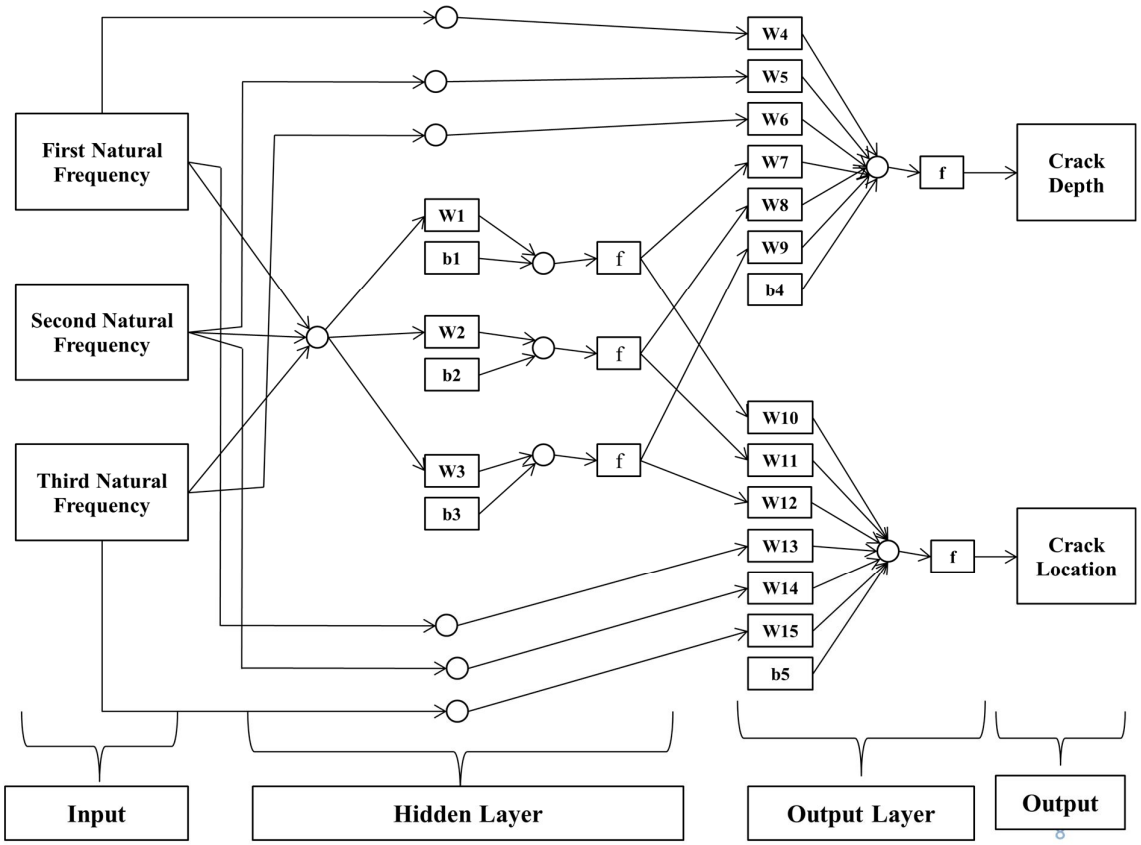

Figure 4.4 Block diagram of cascade forward artificial neural network for crack detection

Backpropagation Algorithmis most commonly used in the multilayer cascade-forward network.Standard backpropagation is a gradient descent algorithm in which the network weights are moved along thenegative of the gradient of the performance function. The term backpropagation refers to the manner in which the gradient is computed for nonlinear multilayer networks. For crack detection method back propagation technique is employed to reduce the error with optimize the inputs relative natural frequencies to achieve the target that is normalized crack location and crack depth ration. Neurons are originated by the number of training data and the convergence of the error during training to a minimum threshold error to control the crack location and crack depth. A measure of the performance of the networkis the instantaneous sum-squared difference between $\Psi_{\text{desired, } n}$ and $\Psi_{\text{actual, } n}$ for the set of presented training patterns

$$Error = \frac{1}{2} \sum_{\substack{all\,training \\ patterns}} \left(\psi_{desired,m} - \psi_{actual,m} \right)^2 \tag{4.3}$$

where, m = output parameters

The error back-propagation method is applied to train the network [Haykin, (2006)]. This method requires the computationof neighbouring error gradients in order to determine appropriate weight corrections to reduce error. For the output layer, the error gradient δ^i (ith layer) is

$$\delta^i = f'\left(N^i\right)\left(\psi_{desired,n} - \psi_{desired,n}\right) \tag{4.4}$$

$$\text{where, } N_j^i = \sum_{n=1}^{z} W_{jn}^i \; y_n^{i-1} + W_j^i u_j \text{ and } W_j^i = f\left(N_j^i\right)$$

i=layer number, j= label for j^{th} neuron in hidden layer, $W_{jn}{}^i$= weight of the connection from neuron n in layer '$i-1$' to neuron j in layer i and u= input neuron

The local gradient for neurons in hidden layer is given by

$$\delta_j^i = f'\left(N_j^i\right)\left(\sum_k \delta_k^{i+1} W_{kj}^{i+1}\right) \tag{4.5}$$

Neurons weight is updated as

$$W_{jn}(t+1) = W_{jn}(t) + \Delta W_{jn}(t+1) \tag{4.6}$$

$$\text{Where, } \Delta W_{jn}(t+1) = \alpha \Delta W_{jt}(t) + \beta \delta_j^i y_n^{i-1}$$

Where, α = momentum coefficient is chosen empiricallyas 0.2 in this computational work; β= learning rate is chosenempirically as 0.35 in this computational work, t = iteration number, the final output from the neural network is

$$\psi_{actual,m} = f\left(N_m^{i_{output}}\right) \tag{4.7}$$

$$\text{where, } f_m^{i_{output}} = \sum_{n=1} W_{mn}^{i_{output}} y_n^{i_{output-1}}$$

Each activation consists of the arrangement of learning sample with alteration of the neuron weight.

4.3 Crack detection by Response Surface Methodology (RSM)

Response surface methodology (RSM) is a statistical tool which explores the relationships between several explanatory variables and one or more response variables. This method was introduced by George E. P. Box and K. B. Wilson in 1951 [N. R. Draper (1992)]. The main idea of RSM is to use a sequence of designed experiments to obtain an optimal response. Box and Wilson suggest using a second-degree polynomial model to do this. This

model is only an approximation, but they use it because such a model is easy to estimate and apply, even when little is known about the relation. Three topic statistical experimental design fundamentals, regression modelling techniques, and elementary optimization methods are generally combined into this methodology. Identifying and fitting from experimental data is required some statistical knowledge. Main objective of RSM is optimization, finding the best set of factor levels to achieve some goal.

The most extensive applications of RSM are in the industrial world, particularly in situations where several input variables potentially influence some performance measure or quality characteristic (the response) of the product or process. If it is easily constructed the graphical display of the relationship between the response and the predictors (the responsesurface), the optimization of this process would be very straight forward. By inspection of the plot, we could identify the values of the process variables which yield to the desired value of the response variable of interest. Unfortunately, in most practical situations, the true response function is unknown. In this case, the field of response surface methodology consists of the experimental strategy for exploring the space of the process variables, empirical statistic modelling to develop an appropriate approximating relationship, and optimization methods for finding the levels or values of the process variables that produce desirable values of the response.

In the applications to damage diagnosis, the experimental strategy consists of the monitoring of the structure in time. When dynamic problems or more complex structures are considered, an approximation is needed. The change in the statistical distribution of the error involved in these problems can be considered as adamage indicator. Its application to a numerical example leads to the formulation of a new method for damage detection and localization. The testing of the method on more thorough examples is main objective of the sections.

4.3.1 Design and architecture of Response Surface Methodology

In many experimental fields has a response variable of interest, y, and a set of input variables, x_1, x_2,….x_k. In some systems the nature of the relationship between y and the x's might be known "exactly", based on the underlying engineering, chemical, or physical principles. Then one could write a model of the form $y = g(x_1, x_{2,\ldots}x_k) + \eta$, where the term η represents the "error" in the system. This type of relationship is often called a mechanistic model. In the more common situation where the underlying mechanism is not fully

understood, the experimenter must approximate the unknown function g with an appropriate empirical model $y = f(x_1, x_2, \ldots, x_k) + \varepsilon$, where ε also accounts for the lack of fit error η_L introduced in the model by the assumed form of $f(.)$. Usually, the function f is a first-order or second-order polynomial in the basic predictors or their transformations. This is empirical model of RSM. In this crack detection method this input variables (q) are normalized crack location and crack depth ratio and response variables are relative values of the first three natural frequencies.

Response Surface Methodology is useful for developing, improving, and optimizing the response variable. In this case, the normalized crack location y is the response variable, and it is a function of normalized crack location and crack depth ratio. It can beexpressed as

$$y = f(x_1, x_2) + e \tag{4.8}$$

The variables x_1, and x_2 are independent variables where the response y dependson them. The dependent variable y is a function of x_1, andx_2 the experimental errorterm, denoted as e. The error term e represents any measurement error on the response, as well as other type of variations not counted in f. It is a statistical error that is assumedto distribute normally with zero mean and variance s^2. In crack detection RSM problems, the true response function f is unknown. In order to develop a proper approximation for f, the experimenter usually starts with a low-order polynomial in some small region. In this approach there is a curvature in the response surface, a higher degree polynomial should be used.

$$Y = C_0 + \sum_{i=1}^{2} C_i x_i + \sum_{i=1}^{2} C_i x_i^2 + \sum_{i,j=1, i\neq j}^{2} C_{ij} x_i x_j \tag{4.9}$$

In each model, the levels of each factor are independent of the levels of other factors. In order to get the most efficient result in the approximation of polynomials the proper experimental design must be used to collect data. Once the data are collected, the method of least square is used to estimate the parameters in the polynomials. The response surface analysis is performed by using the fitted surface. The response surface designsare types of designs for fitting response surface.

There are many designs available for fitting a second-order model. The most popular one is the central composite design (CCD).This design was introduced by Boxand Wilson. It consists of factorial points ($2q$), central points, and axial points. CCD was often developed through a sequential experimentation. When a first-order model shows an evidence of lack of fit, axial points can be added to the quadratic terms with more center points to develop CCD.

The number of center points n_c at the origin and the distance a of the axial runs from the design center are two parameters in the CCD design. The center runs contain information about the curvature of the surface, if the curvature is significant, the additional axial points allow for the experimenter to obtain an efficient estimation of the quadratic terms. Graphical view of a central composite design for two variables is shown in Figure 4.5.

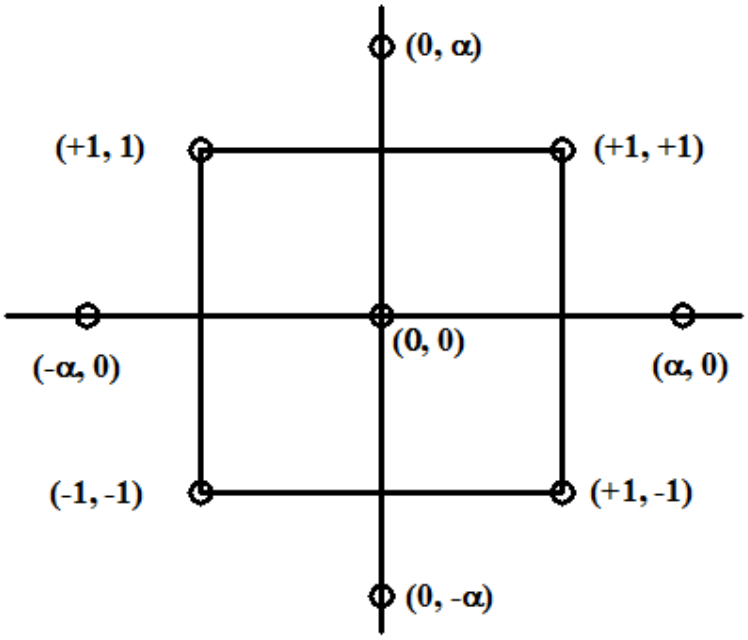

Figure 4.5 Central Composite Design for two variables

There are couples of ways of choosing axis length (a) and number of center point (n_c). First, CCD can run in incomplete blocks. A block is a set of relatively homogeneous experimental conditions so that an experimenter divides the observations into groups that are run in each block. An incomplete block design may be conducted when all treatment combinations cannot be run in each block. In order to protect the shape of the response surface, the block effects need to be orthogonal to treatment effects. This can be done by choosing the correct a and n_c in factorial and axial blocks. Since the reason for using response surface analysis is to located unknown optimization, itmakes sense to use a rotatable design that provides equal precision of estimation of the surface in all directions. For the present approach value of a is taken with considering rotatable CCD design by using $\alpha=2^{a/4}$.Five center points is considered for this methodology.

The analysis of a second-order model is usually done by Minitab software. The analysis of variance for fitting the data to the second-order and contour plots will help

characterize the response surface. The Minitab computes the linear, quadratic, and interactions terms in the model. Analysis of variance for the adequacy of the model is then performed in the subsequent step. Variance indicates that there are significant interactions between the factors or variables. The small probability values (*p*-values) for linear and square terms also point out that their contribution is significant to the model. Since, there are no replicated center points; the software cannot obtain a lack-of- fit. But, small *p*-values for the interactions and the squared terms suggest there is curvature in the response surface. Moreover, the main effects can be referred to as significant at an individual 0.05 significant level. So fitness ratio (*F*) is calculated for 95% level of confidence.

The value which are less than 0.05 are considered significant and the values greater than 0.05 are not significant and the model are adequate to represent the relationship between first three natural frequencies with crack position and depth. The fit summary recommends that the quadratic model is statistically significant for analysis of Regression (R_a). For the appropriate fitting of R_a, the non-significant terms are eliminated by backward elimination process.

4.4 Crack detection by Genetic Algorithm(GA)

A “genetic algorithm” is a modifying stochastic method that inspired of the Darwinian survival-of-the fittest theory, which is based on an opportune combination of random mutations and natural selection, in orderto numerically find optimal values of some specific function. The algorithm acts over a population of *P* potential solutions by applying, iteratively, the “survival of the fittest” principle; in such a way it produces a sequence of new generations of *P* individuals that evolves towards a stationary population where the large majority of surviving solutions do coincide and approachas much as possible the real solution of a practical problem (D. E. Goldberg, 1989).

Genetic Algorithms (GAs) imitate natural selection and is used to perform tasks like search, optimization and classification. GAs outperform the efficiency of conventional optimization techniques in searching non-linear and non-continuous spaces, which are characterized by abstract or poorly understood expert knowledge. Furthermore, to the contrary with the standard algorithms, GAs generate at each iteration a population of points that approach the optimal solution by using stochastic and not deterministic operators. As a result, the search can be deployed without being trapped within local extremes.

A simple genetic algorithm consists of three basic operations: reproduction, crossover and mutation. Reproduction is the process by which strings with better fitness values receive correspondingly better copies in the new generation. Better solutions persist and contribute to better new strings during successive generation and strings with lower fitness values are eliminated. Genetic operator, crossover is the process in which the strings are able to mix and match their desirable qualities in a random fashion. Crossover proceeds in three simple steps. First, two new strings are selected whose fitness value is close to that of the field variables. Second, a random location in both strings is selected. Third, the portions of the strings to the left and right of the randomly selected location in the two strings are exchanged. During the creation of a generation it is possible that the entire population of strings is missing a vital bit of information that is important for determining the correct or the most nearly optimum solution. Future generations that would be created using selection and crossover would not be able to solve this problem. Here mutation becomes important. Occasionally, the value at a certain string location is changed to a zero and vice versa. Mutation thus ensures that the vital bit of information is introduced into the generation. The various process used in GA as follows:

- Selecting the variables
- Define fitness function and solution space
- Specify population size and randomly initialize population
- Fitness value evaluation
- select parents from population
- perform crossover on parents creating population
- perform mutation of population
- determine fitness of population
- re-evaluating the costs and iterating the algorithm until best individual is good enough
- Stopping criteria (Based upon fitness function)

In order to translate into this scenario the crack parameter identification problem of cracked beam with a single cracka GA is designed and is used to detect the relative crack depth and relative crack location. Designed controller uses three inputs and two outputs. The inputs to the Genetic Controller are the relative values of the first three natural frequencies

and the outputs are normalized crack location and crack depth ratio. In this approach, genetic algorithm based crack identification procedure, developed on the basis of the objective function discretization.

4.4.1 Design and architecture of Genetic Algorithm

In genetic algorithms, a chromosome is a set of parameters which define a proposed solution to the problem that the genetic algorithm is trying to solve. Each chromosome is encoded one binary string. Each bit in this string can represent some characteristic of the solution. A number is represented by whole string. One example of encoding the chromosomes into bit strings is shown in Figure 4.6. After obtaining the input relative natural frequencies, a population of individuals, is generated atrandom. A population of individuals represents a candidate solution to the problem. The initial population is then submitted to generic operators, resulting in the evolution of populations through generations. Selection is a genetic operator where the best chromosomes are selected to continue, and the rest are rejected. Individual solutions are selected through a fitness function, where fitter solutions are typically more expected to be selected.

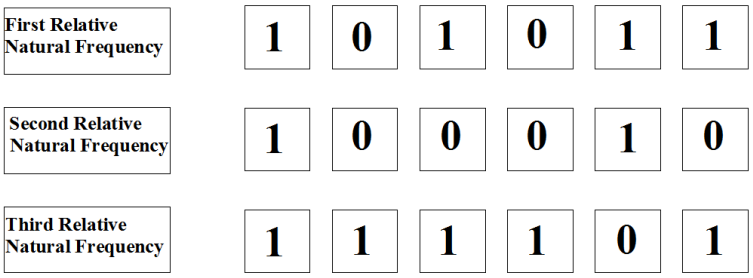

Figure 4.6 Encoding the chromosomes into bit strings

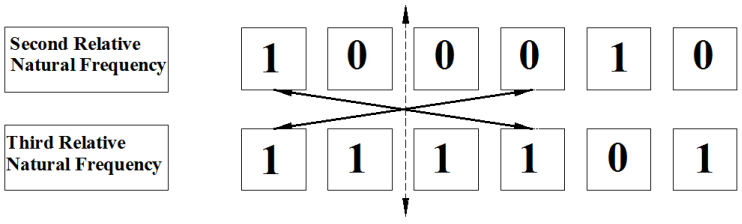

Figure 4.7 Crossover of bit strings

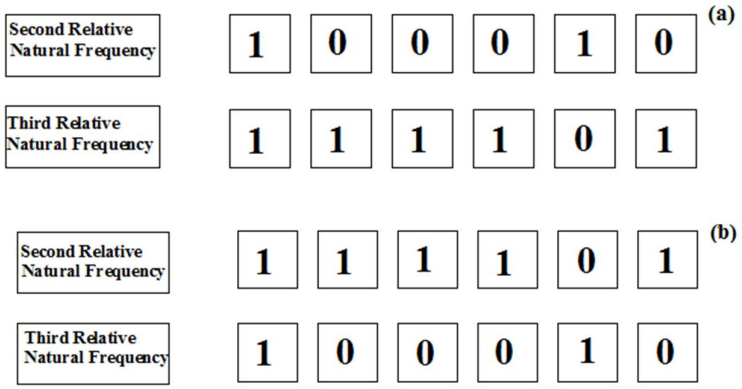

Figure4.8 Mutation of bit strings (a) Before Mutation (b) After Mutation

After that genetic operator used to produce the second generation of populations from those nominated through selection using crossover and mutation. This process is called reproduction. Crossover selects genes from parent chromosomes and creates a new offspring. The simplest way to dothis is to choose randomly some crossover point and everything after and before the point is crossed between the parents and copied. One example of crossover of bit strings is shown in Figure 4.7. After crossover the mutation operator is applied on all the chromosomes except the best chromosome, which is called the best. In the mutation operator the whole chromosome is changed or each bit can beinverted. One example of mutation of bit strings is shown in Figure 4.8. After mutation one generation is completed and in the next generation the mutated natural frequencies is used for calculating relative crack depth and relative crack location. The best fitness value is checked in every generation and if the fitness reaches a certain level, or if the maximum number of iterations is achieved, the algorithm is stopped.

In this study GA method is applied to predict crack depth and location in a structure using natural frequency information. The first three natural frequencies of the beams are used to construct the objective function. The genetic algorithm is applied to predict the global optimal depth and location by minimizing the objective function which is based on numerical or finite element results frequencies (f_n) and calculated regression equation frequencies (f_r).

The process used for prediction of crack in GA as follows:

1. First all variable are selected. The GA begins by defining two variables, crack depth ratio andnormalized location of crack whose values are to be optimized.

2. The fitness function is to be minimized according to the following equation:

$$fitness(l_c, d_c) = \sum_{i=1}^{3} (f_{ni} - f_{ri})^2 \quad (4.10)$$

where,

d_c= depth ratio of the crack

l_c= normalized location of the crack

f_{ni} = numerical and finite element result of normalized first three natural frequencies

f_{ri} = normalized regression field first three natural frequencies function of d_c and l_c

3. Twenty number of initial population is developed.

4. Initial population is collected from Numerical or finite element analysis.

5. Two parents set from initial population using fitness function are selected.

6. The chosen parents are converted to binary string from decimal values

7. The binary string is randomly cut at any point doing crossover

8. The children from the parents are determined.

9. The fitness value is figured out for each variable.

10. Stochastic uniform is used for selection. Only the best chromosomes are selected to continue, and the rest are eliminated.

11. After generating a new population, the process of selection and crossover is repeated and mutation is used on all of the data expect the best children. Uniform mutation is used with rate 0.01 for best fitness value.

12. The process is reevaluated and iterated the algorithm until the fitness value reaches a certain level. Function tolerance and maximum number of generations for each run was set at $1e^{-12}$ and 500 respectively.

4.5 Crack detection byContour Plot Intersection Method

A contour plot is a graphical technique for representing a 3-dimensional surface by plotting constant z slices, called contours, on a 2-dimensional format. That is, given a value for *z*, lines are drawn for connecting the (*x*, *y*) coordinates where that *z* value occurs.

When two contour lines are plotted for first and second modes in same axis of a cracked beam, it is observed that two normalized contour lines may sometime intersect more than one point indicating the existence of crack. In order to point out unique position of crack, assistance of third frequency contour line is required. The intersection of these contours indicates crack location and size. Unknown values of contour lines are obtained by cubic interpolation from adjacent values.

In this method, first three natural frequencies obtained using numerical and finite element analyses are applied. These values are normalized between 0 and 1. At the same time, crack location and depth are also normalized with respect to beam length and beam depth, respectively. The normalized frequencies for a particular beam are plotted against normalized location and normalized depth. It should be pointed out that normalized natural frequency is not only a function of crack depth, and crack location, but also of the different mode number.

Both the crack location and the crack depth influence the changes in the natural frequencies of a cracked beam. Consequently, a particular frequency could correspond to different crack locations and crack depths. This can be observed from the three-dimensional plots of the first three natural frequencies of cantilever and clamped-clamped beams.

For a beam with a single crack with unknown parameters, the following steps are required to predict the crack location, and depth, namely,

- Measurements of the first three natural frequencies;
- Normalization of the measured frequencies;
- Plotting of contour lines from different modes on the same axes;
- Location of the point of intersection of the different contour lines.
- The point of intersection, common to all the three modes, indicates the crack location, and crack depth. This intersection becomes unique due to the fact that any normalized crack frequency can be represented by a governing equation that is dependent on normalized crack depth, normalized crack location and mode number.
- Therefore a minimum of three curves is required to identify the two unknown parameters of normalized crack location and crack depth.

4.6 Crack detection by Adaptive Neuro-Fuzzy Interference System (ANFIS)

An adaptive neuro-fuzzy inference system (ANFIS) is a Takagi–Sugeno fuzzy based artificial neural network. The technique was developed 30 years ago. Since it integrates both neural networks and fuzzy logic principles, it has potential to capture the benefits of both in a single framework. Its inference system corresponds to a set of fuzzy IF–THEN rules that have learning capability to approximate nonlinear functions [Abraham (2005)]. Hence, ANFIS is considered to be a universal estimator.ANFIS works as a small window on the model to show which parameters are actually influenced the prediction output. While neural network works as a black box. The parameters of the membership are adapted to give better matching between input and output during ANFIS training. So that fuzzy system takes on the ability of learning conventional neural network.Flowchart of ANFIS is shown in Figure 4.9.

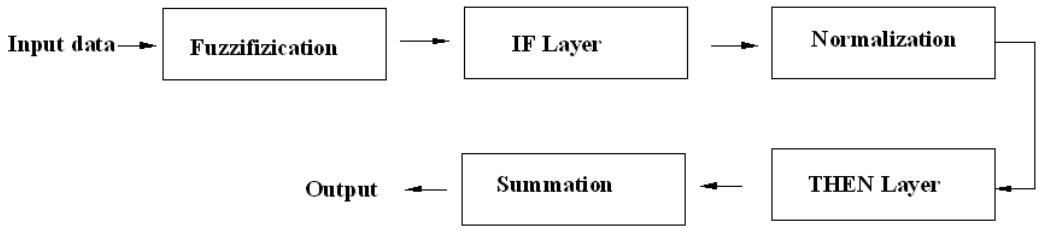

Figure 4.9 Block diagram of ANFIS.

Sugeno fuzzy is a popular fuzzy interference. Sugeno fuzzy is introduced by Sugano [M. Sugano, (1985)]. Sugeno output membership functions are either linear or constant.

The input data and output data are fed into the ANFIS model to extract the rules. The 'fuzzification' layer is set and adapts the parameters for the chosen membership. After that, the strength firing layer is coming and it represents the IF conditions to set the rules. The output of the firing strength is normalized in the normalization layer. Before the final layer, there is another adaptation layer that works as a 'defuzzification' layer of the rules, where the surgeon model parameters are tuned to derive the best matching between input and output. ANFIS by dividing the data space into rectangular sub-spaces (ANFIS-Grid partition model).

The most popular learning algorithm is the hybrid algorithm proposed by Jang (J. S.R. Jang 1991). It is used to adapt the parameters in the adaptive network. This algorithm is a combination of Steepest Descent and Least Squares Estimation (LSE). In this learning

algorithm, there are two passes: the forward and feedback passes. LSE is used during the forward pass to tune consequent parameters, and Steepest Descent is used during the backward pass to tune the antecedent parameters. For each input, the experimental membership function is set to the Gaussian type. While the output membership function is set to the linear type.

After training, the parameter of the membership was adapted to give better matching between input and output, which lead to changing the initial shape of the membership. The more changing of the membership shape before and after the training represents the most effective variables in constructing the model. The hybrid algorithm was used to adapt the membership parameter and the Sugeno polynomial parameters. The step-size adaptation parameter was initialized to 0.01. Fuzzy subtractive clustering has been used to find the fuzzy rules for the ANFIS model.

4.6.1 Design and architecture of Adaptive Neuro-Fuzzy System

The architecture of a simple ANFIS is shown in Figure. 4.9. In forward problem crack detection method ANFIS has two inputs crack depth ratio (d_c/h) and normalized location (l_c/l) and one output frequency ratio (f_c/f). For this model, the rule is set with two fuzzy 'if–then' rules. Rule is expressed as a model develops by Jang et al.(Jang J-SR, Sun CT, Mizutani E, 1997):

If d_c/h is A_k and l_c/l is B_k then

$$\mu_i = p_i (d_c/h) + q_i (l_c/l) + r,\ k=1, 2 \tag{4.11}$$

where A_k and B_k are the k^{th} fuzzy set defined for d_c/h and l_c/l, μ is a linearconsequent function defined in terms of the input variablesand p, q and r are the consequent parameters of the model.

The five layers ANFIS explained as follows:

The first layer is the fuzzy layerthat converts the inputs into a fuzzy set by means ofmembership functions. Every node i in this layer is anadaptive node. The outputs $O_{1,\,i}$of this layer are the fuzzymembership grade of a fuzzy set. The membership relationship between the output and input functions of this layer can be expressed as

$$\begin{aligned} O_{1,i} &= g_{A_i}\left(d_c/h\right), \quad i = 1,2 \\ O_{1,i} &= g_{B_{i-2}}\left(l_c/l\right), \quad i = 3,4 \end{aligned} \tag{4.12}$$

Where g_{Ai}, and g_{Bi} denote the membership functions, these can have various shapes, like triangular–trapezoidal, Gaussian, bell-shaped. Here, the membership function is selected to be triangular function.

$$g_{Ai}(x) = \max\left(\min\left(\frac{\left(d_c/h\right) - m_i}{n_i - m_i}, \frac{n_i - x}{o_i - n_i}\right), 0\right) \quad i = 1,2 \tag{4.13}$$

where $\{m_i, n_i, o_i\}$ is the parameter set of the ANFIS model. Parameters in this layer are referred to as principle parameters.

This layer is the product layerthat consists of a fixed number of nodes labelled by (Ω). The output of this layer is the product of all incoming signals, which is defined as follows:

$$O_{2,i} = w_i = g_{Ai}(x) g_{Bi}(y) \tag{4.14}$$

where the $O_{2,i}$ is the output of the Layer 2. The output signal w_i denotes the firing strength of the rule.

The third layer is the normalised layer, every node i in this layer is a fixed node which arelabelled N. The firing strengths of the i^{th} node of this layer is normalised by calculating the ratio of the i^{th} rule's firing strength to the sum of all rules' firing strengths:

$$0_{3,i} = w_i' = \frac{w_i}{w_1 + w_2}, \quad i = 1,2 \tag{4.15}$$

Where$O_{3,i}$ is the output of Layer 3. The quantity w_i' is known as the normalised firing strength.

The fourth layer is the defuzzification layer, which performs defuzzification by means of fuzzy rule operations. Every node i in this layer is an adaptive node with a node function. The relationship between the inputs and outputs of this layer can be defined as equation 4.16.

$$Q_{4,i} = w_i' \mu_i \left(p_i\left(a/h\right) + q_i\left(l_c/l\right) + r\right), \quad i = 1,2 \tag{4.16}$$

Where $Q_{4,i}$ is the output of Layer 4. The consequent parameters of μ_i in this layer are to be adapted in order tominimise the error between the ANFIS outputs and theircomputed results.

The fifth layer is the output layer, thesingle node in this layer is a fixed node labelled Σ, whichcomputes the overall output by summing all the incoming signals. The output can be expressed as equation 4.17.

$$\left(f_c/f\right)_{output} = Q_{5,i} = \sum_i w_i' \mu_i \tag{4.17}$$

Learning algorithms adapt the parameters of the 1st layer, called principle parameters, and the parameters of the 3rd layer, referred to as consequent parameters, in order to minimise the output error based onthe training data sets until acceptable error is reached.

In this crack detection approach ANFIS method constructs fuzzy inference systems (FIS) whose membership function parameters are adjusted using combination with a least-squares type of method to improve the system performance and also to rapidly and accurately approximate complex functions.The triangular and linear membership functions are used for input data and output data respectively. Hybrid optimization method is applied for training. Number of membership function consider for each parameter is three.

4.7 Crack detection by Hybrid Optimization Technique

Hybrid optimization based crack detection technique is developed in recent years. Two or three combination base optimization sometimes gets more accurate result than single optimization technique. Two hybrid optimization techniques are employed in this thesis. The following section provides a detailed description of those hybrid techniques.

4.7.1 Cascade Neuro-GA Hybrid Technique

The present section builds an incorporated hybrid optimization technique by a combination of Genetic Algorithm and Cascade Artificial Neural Network techniques. First genetic algorithm model isprepared from finite element or experimental result and general regression equation. GA is applied to predict the global optimal depth and location of crack by minimising the fitness function which is constructed based on experimental results (f_e) and general regression field (f_r) as described 4.4 section. The fitness function is to be minimised according to the following equation:

. $$fitness(l_c, d_c) = \sum_{i=1}^{4} \left(f_{ei} - f_{ri}\right)^2 \tag{4.18}$$

f_e is the first four relative natural frequencies which are applied to crack detection system as inputs obtain from experimental results. .f_r is the first four relative general regression field natural frequencies, which are functions of crack location (l_c) and depth ratio (d_c), and are calculated from the general regression cracked-beam model. Stochastic uniform and adaptive feasible mutation are used for selection and mutation respectively. Function

tolerance and maximum number of generations for each run is set at 1e−12 and 500, respectively.

Second step of this hybrid optimization Cascade ANN is employed. Optimized output results (normalized crack location and crack depth ratio) from GA are used as input neurons of neuron network. So this hybrid neural network technique has six input parameter four natural frequency obtain from experimentation with two optimized data output of GA crack location and its depth. Actual (finite element data or experimental data) normalized crack location and crack depth ratio isset as target data of cascade neural network. This training and learning process are same as describe at 4.2 section. The Figure 4.10 present the GA based hybrid techniques for Cascade ANN.

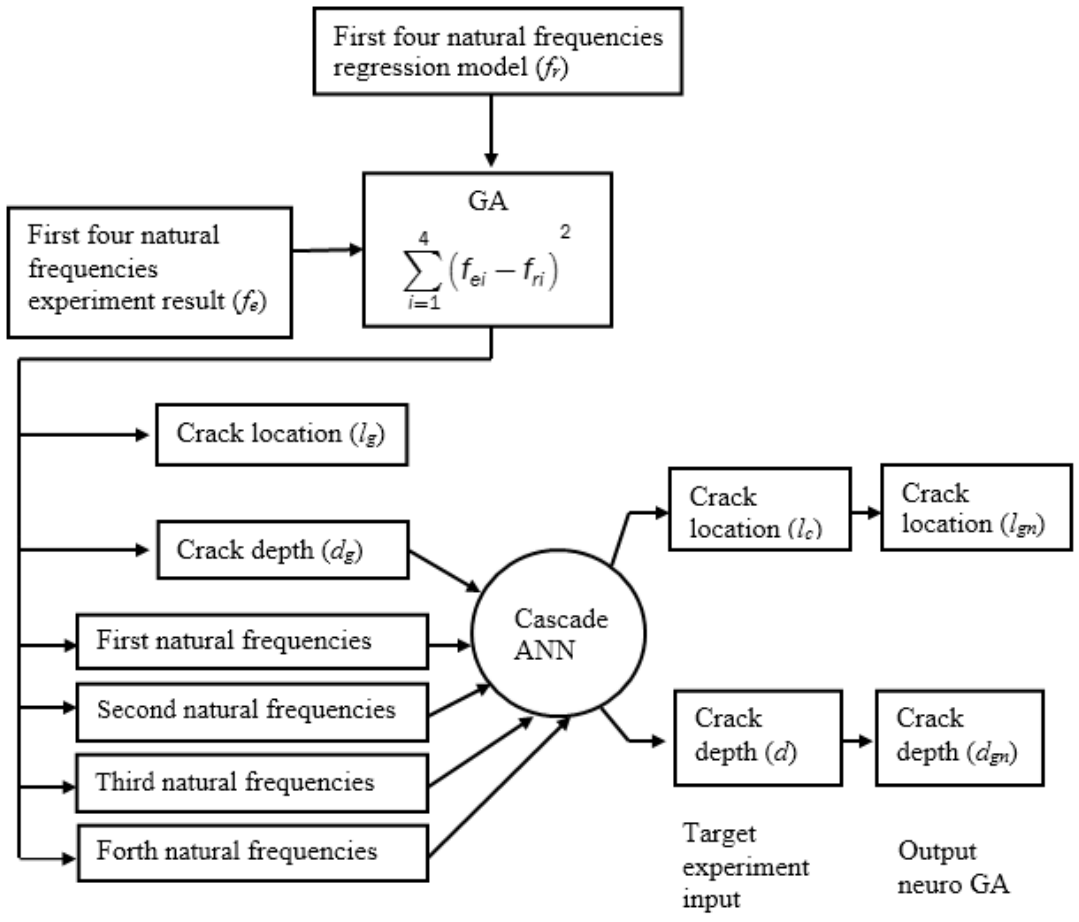

Figure4.10 Block diagram of Neuro-GA technique

4.7.2 Response Surface Methodology with GA

This hybrid technique is predictedthe crack location and its size a beam by two steps. In the first step a statistical regression model developed by response surface methodology as

described 4.3 section. These regression equations are applied in the fitness function of GA. In order to detect crack location and its size fitness function optimized in the second step with the help of GA.

GA is applied to predict the global optimaldepth and location of crack by minimizing the objective (fitness) function which is constructedbased on numerical or experimental frequencies results (f_n) and RSM regression equation (f_r). Now fitness equation (4.19) is optimized by GA.

$$fitness(l_c, d_c) = \sum_{i=1}^{3} (f_{ni} - f_{ri})^2 \tag{4.19}$$

Detail procedure of GA optimization is described at 4.4 section. The Figures 4.11 present the GA based hybrid techniques for Cascade ANN

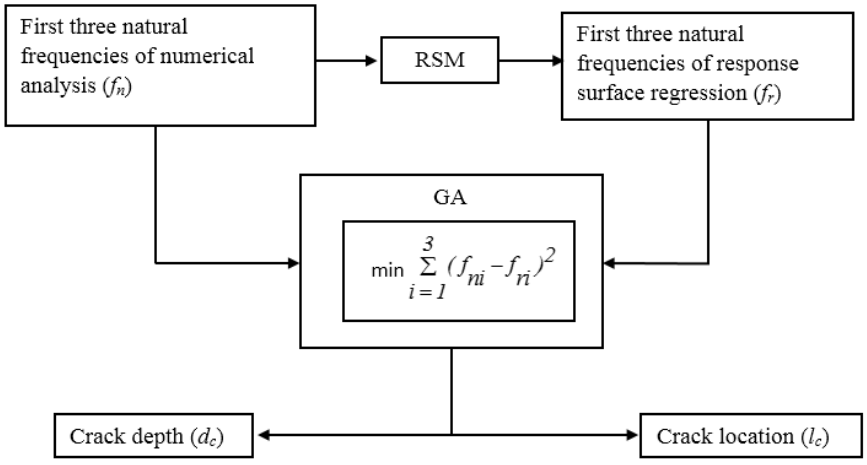

Figure4.11 Block diagram of RSM with GA technique

4.8 Summary

Total five optimizations techniques for crack investigation are described in this chapter namely.Name of those techniques are CANN, ANFIS, RSM, Contour Plot and GA. In addition, two hybrid crack detection techniques such as, RSM with GA and Neuro GA are described. These optimization techniques are employed in subsequent chapter to predict the location and magnitude of the crack by measuring the dynamic characteristics of the vibrating beam.

"*This page is intentionally left blank*"

Chapter 5

RESULTS AND DISCUSSION OF CRACK PARAMETER IDENTIFICATION BY OPTIMIZATION TECHNIQUES

5.1 Introduction, 5.2 Forward Problem 5.2.1 Crack identification of beam using cascade ANN, 5.2.2 Crack identification of beam using ANFIS, 5.3 Inverse Problem, 5.3.1 Crack parameter identification of isometric beam, 5.3.1.1 Crack parameter identification from first three natural frequencies using CANN, 5.3.1.2 Crack parameter identification of isometric beam from first three natural frequencies using ANFIS , 5.3.2 Crack parameter identification of FGM beam, 5.3.2.1 Crack parameter identification from first three natural frequencies using Frequency Contour, 5.3.2.2 Crack parameter identification from first three natural frequencies using RSM, 5.3.2.3 Crack parameter identification from first three natural frequencies using RSM with GA. 5.3.3 Crack parameter identification from experiment result, 5.3.3.1 Crack parameter identification from first four natural frequencies using CANN, 5.3.3.2. Crack parameter identification from first four natural frequencies using GA, 5.3.3.3 Crack parameter identification from first four natural frequencies using Neuro-GA hybrid technique, 5.4 Summary

5.1 Introduction

This section presents the results obtained from all optimization techniques described in chapter 4. An attempt is made to highlight the merit and demerit of those optimization techniques also. First the result of the forward problem is mentioned in section 5.2 followed by results of the inverse problem.

5.2 Forward Problem

Forward problem starts with the causes and then calculates the result. In case of forward problem, input parameters are normalised crack location and crack depth ratio, whereas output of optimization technique is relative natural frequencies. In this thesis, these output values are obtained by two methods namely, CANN and ANFIS. Finally, these values are compared with the output of numerical analysis of crack beam.

Total 80 numbers of cracked beams are considered with different crack parameters. The length (L), thickness (h) and width (w) of the beams are 1.6m, 0.1 m and 0.15 m respectively. The material of beam is chosen as aluminium with Young's modulus of 70 GPa, Poisson ratio of 0.33 and density of 2780 kg/m^3. Since the boundary condition is symmetrical

about mid-point of the beam, prediction analysis is performed on one half of the beam. Following the methods (CANN and ANFIS) mentioned in chapter 4. Percentage errors of predicted results are evaluated using the following equation.

$$Error\% = \left| \frac{Acual\ Value - \Pr edicted\ Value}{Actual\ Value} \right| \times 100 \qquad (5.1)$$

5.2.1 Crack identification of beam using CANN

For the identification of crack location and crack depth by CANN, forward backpropagation algorithm is used. In CANN forward back propagation model, a weight connection is connected from the input to each layer and from each layer to the successive layers. Before training, data sets are normalized between 0 and 1. The data sets having two input parameters (crack depth and location) and three target parameters (first three natural frequencies obtained from numerical analysis) are divided among training purpose and testing purpose. 64 sets of data are used for training purpose and 16 sets of data are utilized for testing purpose. The transigmoid hyperbolic function is used as an active function to reach the optimized result. In order to achieve best target accuracies number of neurons in a particular hidden layer and total number of hidden layers are varied. It is observed that best neural network model for this particular analysis is (2-1-3-3), i.e. 2 input, 3 output and 2 hidden layers in which first layer contains one neuron and second layer contains three neurons. Optimized results along with errors values of crack location and depth obtained from Cascade Artificial Neural Network (CANN) is shown in Table 5.1.

Table 5.1.a CANN result (Forward Problem)

Value of crack parameters		**Relative Natural Frequencies**								
		First			**Second**			**Third**		
Crack Location	**Crack Depth Ratio**	**NUM**	**CANN**	**Error (%)**	**NUM**	**CANN**	**Error (%)**	**NUM**	**CANN**	**Error (%)**
0.1	0.05	0.989	0.984	0.5409	0.993	0.987	0.5255	0.995	0.997	0.1747
0.1	0.1	0.993	0.991	0.1186	0.997	0.996	0.0396	0.999	1.000	0.0904
0.1	0.15	0.995	0.996	0.0807	0.999	0.999	0.0032	1.000	1.000	0.0003
0.1	0.2	0.997	0.998	0.0511	1.000	1.000	0.0365	0.999	1.000	0.0681
0.1	0.25	0.999	0.999	0.0020	1.000	1.000	0.0044	0.997	0.998	0.1189
0.1	0.3	1.000	0.999	0.0282	0.999	0.999	0.0745	0.996	0.995	0.0470
0.1	0.35	1.000	1.000	0.0358	0.997	0.998	0.1001	0.995	0.992	0.2881
0.1	0.4	1.000	1.000	0.0323	0.996	0.997	0.0749	0.996	0.994	0.1590
0.1	0.45	1.000	0.999	0.0162	0.995	0.995	0.0286	0.997	0.997	0.0337
0.1	0.5	0.999	0.999	0.0010	0.995	0.994	0.0932	0.999	0.999	0.0570
0.1	0.55	0.998	0.998	0.0180	0.995	0.993	0.2306	0.999	1.000	0.0354

Table 5.1.b CANN result (Forward Problem)

Value of crack parameters		Relative Natural Frequencies								
		First			Second			Third		
Crack Location	Crack Depth Ratio	NUM	CANN	Error (%)	NUM	CANN	Error (%)	NUM	CANN	Error (%)
0.1	0.6	0.997	0.0525	0.0014	0.996	0.994	0.1735	0.999	1.000	0.0792
0.1	0.65	0.996	0.0979	0.0048	0.997	0.998	0.0497	0.998	1.000	0.2034
0.1	0.7	0.996	0.1221	0.0075	0.999	0.999	0.0929	0.996	0.999	0.2674
0.1	0.75	0.995	0.0684	0.0023	0.999	1.000	0.0382	0.994	0.995	0.0405
0.1	0.8	0.995	0.1448	0.0105	1.000	1.000	0.0117	0.994	0.993	0.0485
0.2	0.05	0.966	0.3090	0.0477	0.977	0.974	0.3534	0.986	0.992	0.6854
0.2	0.1	0.976	0.2593	0.0336	0.989	0.991	0.1936	0.997	0.999	0.2549
0.2	0.15	0.985	0.5503	0.1514	0.997	0.998	0.0853	1.000	1.000	0.0215
0.2	0.2	0.991	0.3429	0.0588	1.000	0.999	0.0816	0.997	0.999	0.2567
0.2	0.25	0.996	0.1050	0.0055	0.999	0.999	0.0417	0.990	0.995	0.5192
0.2	0.3	0.999	0.0263	0.0003	0.995	0.998	0.3204	0.984	0.986	0.1993
0.2	0.35	1.000	0.0763	0.0029	0.989	0.992	0.2697	0.982	0.980	0.2326
0.2	0.4	1.000	0.0497	0.0012	0.984	0.986	0.1407	0.985	0.985	0.0210
0.2	0.45	0.998	0.0373	0.0007	0.981	0.984	0.3075	0.990	0.992	0.2263
0.2	0.5	0.995	0.1209	0.0073	0.980	0.983	0.2441	0.996	0.997	0.0640
0.2	0.55	0.992	0.1402	0.0098	0.982	0.982	0.0242	0.999	0.998	0.1002
0.2	0.6	0.989	0.1456	0.0106	0.986	0.985	0.0725	0.998	0.999	0.0495
0.2	0.65	0.987	0.2905	0.0422	0.990	0.992	0.2068	0.993	0.998	0.5166
0.2	0.7	0.984	0.4511	0.1018	0.995	0.998	0.2620	0.986	0.994	0.8195
0.2	0.75	0.983	0.3248	0.0528	0.999	0.999	0.0695	0.980	0.982	0.1894
0.2	0.8	0.982	0.3306	0.0546	1.000	1.000	0.0258	0.978	0.975	0.2649
0.3	0.05	0.935	0.0600	0.0018	0.958	0.957	0.1086	0.974	0.979	0.4552
0.3	0.1	0.953	0.4187	0.0877	0.980	0.984	0.3938	0.994	0.997	0.3327
0.3	0.15	0.969	0.9633	0.4639	0.994	0.996	0.1723	1.000	0.999	0.1084
0.3	0.2	0.982	0.6391	0.2042	1.000	0.998	0.1600	0.993	0.996	0.3695
0.3	0.25	0.992	0.2028	0.0206	0.997	0.998	0.0902	0.978	0.983	0.4743
0.3	0.3	0.998	0.0485	0.0012	0.988	0.994	0.5821	0.967	0.963	0.3995
0.3	0.35	1.000	0.1613	0.0130	0.977	0.977	0.0482	0.964	0.955	0.8563
0.3	0.4	0.999	0.1041	0.0054	0.966	0.960	0.7069	0.969	0.967	0.2038
0.3	0.45	0.995	0.0753	0.0028	0.960	0.956	0.4245	0.980	0.983	0.2366
0.3	0.5	0.990	0.1955	0.0191	0.958	0.958	0.0093	0.992	0.992	0.0474
0.3	0.55	0.983	0.0851	0.0036	0.962	0.961	0.1306	0.999	0.995	0.3821
0.3	0.6	0.977	0.1929	0.0186	0.970	0.968	0.2011	0.997	0.996	0.1416
0.3	0.65	0.971	0.1981	0.0196	0.980	0.982	0.2674	0.986	0.992	0.5683
0.3	0.7	0.966	0.2919	0.0426	0.990	0.994	0.4127	0.971	0.978	0.7478
0.3	0.75	0.963	0.5639	0.1590	0.997	0.998	0.0577	0.959	0.960	0.0832
0.3	0.8	0.962	0.0505	0.0013	1.000	0.998	0.1297	0.955	0.954	0.1200
0.4	0.05	0.897	0.0898	0.0040	0.938	0.936	0.1797	0.963	0.960	0.3626
0.4	0.1	0.925	0.4864	0.1183	0.969	0.971	0.2255	0.990	0.993	0.2223
0.4	0.15	0.949	0.2288	0.0262	0.990	0.992	0.1851	1.000	0.997	0.3197
0.4	0.2	0.970	0.1470	0.0108	1.000	0.997	0.2870	0.987	0.990	0.2479
0.4	0.25	0.986	0.1837	0.0169	0.995	0.997	0.1367	0.962	0.963	0.1294

Table 5.1.c CANN result (Forward Problem)

Value of crack parameters		Relative Natural Frequencies								
Crack Location	Crack Depth Ratio	First			Second			Third		
		NUM	CANN	Error (%)	NUM	CANN	Error (%)	NUM	CANN	Error (%)
0.4	0.3	0.996	0.993	0.3213	0.979	0.988	0.9173	0.943	0.938	0.4851
0.4	0.35	1.000	0.995	0.4409	0.958	0.961	0.2745	0.939	0.935	0.5041
0.4	0.4	0.998	0.995	0.3516	0.941	0.937	0.3223	0.949	0.951	0.1865
0.4	0.45	0.991	0.991	0.0454	0.930	0.928	0.2104	0.968	0.973	0.5425
0.4	0.5	0.981	0.983	0.2100	0.928	0.929	0.0451	0.987	0.987	0.0423
0.4	0.55	0.969	0.971	0.1376	0.935	0.935	0.0237	0.999	0.992	0.6526
0.4	0.6	0.957	0.956	0.1607	0.948	0.946	0.2195	0.995	0.993	0.2480
0.4	0.65	0.947	0.944	0.2604	0.965	0.967	0.2102	0.976	0.984	0.8248
0.4	0.7	0.939	0.939	0.0579	0.982	0.988	0.6145	0.951	0.951	0.0483
0.4	0.75	0.934	0.937	0.3487	0.995	0.996	0.0798	0.931	0.924	0.7238
0.4	0.8	0.932	0.929	0.2986	1.000	0.997	0.2504	0.924	0.927	0.3795
0.5	0.05	0.858	0.871	1.5350	0.920	0.924	0.4373	0.954	0.954	0.0119
0.5	0.1	0.894	0.888	0.6297	0.957	0.956	0.1731	0.987	0.989	0.2339
0.5	0.15	0.926	0.924	0.2387	0.986	0.985	0.1114	1.000	0.994	0.5824
0.5	0.2	0.955	0.957	0.2090	1.000	0.993	0.6545	0.980	0.979	0.0727
0.5	0.25	0.978	0.979	0.0587	0.993	0.991	0.1849	0.941	0.941	0.0312
0.5	0.3	0.993	0.991	0.2397	0.967	0.968	0.0829	0.915	0.917	0.2577
0.5	0.35	1.000	0.994	0.5643	0.934	0.929	0.5945	0.912	0.915	0.3224
0.5	0.4	0.997	0.992	0.4449	0.907	0.911	0.3549	0.928	0.930	0.1976
0.5	0.45	0.986	0.987	0.0804	0.893	0.904	1.2643	0.954	0.954	0.0508
0.5	0.5	0.969	0.974	0.5477	0.891	0.902	1.2143	0.981	0.975	0.6333
0.5	0.55	0.950	0.954	0.4031	0.902	0.905	0.3223	0.998	0.985	1.3283
0.5	0.6	0.931	0.929	0.1797	0.921	0.914	0.8470	0.993	0.986	0.6235
0.5	0.65	0.915	0.911	0.3553	0.946	0.935	1.2036	0.963	0.973	1.0419
0.5	0.7	0.902	0.902	0.0288	0.972	0.970	0.1784	0.926	0.928	0.1662
0.5	0.75	0.894	0.896	0.1664	0.992	0.990	0.1960	0.898	0.899	0.0707
0.5	0.8	0.892	0.889	0.2561	1.000	0.995	0.5228	0.887	0.896	0.9939

5.2.2 Crack identification of beam using ANFIS

In case of ANFIS, the same numbers of data sets are used for training and testing purposes has been carried out for CANN. The triangular and linear membership method is applied for training purpose. Hybrid optimization algorithm is applied for training Number of membership function considered for each parameter is three. ANFIS optimized results with error are shown in Table 5.2.

Table 5.2 a ANFIS result (Forward Problem)

Value of crack parameters		Relative Natural Frequencies								
Crack Location	Crack Depth Ratio	First			Second			Third		
		NUM	ANFIS	Error (%)	NUM	ANFIS	Error (%)	NUM	ANFIS	Error (%)
0.1	0.05	0.989	0.989	0.0188	0.993	0.993	0.0377	0.995	0.995	0.0125
0.1	0.1	0.993	0.993	0.0086	0.997	0.996	0.0342	0.999	1.000	0.0706

Table 5.2 b ANFIS result (Forward Problem)

Value of crack parameters		Relative Natural Frequencies								
		First			Second			Third		
Crack Location	Crack Depth Ratio	NUM	ANFIS	Error (%)	NUM	ANFIS	Error (%)	NUM	ANFIS	Error (%)
0.1	0.15	0.995	0.995	0.0141	0.999	0.999	0.0078	1.000	0.999	0.0902
0.1	0.2	0.997	0.997	0.0204	1.000	1.000	0.0109	0.999	0.998	0.0720
0.1	0.25	0.999	0.999	0.0110	1.000	1.000	0.0003	0.997	0.998	0.0458
0.1	0.3	1.000	0.999	0.0168	0.999	0.999	0.0086	0.996	0.997	0.1465
0.1	0.35	1.000	1.000	0.0000	0.997	0.997	0.0242	0.995	0.996	0.1231
0.1	0.4	1.000	1.000	0.0099	0.996	0.996	0.0107	0.996	0.995	0.0364
0.1	0.45	1.000	1.000	0.0156	0.995	0.994	0.0462	0.997	0.997	0.0229
0.1	0.5	0.999	0.999	0.0097	0.995	0.995	0.0159	0.999	0.998	0.0783
0.1	0.55	0.998	0.998	0.0039	0.995	0.995	0.0298	0.999	0.998	0.1226
0.1	0.6	0.997	0.997	0.0158	0.996	0.996	0.0195	0.999	0.998	0.0955
0.1	0.65	0.996	0.997	0.0069	0.997	0.997	0.0105	0.998	0.998	0.0022
0.1	0.7	0.996	0.996	0.0030	0.999	0.998	0.0271	0.996	0.997	0.0997
0.1	0.75	0.995	0.995	0.0347	0.999	0.999	0.0309	0.994	0.995	0.1268
0.1	0.8	0.995	0.997	0.1213	1.000	1.000	0.0231	0.994	0.994	0.0088
0.2	0.05	0.966	0.966	0.0367	0.977	0.977	0.0019	0.986	0.985	0.0117
0.2	0.1	0.976	0.976	0.0017	0.989	0.989	0.0594	0.997	1.001	0.4534
0.2	0.15	0.985	0.985	0.0139	0.997	0.998	0.0816	1.000	0.995	0.4499
0.2	0.2	0.991	0.991	0.0214	1.000	1.000	0.0042	0.997	0.991	0.5395
0.2	0.25	0.996	0.996	0.0278	0.999	0.999	0.0056	0.990	0.988	0.1989
0.2	0.3	0.999	0.999	0.0337	0.995	0.995	0.0081	0.984	0.985	0.1456
0.2	0.35	1.000	1.000	0.0016	0.989	0.990	0.0230	0.982	0.984	0.1735
0.2	0.4	1.000	1.000	0.0030	0.984	0.983	0.0988	0.985	0.983	0.1411
0.2	0.45	0.998	0.998	0.0045	0.981	0.979	0.2222	0.990	0.992	0.1864
0.2	0.5	0.995	0.995	0.0552	0.980	0.980	0.0152	0.996	0.996	0.0342
0.2	0.55	0.992	0.999	0.6757	0.982	0.983	0.0870	0.999	0.998	0.0968
0.2	0.6	0.989	0.989	0.0021	0.986	0.986	0.0438	0.998	0.998	0.0315
0.2	0.65	0.987	0.987	0.0285	0.990	0.990	0.0533	0.993	0.995	0.2264
0.2	0.7	0.984	0.985	0.0393	0.995	0.994	0.0757	0.986	0.991	0.4524
0.2	0.75	0.983	0.983	0.0171	0.999	0.997	0.1019	0.980	0.983	0.3298
0.2	0.8	0.982	0.983	0.0330	1.000	1.000	0.0231	0.978	0.974	0.3837
0.3	0.05	0.935	0.935	0.0109	0.958	0.959	0.0445	0.974	0.974	0.0193
0.3	0.1	0.953	0.954	0.0587	0.980	0.979	0.1103	0.994	1.000	0.6352
0.3	0.15	0.969	0.969	0.0245	0.994	0.996	0.1709	1.000	0.990	1.0003
0.3	0.2	0.982	0.982	0.0200	1.000	1.001	0.1191	0.993	0.982	1.1107
0.3	0.25	0.992	0.991	0.0539	0.997	0.997	0.0019	0.978	0.975	0.3029
0.3	0.3	0.998	0.997	0.0553	0.988	0.988	0.0106	0.967	0.971	0.4427
0.3	0.35	1.000	1.000	0.0241	0.977	0.977	0.0372	0.964	0.968	0.4874
0.3	0.4	0.999	0.999	0.0255	0.966	0.965	0.1282	0.969	0.968	0.1590
0.3	0.45	0.995	0.996	0.0783	0.960	0.957	0.3344	0.980	0.983	0.3049
0.3	0.5	0.990	0.989	0.0469	0.958	0.959	0.1008	0.992	0.991	0.1478
0.3	0.55	0.983	0.983	0.0143	0.962	0.964	0.2232	0.999	0.994	0.5257
0.3	0.6	0.977	0.977	0.0589	0.970	0.971	0.1097	0.997	0.993	0.4167
0.3	0.65	0.971	0.972	0.1224	0.980	0.979	0.0635	0.986	0.988	0.1659
0.3	0.7	0.966	0.967	0.0974	0.990	0.989	0.0947	0.971	0.978	0.7348
0.3	0.75	0.963	0.962	0.0472	0.997	0.995	0.1740	0.959	0.965	0.6189

Table 5.2 c ANFIS result (Forward Problem)

Value of crack parameters		Relative Natural Frequencies								
Crack Location	Crack Depth Ratio	First			Second			Third		
		NUM	ANFIS	Error (%)	NUM	ANFIS	Error (%)	NUM	ANFIS	Error (%)
0.3	0.8	0.962	0.961	0.0435	1.000	1.001	0.1318	0.955	0.948	0.6968
0.4	0.05	0.897	0.896	0.1565	0.938	0.940	0.1618	0.963	0.962	0.1395
0.4	0.1	0.925	0.926	0.1211	0.969	0.960	0.9059	0.990	1.015	2.4505
0.4	0.15	0.949	0.951	0.1634	0.990	0.988	0.2557	1.000	0.997	0.3329
0.4	0.2	0.970	0.971	0.0935	1.000	1.000	0.0189	0.987	0.981	0.6250
0.4	0.25	0.986	0.985	0.0176	0.995	0.996	0.0429	0.962	0.968	0.6563
0.4	0.3	0.996	0.995	0.0742	0.979	0.980	0.1223	0.943	0.958	1.5799
0.4	0.35	1.000	0.999	0.0486	0.958	0.960	0.1256	0.939	0.950	1.1168
0.4	0.4	0.998	0.999	0.0550	0.941	0.940	0.0312	0.949	0.944	0.5402
0.4	0.45	0.991	0.993	0.1468	0.930	0.927	0.2776	0.968	0.971	0.2955
0.4	0.5	0.981	0.980	0.1708	0.928	0.930	0.1447	0.987	0.982	0.5231
0.4	0.55	0.969	0.968	0.1740	0.935	0.937	0.2110	0.999	0.987	1.2170
0.4	0.6	0.957	0.957	0.0567	0.948	0.948	0.0275	0.995	0.985	1.0401
0.4	0.65	0.947	0.948	0.0696	0.965	0.964	0.1449	0.976	0.976	0.0368
0.4	0.7	0.939	0.940	0.0968	0.982	0.982	0.0060	0.951	0.961	1.1041
0.4	0.75	0.934	0.933	0.0791	0.995	0.993	0.1882	0.931	0.940	0.9660
0.4	0.8	0.932	0.932	0.0333	1.000	1.002	0.2405	0.924	0.913	1.1654
0.5	0.05	0.858	0.851	0.9011	0.920	0.937	1.9211	0.954	0.923	3.2559
0.5	0.1	0.894	0.893	0.0955	0.957	0.956	0.1583	0.987	1.006	1.8722
0.5	0.15	0.926	0.928	0.1690	0.986	0.988	0.1871	1.000	0.983	1.6822
0.5	0.2	0.955	0.956	0.0958	1.000	1.001	0.1378	0.980	0.964	1.6222
0.5	0.25	0.978	0.977	0.1108	0.993	0.991	0.1573	0.941	0.949	0.8346
0.5	0.3	0.993	0.991	0.2498	0.967	0.967	0.0250	0.915	0.936	2.3991
0.5	0.35	1.000	0.998	0.2133	0.934	0.934	0.0155	0.912	0.927	1.6742
0.5	0.4	0.997	0.997	0.0479	0.907	0.907	0.0073	0.928	0.921	0.7280
0.5	0.45	0.986	0.988	0.2656	0.893	0.891	0.1850	0.954	0.959	0.5786
0.5	0.5	0.969	0.967	0.2145	0.891	0.894	0.3037	0.981	0.975	0.6662
0.5	0.55	0.950	0.948	0.2250	0.902	0.905	0.3077	0.998	0.981	1.7658
0.5	0.6	0.931	0.931	0.0431	0.921	0.922	0.0460	0.993	0.978	1.4761
0.5	0.65	0.915	0.916	0.1232	0.946	0.945	0.1840	0.963	0.966	0.3068
0.5	0.7	0.902	0.903	0.0986	0.972	0.972	0.0182	0.926	0.946	2.0881
0.5	0.75	0.894	0.892	0.2177	0.992	0.988	0.4145	0.898	0.916	2.0743
0.5	0.8	0.892	0.891	0.0971	1.000	1.000	0.0231	0.887	0.879	0.9321

Table 5.3 shows the average and maximum percentage error of CANN and ANFIS analysis when compared with the output of numerical analysis. The table indicates that of predicted results error percentages are quite small for both the techniques. However, for the prediction of first two natural frequencies ANFIS is better than CANN whereas for the case of third frequency, reverse is true.

Comparative results of three natural frequencies obtained by optimization techniques along with three different crack depths are shown in Figure 5.1. Results show prediction of frequencies by both techniques match quite well with that of numerical and ANSYS analysis.

Table 5.3 Percentage errors of natural frequencies using CANN and ANFIS method

	CANN		ANFIS	
	Average Error	**Maximum Error**	**Average Error**	**Maximum Error**
First Mode	0.237%	1.534%	0.085%	0.901%
Second Mode	0.259%	1.264%	0.126%	1.921%
Third Mode	0.175%	1.328%	0.623%	3.256%

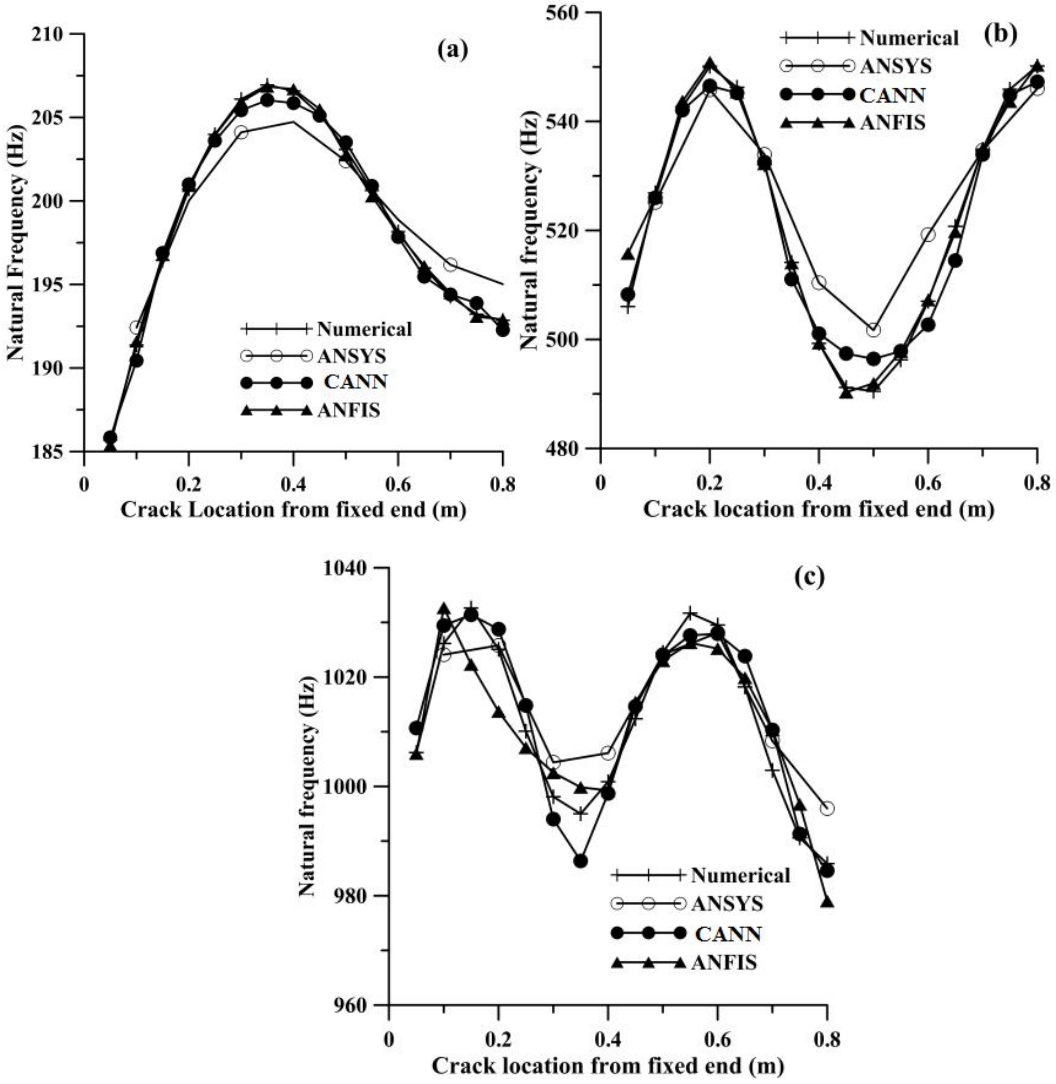

Figure 5.1 (a) First natural frequencies of clamped-clamped beams with an edge crack at varying locations for a crack size 0.04 m, (b) Second natural frequencies of clamped-clamped beams with an edge crack at varying locations for a crack size 0.05 m and (c) Third natural frequencies of clamped-clamped beams with an edge crack at varying locations for a crack size of 0.03 m

5.3 Inverse Problem

Inverse theory is capable of doing much more than just estimating model parameters. It can be used to estimate the quality of the predicted model parameters. It is very useful

because it generally provides information about a physical parameter that is difficult to observe in naked eyes. In inverse problem, a relationship is established between vibrational parameters and crack parameters. As a result unknown crack parameter can be evaluated with the help of known vibrational parameters obtained from numerical analysis or experimental investigation. In section 5.3.1 and 5.3.2 crack parameters are identified for isometric and FGM beams respectively based on numerical analysis. In section 5.3.3, crack parameters of isometric beams are determined based on experimental results.

5.3.1 Crack parameter identification of isometric beam

Crack parameters of isometric beams are predicted using two different optimization techniques namely, CANN and ANFIS. Physical and material properties are same as describe in 5.2 section.

5.3.1.1 Crack parameter identification from first three natural frequencies using CANN

A total number of 56 data patterns are used for training network. The tansigmoid hyperbolic function is used as an activation function to reach the optimized result. In order to achieve best target accuracy number of neurons in a hidden layer and total numbers of hidden layers are varied.

Neural network model for this analysis is (3-4-2) i.e. neurons of input, hidden and output are 3, 4 and 2 respectively. It has been observed that the best value of regression (R) analysis is found to be 0.99865 as shown in Figure 5.2.

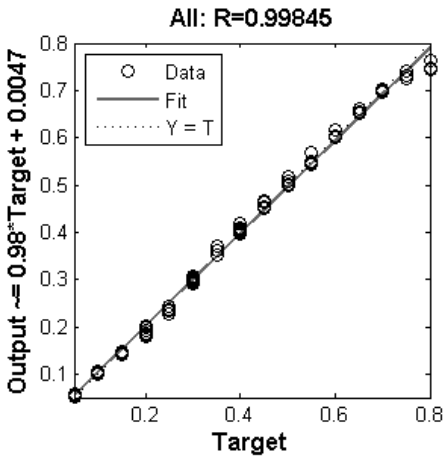

Figure 5.2 Regression plot of CANN for natural frequencies and crack parameter network

Table 5.4 a CANN result (Inverse Problem)

Output of Numerical analysis			**Input in Numerical analysis**		**CANN Output**		**Error %**	
Relative natural frequencies			**Crack parameter**		**Crack parameter**		**Depth**	**Location**
			Depth (m)	**Location (m)**	**Depth (m)**	**Location (m)**		
First	**Second**	**Third**	d_c	l_c	d_c^*	l_c^*	E_h^*	E_L^*
0.989	0.991	0.981	0.01	0.05	0.015	0.048	4.890	0.10
0.992	0.994	0.985	0.01	0.1	0.014	0.233	4.375	8.30
0.995	0.997	0.985	0.01	0.15	0.014	0.239	3.590	5.59
0.997	0.998	0.984	0.01	0.2	0.013	0.405	2.760	12.78
0.998	0.998	0.983	0.01	0.25	0.012	0.537	2.222	17.96
0.999	0.997	0.983	0.01	0.3	0.012	0.509	2.117	13.06
1.000	0.995	0.982	0.01	0.35	0.012	0.446	2.163	5.98
1.000	0.994	0.981	0.01	0.4	0.012	0.439	2.124	2.42
1.000	0.992	0.982	0.01	0.45	0.012	0.472	2.078	1.35
0.999	0.993	0.983	0.01	0.5	0.012	0.490	2.183	0.64
0.998	0.993	0.984	0.01	0.55	0.012	0.477	2.398	4.57
0.997	0.994	0.984	0.01	0.6	0.013	0.473	2.568	7.94
0.996	0.995	0.983	0.01	0.65	0.013	0.512	2.682	8.64
0.996	0.996	0.982	0.01	0.7	0.013	0.575	2.878	7.81
0.995	0.997	0.981	0.01	0.75	0.013	0.618	3.177	8.23
0.996	0.998	0.979	0.01	0.8	0.013	0.631	3.336	10.56
0.966	0.975	0.971	0.02	0.05	0.026	0.248	5.651	12.38
0.976	0.987	0.987	0.02	0.1	0.025	0.051	5.423	3.09
0.985	0.996	0.981	0.02	0.15	0.020	0.052	0.235	6.15
0.991	0.998	0.977	0.02	0.2	0.016	0.257	4.448	3.55
0.996	0.997	0.974	0.02	0.25	0.014	0.516	5.529	16.60
0.999	0.992	0.971	0.02	0.3	0.020	0.231	0.434	4.34
1.000	0.987	0.970	0.02	0.35	0.022	0.353	1.900	0.18
0.999	0.981	0.969	0.02	0.4	0.021	0.394	0.920	0.39
0.998	0.977	0.978	0.02	0.45	0.018	0.371	2.453	4.97
0.995	0.978	0.982	0.02	0.5	0.015	0.479	5.044	1.30
0.999	0.981	0.984	0.02	0.55	0.015	0.588	4.516	2.39
0.989	0.984	0.984	0.02	0.6	0.016	0.530	4.186	4.35
0.987	0.988	0.981	0.02	0.65	0.016	0.552	4.198	6.10
0.985	0.992	0.976	0.02	0.7	0.019	0.772	0.786	4.49
0.983	0.995	0.969	0.02	0.75	0.024	0.792	3.516	2.61
0.983	0.998	0.960	0.02	0.8	0.025	0.792	4.780	0.51
0.935	0.957	0.960	0.03	0.05	0.042	0.102	11.650	3.23
0.954	0.976	0.986	0.03	0.1	0.039	0.050	9.056	3.12
0.969	0.993	0.976	0.03	0.15	0.032	0.050	1.685	6.25
0.982	0.999	0.967	0.03	0.2	0.024	0.165	6.033	2.19
0.991	0.995	0.961	0.03	0.25	0.028	0.221	2.294	1.80
0.997	0.986	0.957	0.03	0.3	0.031	0.327	1.183	1.67
1.000	0.975	0.954	0.03	0.35	0.026	0.339	4.443	0.66
0.999	0.963	0.954	0.03	0.4	0.028	0.366	1.984	2.12
0.996	0.955	0.969	0.03	0.45	0.034	0.476	4.211	1.65

Table 5.4 b CANN result (Inverse Problem)

Output of Numerical analysis			**Input in Numerical analysis**		**CANN Output**		**Error %**	
Relative natural frequencies			**Crack parameter**		**Crack parameter**		**Depth**	**Location**
			Depth (m)	**Location (m)**	**Depth (m)**	**Location (m)**		
First	**Second**	**Third**	d_c	l_c	d_c^*	l_c^*	E_h^*	E_L^*
0.989	0.957	0.976	0.03	0.5	0.03	0.503	0.050	0.19
0.983	0.962	0.979	0.03	0.55	0.029	0.664	1.372	7.15
0.977	0.969	0.978	0.03	0.6	0.027	0.587	2.687	0.84
0.972	0.977	0.973	0.03	0.65	0.023	0.530	7.269	7.49
0.967	0.987	0.964	0.03	0.7	0.027	0.800	2.624	6.25
0.962	0.993	0.951	0.03	0.75	0.029	0.800	1.064	3.12
0.961	0.999	0.934	0.03	0.8	0.03	0.799	0.098	0.05
0.896	0.937	0.948	0.04	0.05	0.05	0.056	9.593	0.39
0.926	0.958	1.000	0.04	0.1	0.045	0.051	4.780	3.08
0.951	0.986	0.982	0.04	0.15	0.041	0.050	1.390	6.23
0.970	0.998	0.967	0.04	0.2	0.034	0.206	6.142	0.35
0.985	0.994	0.954	0.04	0.25	0.035	0.069	4.769	11.32
0.995	0.978	0.944	0.04	0.3	0.041	0.267	1.474	2.04
0.999	0.958	0.936	0.04	0.35	0.038	0.398	1.946	2.98
0.999	0.938	0.931	0.04	0.4	0.041	0.401	0.779	0.08
0.993	0.925	0.957	0.04	0.45	0.041	0.443	1.492	0.44
0.979	0.928	0.968	0.04	0.5	0.044	0.367	4.307	8.29
0.968	0.935	0.972	0.04	0.55	0.046	0.646	5.726	6.00
0.957	0.946	0.970	0.04	0.6	0.042	0.569	1.618	1.91
0.947	0.961	0.962	0.04	0.65	0.033	0.643	7.058	0.42
0.939	0.980	0.947	0.04	0.7	0.042	0.800	2.118	6.25
0.933	0.991	0.926	0.04	0.75	0.044	0.800	3.649	3.12
0.932	1.000	0.900	0.04	0.8	0.044	0.800	3.890	0.01
0.850	0.935	0.909	0.05	0.05	0.05	0.052	0.264	0.14
0.893	0.954	0.991	0.05	0.1	0.046	0.064	4.213	2.22
0.928	0.986	0.969	0.05	0.15	0.046	0.052	4.338	6.12
0.956	0.999	0.950	0.05	0.2	0.036	0.267	14.226	4.16
0.977	0.989	0.935	0.05	0.25	0.042	0.052	8.163	12.40
0.991	0.965	0.923	0.05	0.3	0.049	0.306	0.849	0.36
0.998	0.932	0.914	0.05	0.35	0.049	0.339	1.058	0.71
0.997	0.905	0.908	0.05	0.4	0.049	0.367	0.535	2.09
0.988	0.889	0.945	0.05	0.45	0.049	0.463	0.808	0.80
0.967	0.892	0.960	0.05	0.5	0.048	0.507	1.716	0.43
0.948	0.903	0.967	0.05	0.55	0.049	0.571	0.629	1.30
0.931	0.920	0.964	0.05	0.6	0.046	0.351	4.102	15.56
0.916	0.942	0.952	0.05	0.65	0.049	0.620	1.011	1.88
0.903	0.970	0.932	0.05	0.7	0.049	0.800	0.878	6.25
0.892	0.986	0.903	0.05	0.75	0.049	0.800	0.688	3.12
0.891	0.998	0.866	0.05	0.8	0.049	0.800	0.566	0.00
Crack Depth Average Error 3.275% Maximum Error 14.23% Crack Location Average Error 4.34% Maximum Error 17.96%								

Once prediction of crack location and depth are obtained from CANN, they are compared with input crack parameters and the percentage of errors are computed by following equation

$$E_h^* = \left| \frac{d_c - d_c^*}{h} \right| \times 100; E_L^* = \left| \frac{l_c - l_c^*}{L} \right| \times 100 \tag{5.2}$$

Where d_c and l_c are the actual crack depth and crack location, respectively, d_c^* and l_c^* are the predicted crack depth and crack location, respectively, found by CANN.

The values of crack location and crack depth are obtained from CANN using first three relative natural frequencies of the beams as input to the optimization process. The frequencies are obtained from numerical analysis with known crack depths and locations. Deviation of CANN optimized results from the actual crack location and its depth values used during analysis are shown in Table 5.4. Result shows that an average error is less than 5% for both crack location and depth. In a few cases errors are significant (greater than 10%) especially for the prediction of location. Overall optimization results are reasonably close to actual crack parameters.

Table 5.5 Actual and predicted results of cracked clamped-clamped beams using CANN

Case Number	Crack depth and location from fixed end in meter (Numerical input)	Relative Natural Frequency	Predicted crack depth and location from fixed end in meter (From CANN output)	Error (%)
1	d_c =0.01 l_c=0.175	First - 0.973917 second-0.996864 Third-0.997766	d_c^* =0.013 l_c^* =0.031	E_h^* =3.1 E_L^* =8.46
2	d_c=0.01 l_c=0.375	First - 1 Second-0.968174 Third-0.956722	d_c^* =0.012 l_c^* =0.044	E_h^* =2.1 E_L^* =3.75
3	d_c =0.01 l_c=0.775	First - 0.967948 Second-0.996362 Third-0.946015	d_c^* =0.013 l_c^* =0.625	E_h^* =3.3 E_L^* =9.34
4	d_c=0.03 l_c=0.175	First - 0.830731 Second-0.981365 Third-0.978877	d_c^* =0.03 l_c^* =0.05	E_h^* =0.02 E_L^* =7.78
5	d_c =0.03 l_c=0.375	First - 0.99926 Second-0.73565 Third-0.693592	d_c^* =0.034 l_c^* =0.26	E_h^* =4.22 E_L^* =2.19
6	d_c=0.03 l_c=0.775	First - 0.73458 Second-0.980897 Third-0.618174	d_c^* =0.03 l_c^* =0.8	E_h^* =0.14 E_L^* =1.54

In the next stage, an attempt is made to identify unknown crack parameter (crack depth and location) of a using CANN when natural frequencies are fed as input. Table 5.5 shows predicted crack parameters for six different clamped-clamped beams. Result shows that all error percentage is moderate (less than 10%) for all cases. In a few cases, errors are quite less. It may be highlighted that prediction of crack depth is better than that of crack location. This is due to the fact that relations between relative natural frequencies and crack locations are very complex. Overall this method is quite relevant for detection of crack in clamped–clamped beam.

5.3.1.2 Crack parameter identification of isometric beam from first three natural frequencies using ANFIS

Crack locations with its depths are used as an input to ANFIS. Numerical results of first three natural frequencies are used as an output of ANFIS. Total 56 data pattern are used for training network. Total 12 data pattern are used for testing and the rest for checking purpose. The Gaussian and constant membership functions are used for input data and output data respectively. Hybrid optimization method is applied for training. Number of membership function considered for each parameter is five. Therefore number of fuzzy rule is $(5)^3$ i.e. 125. Structure of this ANFIS model is shown in Figure 5.3.

After 1012 epochs, model gives optimal results. The corresponding value of training error is found to be 0.0152. Once prediction of crack location and depth are obtained from ANFIS, they are compared with numerical results and the percentage of errors are computed by following equation

$$E_h^* = \left| \frac{d_c - d_c^{**}}{h} \right| \times 100; E_L^* = \left| \frac{l_c - l_c^{**}}{L} \right| \times 100 \qquad (5.3)$$

where d_c and l_c are the actual crack depth and crack location, respectively, d_c^{**} and l_c^{**} are the predicted crack depth and crack location, respectively, found by ANFIS.

From the ANFIS optimized analysis, deviation of the crack parameters from crack location and its depth values used in numerical analysis are shown in Table 5.6. Result shows that an average error for prediction of crack depth size is very less (less than 3%) where as an average error for prediction of crack location is not very small (near 9%). In a few cases, errors are quite large (greater than 20%) especially for the prediction of location. Overall performance of optimization of ANFIS is less than CANN method. Performance can be

improved by rising membership number and fuzzy rule number. However increase of membership by any extent is impractical for structural health monitoring. Increase of fuzzy rule leads to increase in operation time and complexity as large number of fuzzy rule means more processing time.

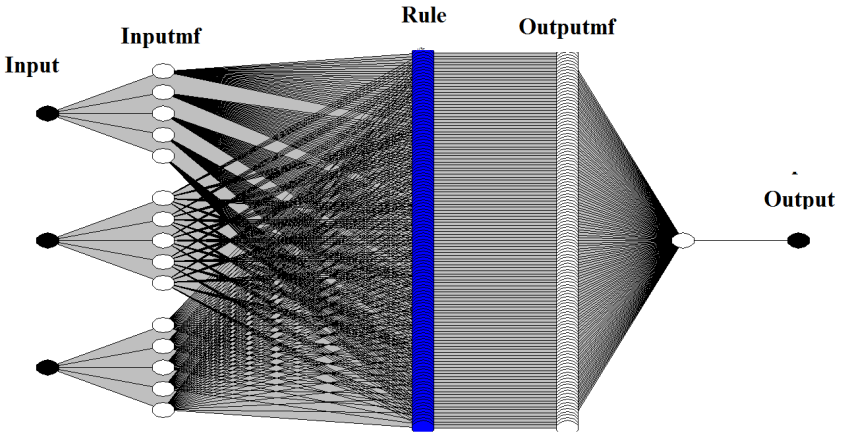

Figure 5.3 ANFIS model structure

Table 5.6 a ANFIS result (Inverse Problem)

Output of Numerical analysis			**Input in Numerical analysis**		**ANFIS Output**		**Error %**	
Relative natural frequencies			**Crack parameter**		**Crack parameter**		**Depth**	**Location**
			Depth (m)	**Location (m)**	**Depth (m)**	**Location (m)**		
0.989	0.991	0.981	0.01	0.05	0.0171	0.039	7.1	0.69
0.992	0.994	0.985	0.01	0.1	0.0114	0.036	1.4	4.00
0.995	0.997	0.985	0.01	0.15	0.0092	0.378	0.77	14.25
0.997	0.998	0.984	0.01	0.2	0.0082	0.051	1.8	9.31
0.998	0.998	0.983	0.01	0.25	0.008	0.458	1.97	13.00
0.999	0.997	0.983	0.01	0.3	0.0086	0.258	1.4	2.63
1.000	0.995	0.982	0.01	0.35	0.0096	0.291	0.37	3.69
1.000	0.994	0.981	0.01	0.4	0.0113	0.396	1.3	0.25
1.000	0.992	0.982	0.01	0.45	0.0107	0.434	0.7	1.00
0.999	0.993	0.983	0.01	0.5	0.0101	0.465	0.1	2.19
0.998	0.993	0.984	0.01	0.55	0.0099	0.472	0.07	4.88
0.997	0.994	0.984	0.01	0.6	0.0098	0.459	0.16	8.81
0.996	0.995	0.983	0.01	0.65	0.0102	0.426	0.2	14.00
0.996	0.996	0.982	0.01	0.7	0.0107	0.439	0.7	16.31
0.995	0.997	0.981	0.01	0.75	0.0118	0.374	1.8	23.50
0.996	0.998	0.979	0.01	0.8	0.0121	0.390	2.1	25.63
0.966	0.975	0.971	0.02	0.05	0.0321	0.282	12.1	14.50
0.976	0.987	0.987	0.02	0.1	0.022	0.410	2	19.38
0.985	0.996	0.981	0.02	0.15	0.0177	0.196	2.3	2.88
0.991	0.998	0.977	0.02	0.2	0.0165	0.199	3.5	0.06

Table 5.6 b ANFIS result (Inverse Problem)

Output of Numerical analysis			**Input in Numerical analysis**		**ANFIS Output**		**Error %**	
Relative natural frequencies			**Crack parameter**		**Crack parameter**		**Depth**	**Location**
			Depth (m)	**Location (m)**	**Depth (m)**	**Location (m)**		
0.996	0.997	0.974	0.02	0.25	0.0173	0.353	2.7	6.44
0.999	0.992	0.971	0.02	0.3	0.0193	0.233	0.7	4.19
1.000	0.987	0.970	0.02	0.35	0.0215	0.319	1.5	1.94
0.999	0.981	0.969	0.02	0.4	0.0235	0.249	3.5	9.44
0.998	0.977	0.978	0.02	0.45	0.0206	0.378	0.6	4.50
0.995	0.978	0.982	0.02	0.5	0.0188	0.506	1.2	0.38
0.999	0.981	0.984	0.02	0.55	0.0153	0.339	4.7	13.19
0.989	0.984	0.984	0.02	0.6	0.0179	0.643	2.1	2.69
0.987	0.988	0.981	0.02	0.65	0.0191	0.366	0.9	17.75
0.985	0.992	0.976	0.02	0.7	0.0214	0.497	1.4	12.69
0.983	0.995	0.969	0.02	0.75	0.0255	0.520	5.5	14.38
0.983	0.998	0.960	0.02	0.8	0.0304	0.537	10.4	16.44
0.935	0.957	0.960	0.03	0.05	0.0363	0.05	6.3	0.00
0.954	0.976	0.986	0.03	0.1	0.0344	0.349	4.4	15.56
0.969	0.993	0.976	0.03	0.15	0.0284	0.588	1.6	27.38
0.982	0.999	0.967	0.03	0.2	0.0263	0.502	3.7	18.88
0.991	0.995	0.961	0.03	0.25	0.0282	0.394	1.8	9.00
0.997	0.986	0.957	0.03	0.3	0.0308	0.393	0.8	5.81
1.000	0.975	0.954	0.03	0.35	0.0323	0.400	2.3	3.13
0.999	0.963	0.954	0.03	0.4	0.0327	0.403	2.7	0.19
0.996	0.955	0.969	0.03	0.45	0.0304	0.479	0.4	1.81
0.989	0.957	0.976	0.03	0.5	0.0291	0.454	0.9	2.88
0.983	0.962	0.979	0.03	0.55	0.028	0.450	2	6.25
0.977	0.969	0.978	0.03	0.6	0.0282	0.453	1.8	9.19
0.972	0.977	0.973	0.03	0.65	0.0297	0.375	0.3	17.19
0.967	0.987	0.964	0.03	0.7	0.033	0.454	3	15.38
0.962	0.993	0.951	0.03	0.75	0.0368	0.545	6.8	12.81
0.961	0.999	0.934	0.03	0.8	0.0403	0.489	10.3	19.44
0.896	0.937	0.948	0.04	0.05	0.04	0.5	0	28.13
0.926	0.958	1.000	0.04	0.1	0.039	0.504	1	25.25
0.951	0.986	0.982	0.04	0.15	0.0373	0.431	2.7	17.56
0.970	0.998	0.967	0.04	0.2	0.0306	0.513	9.4	19.56
0.985	0.994	0.954	0.04	0.25	0.0337	0.574	6.3	20.25
0.995	0.978	0.944	0.04	0.3	0.0379	0.550	2.1	15.63
0.999	0.958	0.936	0.04	0.35	0.0364	0.327	3.6	1.44
0.999	0.938	0.931	0.04	0.4	0.0391	0.416	0.9	1.00
0.993	0.925	0.957	0.04	0.45	0.0394	0.528	0.6	4.88
0.979	0.928	0.968	0.04	0.5	0.0403	0.569	0.3	4.31
0.968	0.935	0.972	0.04	0.55	0.0405	0.602	0.5	3.25
0.957	0.946	0.970	0.04	0.6	0.0337	0.604	6.3	0.25

Table 5.6 c ANFIS result (Inverse Problem)

Output of Numerical analysis			**Input in Numerical analysis**		**ANFIS Output**		**Error %**	
Relative natural frequencies			**Crack parameter**		**Crack parameter**		**Depth**	**Location**
			Depth (m)	**Location (m)**	**Depth (m)**	**Location (m)**		
0.947	0.961	0.962	0.04	0.65	0.0364	0.400	3.6	15.63
0.939	0.980	0.947	0.04	0.7	0.0377	0.606	2.3	5.88
0.933	0.991	0.926	0.04	0.75	0.04	0.648	0	6.38
0.932	1.000	0.900	0.04	0.8	0.04	0.655	0	9.06
0.850	0.935	0.909	0.05	0.05	0.0568	0.001	6.8	3.06
0.893	0.954	0.991	0.05	0.1	0.0503	0.387	0.3	17.94
0.928	0.986	0.969	0.05	0.15	0.0505	0.15	0.5	0.00
0.956	0.999	0.950	0.05	0.2	0.0375	0.2	12.5	0.00
0.977	0.989	0.935	0.05	0.25	0.0424	0.249	7.6	0.06
0.991	0.965	0.923	0.05	0.3	0.05	0.3	0	0.00
0.998	0.932	0.914	0.05	0.35	0.0502	0.659	0.2	19.31
0.997	0.905	0.908	0.05	0.4	0.05	0.4	0	0.00
0.988	0.889	0.945	0.05	0.45	0.0503	0.751	0.3	18.81
0.967	0.892	0.960	0.05	0.5	0.0499	0.765	0.1	16.56
0.948	0.903	0.967	0.05	0.55	0.0689	0.102	18.9	28.00
0.931	0.920	0.964	0.05	0.6	0.0504	0.415	0.4	11.56
0.916	0.942	0.952	0.05	0.65	0.0499	0.664	0.1	0.88
0.903	0.970	0.932	0.05	0.7	0.0498	0.799	0.2	6.19
0.892	0.986	0.903	0.05	0.75	0.05	0.799	0	3.06
0.891	0.998	0.866	0.05	0.8	0.0499	0.804	0.1	0.25
Crack Depth Average Error 2.67% Maximum Error 18.9% Crack Location Average Error 9.42% Maximum Error 28.13%								

In order to determine unknown crack parameter from arbitrary cracked beam with known natural frequencies, results are simulated with ANFIS model. Six sets unknown crack parameters (location and depth) are predicted for six clamped –clamped beam having crack with different depth and locations. Result shown in Table 5.7 indicates that in a few cases errors are high (greater than 15 %) otherwise errors are moderate (less than10%). Overall this method is quite reasonable for detection of crack especially for clamped–clamped beam.

Table 5.7 Actual and predicted results of cracked clamped-clamped beams using ANFIS

Case Number	Crack depth and location from fixed end in meter (Numerical input)	Relative Natural Frequency	Predicted crack depth and location from fixed end in meter (From ANFIS output)	Error %
1	d_c =0.01 l_c=0.175	First - 0.973917 second-0.996864 Third-0.997766	d_c^{**} =0.007 l_c^{**} =0.045	E_h^{**} =2.9 E_L^{**} =17.19
2	d_c=0.01 l_c=0.375	First - 1 Second-0.968174 Third-0.956722	d_c^{**} =0.012 l_c^{**} =0.395	E_h^{**} =2.2 E_L^{**} =1.25
3	d_c =0.01 l_c=0.775	First - 0.967948 Second-0.996362 Third-0.946015	d_c^{**} =0.013 l_c^{**} =0.575	E_h^{**} =2.9 E_L^{**} =12.5
4	d_c=0.03 l_c=0.175	First - 0.830731 Second-0.981365 Third-0.978877	d_c^{**} =0.014 l_c^{**} =0.465	E_h^{**} =15.60 E_L^{**} =18.13
5	d_c =0.03 l_c=0.375	First - 0.99926 Second-0.73565 Third-0.693592	d_c^{**} =0.031 l_c^{**} =0.391	E_h^{**} =1.3 E_L^{**} =1
6	d_c=0.03 l_c=0.775	First - 0.73458 Second-0.980897 Third-0.618174	d_c^{**} =0.02 l_c^{**} =0.754	E_h^{**} =10.10 E_L^{**} =1.31

5.3.2 Crack parameter identification of FGM beam

In this section, an attempt is made to identify the crack parameters of FGM beam using frequency contour plot, RSM and RSM with GA.

Geometric and material properties of beam are taken as E_1=70 GPa, ν=0.33, ρ_1=2780 Kg/m^3, L/h=16, h=0.1 m, d_c/h =0.2 & 0.4, ι =5/6. ι represents correlation factor between two layers.

First three natural frequencies of cracked clamped-clamped beam and cantilever beam with different crack size and two material gradient k=5 and k=0.2 are obtain by numerical analysis. Now crack parameters are evaluated with the help of known first three natural frequencies using different methods mentioned in the following section.

5.3.2.1 Crack parameter identification from first three natural frequencies using Frequency Contour Plot

For prediction of crack using frequency contour method, different crack conditions with crack sizes are considered at three different crack locations of the beams. In case of clamped–clamped beam, cracks are situated at 0.0175, 0.375 and 0.775 m from the fixed end

with crack sizes (d_c= 0.01 and 0.03) whereas for cantilever beam, they are supposed to be at 0.15, 0.45 and 1.25 m from the fixed end with crack sizes (d_c= 0.02 and 0.04), respectively.

Figures 5.4 and 5.5 show contour plots of normalised natural frequencies for clamped–clamped beam (k = 0.2) and cantilever beam (k = 5) with various normalised crack location and normalised crack depth, respectively. All three frequencies for a particular value of crack depth oscillate as the crack location moves from the fixed end to another fixed end (Figure 5.4). Number of oscillations increases with mode number. Since the boundary condition is symmetric about mid-point of the beam, contour plots of normalised frequencies are also symmetrical for clamped–clamped beam. For Figure 5.5 (a), it is observed that first normalised natural frequency is monotonically increased as the crack location moves from the fixed end to the free end for a particular value of crack depth. On the other hand, the second and third natural frequencies oscillate under the same situations (Figure 5.5 (b) and (c)). Normalised natural frequency is not only a function of crack depth, and crack location, but also of the different mode number

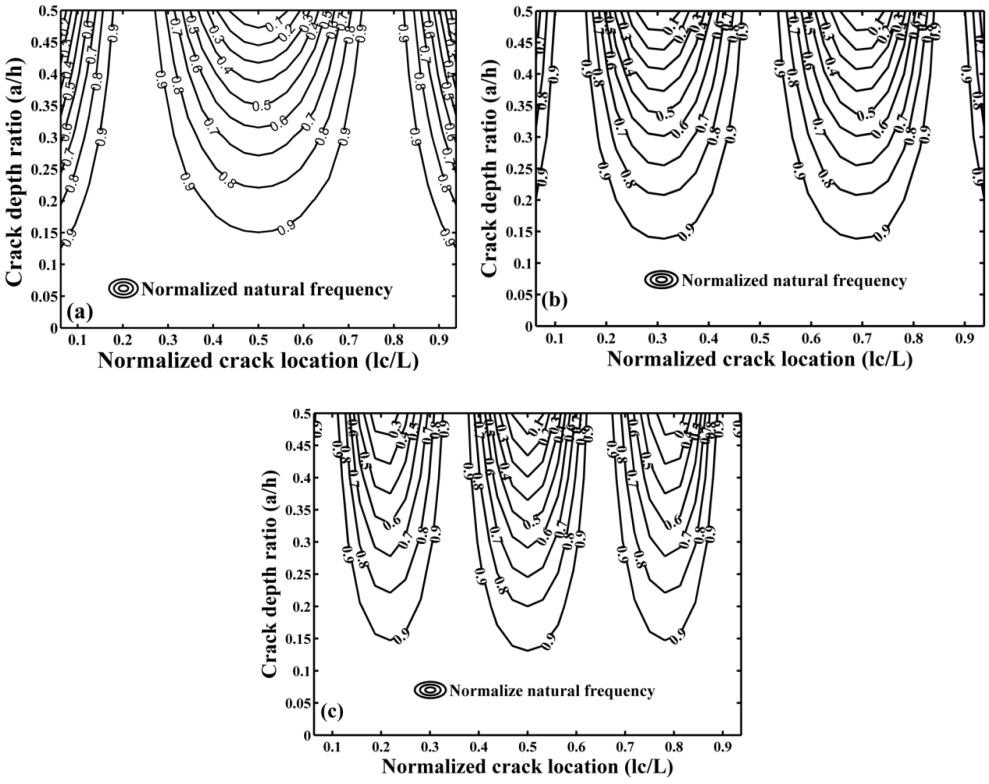

Figure 5.4 First natural frequency contour plots for clamped–clamped FGM beam (k = 0.2) with single transverse crack, (b) second natural frequency contour plots for clamped–clamped FGM beam (k = 0.2) with single transverse crack and (c) third natural frequency contour plots for clamped–clamped FGM beam (k = 0.2) with single transverse crack.

The location and size corresponding to any point on the curve (Figures 5.4 and 5.5) would become the possible crack location and size. So for a single crack beam, two reference normalised frequencies are theoretically sufficient to predict two unknown parameters, say, crack location and depth.

Figure 5.6 shows prediction of crack location and size with help of frequency contour curve for six different crack scenarios of clamped–clamped beam with material gradient k = 0.2. Being symmetric on about the mid-point, half of the beam is analysis for prediction of crack. Figure 5.7 shows prediction of crack location and size with help of frequency contour curve for six different crack scenarios of cantilever beam with material gradient k = 5.

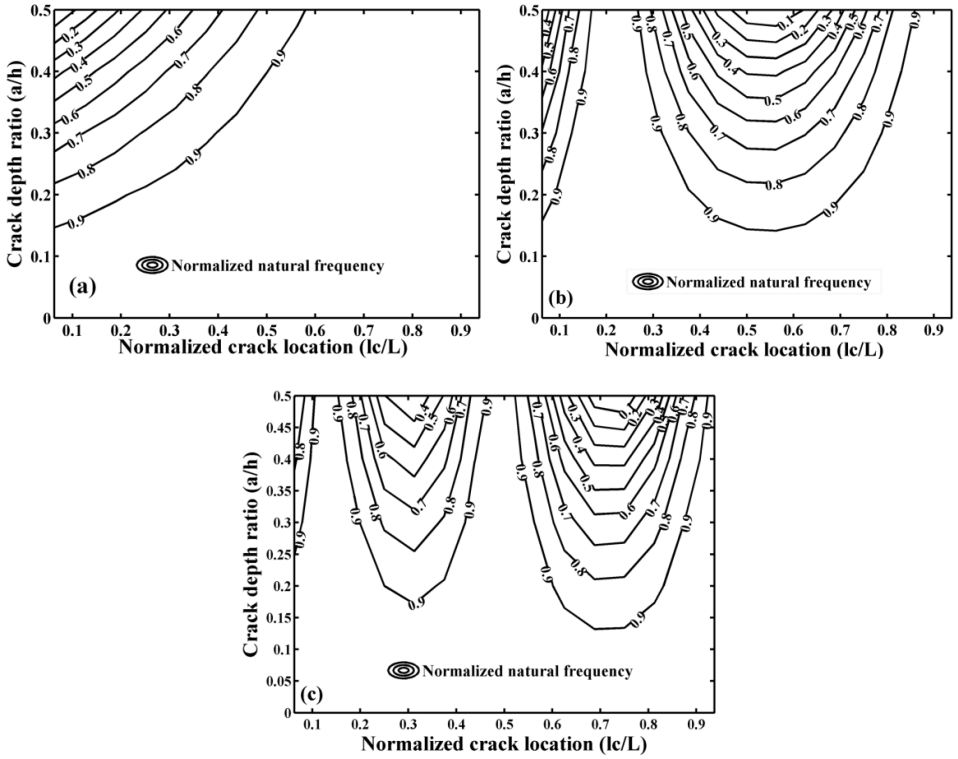

Figure 5.5 First natural frequency contour plots for cantilever FGM beam (k = 5) with single transverse crack, (b) second natural frequency contour plots for cantilever FGM beam (k = 5) with single transverse crack and (c) third natural frequency contour plots for cantilever FGM beam (k = 5) with single transverse crack.

However, in a few cases, the three contour curves do not intersect at one point. Due to the presence of the measurement and modelling errors, pairs of contour lines intersected three different points and produced a triangle. The centroid of this triangle is taken as the crack location and depth. Another difficulty is observed in some cases where two sets of three pairs of intersections are present (Figure 5.6 (c)). In that case, smaller triangle is considered for crack prediction.

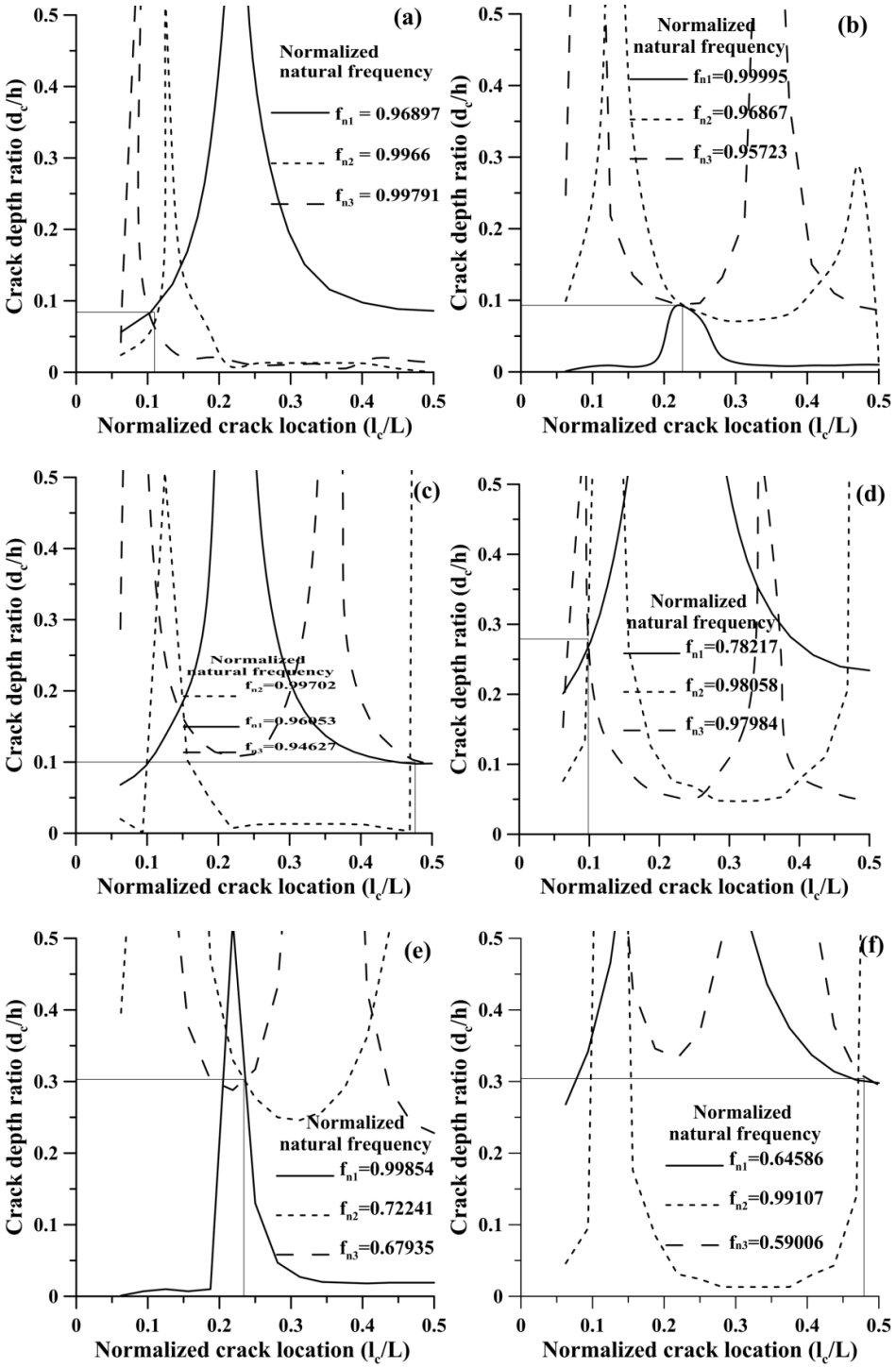

Figure 5.6 (a) Crack prediction using frequency contours of first natural frequencies in clamped-clamped beam (first —, second -----, third——): case 1, (b) Crack prediction using frequency contours of first natural frequencies in clamped-clamped beam (frist —, second -----, third ——): case 2, (c) Crack prediction using frequency contours of first natural frequencies in clamped-clamped beam (frist —, second -----, third ——): case 3, (d) Crack prediction using frequency contours of first natural frequencies in clamped-clamped beam (frist —, second -----, third ——): case 4, (e) Crack prediction using frequency contours of first natural frequencies in cantilever beam (first —, second -----, third — —): case 5, (f) Crack prediction using frequency contours of first natural frequencies in cantilever beam (first —, second -----, third — —): case 6.

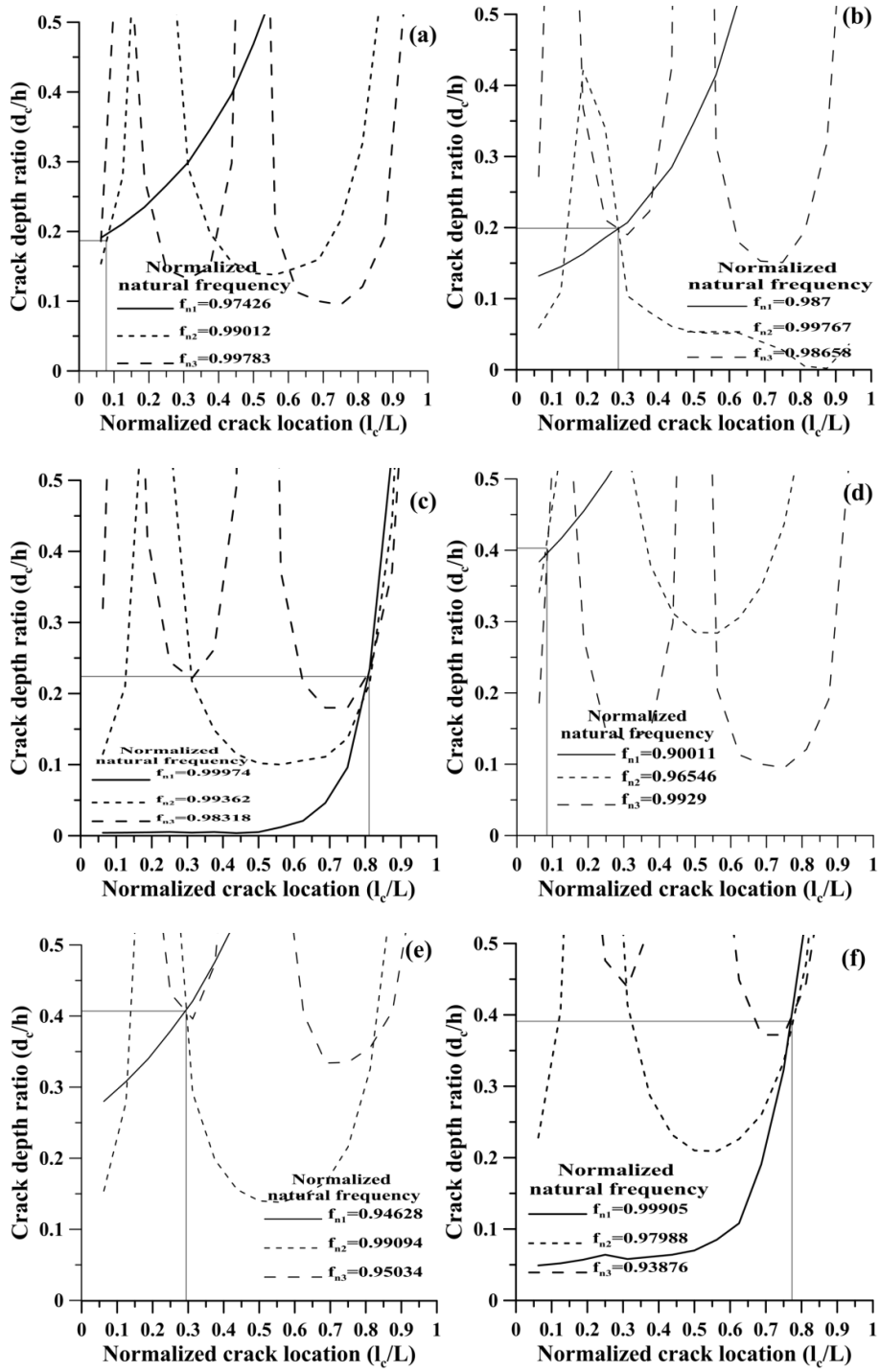

Figure 5.7 (a) Crack prediction using frequency contours of first natural frequencies in cantilever beam (frist —, second -----, third ——): case 1, (b) Crack prediction using frequency contours of first natural frequencies in cantilever beam (frist —, second -----, third ——): case 2, (c) Crack prediction using frequency contours of first natural frequencies in cantilever beam (frist —, second -----, third ——): case 3, (d) Crack prediction using frequency contours of first natural frequencies in cantilever beam (frist —, second -----, third ——): case 4, (e) Crack prediction using frequency contours of first natural frequencies in cantilever beam (frist —, second -----, third ——): case 5, (f) Crack prediction using frequency contours of first natural frequencies in cantilever beam (frist —, second -----, third ——): case 6

Once prediction of crack location and depth are obtained from contour line intersection, they are compared with numerical results and the percentage of errors is computed by the following equation.

$$E_h^{'} = \left|\frac{d_c - d_c^{'}}{h}\right| \times 100; E_L^{'} = \left|\frac{l_c - l_c^{'}}{L}\right| \times 100 \qquad (5.4)$$

Where d_c and l_c are the actual crack depth and crack location respectively, $d_c^{'}$ and $l_c^{'}$ are the predicted crack depth and crack location respectively found by intersection.

Table 5.8 Actual and predicted results of cracked clamped-clamped beam using Frequency Contours method

Case Number	Crack depth and location from fixed end in meter (Numerical input)	Relative Natural Frequency	Predicted crack depth and location from fixed end in meter (From contour plot)	Error %
1	d_c= 0.01 l_c= 0.175	First - 0.968972 Second-0.996604 Third-0.997908	$d_c^{'}$ =0.0084 $l_c^{'}$ =0.17529	$E_h^{'}$ = 1.6 $E_L^{'}$ = 0.02
2	d_c= 0.01 l_c= 0.375	First - 0.999948 Second-0.968677 Third-0.957228	$d_c^{'}$ =0.0093 $l_c^{'}$ = 0.361	$E_h^{'}$ = 0.7 $E_L^{'}$ = 0.88
3	d_c = 0.01 l_c= 0.775	First - 0.960534 Second-0.997017 Third-0.946271	$d_c^{'}$ =0.01 $l_c^{'}$ =0.7623	$E_h^{'}$ =0 $E_L^{'}$ = 0.79
4	d_c = 0.03 l_c= 0. 175	First - 0.782173 Second-0.980583 Third-0.979836	$d_c^{'}$ = 0.0279 $l_c^{'}$ = 0.1578	$E_h^{'}$ = 2.1 $E_L^{'}$ = 1.08
5	d_c = 0.03 l_c= 0.375	First - 0.998541 Second-0.722414 Third-0.679349	$d_c^{'}$ = 0.0303 $l_c^{'}$ = 0.3748	$E_h^{'}$ = 0.3 $E_L^{'}$ = 0.01
6	d_c=0.03 l_c=0.775	First - 0.645861 Second-0.991066 Third-0.590062	$d_c^{'}$ =0.0304 $l_c^{'}$ = 0.767	$E_h^{'}$ = 0.4 $E_L^{'}$ = 0.5

Table 5.8 and 5.9 present the predicted results of clamped-clamped and cantilever beam, respectively. For clamped-clamped beam, maximum errors of 2.1 % and 1.08 % are observed for crack depth and crack location whereas average errors are 0.85 % and 0.55 % for all six crack scenario. In case of cantilever beam, maximum errors of 1.3 % and 2.94 % are obtained for depth and location parameters respectively, average errors are fond to be 0.75 % and 1.36 %. Since total number of cracked beam sample is higher for clamped-clamped beam (75 number of sample for 800 mm of beam length) than that of cantilever beam (75 number of sample for 1600 mm of beam length), predicted results of clamped-clamped beam is found to be more accurate. It is also observed that when crack depth is small, error in prediction of location deteriorates. Prediction of crack size is not very good

when crack is located near the fixed end in case of clamped-clamped beam. Similar observation is noticed in case of cantilever beam when crack is located near the free end.

Table 5.9 Actual and predicted results of cracked cantilever beams using Frequency Contours method

Case Number	Crack depth and location from fixed end in meter (Numerical input)	Relative Natural Frequency	Predicted crack depth and location from fixed end in meter (From contour plot)	Error%
1	d_c =0.02 l_c=0.15	First - 0.974263 Second-0.99012 Third-0.997828	$d_c^{'}$ = 0.0187 $l_c^{'}$ =0.1243	$E_h^{'}$ = 1.3 $E_L^{'}$ =1.61
2	d_c =0.02 l_c=0.45	First - 0.987 Second-0.997671 Third-0.986582	$d_c^{'}$ = 0.0199 $l_c^{'}$ = 0.4592	$E_h^{'}$ = 0.1 $E_L^{'}$ = 0.58
3	d_c =0.02 l_c=1.25	First - 0.999735 Second-0.993617 Third-0.983179	$d_c^{'}$ = 0.0224 $l_c^{'}$ = 1.297	$E_h^{'}$ = 1.2 $E_L^{'}$ = 2.94
4	d_c =0.04 l_c=0.15	First - 0.900113 Second-0.965461 Third-0.992901	$d_c^{'}$ = 0.0403 $l_c^{'}$ = 0.1346	$E_h^{'}$ = 0.3 $E_L^{'}$ = 0.96
5	d_c=0.04 l_c=0.45	First - 0.946283 Second-0.990937 Third-0.950342	$d_c^{'}$ = 0.0407 $l_c^{'}$ = 0.4706	$E_h^{'}$ = 0.7 $E_L^{'}$ = 1.29
6	d_c =0.04 l_c=1.25	First - 0.999051 Second-0.979883 Third-0.938758	$d_c^{'}$ = 0.0391 $l_c^{'}$ = 1.2379	$E_h^{'}$ = 0.9 $E_L^{'}$ = 0.76

In order to ascertain the efficacy of the proposed technique, contour plots have been generated from the data used by Owolabi et al. (2003) and crack depth and its location are obtained. Table 5.10 shows that the present procedure exhibits almost same level of accuracy if not more.

Table 5.10 Comparison of contour plot crack detection of cracked beam by first three natural frequencies

Beam Condition	Experimental result (Input)		Normalized frequency			Owolabi et al.				Present study			
						Depth		Location		Depth		Location	
	Depth	Location	First	Second	Third	Output	Error %	Output	Error %	Output	Error %	Output	Error %
Clamped-clamped	0.1	0.4375	0.998	0.999	0.993	0.109	9	0.447	2.17	0.101	1	0.446	1.94
Simply supported	0.3	0.1875	0.988	0.971	0.983	0.191	1.87	0.295	1.67	0.186	0.8	0.298	0.67

5.3.2.2 Crack parameter identification from first three natural frequencies using RSM

In order to check the applicability of the regression model, frequencies obtained by the numerical analysis are compared with the predicted value from the model for all the results. As a test case, only first natural frequency for first portion of cantilever beam (k =

0.2) is shown in Figure 5.8. Since most of the points fall on a straight line, it implies that the data are normal, it may be inferred that the regression model is reasonably well fitted with the observed values. In addition, the plot of the residues vs. predicted frequencies (Figure 5.9) illustrates that there is no noticeable pattern or unusual structure present in the data. It is observed from the Figure that the residues, which are calculated as the difference between the predicted and observed value, lies in the range of −0.0068 to 0.0084. Similar procedure is followed for all crack scenarios for the first three natural frequencies of cantilever beam (k = 0.2) and clamped–clamped beam (k = 5).

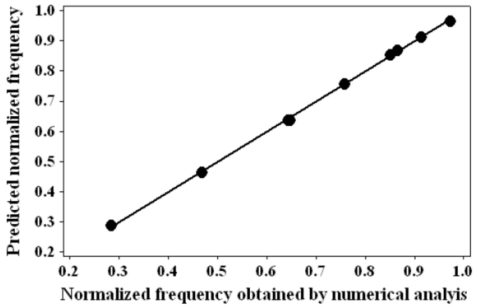

Figure 5.8 Predicted frequencies vs. Frequency obtained by numerical analysis

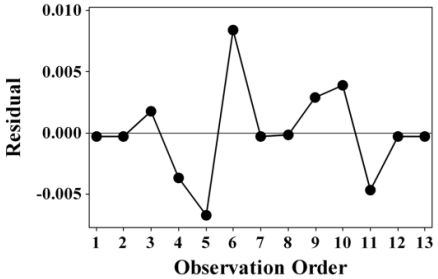

Figure 5.9 Residual vs. Observation Order

In order to obtain the regression equations of the response surface model for first three natural frequencies, the beam is divided into three equal portions as given below.

For cantilever beam, the beam length being 1.6 m, first portion is fixed end to 0.533 m, second portion is between 0.533 m and 1.067 m from fixed end and the third portion is from 1.067 m to free end. In case of both end clamped beam, first portion is fixed end to 0.325 m from fixed end, second portion is 0.325 m from fixed end to 0.575 m from fixed end and third portion is 0.575m from fixed end to 0.8 m from fixed end (i.e. middle of the beam).

Detailed description of that RSM technique is described in 4.3 section. After eliminating the non-significant terms, the final response equations in terms of the crack depth

(d_c) and location (l_c) values of independent variable for frequencies(f) of clamped-clamped beam for a gradation relation of k = 0.2 are given as:

$$f_{1f} = 1.0518 - 24.7434 \times d_c + 0.987 \times l_c - 115.575 \times d_c \times d_c + 110.123 \times d_c \times l_c - 5.6797 \times l_c \times l_c \quad (5.5)$$

$$f_{1s} = 0.3611 - 0.8368 \times d_c + 6.254 \times l_c - 14.7508 \times l_c \times l_c \quad (5.6)$$

$$f_{1t} = 0.1577 + 21.4087 \times d_c + 6.794 \times l_c - 132.429 \times d_c \times l_c - 11.0708 \times l_c \times l_c \quad (5.7)$$

$$f_{2f} = -0.163 + 28.0838 \times d_c + 4.1836 \times l_c - 63.5279 \times d_c \times d_c - 61.549 \times d_c \times l_c - 3.5476 \times l_c \times l_c \quad (5.8)$$

$$f_{2s} = 2.7245 + 12.6567 \times d_c - 7.9579 \times l_c - 339.855 \times d_c \times d_c - 34.9295 \times d_c \times l_c + 9.2371 \times l_c \times l_c \quad (5.9)$$

$$f_{2t} = 1.788 - 57.0413 \times d_c - 1.688 \times l_c - 92.0313 \times d_c \times d_c + 117.462 \times d_c \times l_c \quad (5.10)$$

$$f_{3f} = 2.0751 + 32.3451 \times d_c - 3.7346 \times l_c - 379.489 \times d_c \times d_c - 44.49 \times d_c \times l_c \quad (5.11)$$

$$f_{3s} = -0.1393 - 73.335 \times d_c + 4.8464 \times l_c - 99.6345 \times d_c \times d_c + 104.015 \times d_c \times l_c - 4.58563 \times l_c \times l_c \quad (5.12)$$

$$f_{3t} = 1.684 + 97.7766 \times d_c - 4.0583 \times l_c - 196.926 \times d_c \times d_c - 144.937 \times d_c \times l_c + 4.4429 \times l_c \times l_c \quad (5.13)$$

Similar type of methodology is applied and equations are generated for cantilever FGM beam with k=5. Regression equations are given as:

$$f_{1f} = 1.08305 - 7.29249\, d_c - 0.279307\, l_c - 324.443\, d_c \times d_c + 32.5235\, d_c \times l_c - 0.261577 l_c \times l_c \quad (5.14)$$

$$f_{1s} = 0.722298 - 9.61433\, d_c + 2.3986\, l_c + 26.738\, d_c \times l_c - 4.51466\, l_c \times l_c \quad (5.15)$$

$$f_{1t} = 0.392128 + 15.009\, d_c + 3.15202\, l_c - 69.153\, d_c \times l_c - 2.81377\, l_c \times l_c \quad (5.16)$$

$$f_{2f} = 0.994091 - 11.432\, d_c + 0.229978\, l_c - 93.6326\, d_c \times d_c + 16.0692\, d_c \times l_c - 0.296463\, l_c \times l_c \quad (5.17)$$

$$f_{2s} = 2.26795 + 17.7549\, d_c - 3.56527\, l_c - 422.851\, d_c \times d_c - 18.508\, d_c \times l_c + 2.39371\, l_c \times l_c \quad (5.18)$$

$$f_{2t} = -2.18311 - 1.22872\, d_c + 8.19855\, l_c - 5.4055\, d_c \times d_c - 5.24052\, l_c \times l_c \quad (5.19)$$

$$f_{3f} = 0.883229 - 1.95226\, d_c + 0.199421\, l_c - 2.8281\, d_c \times d_c + 1.524\, d_c \times l_c - 0.084431 l_c \times l_c \quad (5.20)$$

$$f_{3s} = -0.308882 - 49.6415\, d_c + 2.58748\, l_c - 99.716\, d_c \times d_c + 39.3038\, d_c \times l_c - 1.23249\, l_c \times l_c \quad (5.21)$$

$$f_{3t} = 2.87749 - 103.405\, d_c - 1.52136\, l_c - 391.709\, d_c \times d_c + 85.3985\, d_c \times l_c \quad (5.22)$$

Suffix of f is denoted as first three natural frequencies (*1*, *2* and *3*) and first, second and third portion of beam (*f*, *s* and *t*).

Now first, second and third natural frequency equations are solved for any portion of the beam. If values of crack location and its depth is not unique then average value is taken. Altogether six different crack scenario are predicted for both clamped-clamped (k=0.2) beam and cantilever (k=5) FGM beam by solving the regression equations. Percentage errors are calculated by following equation

$$E_h'' = \left|\frac{d_c - d_c''}{h}\right| \times 100; E_L'' = \left|\frac{l_c - l_c''}{L}\right| \times 100 \tag{5.23}$$

where d_c and l_c are the actual crack depth and crack location respectively, d_c'' and l_c'' are the predicted crack depth and crack location respectively generate by GA.

Table 5.11 Actual and predicted results of cracked clamped-clamped beam using RSM

Case Number	Crack depth and location from fixed end in meter (Numerical input)	Relative Natural Frequency	Predicted crack depth and location from fixed end in meter (From RSM result)	Error %
1	d_c= 0.01 l_c= 0.175	First - 0.968972 Second-0.996604 Third-0.997908	d_c''=0.012 l_c''=0.178	E_h''=2 E_L''=0.19
2	d_c= 0.01 l_c= 0.375	First - 0.999948 Second-0.968677 Third-0.957228	d_c''=0.014 l_c''= 0.438	E_h''=4 E_L''=3.94
3	d_c = 0.01 l_c= 0.775	First - 0.960534 Second-0.997017 Third-0.946271	d_c''=0.01 l_c''=0.739	E_h''=0 E_L''=2.25
4	d_c = 0.03 l_c= 0. 175	First - 0.782173 Second-0.980583 Third-0.979836	d_c''= 0.0279 l_c''= 0.1578	E_h''=2.1 E_L''=1.08
5	d_c = 0.03 l_c= 0.375	First - 0.998541 Second-0.722414 Third-0.679349	d_c''= 0.0278 l_c''= 0.358	E_h''=2.2 E_L''= 1.06
6	d_c=0.03 l_c=0.775	First - 0.645861 Second-0.991066 Third-0.590062	d_c''=0.0298 l_c''= 0.776	E_h''=0.2 E_L''= 0.06

Tables 5.11 and 5.12 present the predicted results of clamped-clamped and cantilever beam, respectively. For clamped-clamped beam, maximum errors of 4 % and 3.94 % are observed for crack depth and crack location respectively whereas average errors are 1.75 % and 1.43 % for all six crack scenario. In case of cantilever beam, maximum errors of 4 % and 3.13 % are obtained for depth and location parameters respectively, average errors are fond to

be 2.17 % and 2.01 %. Since total number of cracked beam sample is higher for clamped-clamped beam (75 number of sample for 800 mm of beam length) than that of cantilever beam (75 number of sample for 1600 mm of beam length), predicted results of clamped-clamped beam is found to be more accurate. It is observed that in all cases errors are less than 5%.

Table 5.12 Actual and predicted results of cracked cantilever beams using RSM

Case Number	Crack depth and location from fixed end in meter (Numerical input)	Relative Natural Frequency	Predicted crack depth and location from fixed end in meter (From RSM result)	Error%
1	d_c =0.02 l_c=0.15	First - 0.974263 Second-0.99012 Third-0.997828	d_c'' =0.02 l_c'' =0.187	E_h'' =0 E_L'' =2.31
2	d_c =0.02 l_c=0.45	First - 0.987 Second-0.997671 Third-0.986582	d_c'' =0.018 l_c'' =0.4	E_h'' =2 E_L'' =3.12
3	d_c =0.02 l_c=1.25	First - 0.999735 Second-0.993617 Third-0.983179	d_c'' =0.024 l_c'' =1.28	E_h'' =4 E_L'' =1.88
4	d_c =0.04 l_c=0.15	First - 0.900113 Second-0.965461 Third-0.992901	d_c'' =0.042 l_c'' =0.144	E_h'' =2 E_L'' =0.375
5	d_c=0.04 l_c=0.45	First - 0.946283 Second-0.990937 Third-0.950342	d_c'' =0.042 l_c'' l_c^* =0.5	E_h'' =2 E_L'' =3.13
6	d_c =0.04 l_c=1.25	First - 0.999051 Second-0.979883 Third-0.938758	d_c'' =0.043 l_c'' =1.27	E_h'' =3 E_L'' =1.25

5.3.2.3 Crack parameter identification from first three natural frequencies using RSM with GA.

Altogether six different crack scenario are predicted for both clamped-clamped (k=0.2) beam and cantilever (k=5) FGM beam. For each type of beam, three different RSM regression models have been developed for three segments of the beam length against each frequency. All these regression models are tested for fitness function and the best fitness value along with corresponding crack depth and crack location are chosen for optimal result. As an example, two fitness plots as a function of generation number are shown in Figure 5.10.

Predicted results are compared with actual value and percentage errors are evaluated using the following equation.

$$E_h''' = \left|\frac{d_c - d_c'''}{h}\right| \times 100; E_L''' = \left|\frac{l_c - l_c'''}{L}\right| \times 100 \tag{5.24}$$

where d_c and l_c are the actual crack depth and crack location respectively, d_c''' and l_c''' are the predicted crack depth and crack location respectively generate by GA.

Actual and predicted results of clamped- clamped and cantilever beams are shown in Tables 5.13 and 5.14, respectively. For clamped-clamped beam, maximum errors of 3 % and 6.5 % are observed for crack depth and crack location, respectively whereas average errors are found to be 0.84% and 2.36% respectively of all six crack scenario.

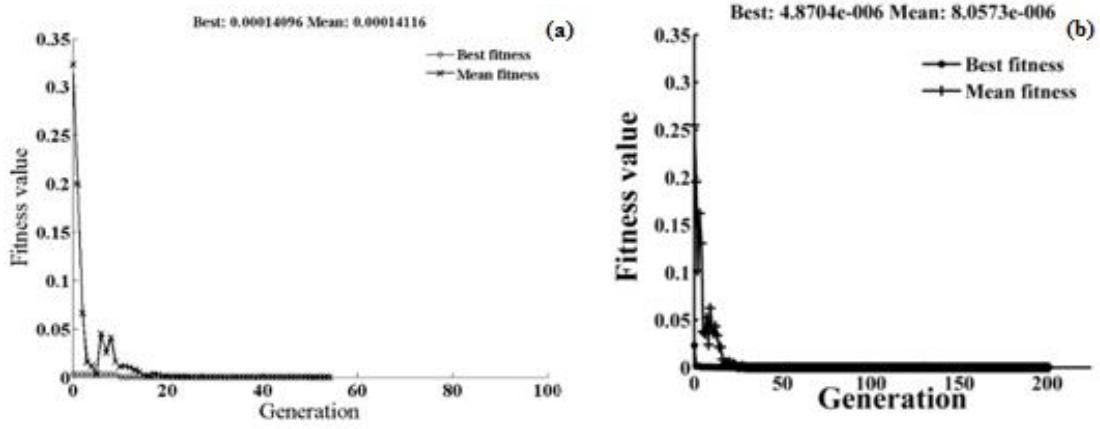

Figure 5.10 (a) Fitness function value as a function of generation number: case number 1 of FGM (k = 0.2) clamped–clamped beam, (b) fitness function value as a function of generation number: case number 6 of FGM (k = 5) cantilever beam.

In case of cantilever beam maximum errors of 4 % and 3.38 % are observed for crack depth and crack location, respectively with an average errors of 2.17 % and 1.81 % when all six crack scenario are considered. Due to higher resolution, result of prediction of crack is found to be better for clamped-clamped beam than that of cantilever beam. Same trend is observed in case of prediction by contour plot intersection method. One point is observed that when crack depth is very small, prediction of location is not very accurate as vibration response is less sensitive to small crack. Although a few results are not as good as previous method, this method is quite suitable for detection of crack especially for clamped-clamped beam

Table 5.13 Actual and predicted results of cracked clamped-clamped beams using RSM with GA

Case Number	Crack depth and location from fixed end in meter (Numerical input)	Relative Natural Frequency	Predicted crack depth and location from fixed end in meter (From RSM-GA result)	Error %
1	d_c = 0.01 l_c= 0.175	First - 0.968972 Second-0.996604 Third-0.997908	d_c''' =0.012 l_c''' =0.178	E_h''' =2 E_L''' =0.19
2	d_c = 0.01 l_c= 0.375	First - 0.999948 Second-0.968677 Third-0.957228	d_c''' =0.01 l_c''' = 0.479	E_h''' =0 E_L''' =6.5
3	d_c = 0.01 l_c= 0.775	First - 0.960534 Second-0.997017 Third-0.946271	d_c''' =0.01 l_c''' =0.676	E_h''' =0 E_L''' =6.19
4	d_c = 0.03 l_c= 0. 175	First - 0.782173 Second-0.980583 Third-0.979836	d_c''' = 0.027 l_c''' =0.158	E_h''' = 3 E_L''' =1.07
5	d_c = 0.03 l_c= 0.375	First - 0.998541 Second-0.722414 Third-0.679349	d_c''' = 0.03 l_c''' =0.374	E_h''' =0 E_L''' = 0.06
6	d_c =0.03 l_c=0.775	First - 0.645861 Second-0.991066 Third-0.590062	d_c''' =0.03 l_c''' = 0.777	E_h''' =0 E_L''' = 0.13

Table 5.14 Actual and predicted results of cracked cantilever cracked beams using RSM with GA

Case Number	Crack depth and location from fixed end in meter (Numerical input)	Relative Natural Frequency	Predicted crack depth and location from fixed end in meter (From RSM-GA results)	Error %
1	d_c =0.02 l_c=0.15	First - 0.974263 Second-0.99012 Third-0.997828	d_c''' =0.022 l_c''' =0.204	E_h''' =2 E_L''' =3.38
2	d_c=0.02 l_c=0.45	First - 0.987 Second-0.997671 Third-0.986582	d_c''' =0.023 l_c''' =0.431	E_h''' =3 E_L''' =1.19
3	d_c =0.02 l_c=1.25	First - 0.999735 Second-0.993617 Third-0.983179	d_c''' =0.024 l_c''' =1.275	E_h''' =4 E_L''' =1.56
4	d_c =0.04 l_c=0.15	First - 0.900113 Second-0.965461 Third-0.992901	d_c''' =0.038 l_c''' =0.116	E_h''' =2 E_L''' =2.13
5	d_c =0.04 l_c=0.45	First - 0.946283 Second-0.990937 Third-0.950342	d_c''' =0.04 l_c''' =0.476	E_h''' =0 E_L''' =1.63
6	d_c =0.04 l_c=1.25	First - 0.999051 Second-0.979883 Third-0.938758	d_c''' =0.042 l_c''' =1.265	E_h''' =2 E_L''' =0.94

5.3.3 Crack parameter identification from experiment result

Free vibration experimentation is carried out for a series of cracked cantilever beams and first four natural frequencies are obtained. Geometric and material properties of beam are taken as E = 70 GPa, ν = 0.33, ρ = 2645 kg/m^3, L=850 mm, h=10mm, width =50mm. Three crack depth ratios (d_c/h= 0.2, 0.4 and 0.6) of cracked beam are taken. Normalized crack location (l/L) is varied from 0.0588 to 0.8824. First four natural frequencies in transverse direction are evaluated. Now those natural frequencies are used for input optimization technique for evaluation of crack location and depth using CANN, GA and Neuro-GA hybrid technique.

5.3.3.1 Crack parameter identification from first four natural frequencies using CANN

Forward back propagation algorithm is applied for analysis using cascade artificial neural network. Cascade algorithm starts with a single layer network to which hidden units are then added one by one. Total 24 data sets obtain from experimentation having four inputs (first four natural frequencies) and two targets (crack depth and location) are divided among training, validation and testing purposes. Ratio of data set for training, validation and testing are 4:1:1. Levenberg-Marquardt optimization and gradient descent with momentum weight and bias are chosen for training function and learning function respectively. The tansigmoid hyperbolic function is used as an activation function to reach the optimized result. In order to achieve best target accuracies, number of neurons in a particular hidden layer and total number of hidden layers are varied. During prediction of depth and location of crack in cascade ANN, it has been observed that best MSE value of validation performance is 0.00987 at 47 epochs. Corresponding Regression value is 0.9143. Neural network model for this analysis consists of 3 inputs, 2 output and 2 hidden layer having three neurons each.

Predicted results are compared with actual value and percentage errors are evaluated using the following equation

$$E_h^{\#} = \left| \frac{d_c - d_c^{\#}}{h} \right| \times 100; E_L^{\#} = \left| \frac{l_c - l_c^{\#}}{L} \right| \times 100 \qquad (5.25)$$

Where a_c and l_c are the actual crack depth and crack location respectively, $d_c^{\#}$ and $l_c^{\#}$ are the predicted crack depth and crack location respectively found by GA.

Table 5.15 present the predicted results of CANN optimization technique for cantilever beam, respectively. For maximum errors of 15.91 % and 19.21 % are observed for crack location and crack depth whereas average errors are 4.21 % and 2.99 % for all 24 crack scenario. Four cases large amount (greater than 10%) of error is present for prediction of location whereas only one case large amount (greater than 10%) of error is present for prediction of depth. Predicted results of crack depth are found to be more accurate than location. Over all crack prediction is reasonable well with few amount of experimental dada using CANN.

Table 5.15 CANN optimization results of cantilever beam with error

Case No	**Normalized Natural Frequencies**				**Experiment**		**CANN**		**Error (%)**	
	First	**Second**	**Third**	**Forth**	l_c/L	d_c/h	$l_c^{\#}/L$	$d_c^{\#}/h$	$E_L^{\#}$	$E_h^{\#}$
1	0.821	0.667	0.495	0.950	0.059	0.2	0.123	0.211	6.387	1.127
2	0.866	0.971	0.600	0.902	0.176	0.2	0.180	0.210	0.348	1.030
3	0.911	0.715	0.495	0.950	0.294	0.2	0.297	0.208	0.285	0.823
4	0.643	0.429	0.493	0.852	0.059	0.4	0.067	0.414	0.777	1.449
5	0.732	0.928	0.710	0.654	0.176	0.4	0.135	0.392	4.109	0.841
6	0.821	0.595	0.391	0.802	0.294	0.4	0.304	0.303	0.959	9.727
7	0.000	0.142	0.210	0.902	0.059	0.6	0.059	0.600	0.000	0.014
8	0.375	0.880	0.594	0.213	0.176	0.6	0.217	0.598	4.063	0.227
9	0.554	0.715	0.000	0.754	0.294	0.6	0.306	0.593	1.141	0.729
10	0.955	0.694	0.570	0.944	0.412	0.2	0.458	0.212	4.588	1.160
11	0.955	0.643	0.600	0.796	0.529	0.2	0.689	0.273	15.918	7.329
12	1.000	0.715	0.495	0.964	0.647	0.2	0.597	0.206	4.990	0.649
13	0.866	0.424	0.706	0.816	0.412	0.4	0.355	0.373	5.705	2.745
14	0.911	0.310	0.810	0.556	0.529	0.4	0.514	0.430	1.514	3.009
15	1.000	0.643	0.594	1.000	0.647	0.4	0.542	0.208	10.469	19.207
16	0.777	0.258	0.511	0.722	0.412	0.6	0.347	0.597	6.511	0.252
17	0.911	0.000	0.810	0.261	0.529	0.6	0.524	0.594	0.500	0.582
18	0.955	0.286	0.087	1.000	0.647	0.6	0.647	0.594	0.037	0.571
19	1.000	0.976	0.702	0.758	0.765	0.2	0.754	0.264	1.111	6.351
20	1.000	1.000	0.890	0.910	0.882	0.2	0.860	0.225	4.236	2.456
21	1.000	0.930	0.501	0.516	0.765	0.4	0.866	0.450	10.082	4.987
22	1.000	0.930	0.691	0.633	0.882	0.4	0.833	0.387	4.963	1.269
23	0.957	0.790	0.000	0.000	0.765	0.6	0.882	0.600	11.763	0.001
24	1.000	1.000	0.421	0.363	0.882	0.6	0.878	0.548	0.460	5.233

5.3.3.2 Crack parameter identification from first four natural frequencies using GA

GA is applied to predict the global optimal depth and location of crack by minimising the fitness function which is constructed based on experimental results *(f_e)* and general regression (f_r).

The fitness function is to be minimised according to the following equation:

$$fitness(l_c, d_c) = \sum_{i=1}^{4} \left(f_{ei} - f_{ri}\right)^2 \tag{5.26}$$

Where, f_e is the first four natural frequencies which are applied to crack detection system as inputs obtain from experimental results. .f_r is the first four natural frequencies, which are functions of crack location (l_c) and its depth (d_c), and are calculated from the general regression cracked-beam model.

Table 5.16 GA optimization of cantilever beam with error

Case No	Normalized natural frequencies				Experiment		GA		Error (%)	
	First	Second	Third	Forth	l_c/L	d_c/h	$l_c^{\#\#} / L$	$d_c^{\#\#} / h$	$E_L^{\#\#}$	$E_h^{\#\#}$
1	0.821	0.667	0.495	0.950	0.059	0.2	0.068	0.233	0.941	3.3
2	0.866	0.971	0.600	0.902	0.176	0.2	0.120	0.139	5.647	6.1
3	0.911	0.715	0.495	0.950	0.294	0.2	0.288	0.225	0.588	2.5
4	0.643	0.429	0.493	0.852	0.059	0.4	0.061	0.377	0.235	2.3
5	0.732	0.928	0.710	0.654	0.176	0.4	0.153	0.398	2.353	0.2
6	0.821	0.595	0.391	0.802	0.294	0.4	0.300	0.426	0.588	2.6
7	0.000	0.142	0.210	0.902	0.059	0.6	0.059	0.600	0.000	0
8	0.375	0.880	0.594	0.213	0.176	0.6	0.182	0.586	0.588	1.4
9	0.554	0.715	0.000	0.754	0.294	0.6	0.306	0.600	1.176	0
10	0.955	0.694	0.570	0.944	0.412	0.2	0.412	0.267	0.000	6.7
11	0.955	0.643	0.600	0.796	0.529	0.2	0.444	0.252	8.588	5.2
12	1.000	0.715	0.495	0.964	0.647	0.2	0.614	0.240	3.294	4
13	0.866	0.424	0.706	0.816	0.412	0.4	0.428	0.364	1.647	3.6
14	0.911	0.310	0.810	0.556	0.529	0.4	0.521	0.415	0.824	1.5
15	1.000	0.643	0.594	1.000	0.647	0.4	0.613	0.294	3.412	10.6
16	0.777	0.258	0.511	0.722	0.412	0.6	0.614	0.543	20.235	5.7
17	0.911	0.000	0.810	0.261	0.529	0.6	0.562	0.600	3.294	0
18	0.955	0.286	0.087	1.000	0.647	0.6	0.680	0.669	3.294	6.9
19	1.000	0.976	0.702	0.758	0.765	0.2	0.771	0.227	0.588	2.7
20	1.000	1.000	0.890	0.910	0.882	0.2	0.891	0.178	0.824	2.2
21	1.000	0.930	0.501	0.516	0.765	0.4	0.722	0.329	4.235	7.1
22	1.000	0.930	0.691	0.633	0.882	0.4	0.809	0.426	7.294	2.6
23	0.957	0.790	0.000	0.000	0.765	0.6	0.751	0.592	1.412	0.8
24	1.000	1.000	0.421	0.363	0.882	0.6	0.894	0.607	1.176	0.7

Stochastic uniform and adaptive feasible mutation are used for selection and mutation respectively. Function tolerance and maximum number of generations for each run is set at $1e^{-12}$ and 500, respectively

All 24 crack scenario are tested for fitness function of GA and the best cost value along with corresponding crack depth and crack location are chosen for optimal result. Results of GA are shown in Table 4.15. The percentage of errors is computed by the following equation.

$$E_h^{\#\#} = \left| \frac{d_c - d_c^{\#\#}}{h} \right| \times 100; E_L^{\#\#} = \left| \frac{l_c - l_c^{\#\#}}{L} \right| \times 100 \tag{5.27}$$

Where a_c and l_c are the actual crack depth and crack location respectively, $a_c^{\#\#}$ and $l_c^{\#\#}$ are the predicted crack depth and crack location respectively found by GA.

Table 5.16 present the predicted results of GA optimization technique of cantilever beam. The maximum errors of 20.2% and 10.6 % are observed for crack location and crack depth whereas average errors are 3.01 % and 3.27 % for all 24 crack scenario. Accuracy of prediction of location and depth is nearly equal in GA method. Overall average value of prediction error is very similar to CANN method.

5.3.3.3 Crack parameter identification from first four natural frequencies using Neuro-GA hybrid technique

Altogether 24 different crack scenarios are optimized by Neuro-GA hybrid technique. First genetic algorithm model is prepared from experimental result and general regression equation as per describe in section 5.3.3.2.

All 24 optimized output results (crack parameters) of GA with experimental results (natural frequencies) are used as input parameters of this hybrid neural network. For CANN modelling same procedure is followed as per describe in section 5.3.3.1. MSE value of validation performance is 0.00987 at 47 epochs in this technique. Corresponding regression value is 0.9143. Neural network model for this analysis consists of 3 inputs, 2 output and 3 hidden layer having three neurons.

Predicted results are compared with actual value and percentage errors are evaluated using the following equation

$$E_h^{\#\#\#} = \left| \frac{d_c - d_c^{\#\#\#}}{h} \right| \times 100; E_L^{\#\#\#} = \left| \frac{l_c - l_c^{\#\#\#}}{L} \right| \times 100 \qquad (5.28)$$

Where a_c and l_c are the actual crack depth and crack location respectively, $a_c^{\#\#\#}$ and $l_c^{\#\#\#}$ are the predicted crack depth and crack location respectively found by Neuro-GA.

Results of neuro-GA are shown in Table 5.17 In this technique maximum errors of 15.35% and 8.7 % are observed for crack location and crack depth whereas average errors are 2.57 % and 1.45 % for all 24 crack scenario. Result shows that accuracy prediction trough Neuro-GA is better than homogeneous optimization of CANN or GA techniques.

Table 5.17 Neuro GA optimization of cantilever beam with error

Case No	Normalized natural frequencies				Experiment		Neuro-GA		Error (%)	
	First	Second	Third	Forth	l_c/L	d_c/h	$l_c^{\#\#\#}/L$	$d_c^{\#\#\#}/h$	$E_L^{\#\#\#}$	$E_h^{\#\#\#}$
1	0.821	0.667	0.495	0.950	0.059	0.2	0.079	0.200	2.062	0.040
2	0.866	0.971	0.600	0.902	0.176	0.2	0.174	0.200	0.245	0.007
3	0.911	0.715	0.495	0.950	0.294	0.2	0.307	0.201	1.267	0.078
4	0.643	0.429	0.493	0.852	0.059	0.4	0.063	0.401	0.427	0.100
5	0.732	0.928	0.710	0.654	0.176	0.4	0.258	0.344	8.126	5.572
6	0.821	0.595	0.391	0.802	0.294	0.4	0.302	0.405	0.791	0.454
7	0.000	0.142	0.210	0.902	0.059	0.6	0.059	0.600	0.006	0.000
8	0.375	0.880	0.594	0.213	0.176	0.6	0.179	0.600	0.267	0.007
9	0.554	0.715	0.000	0.754	0.294	0.6	0.242	0.600	5.252	0.001
10	0.955	0.694	0.570	0.944	0.412	0.2	0.565	0.206	15.335	0.629
11	0.955	0.643	0.600	0.796	0.529	0.2	0.512	0.202	1.748	0.229
12	1.000	0.715	0.495	0.964	0.647	0.2	0.631	0.204	1.572	0.376
13	0.866	0.424	0.706	0.816	0.412	0.4	0.403	0.400	0.913	0.041
14	0.911	0.310	0.810	0.556	0.529	0.4	0.531	0.402	0.174	0.153
15	1.000	0.643	0.594	1.000	0.647	0.4	0.710	0.321	6.291	7.857
16	0.777	0.258	0.511	0.722	0.412	0.6	0.435	0.600	2.331	0.002
17	0.911	0.000	0.810	0.261	0.529	0.6	0.561	0.600	3.136	0.027
18	0.955	0.286	0.087	1.000	0.647	0.6	0.655	0.600	0.797	0.012
19	1.000	0.976	0.702	0.758	0.765	0.2	0.770	0.200	0.539	0.041
20	1.000	1.000	0.890	0.910	0.882	0.2	0.873	0.201	0.906	0.069
21	1.000	0.930	0.501	0.516	0.765	0.4	0.832	0.313	6.737	8.698
22	1.000	0.930	0.691	0.633	0.882	0.4	0.867	0.402	1.536	0.204
23	0.957	0.790	0.000	0.000	0.765	0.6	0.753	0.599	1.141	0.114
24	1.000	1.000	0.421	0.363	0.882	0.6	0.882	0.599	0.025	0.112

5.4 Summary

Different optimization techniques in this crack investigation have been implemented in this section. In the 'Forward technique' crack location and relative crack depth are used as input whereas outputs are natural frequencies. Then results are compare with numerical and FEM results. The changes in the relative frequency caused by the existence of transverse crack within beam with different location and their sizes are studied in the technique. For 'Inverse techniques' results obtain from numerical analysis and experiment are applied for input parameter of optimization techniques whereas crack parameter are applied for output parameter. After the model develops results are comparing with actual case i.e. numerical and experimental inputs. Then optimization model are used for investigated unknown crack parameter. Percentages of errors are calculated for all optimization techniques. Errors are quite small most of cases. Results of those techniques are also compared. Overall optimization techniques are employed for identify crack parameters from globally changes are vibration parameters.

Chapter 6

CRACK IDENTIFICATIONBY PORFILE ANALYSIS OF MODE SHAPE

Outline of the Chapter**:** *6.1 Introduction, 6.2 Wavelet Transform Method, 6.2.1 Introduction of Wavelet Transform, 6.2.2 Design of Wavelet Transform for Crack Identification, 6.3 Fractal Dimension (FD) method, 6.3.1 Introduction of FD method, 6.3.2 Design of FD method for Crack Identification, 6.4 Curvature Method,6.4.1 Design of Curvature Method for Crack Identification,6.5 Irregularity extracted method, 6.5.1 Design of Irregularity extracted method, 6.6 Result and Discussion, 6.6.1 Identification of Crack Rotating Cantilever Beam by Continuous Wavelet Transform, 6.6.2 Identification of Crack Rotating Cantilever Beam by FD Method, 6.6.3. Identification of Crack Rotating Cantilever Beam by Curvature Method, 6.6.4 Identification of Crack Cantilever Beam by Irregularity Extracted Method, 6.6.5 Identification of Crack Cantilever Beam from Experimental Results by Irregularity Extracted Method, 6.7 Summary*

6.1 Introduction

Mode shape is a natural way to determine the vibration pattern of structures under given operating conditions. Vibration measurements are carried out at different points and directions on the structure. From these measurements, vibration pattern can be shown as a geometry model of the structure in the term of mode shapes because it provides the geometric features of the structures for operating conditions. However, mode shape itself cannot be used directly visualised to detect damage locations. The idea of using mode shapes as crack identification tool is due to the fact that the presence of a crack causes changes in the modal characteristics.

The advantage of using mode shapes is that changes in mode shapes are much more sensitive compared to changes in natural frequencies. Using mode shapes, however, has some drawbacks. The presence of damage may not significantly influence mode shapes of the lower modes usually measured. Furthermore, environmental noise and choice of sensors used can considerably affect the accuracy of the damage detection procedure.

The mode shape itself cannot be used directly to visualise the presence of crack in a structure Arbitrary mode shape associated with damaged structure contains local singularity information, which can be detected by shape profile analysis. Therefore mode shapes of cracked beams are captured first. Then they are subjected to various profile analysis

techniques to ascertain the presence of crack in beam. The methods utilised in the present thesis are mentioned.

6.2 Wavelet Transform Method

A wavelet is a wave-like oscillation with amplitude that starts out at zero, increases, and then decreases back to zero. Generally, wavelets are purposefully crafted to have specific properties that make them useful for signal processing. Wavelets can be combined, using a "reverse, shift, multiply and sum" technique called convolution, with portions of an unknown signal to extract information from the unknown signal.

6.2.1 Introduction of Wavelet Transform

Wavelet transform is a tool that cuts up data, functions or operators into different frequency components and then studies each component with a resolution matched to its scale. A wavelet is a small wave which has its energy concentrated in time. It has an oscillating wavelike characteristic but also has the ability to allow simultaneous time and frequency analysis and it is suitable tool for transient, non-stationary or time-varying phenomena. Just as the Fourier transform decomposes a signal into a family of complex sinusoidal, the wavelet transform decomposes a signal into a family of wavelets.The main difference is that wavelets are localized in both time and frequency whereas the standard Fourier transform is only localized in frequency. Unlike sinusoids, which are symmetric smooth and regular, wavelets can be symmetric or asymmetric, sharp or smooth, regular or irregular. There are two type wavelet transform phenomena one is time-frequency base and another is position-frequency base.Wavelet analysis is capable of revealing aspects of data that other signal analysis techniques miss aspects such as trends, breakdown points, discontinuities in higher derivatives, and self-similarity. Further, because it affords a different view of data than those presented by traditional techniques, wavelet analysis can often compress or de-noise a signal without appreciable degradation.

There are different types of wavelet family present in literature. Commonly wavelet families are Haar, Morlet, Mexican Hat, Mayer, Daubechies, Bio orthogonal, and Symlets. Wavelet transform are two types Continuous Wavelet Transform, Discrete Wavelet Transform.

Continuous wavelet transform (CWT) works as like Fourier transform. In the Fourier transform, the analyzing functions are complex exponentials, $e^{j\omega t}$. The resulting transform is

a function of a single variable, ω. In the short-time Fourier transform (STFT), the analyzing functions are windowed complex exponentials, $w(t)e^{j\omega t}$, and the result is a function of two variables. The STFT coefficients, F (ω,τ), represent the match between the signal and a sinusoid with angular frequency ω in an interval of a specified length cantered at t.

In CWT, the analyzing function is a wavelet, ψ. The CWT compares the signal to shifted and compressed or stretched versions of a wavelet. Stretching or compressing a function is collectively referred to as dilation or scaling and corresponds to the physical view of scale. By comparing the signal to the wavelet at various scales and positions it is obtained a function of two variables. The two-dimensional representation of a one-dimensional signal is redundant. If the wavelet is complex-valued, the CWT is a complex-valued function of scale and position. If the signal is real-valued, the CWT is a real-valued function of scale and position .For a scale parameter, $s>0$, and position, b, the CWT is

$$C(s,b:f(x),\psi(x))=\int_{-\infty}^{\infty} f(x)\frac{1}{\sqrt{s}}\psi^{*}\left(\frac{x-b}{s}\right)dx \tag{6.1}$$

By continuously varying the values of the scale parameter, a, and the position parameter, b, obtain the cwt coefficients $C(s, b: f(x), \psi(x))$, $\psi^{*}$is the complex conjugate of ψ. The basic function ψ is represented as

$$\psi_{j,k}(x)=2^{j/2}\psi\left(2^{j}x-k\right) \tag{6.2}$$

The results of the transform are wavelet coefficient that show how well a wavelet function correlates with the signal analyzed. Hence, sharp transitions in $f(x)$ create wavelet coefficient with large amplitude and this precisely is the basis of the proposed identification method.

CWT is highly redundant, not necessary to use the full domain of $C(s, b)$ to reconstruct $f(x)$.$C(s, b)$ can also be represented as

$$C(s,b)=\left(f(x),\psi^{*}_{s,b}(x)\right) \tag{6.3}$$

Therefore, CWT is a collection of inner products of a signal $f(x)$ and the translated and dilated wavelets $\psi_{s,b}(x)$.

The Discrete Wavelet Transform (DWT), which is based on sub-band coding, is found to yield a fast computation of Wavelet Transform. It is easy to implement and reduces the computation time and resources required.

In CWT, the signals are analyzed using a set of basic functions which relate to each other by simple scaling and translation. In the case of DWT, a time-scale representation of the digital signal is obtained using digital filtering techniques. The signal to be analyzed is passed through filters with different cut off frequencies at different scales.

DWT adopts dyadic scales and translations in order to reduce the amount of computation, which results in better efficiency of calculation. Filters of different cut off frequencies are used for the analysis of the signal at different scales. The signal is passed through a series of high-pass filters to analyze the high frequencies and through a series of low-pass filters to analyze the low frequencies.

DWT signal can be represent as

$$cD_J(k) = \int_{-\infty}^{\infty} f(x)\psi_{J,k}(x)dx \tag{6.4}$$

where, cD_J (k) is the J detail coefficients

At level j DWT function also be represent as

$$D_j(x) = \sum_{k=-\infty}^{\infty} cD_j(k)\psi_{j,k}(x) \tag{6.5}$$

The approximation at level J is define as

$$A_J(x) = \sum_{k=-\infty}^{\infty} cA_J(k)\phi_{j,k}(x) \tag{6.6}$$

The original function can be expressed as the sun of its approximation at level J plus all its detail up to the same level. Finally the signal $f(x)$ is defined as

$$f(x) = A_J(x) + \sum_{j \le J} D_j(x) \tag{6.7}$$

If $f(x)$ is a response signal, typically the deflection curve the signal $D_j(x)$ contains the information necessary to detect the cracks in the structure.

6.2.2 Design of Wavelet Transform for Crack Identification

All wavelet analysis is performed in MATLAB Wavelet Toolbox. The mode shapes profile obtained from finite element analysis and experiment are used as an input signal in Wavelet Toolbox. Analysis is carried out for the first four mode shapes in the transverse direction. CWT with scales of 1 – 64 is implemented for profile analysis. Bi-orthogonal 6.8 wavelet is chosen for analysing wavelet. Bi-orthogonal 6.8 decomposition scaling function

and decomposition wavelet function shown in Figure6.1.Bi-orthogonal wavelet is preferred for this analysis because in this wavelet analysis scaling function exit, DWT is possible and also fast algorithm is available.

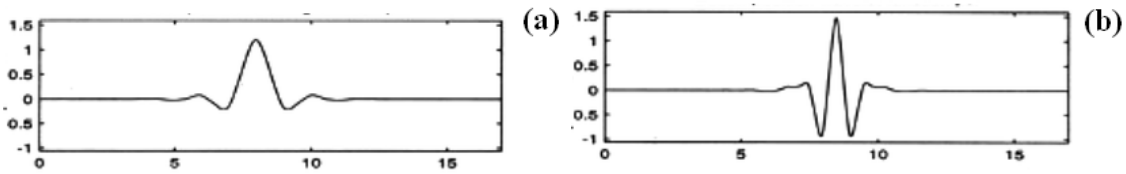

Figure6.1 Bi orthogonal 6.8 wavelet (a) decomposition scaling function (b) decomposition of wavelet function

Result obtained in CWT analysis is plotted with different scale. Large values of scale *s* correspond to big wavelets and thus are suitable for coarse features of *f*(*x*). While low values of scale s correspond to small wavelets correspond to fine details of *f*(*x*).

Result is also plotted using different sampling distances. It is observed that the resolution (sampling point per cm) plays an important role in practical application of the damage detection procedure. However, a very high resolution may be prohibited from the practical view point.

6.3 Fractal Dimension (FD) method

The fractal dimension (FD) of a waveform represents a powerful tool for transient detection. In case of electroencephalograms (EEG) and electrocardiograms (ECG), this feature has been used to identify and distinguish specific states of physiologic function. A variety of algorithms are available for the computation of FD.

6.3.1 Introduction of FD.

Fractal Dimension (FD) has become an efficient tool to extract damage information from mode shapes data. Damage induces changes in the dynamic properties of a structure causing irregularity of local mode shape. This irregularity produces abrupt peak composed of high-magnitude estimates of FD, with the position and magnitude of the peak indicating the location and severity of the damage in a quantitative manner. Among the various waveforms of fractal dimensions available, the Katz's fractal dimension is used as a quantitative measure of the local variation of geometry complexity of the mode shape in the space domain, due to its easy and simple implementation.

The Katz FD of a two-dimensional waveform signal is defined by [M. J. Katz (1988)]

$$D = \frac{\log_{10}(L)}{\log_{10}(d)} \tag{6.8}$$

where L is the length of the curve or sum of distances between successive points and d is the diameter estimated as the distance between the first point of the sequence and the point of the sequence that provides the furthest distance

Mathematically,

$$\mathrm{L} = \sum_{\mathrm{i}=1}^{\mathrm{N}-1} \mathrm{dist}(\mathrm{i},\mathrm{i}+1) \tag{6.9}$$

Considering the distance between each point of the sequence and the first, point *i* is the one that maximizes the distance with respect to the first point.

The FD computed in this manner depends on the measurement units used. If the units are different then the Katz's FD approach solved this problem by dividing the length by average step or average distance between the successive points $\bar{a}$. The normalization results in

$$\mathrm{D} = \frac{\log_{10}\left(\mathrm{L}/\bar{\mathrm{a}}\right)}{\log_{10}\left(\mathrm{d}/\bar{\mathrm{a}}\right)} \tag{6.10}$$

Defining n as the number of steps in the curve, then $n=L/\bar{a}$. Then equation 6.10 written as,

$$D = \frac{\log_{10}(n)}{\log_{10}\left(\frac{d}{L}\right) + \log_{10}(n)} \tag{6.11}$$

6.3.2 Design of FD method for Crack Identification

FD analysis has become a growing tool to provide insight into mode shapes for detecting damage. The sharp peak of the FD curve indicates irregularity of detecting curve i.e. the location of the damage. However, when the second and third mode shapes is considered, the above FD approach may give some misleading peak information in the location of maximum and minimum point in a curve profile. To overcome this deficiency, some adjustment is applied on the FD method. Value of abscissa of all point in detecting mode shape curve is multiplied by sum scale factor. The method is express as

$$x_i^* = sx_i \tag{6.12}$$

x_i^* is the new i^{th} sampling abscissa and s is the scale factor.

All FD analysis is performed on mode shape obtained from FEM and experimental data for detecting crack

6.4 Curvature Method

A crack reduces the stiffness of the structure which is associated with the strain energy. The basic concept of the modal strain energy method is to use the change of modal strain energy due to the damage occurrence to define an index which can be used to identify the damage location in structure.

6.4.1 Design of Curvature Method for Crack Identification

Curvature mode shapes are related to the flexural stiffness of beam cross-sections. Curvature data points at any section of beam is evaluated by

$$k = M / EI \tag{6.13}$$

and strain energy as

$$U = \frac{1}{2}\int EIk^2 dx \tag{6.14}$$

Where k is the curvature at a section, M is the bending moment at a section, E is the modulus of elasticity and I is the second moment of the cross-sectional area.U is the strain energy of the beam.

If crack or other damage is introduced in a structure, it reduces the (EI) of the structure at the cracked section or in the damaged region, which increases the magnitude of curvature at that section of the structure. The changes in the curvature are local in nature and hence can be used to detect and locate a crack or damage in the structure. Curvature mode shape is determined from the equation 6.15.

$$k = \left(\frac{\partial^2 y}{\partial x^2}\right)^2 \tag{6.15}$$

Where y is the displacement of sample point taking from beam at different mode shape condition and x is the abscissa of mode profile. After getting curvature of each section square of curvature is plotted along beam length.

6.5 Irregularity extracted method

Any noisy profile includes two parts: the smooth part which is the ideal defection of the structure without noise, and the unsmooth part which contains the irregularities induced by noise. Sometime irregular part is overshadowed by the stronger smooth part of the profile. In the irregularity extracted method, noisy profiles divided into parts and then weak noisy profile is found out.

6.5.1 Design of Irregularity Extracted method for Crack Identification

In this process, the mode shape is treated as profile of a curve. The change induced by damage becomes their regularity of this curve. Hence, damage can be detected by directly examining the irregularity of the curve.

A measured mode shape of a damaged beam is shown by the solid line in Figure 6.2(a). It consists of two parts: (1) the smooth part [Figure 6.2(b)] showing the mode shapes of the structure without damage and measurement noise and (2) the non-smooth part. [Figure6 2(c)] showing the irregularities induced by the damage in the structure and measurement noise. Only the latter part contains the information of damage. This irregular part shown in Figure 6.2(c), however, is generally overshadowed by the smooth part of the mode shape because the signal prompting the smooth part is much stronger, as demonstrated in Figure 6.2(a). It is thus difficult to detect damage by merely examining the mode shape. To overcome this difficulty, the irregular part is extracted from the whole mode shape. Without the influence of the smooth part of the mode shape, the irregularity induced by damage can be magnified significantly as shown in Figure6.2(c). Thus, the damage can be detected easily by visual examining the irregular part of the mode shape of Figure 6.2(c). Bearing in mind the analogy between the mode shape and profile of a curve, the damage Figure 6.2(c) can be easily extracted as the irregularity of the curve of the mode shape shown inFigure6.2 (a). To this end, a filter is used to eliminate the global effect of the smooth part of the mode shape of Figure6.2 (b) from the measured mode shape. Consequently, only the irregularities indicating local features of the mode shape are left and magnified on the irregularity profile in Figure 6.2 (c).

The irregularity profiles (R) separate from the waviness of the mode shape profile is defined as

$$w(x_0) = \int_{-\infty}^{\infty} z(x_0 + x)h(x)dx \tag{6.16}$$

$$R(x_0) = z(x_0) - w(x_0) \tag{6.17}$$

where z is the deflection of the mode shape which is obtained numerically or experimentally; w and R are waviness and roughness of the mode shape profile, respectively; h(x) is the filtration weighted function.

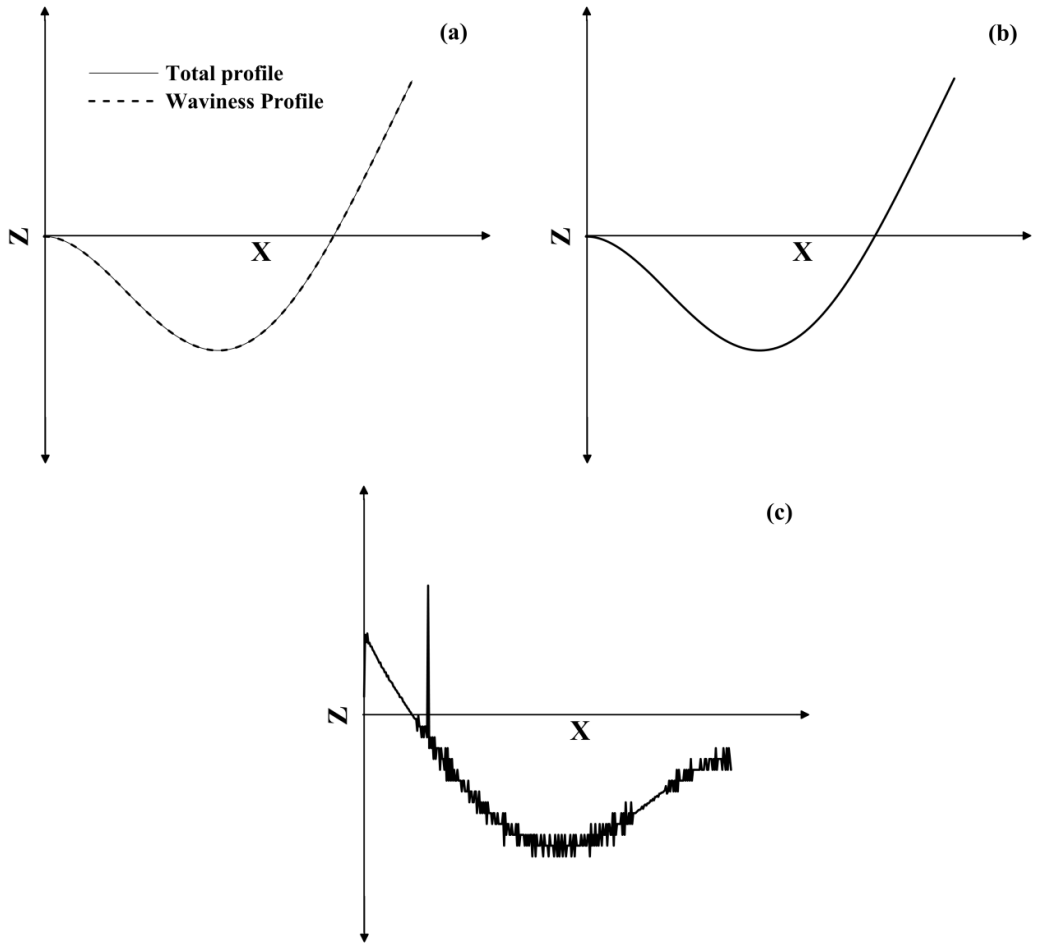

Figure6.2 Extracting irregularity from total mode shape (a) Total Profile, (b) Waviness Profile (c) Roughness Profile

There are many filters available in the literature (ASME B46.1-1995, 1996; Raju et al., 2002). The most widely used one is Gaussian filter. This filter uses the following weighted function:

$$h(x) = \frac{1}{\alpha\lambda_c}\exp\left(-\pi\left(\frac{x}{\alpha\lambda_c}\right)^2\right) \tag{5.18}$$

where, $\alpha = \sqrt{\ln 2/\pi}$ and λ_c is the cut-off wave-length.

Triangular filter is another frequently-used one with weighted function given by:

$$h(x) = \frac{1}{B} - \left(\frac{1}{B}\right)^2 |x| \tag{5.19}$$

where, B is the cut-off length of the filter. Compared with Gaussian filter, the triangular filter is much simpler.

6.6 Result and Discussion

In the following section, cracks are identified on rotating beams by various methods described in the previous section

6.6.1 Identification of Crack on Rotating Cantilever Beam by Continuous Wavelet Transform

First finite element program is used for free vibration of the rotating cracked beams. The length (L), thickness (h) and width (w) of the beams are set to be 500 mm, 10 mm and 15 mm respectively. Left end of the beam is placed 50 mm from global origin in X direction. The beam is made of aluminium with Young's modulus of 69 GPa, Poisson's ratio of 0.33 and density of 2700 kg/m^3.

The first three mode shapes for transverse vibration of cracked rotating beams are plotted for subsequent application of wavelet analysis for crack detection. The depth of the crack is varied from 1 mm to 5 mm with different location starting from 50 mm to 450 mm from fixed end. Four different rotational speed 50 rad/s, 100 rad/s, 150 rad/s and 200 rad/s of beams are considered for analysis.

In order to determinate crack identification of rotating cantilever beam, mode shapes of beam use as an input signal of wavelet analysis.

The CWT transform is implemented for three different scales, namely 1, 8 and 64 with "bior 6.8" as the analysing wavelet. A rotating beam having crack at a location 50 mm from fixed end with 3 mm crack depth is considered. The rotational speed of the beam is 100 rad/s. Crack investigation is carried out with resolution 5 i.e. taking 5 sampling point per centimetre along the beam length. The results of the wavelet analysis of first mode shape of the beam are presented in Figure 6.3. Figure 6.3a shows CWT coefficients are very noisy along the beam length. If the scale is too high (scale 64), there is no evidence of crack in CWT plot (Figure6.3c). A medium scale (scale 8) of CWT shows a better result (Figure6.3b) so far as crack detection is concerned.

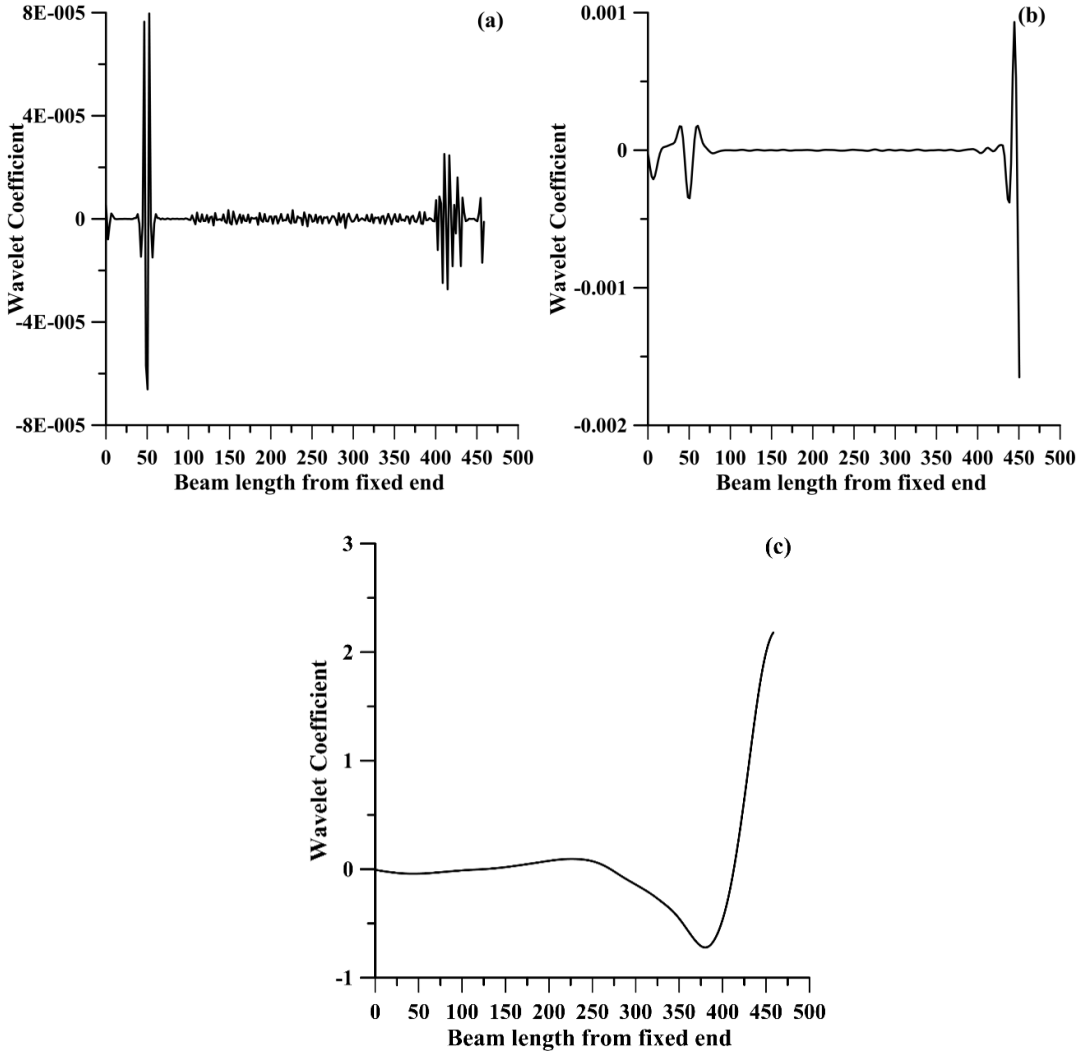

Figure6.3 Wavelet coefficient for (a) Scale 2, (b) Scale 8 and (c) Scale 64.

It is observed that the resolution (sampling point per cm) plays an important role in practical application of the damage detection procedure. However, a very high resolution may be prohibited from the practical view point. The results presented in previous section are based on a sampling distance of the mode shape data of 2 mm. Now the modal displacement data are sampled at distance interval of 10 mm (r = 1 *i.e.* 1 sampling point per cm), 2 mm (r = 5 *i.e.* 5 sampling point per cm), and 0.5 mm (r = 20 *i.e.* 20 sampling point per cm) of a cracked beam with 3 mm crack depth at a crack location of 50 mm from fixed end and rotational speed of 100 rad/s. Figure6.4 shows the CWT result with scale 8 and three different resolutions. Higher resolution produces better results as can be seen from Figure 6.4(a).

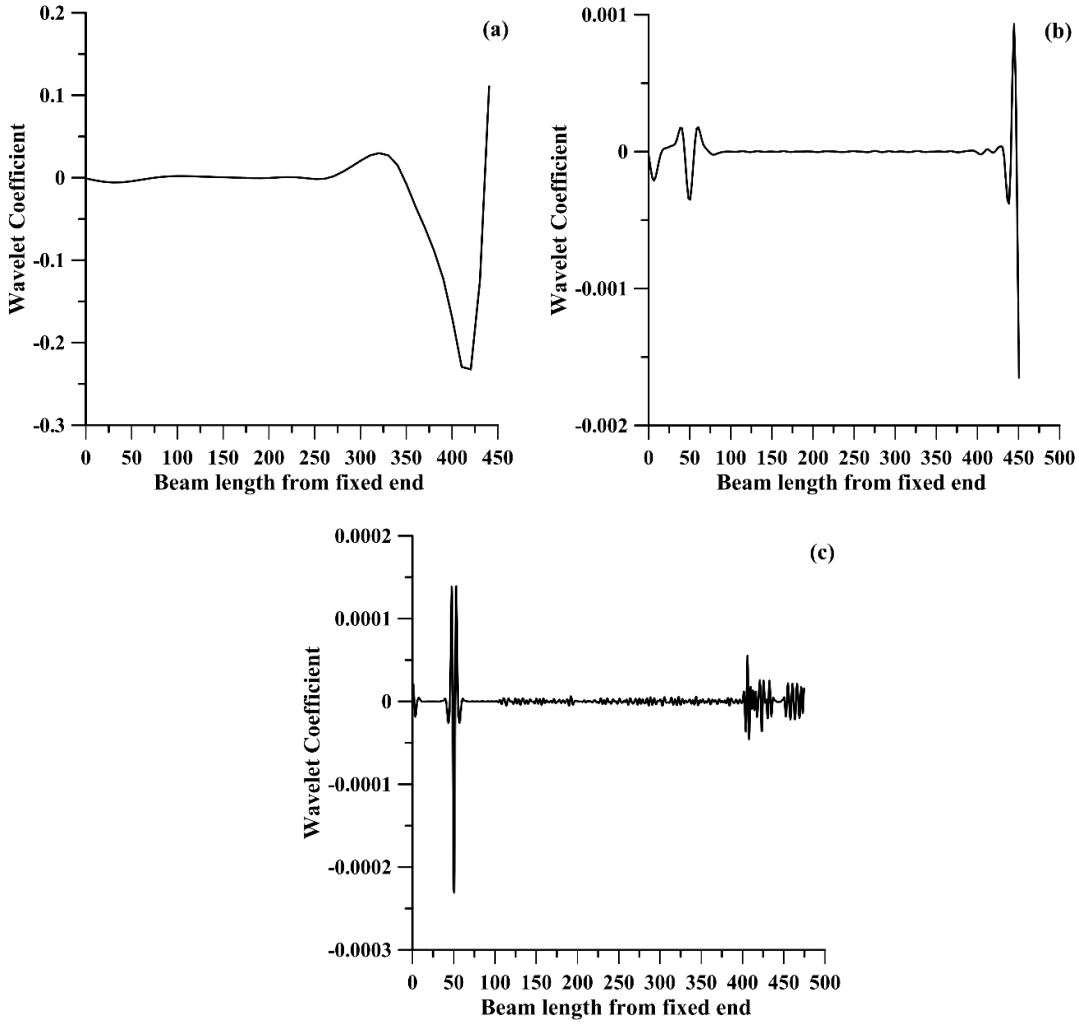

Figure 6.4 Wavelet coefficient plot for (a) resolution, r = 1, (b) resolution, r = 5 and (c) resolution, r = 20

Using the **s**ame beam, wavelet analysis is performed on second and third mode shapes as well. Figure 6.5 shows CWT coefficient plot of second and third mode shapes respectively with s = 8 and r = 20. Figures exhibits better detection of crack location compared to that obtained for first mode shape

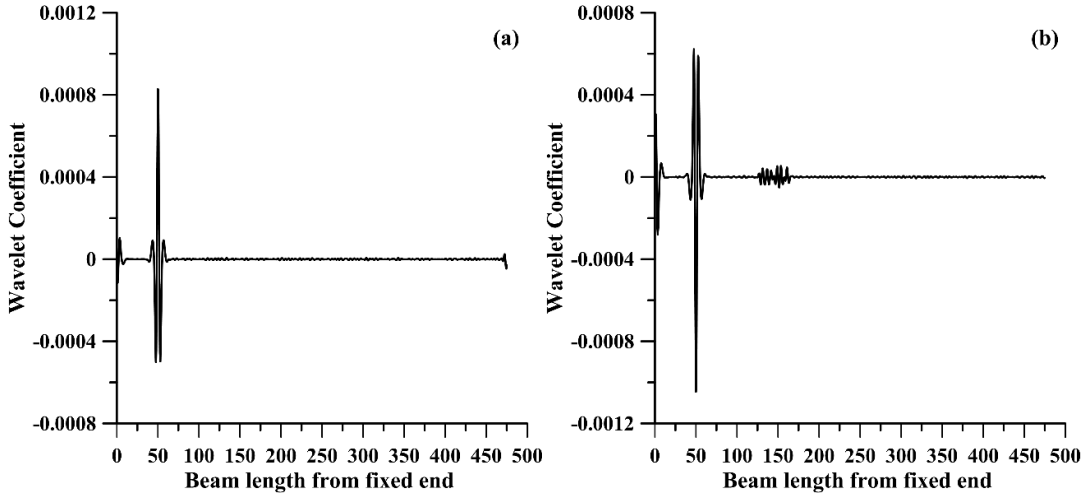

Figure 6.5 Wavelet coefficient plot for (a) second mode shape and (b) third mode shape

Now crack investigation form mode shape profile at different locations of crack. Two cracked beams are taken each having crack with 3 mm depth at a distance of 250 mm and 450 mm from fixed end, respectively. Rotational speed of both the beams is 100 rad/s. Scale and Resolution for the wavelet analysis are taken as 8 and 20 respectively. In this case, third mode shape is taken as input signal of wavelet analysis. Figure6.6 shows the result. From the plots it is evident that there is a crack at a distance of 250 mm and 450 mm from fixed end.

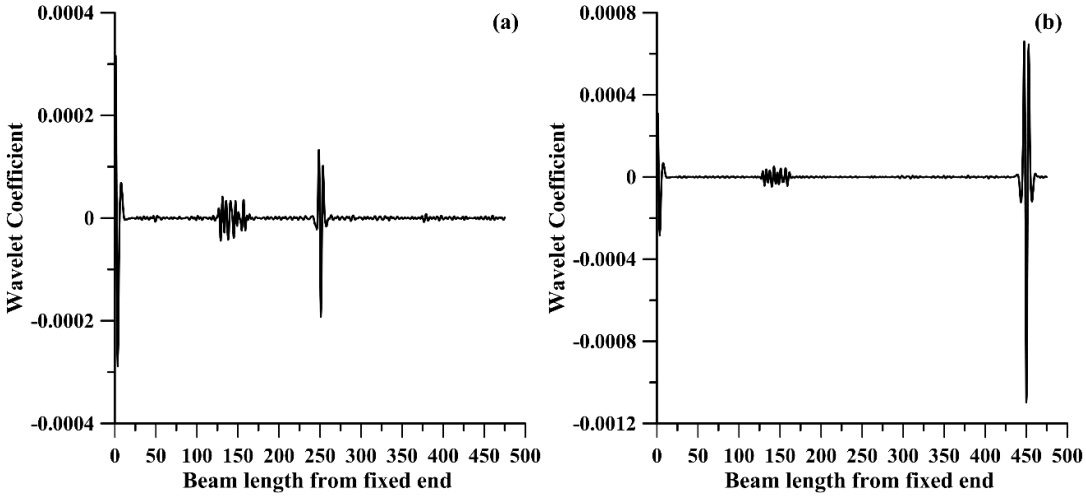

Figure 6.6 CWT plot for (a) location 250 mm from fixed end and (b) location 450 mm from fixed end

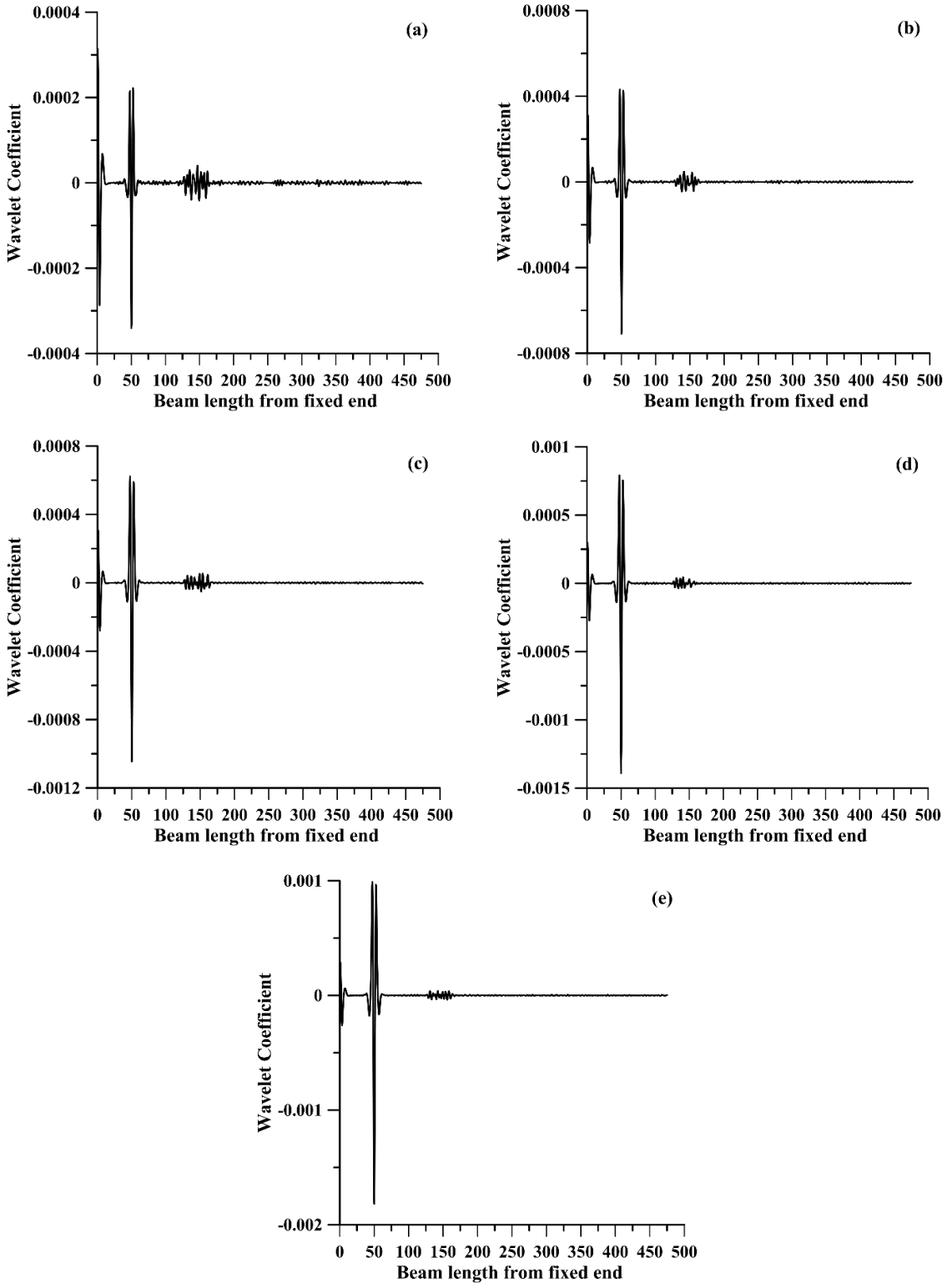

Figure 6.7 CWT plot for crack depth (a) 1mm, (b) 2 mm, (c) 3 mm, (d) 4 mm and (e) 5mm

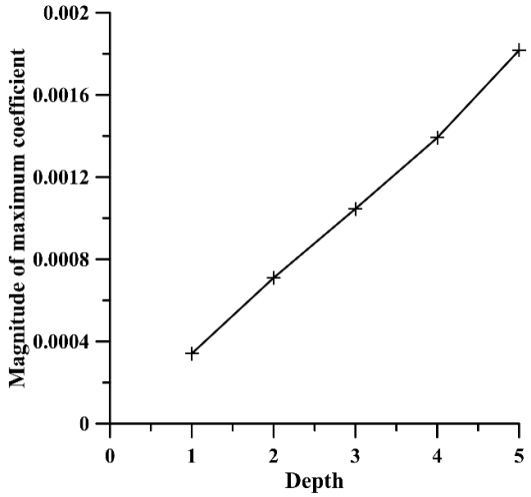

Figure6.8 Wavelet coefficients vs. Depth

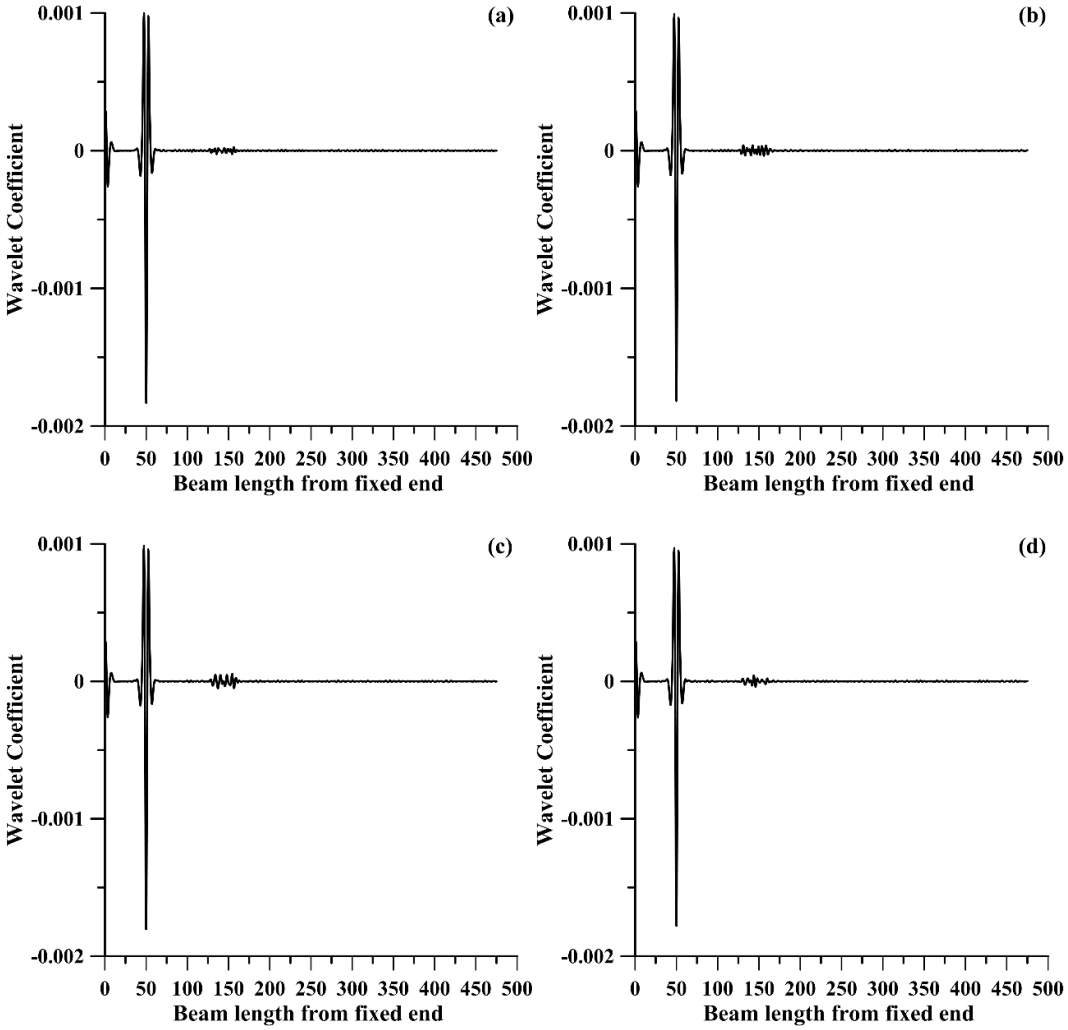

Figure 6.9 CWT plot for different rotating speed (a) 50 rad/s, (b) 100 rad/s, (c) 150 rad/s and (d) 200 rad/s

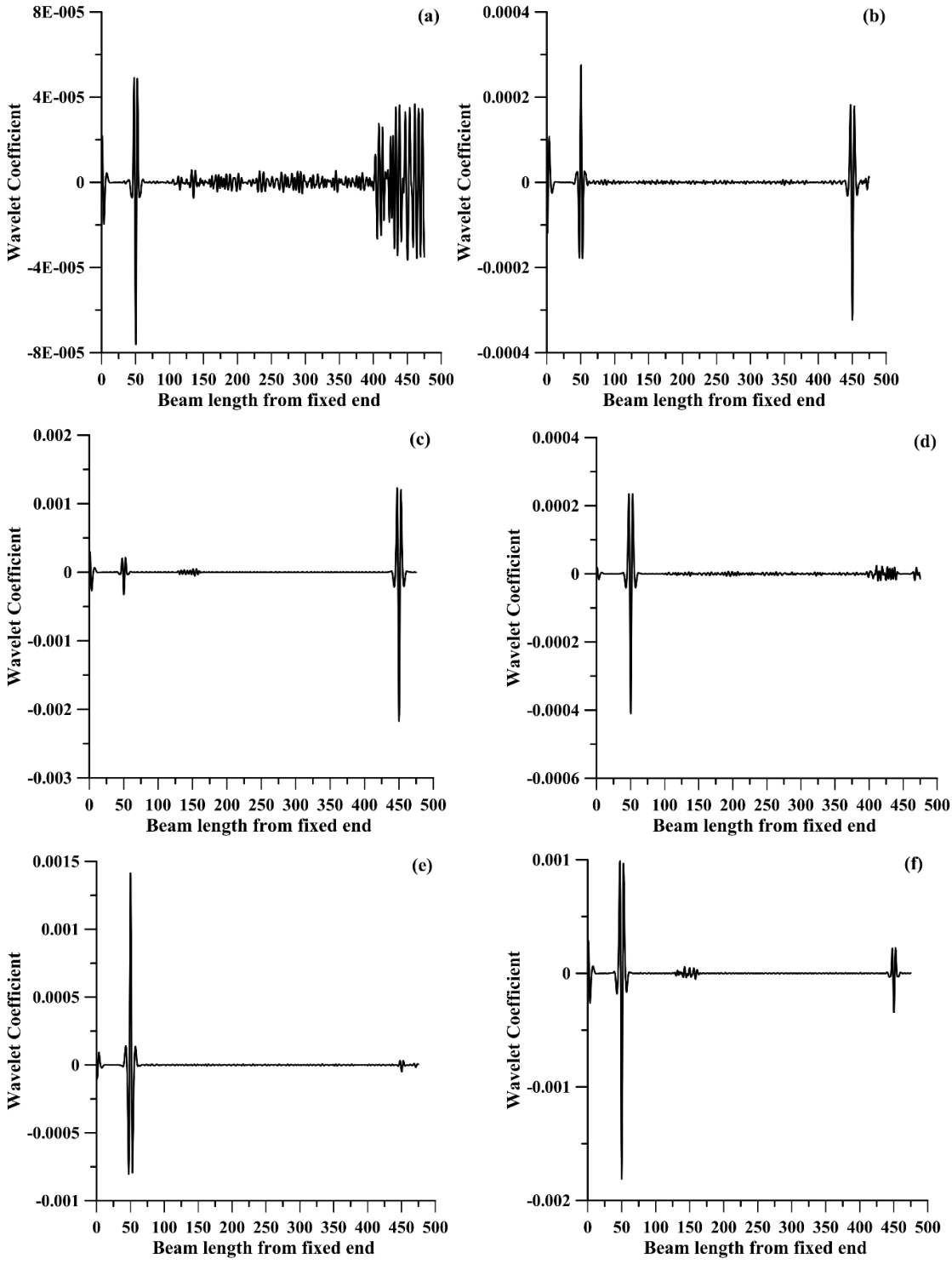

Figure 6.10 CWT plot of double cracked beam with 1 mm and 5 mm crack depth at location 50 mm and 450 mm from fixed end respectively (a) first mode, (b) second mode and (c) third mode and CWT plot of double cracked beam with 5 mm and 1 mm crack depth at location 50 mm and 450 mm from fixed end respectively (d) first mode, (e) second mode and (f) third mode

Now crack investigation form mode shape profile at same locations of crack with different sizes is carried out. Three cracked beams are taken with 1 mm, 2 mm, 3mm, 4mm

and 5 mm crack depth at a crack location of 50 mm from fixed end. Rotational speed of the beam is assumed to be 100 rad/s. As usual, third mode shape is taken as input signal of wavelet analysis. Sampling interval of the mode shape data is 0.5 mm. Figure 6.7 shows CWT results with scale 8. It is observed that the magnitude of coefficient is increased with depth of crack.It is observed that if maximum wavelet coefficient is plotted against crack depth, a straight line relationship is obtained (Figure 6.8).

Crack prediction is examined by wavelet analysis for different rotating speed of same cracked beam. A cracked beam is taken with 5 mm crack depth at crack location 50 mm from fixed end. Now this beam is rotated about Y axis in four different speeds 50 rad/s, 100 rad/s, 150 rad/s and 200 rad/s. Third mode shape of this beam is carried out for wavelet analysis. Scale and resolution for this analysis is taken 8 and 20 respectively. Figure 6.9 are shown wavelet coefficient of this mode shape. Results shows that value of maximum coefficient for rotating speed are nearly equal. The magnitude of coefficients slightly decreases with rotating speed from 0.00183 to 0.00178.

Similar investigation is carried out for detection of multiple cracks also. Two double cracked rotating beams (100 rad/s) are taken for analysis. One cracked beam has a big crack (5mm depth) near fixed end (50 mm from fixed end) and a small crack (1mm depth) near free end (50 mm from free end). Other cracked beam has a small crack (1mm depth) near fixed end (50 mm from fixed end) and a big crack (1mm depth) near free end (50 mm from free end). First three mode shapes are used as an input signal of wavelet analysis in CWT results are shown in Figure 6.10. Figures 6.10 (a) and 6.10 (d) shows that it is difficult to identify crack location from first mode shape only. For wavelet analysis of second mode shape clearly shows the crack location (Figures 6.10b, 6.10e). Crack location is identified easily when it is located near fixed end. For third mode shape analysis result (Figure 6.10f) captures crack size are more prominent than second mode shape analysis for location of evidence of crack.

Next investigation is carried out for a rotating (100 rad/s) cantilever beam with three cracks. Locations of cracks on the beam are 50 mm (near fixed end), 250 mm (at middle) and 450 mm (near free end) from fixed end with same depth of 3 mm depth. Wavelet analysis is performed on second and third mode shape obtained from of FEM. The results are shown in Figures6.11 and 6.12. The figures depicts that in case of second mode shape (Figure 6.11) wavelet coefficient is more severe at middle position and less severe at near free end whereas for third mode shape wavelet coefficient is less severe at middle position and near both end is more severe.

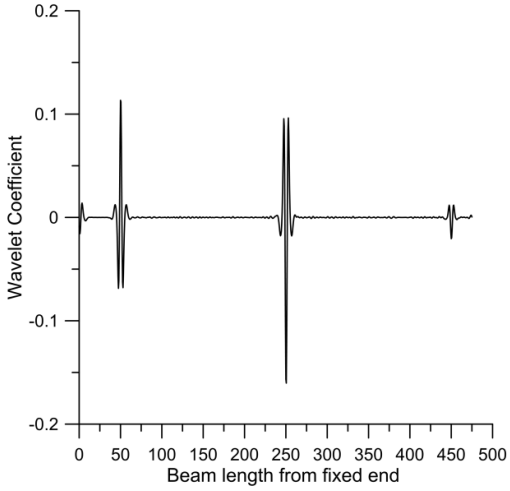

Figure 6.11 CWT plot of triple cracked beam with for second mode shape

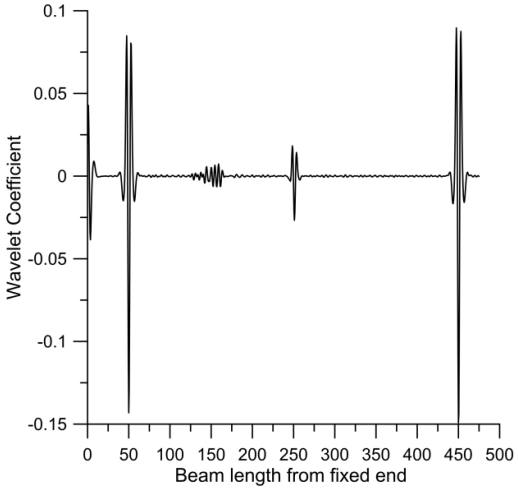

Figure 6.12 CWT plot of triple cracked beam with for third mode shape

6.6.2 Identification of Crack on Rotating Cantilever Beam by Fractal Dimension Method.

Free vibration finite element analysis is carried out on a series of cracked beams. The depth of the crack is varied from 1mm to 5 mm with different starting from 50 mm from fixed end to 450 mm from fixed end. Other properties of the beam are kept same as mentioned in section 6.6.1. Three different rotational speeds 50 rad/s, 100 rad/s, and 200 rad/s are considered for analysis.

The modal displacement data are sampled from the top surface of beam at distance interval of 10mm (r=1 or 1 sampling point per cm), 5 mm (r=2 or 2 sampling point per cm), 2mm (r=5 or 5 sampling point per cm) and 0.5 mm (r=20 or 20 sampling point per cm) of cracked beam at crack location 50 mm from fixed end with 3 mm crack depth. Beam is rotated at 100 rad/s speed. FD analysis is performed with first mode shape. FD analysis is carried out for four different resolution i.e. r=1, 2, 5 and 20.Results are shown in Figure 6.13. It is observed that better result is obtained in higher resolution (Figure 6.13d).

Next FD analysis is carried out for different crack location. Two cracked beam are taken with 3mm depth at a distance 250 mm and 450 mm from fixed end. Rotational speed of the beam is 100 rad/s. First mode shape is used for FD analysis with resolution 20. From Figure 6.14a it is evident that there is a crack at a distance of 250 mm from fixed end. However there is no evidence of crack at a distance of 450 mm from fixed end (Figure 6.14b).

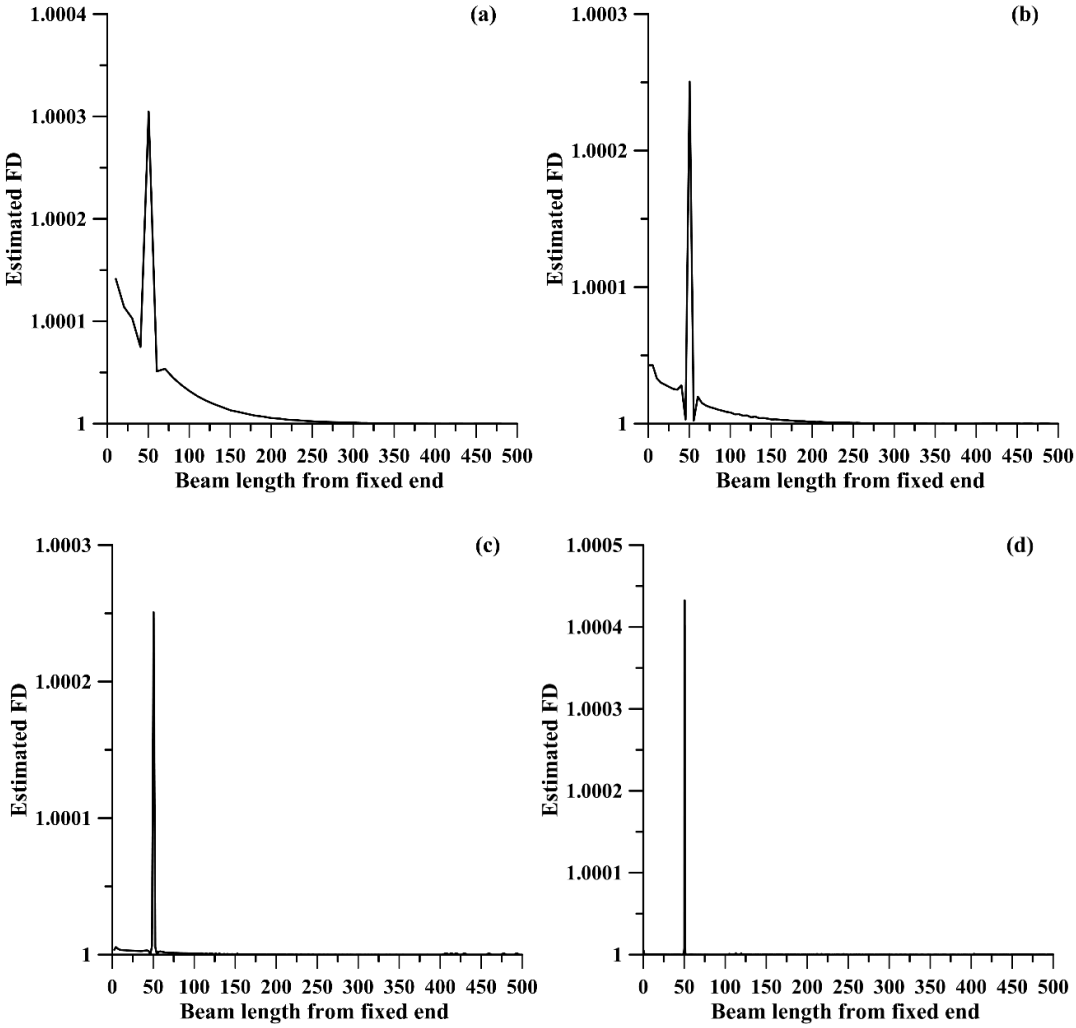

Figure 6.13 FD plot (a) r=1, (b) r=2, (c) r=5 and (d) r=20

In order to overcome this discrepancy in the result, an investigation is carried out with the same beam. Second and third mode shape are used for FD analysis with resolution 20 and scale factor 1. Figure 6.15 shows that there is no evidence of crack at location 450 mm from fixed end for both curves. In addition a few misleading peaks are observed in the FD plot.

Now FD analysis is performed with scale factor 2, 5 and 10. Results of FD analysis with different scale factors are shown in Figures 6.16-6.18. It is observed that when the scale factor is increased identification of crack becomes more prominent for evident of crack at location 450 mm from fixed end. And it is also observed that FD analysis on third mode shapes (Figures 6.16a, 6.17a and 6.18a) gives better results than those of second mode shapes (Figures 6.16b, 6.17b and 6.18c) for same scale factor.

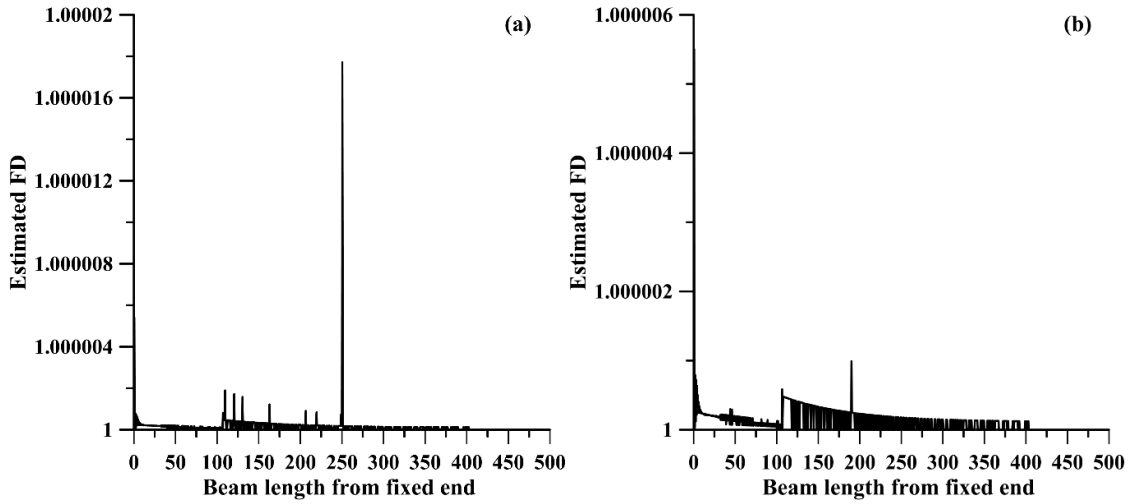

Figure 6.14 FD plot (a) at crack location 250 mm from fixed end and (b) at crack location 450 mm from fixed end

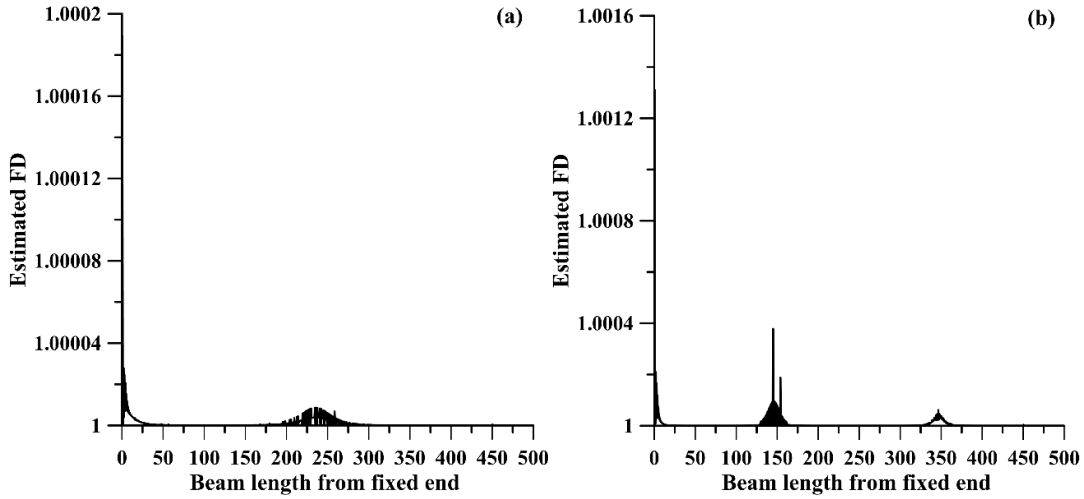

Figure 6.15 FD plot at crack location 450 mm for (a) second mode and (b) third mode

FD analysis is now carried out with different crack depth at same location. Four cracked beam are taken having with 1mm, 2 mm, 3 mm, 4 mm and 5 mm crack depth at crack location of 50 mm from fixed end. Rotational speed of the beam is kept at 100 rad/s. Based on the previous observation, third mode shape is taken as input for FD analysis for subsequent analysis. FD analysis result is shown in Figure 6.19. It is observed that estimated value of FD is increasing with the increase in crack depth. Neat FD value is obtained by subtracting one from actual estimated FD value. Now square root of maximum estimated neat FD value is plotted against crack depth (Figure 6.20). A straight line relationship is observed in Figure 6.20.

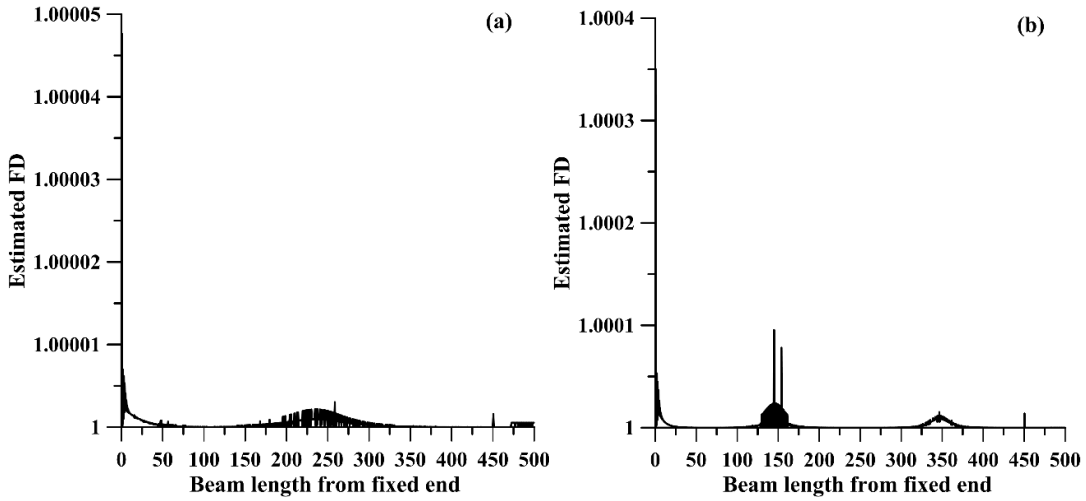

Figure 6.16 FD plot at crack location 450 mm with s=2 (a) second mode and (b) third mode

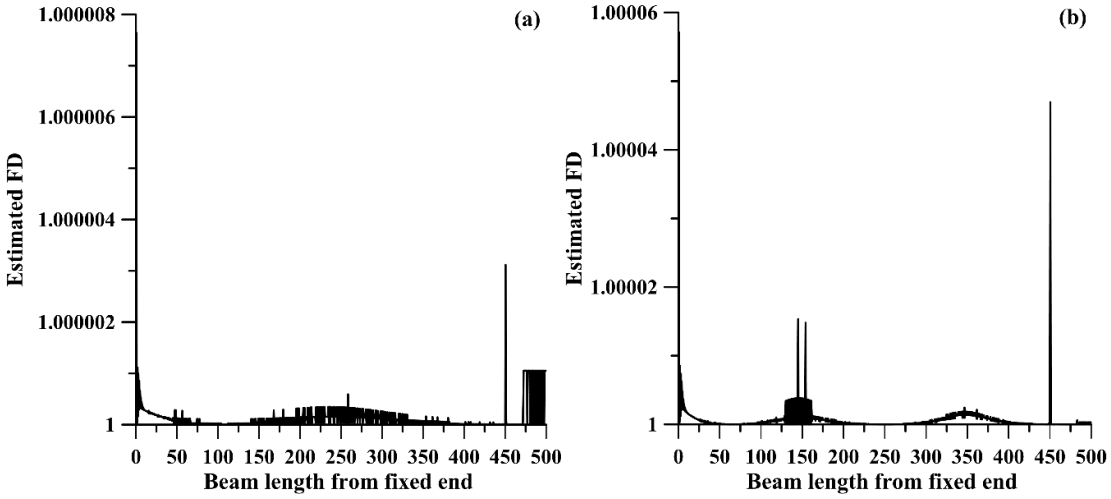

Figure 6.17 FD plot at crack location 450 mm with s=5 (a) second mode and (b) third mode

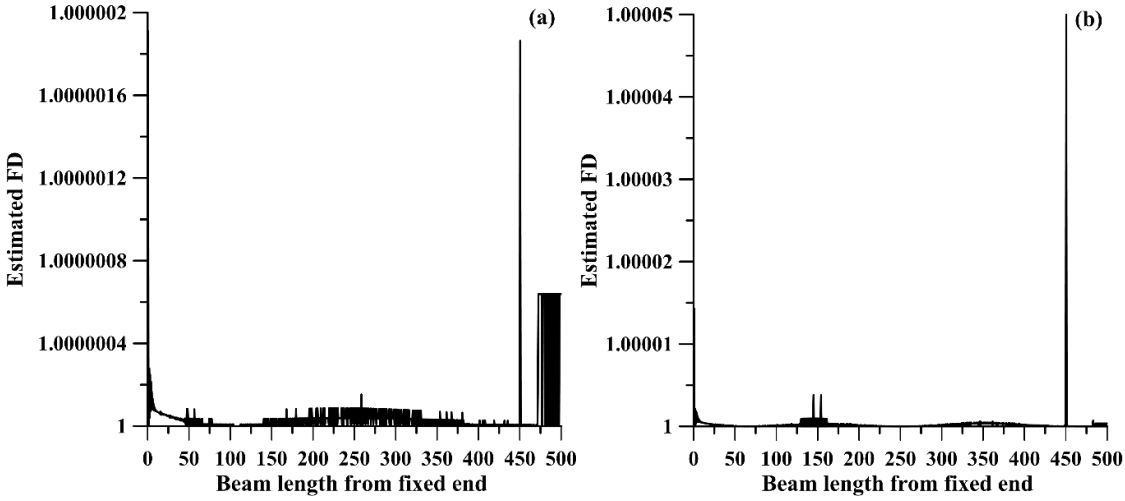

Figure 6.18 FD plot at crack location 450 mm with s=10 (a) second mode and (b) third mode

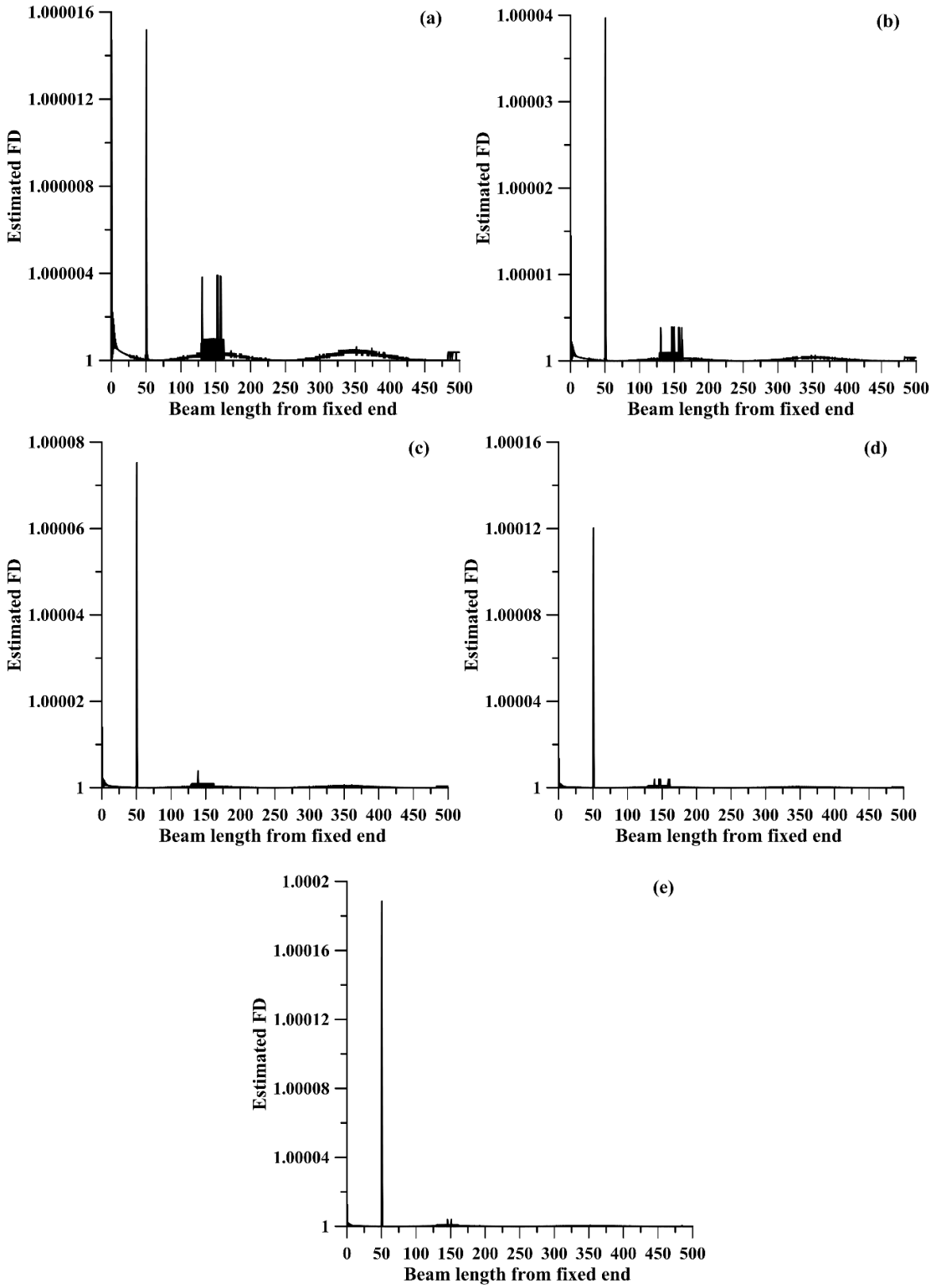

Figure 6.19 FD plot for crack depth (a) 1mm, (b) 2 mm, (c) 3mm, (d) 4 mm and (e) 5 mm

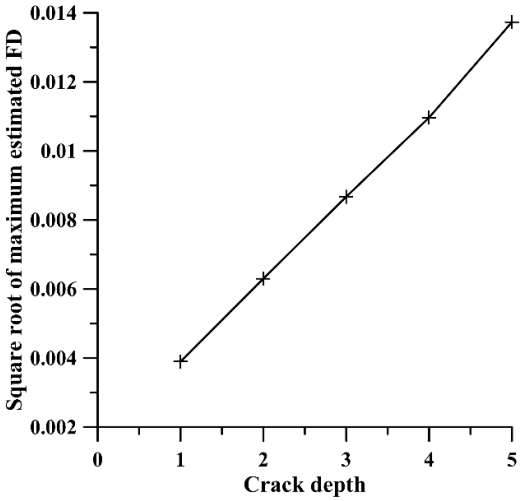

Figure 6.20 Square root of neat estimated FD vs. Depth

Now influence of rotating speed on FD analysis is determined. A cracked beam is taken with 5 mm crack depth at crack location 50 mm from fixed end. The beam is allowed to rotated about Y axis with four different speeds 50 rad/s, 100 rad/s, 150 rad/s and 200 rad/s. Third mode shape of this beam is considered for FD analysis with scale factor 10 and resolution 20.Figure 6.21shows estimated FD of this mode shape. It is depicted that the magnitudes of coefficients slightly decreases with rotating speed from 1.000189 to 1.000177. The centrifugal force introduced by the rotational speed reduces the localization effect of crack on mode shape of beam.

Similar investigation is carried out for detection of multiple cracks as well. Two double cracked rotating beams (100 rad/s) are taken for analysis. One cracked beam has a big crack 5mm depth at a location of 50 mm from fixed end and a small crack of 1mm depth at a distance 50 mm from free end. Other cracked beam has a small crack (1mm depth) near fixed end (50 mm from fixed end) and a big crack (1mm depth) near free end (50 mm from free end). Both second and third mode shapes are used for FD analysis. Figures 6.22 and 6.23 illustrate FD results. Figure 6.22a indicates that it is very difficult to identify crack location near free end by second mode shape when crack is small. However from FD analysis of third shape, presences of cracks are evident for both cases (Figure 6.23).

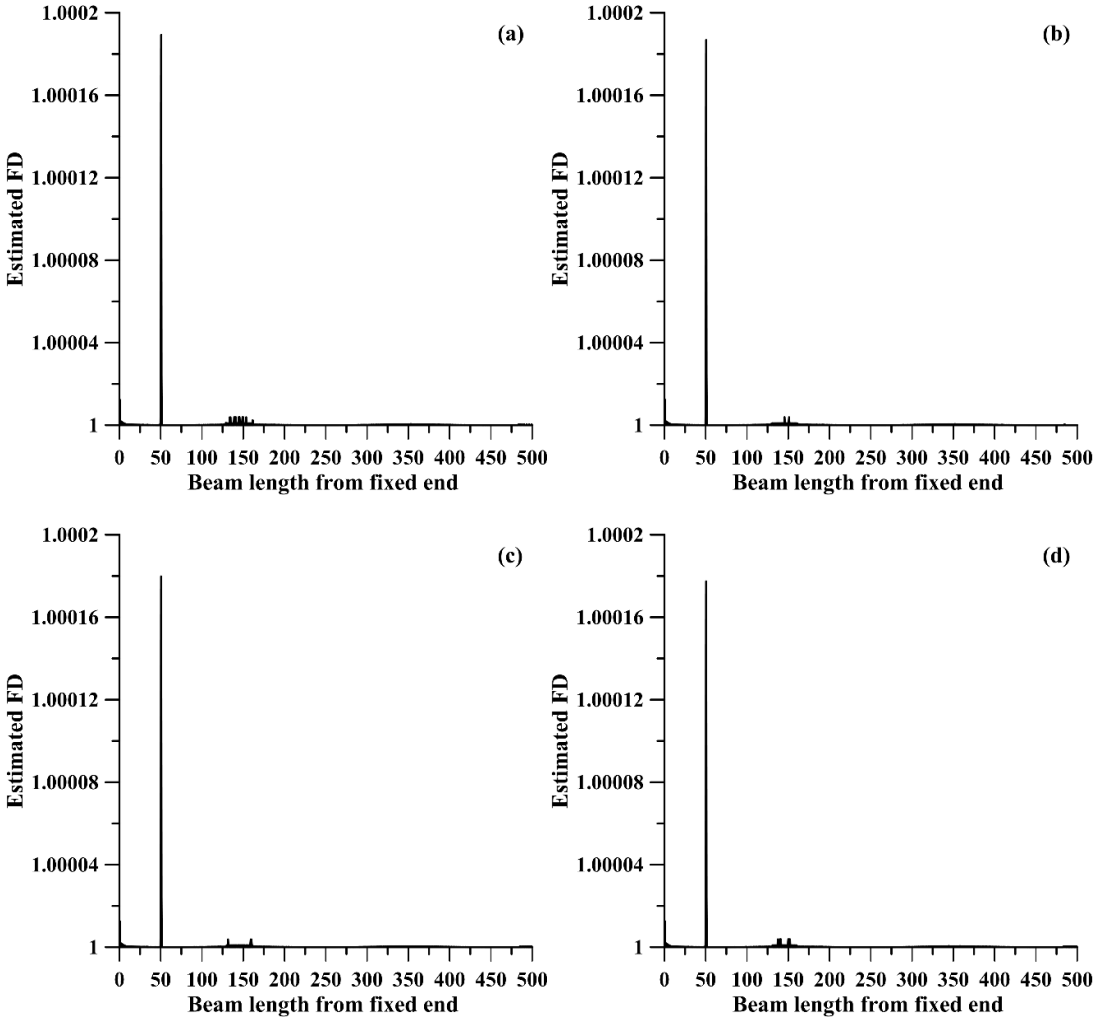

Figure 6.21 FD plot for rotating speed (a) 50 rad/s, (b) 100 rad/s, (c) 150 rad/s and (d) 200 rad/s

Investigation is carried out for a rotating (100 rad/s) cantilever beam with three cracks. Locations of cracks on the beam are 50 mm, 250 mm and 450 mm from fixed end having same depth 3mm. Both second and third mode shape results of FEM are performed for FD analysis. Figures 6.24 and 6.25 are shown the FD results. Result shows that in case of second mode shape (Figure 6.24) estimated FD is more severe at middle position and less severe at near free end whereas for third mode shape (Figure 6.25) estimated FD is more severe at near fixed end and less severe at middle position. This occurs due to the fact that point of inflection present at middle position of the beam in case of third mode shape whereas point of inflection is far away from middle position of the beam in case of second mode shape.

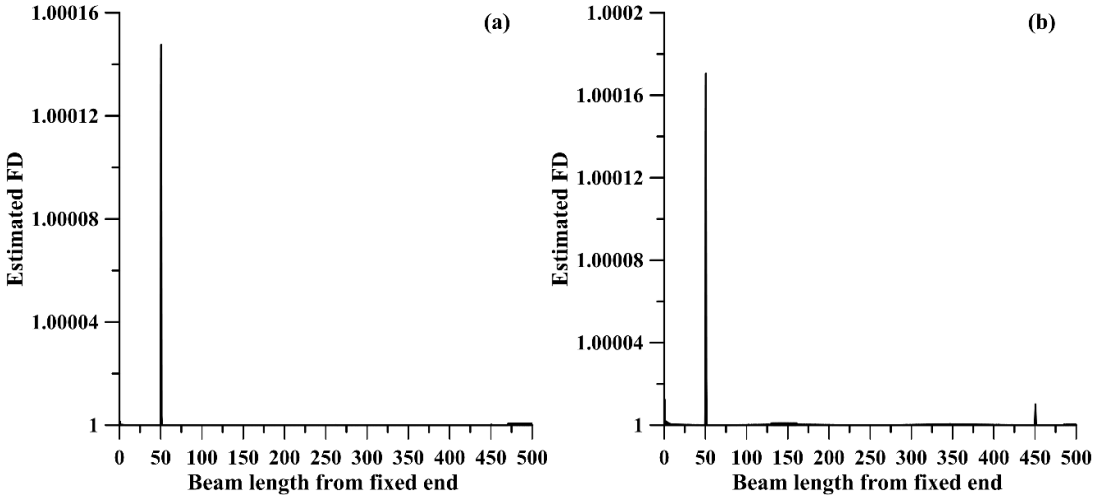

Figure 6.22 FD plots of double cracked beam with5 mm and 1mm crack depth at location 50 mm and 450 mm from fixed end respectively for (a) second mode and (b) third mode

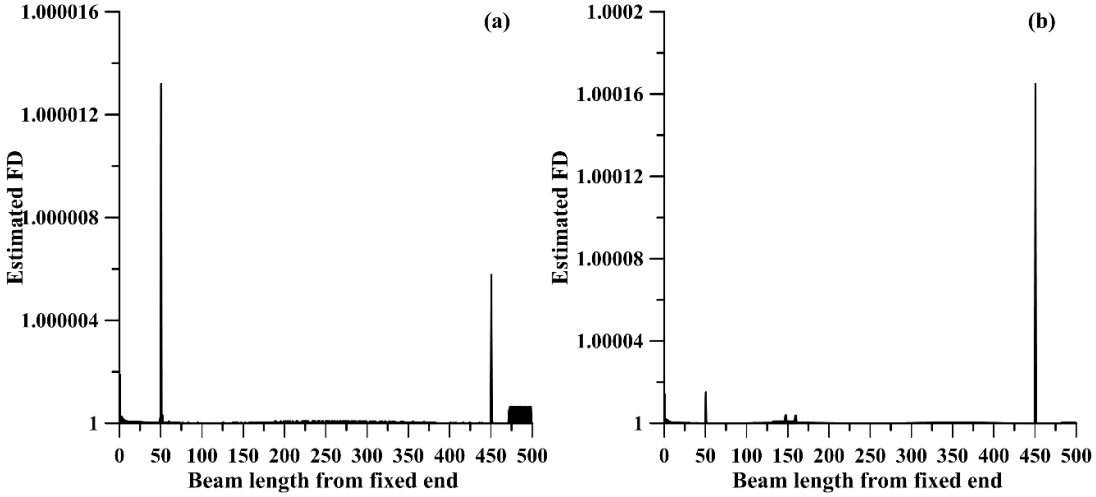

Figure 6.23 FD plot of double cracked beam with 1 mm and 5 mm crack depth at location 50 mm and 450 mm from fixed end respectively for (a) second mode and (b) third mode

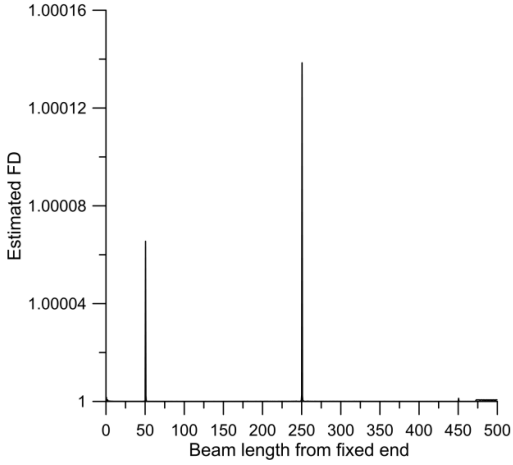

Figure 6.24 FD plot of triple cracked beam with for second mode shape

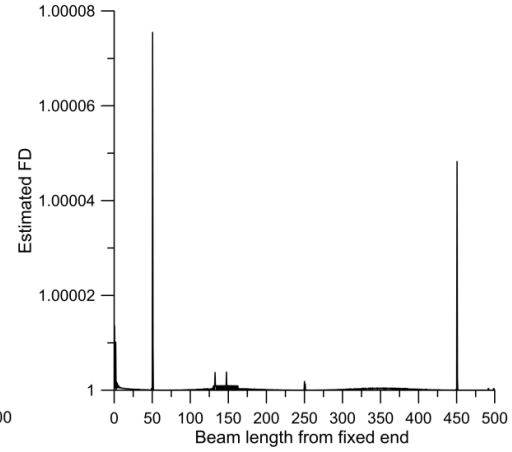

Figure 6.25 FD plot of triple cracked beam with for third mode shape

6.6.3 Identification of Crack on Rotating Cantilever Beam by Curvature Method

Free vibration analysis is carried out by series rotating cracked beams. Material and physical properties of the beam are kept same as in section 6.6.1. Crack parameters and rotational speed of cracked beams are taken from section 6.6.2.

Similar kind analysis is performed on rotating crack beam by curvature method with different resolution. The modal displacement data are sampled from the top surface of beam at distance interval of 10 mm (r=1 or 1 sampling point per cm), 2 mm (r=5 or 5 sampling point per cm) and 0.5 mm (r=20 or 20 sampling point per cm) of cracked beam at crack location 50 mm from fixed end with 3 mm crack depth. Beam is rotated at 100 rad/s speed. Curvature analysis is performed with first mode shape. Figure 6.26 illustrates the curvature plot in which variation of k^2 values are plotted along the beam length for different values of sampling point. The location of crack is evident at 50 mm from fixed end. Better result is shown in higher resolution [Figure 6.26(c)]

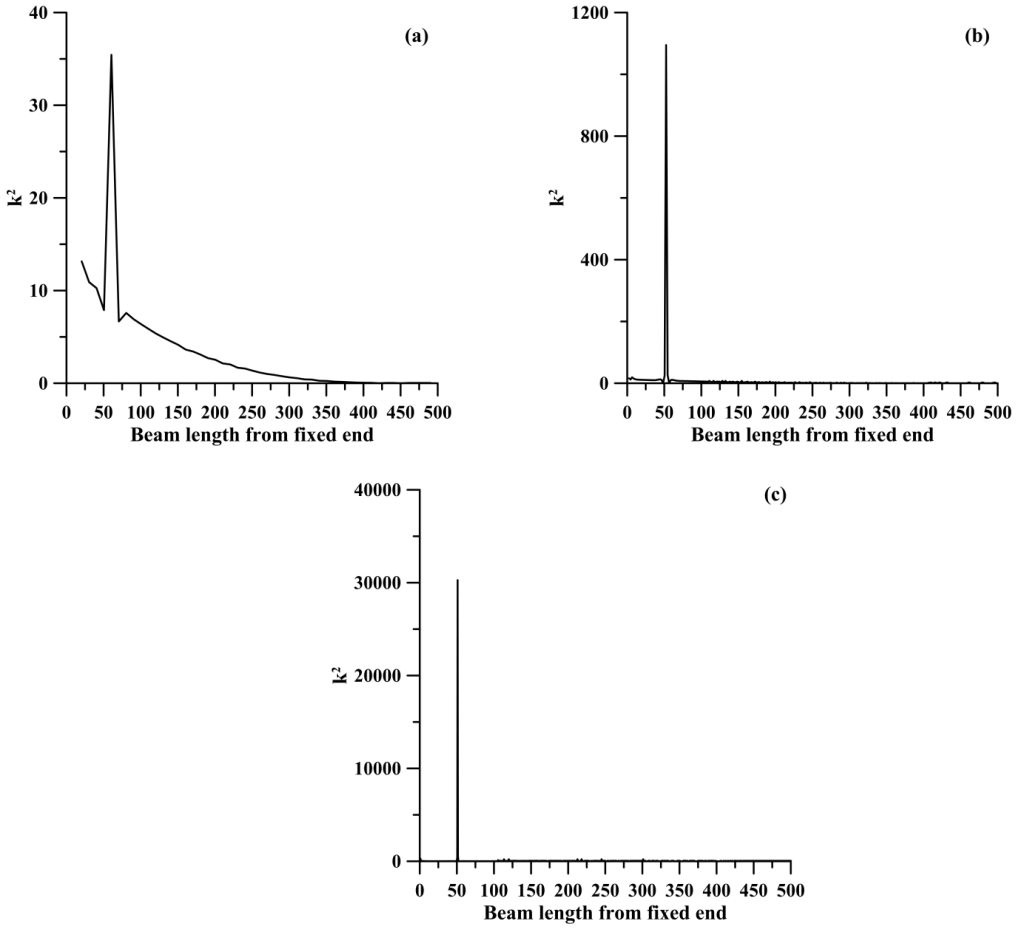

Figure 6.26 Curvature plot for (a) r=1, (b) r=5, (c) r=20

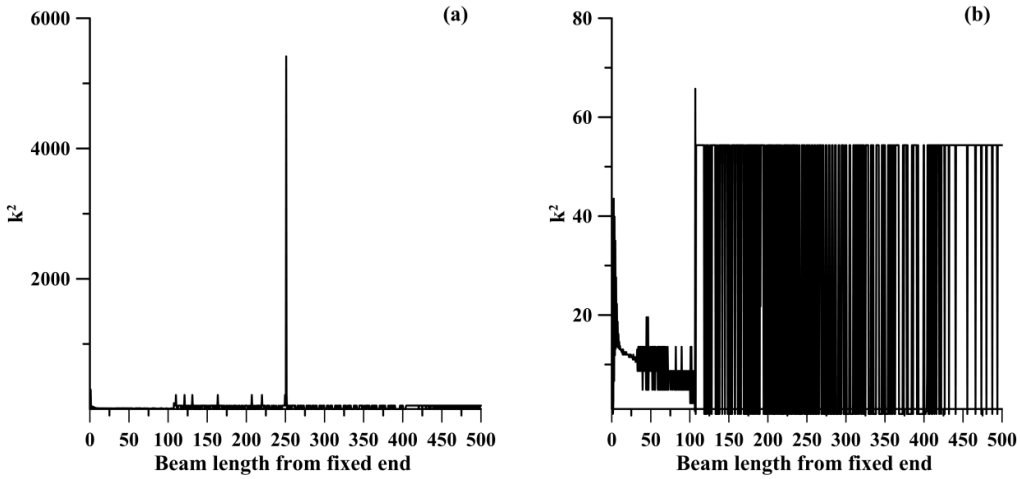

Figure 6.27 Curvature plot for first mode at crack location (a) 250 mm and (b) 450 mm from fixed end

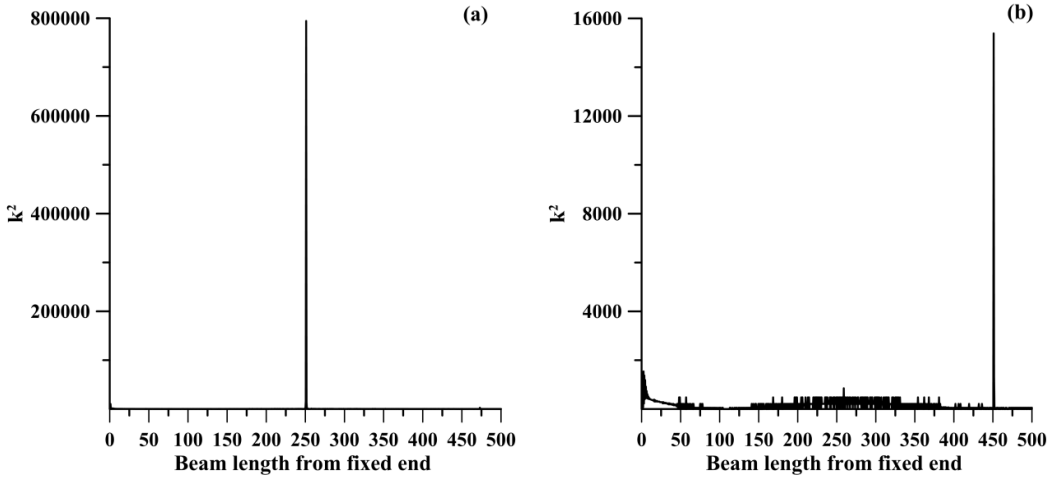

Figure 6.28 Curvature plots for second mode at crack location (a) 250 mm and (b) 450 mm from fixed end

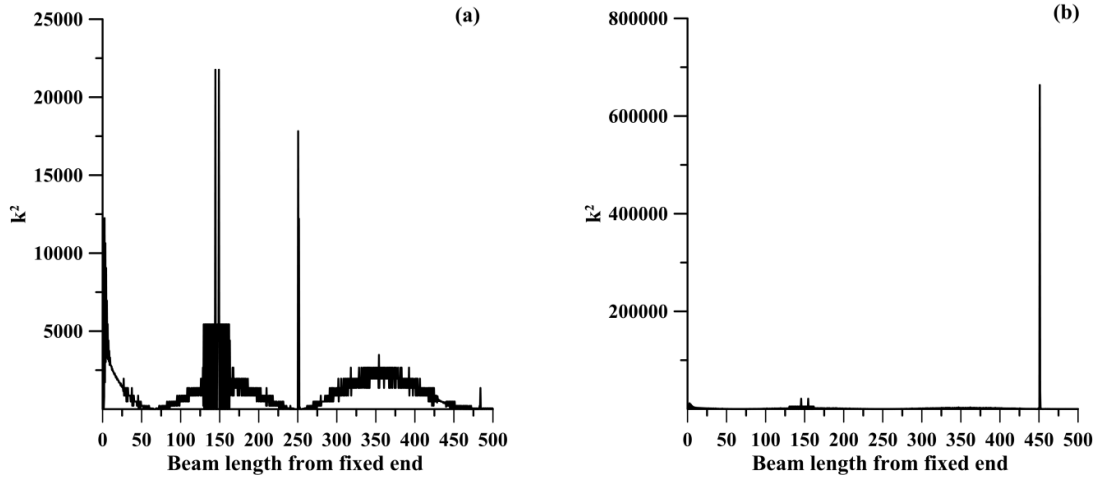

Figure 6.29 Curvature plots for second mode at crack location (a) 250 mm and (b) 450 mm from fixed end

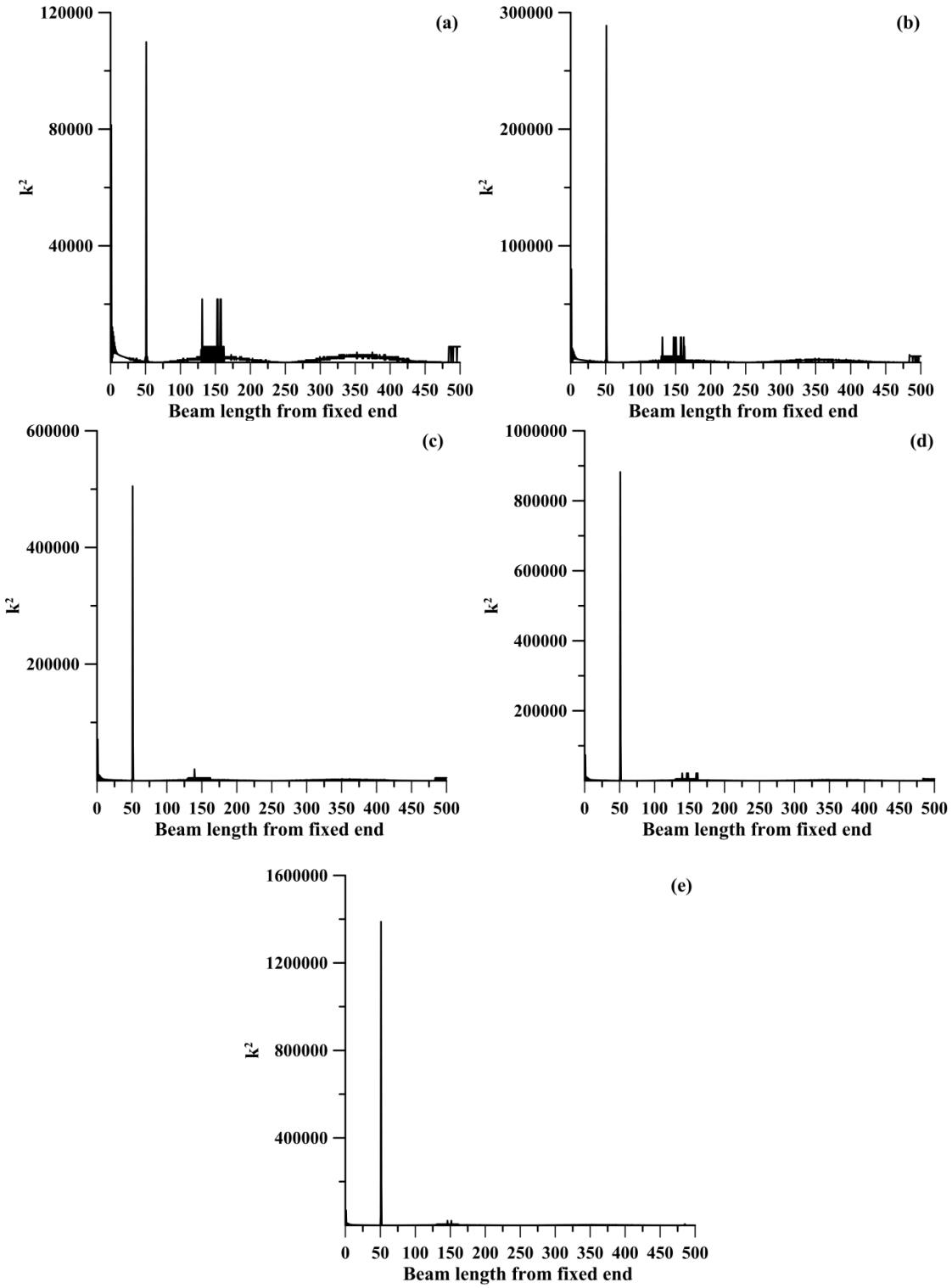

Figure 6.30 Curvature plot for crack depth (a) 1mm, (b) 2 mm, (c) 3 mm, (d) 4 mm and (e) 5 mm

Now curvature analysis is performed different location of crack on rotating cantilever beam. Two cracked beam are taken with 3mm depth at a distance 250 mm and 450 mm from fixed end. Rotational speed of the beam is 100 rad/s. All three mode shapes, first, second and

third are used for curvature analysis with resolution 20. Figures 6.27-6.29 are shown the curvature analysis result.

From the plots it is evident that there is a crack at a distance of 250 mm from fixed end (Figures 6.27a, 6.28a and 6.29a). But in case of second mode shape it has been observed that no disturbance is present in curvature plot other than crack location (Figure 6.28a). From Figure6.27b it has been observed that it is not possible to detect any damage in particular location. For in case of second mode and third mode shape (Figures 6.28b and 6.29b) they are clearly shown that there is a crack at 450 mm from fixed end. But Figure 6.29b shows more clear result with less misleading peak.

Similar curvature analysis is performed with various cracked beam having deferent crack depth (1mm, 2mm, 3mm, 4mm and 5mm) at same location at 50 mm from fixed end. Rotational speed is given in beam 100 rad/s. Third mode shape is taken as input of curvature analysis. Figure 6.30 is shown the result. The values of square of curvature are increased with depth of crack. Curvature at position of crack is plotted against crack depth (Figure 6.31).

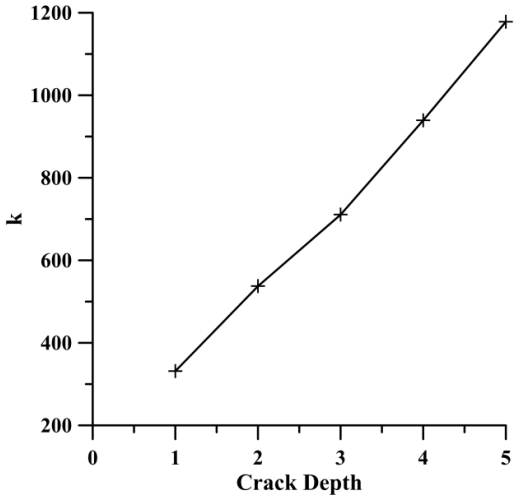

Figure 6.31 Curvatures vs. Crack Depth

A cracked beam is taken with 5 mm crack depth at crack location 50 mm from fixed end. Now this beam is rotated about Y axis in four different speeds 50 rad/s, 100 rad/s, 150 rad/s and 200 rad/s. Third mode shape of this beam is carried out for FD analysis with scale factor 10 and resolution 20.Figure 6.32 is shown wavelet coefficient of this mode shape. Results show that maximum values of square of curvature for rotating speed are nearly equal. The magnitudes of coefficients are slightly decreases with rotating speed from 1406670 to 1316548.

Similar investigation is carried out for detection of multiple cracks also. Two double cracked rotating beams (100 rad/s) are taken for analysis. One cracked beam has a big crack (5mm depth) near fixed end (50 mm from fixed end) and a small crack (1mm depth) near free end (50 mm from free end). Other cracked beam has a small crack (1mm depth) near fixed end (50 mm from fixed end) and a big crack (1mm depth) near free end (50 mm from free end). Both second and third mode shapes are used for FD analysis. Figures 6.32 and 6.33 are shown the CWT results. Figure 6.32a shows that very difficult to identify crack location at near free end by second mode shape for small crack. For FD analysis of third shape is clearly shown evident of crack for both cases (Figures 6.32b and 6.33b).

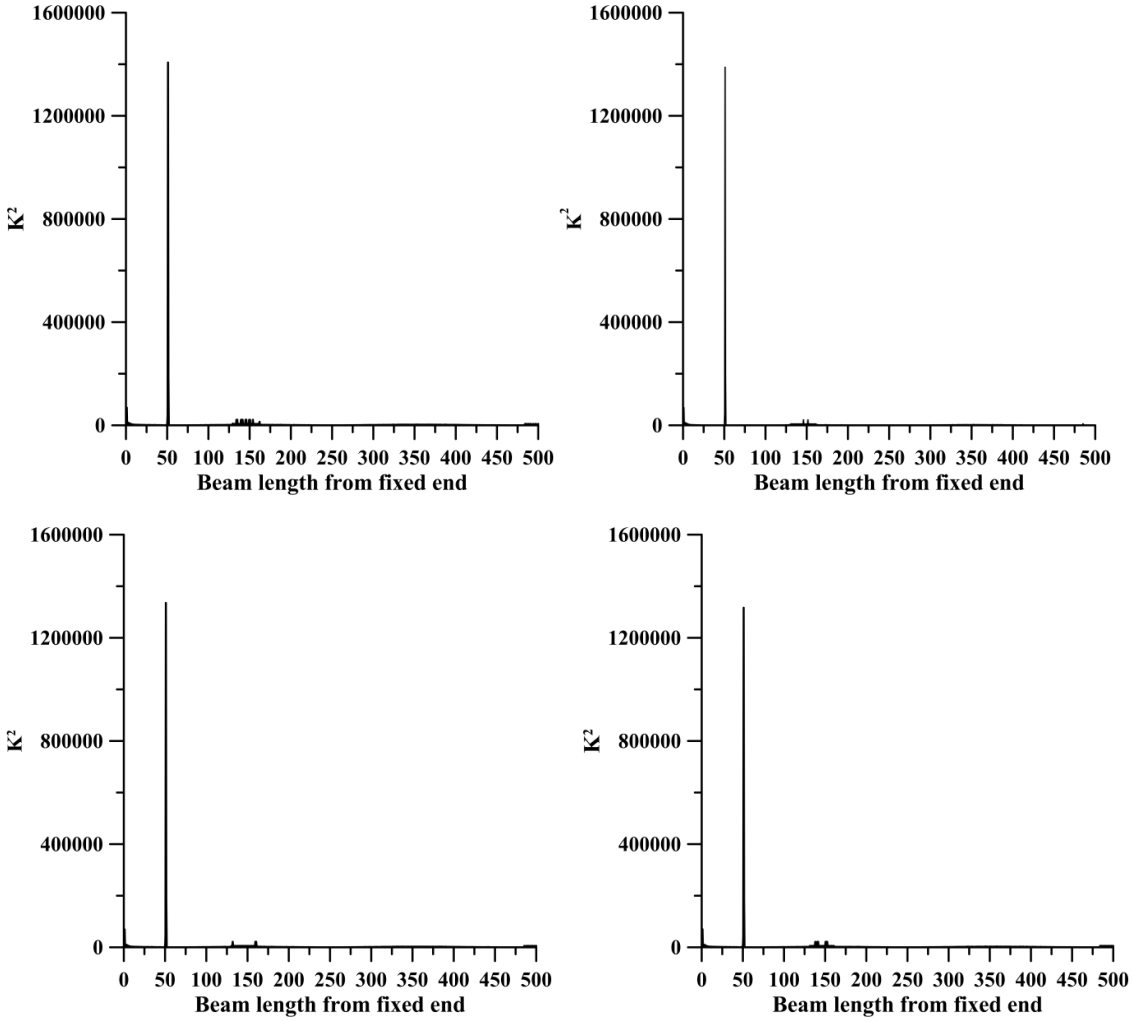

Figure 6.32 Curvature plot for rotating speed (a) 50 rad/s, (b) 100 rad/s, (c) 150 rad/s and (d) 200 rad/s

Now investigation is carried out for a rotating (100 rad/s) cantilever beam with three cracks. Locations of cracks of the beam are 50 mm (near fixed end), 250 mm (at middle) and 450 mm (near free end) from fixed end with same size (3 mm depth). Both second and third

mode shape results of FEM are performed for Curvature analysis. Figures 6.35 and 6.36 are shown the Curvature analysis results. Result shows that in case of second mode shape (Figure6.35) curvature value is more severe at middle position and less severe at near free end whereas for third mode shape curvature value is more severe at near free end and less severe at middle position.

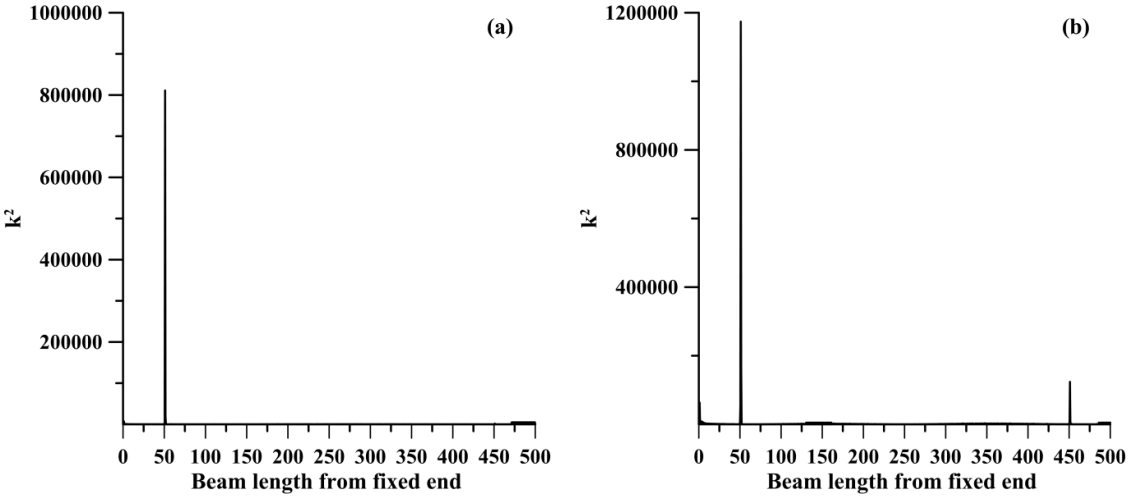

Figure 6.33 Curvature plot of double cracked beam with 5 mm and 1mm crack depth at location 50 mm and 450 mm from fixed end respectively for (a) second mode and (b) third mode

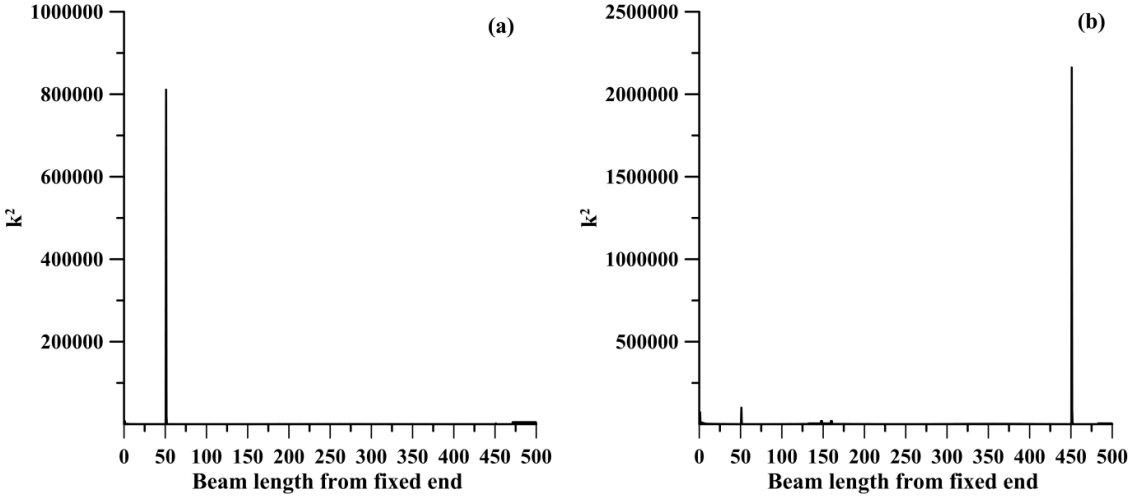

Figure 6.34 Curvature plot of double cracked beam with 1 mm and 5 mm crack depth at location 50 mm and 450 mm from fixed end respectively for (a) second mode and (b) third mode

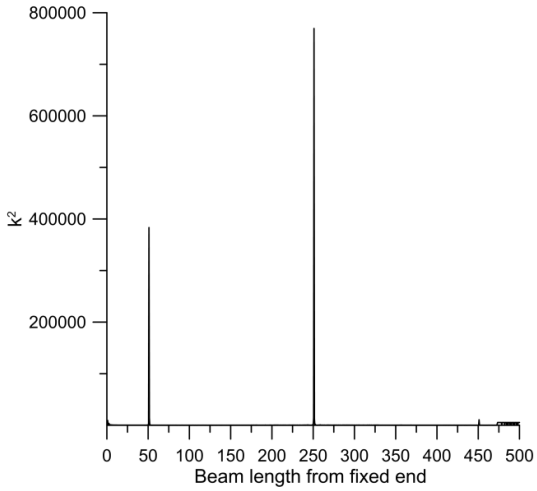

Figure 6.35 Curvature plot of triple cracked beam with for second mode shape

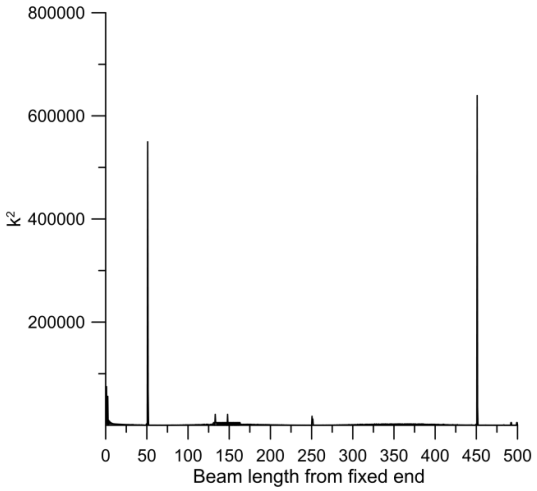

Figure 6.36 Curvature plot of triple cracked beam with for third mode shape

6.6.4 Identification of Crack Cantilever Beam by Irregularity Extracted Method

First free vibration is carried out series of cracked cantilever beam. First four natural frequencies of the cantilever beam under transverse vibration are obtained by finite element analysis. Geometrical and physical properties are shown in the Table 6.1.The corresponding mode shapes profiles are also captured. These profiles are used for damage detection of beam by different filtration technique.

Free vibration finite element analysis is carried out on a series of cracked cantilever beams with three crack sizes (crack depth ratio (d_c/h= 0.2, 0.4 and 0.6)). Vibration analysis is performed on cracked beam with eight different crack locations (l_c/L =0 0588, 0.1765, 0.2941, 0.4118, 0.5294, 0.6471, 0.7059 and 0.7647). In case of double cracked beam, three cracked beams are analysed with three different crack scenarios.

First four mode shapes are developed by finite element analysis of a cracked beam with crack d_c/h =0.4 at l_c/L = 0.1765. Roughness measurement is determined for same crack beam as describe previous section. Figure 6.37 shows that result of roughness filtration with cut off length for all four mode shapes for triangular filtration. Results exhibits better detection of crack location at l_c/L = 0.1765 for first and forth mode than second and third. Roughness values for Gaussian filtration plot are much less than triangular filtration plot but irregularity does not differ much. Hence, triangular filtration is considered for further investigation.

Investigation is also made with other crack location. A cracked beam is taken crack size d_c/h=0.4 at crack location at l_c/L = 0.7059. Roughness plot is shown in the Figure 6.38. Results exhibits better detection of crack location at l_c/L = 0.7059 for second and third mode than first and forth. It is evident from the results (Figures 6.38) that in case of first mode shape roughness value is more prominent corresponding to crack position at near fixed position whereas for second, third and froth mode shapes roughness values are prominent at anti nodal point (maximum displacement).This is due to the fact that bending moment is maximum at fixed end for first mode whereas, in case of second, third and froth mode irregularly effect is more prominent at point of inflection.

Table 6.1 Geometric and physical properties of Cantilever beam

Density (kg/m^3)	Poisson Ratio	Elasticity Modulus (GPa)	Length (L) (mm)	Thickness (W) (mm)	Depth (h) (mm)
2700	0.33	68.3	850	50	10

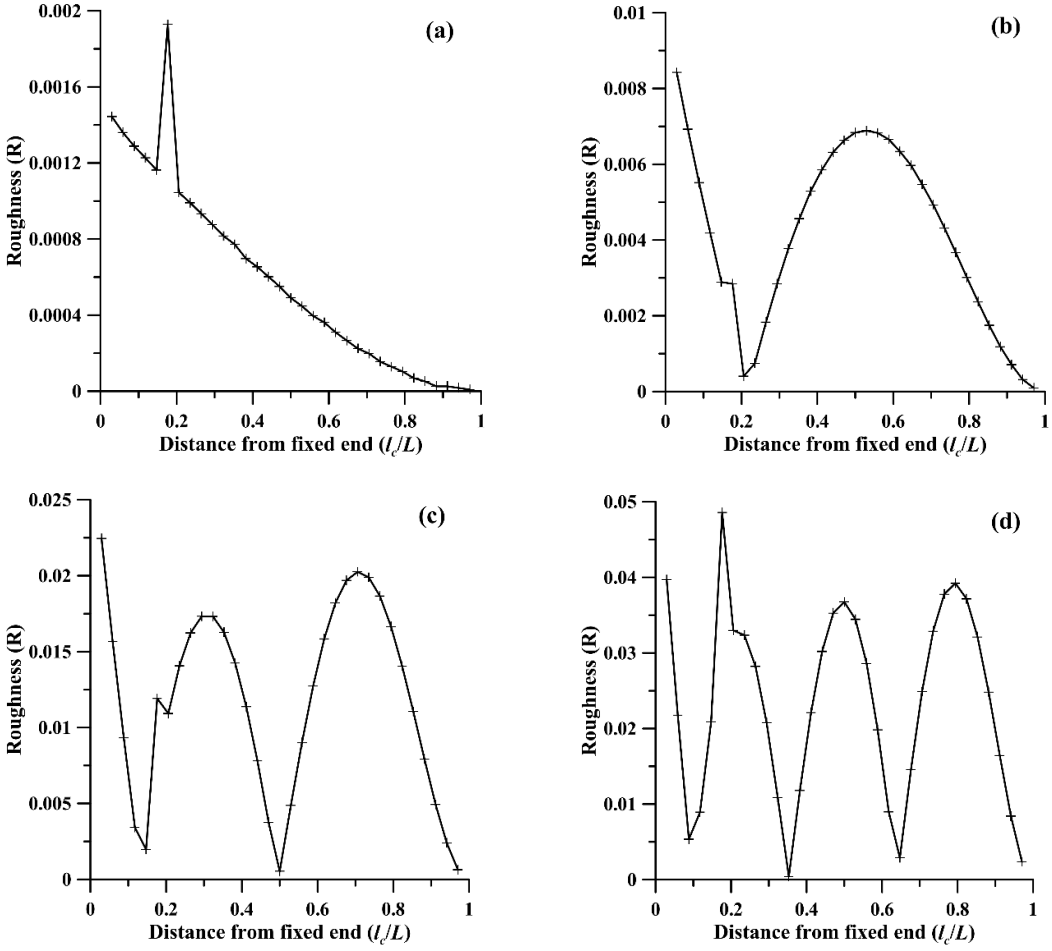

Figure 6.37 Filtration result of the single cracked beam (crack location at l_c/L = 0.1765) based on triangular filtration (a) First mode, (b) Second mode, (c) Third mode, (d) Forth mode.

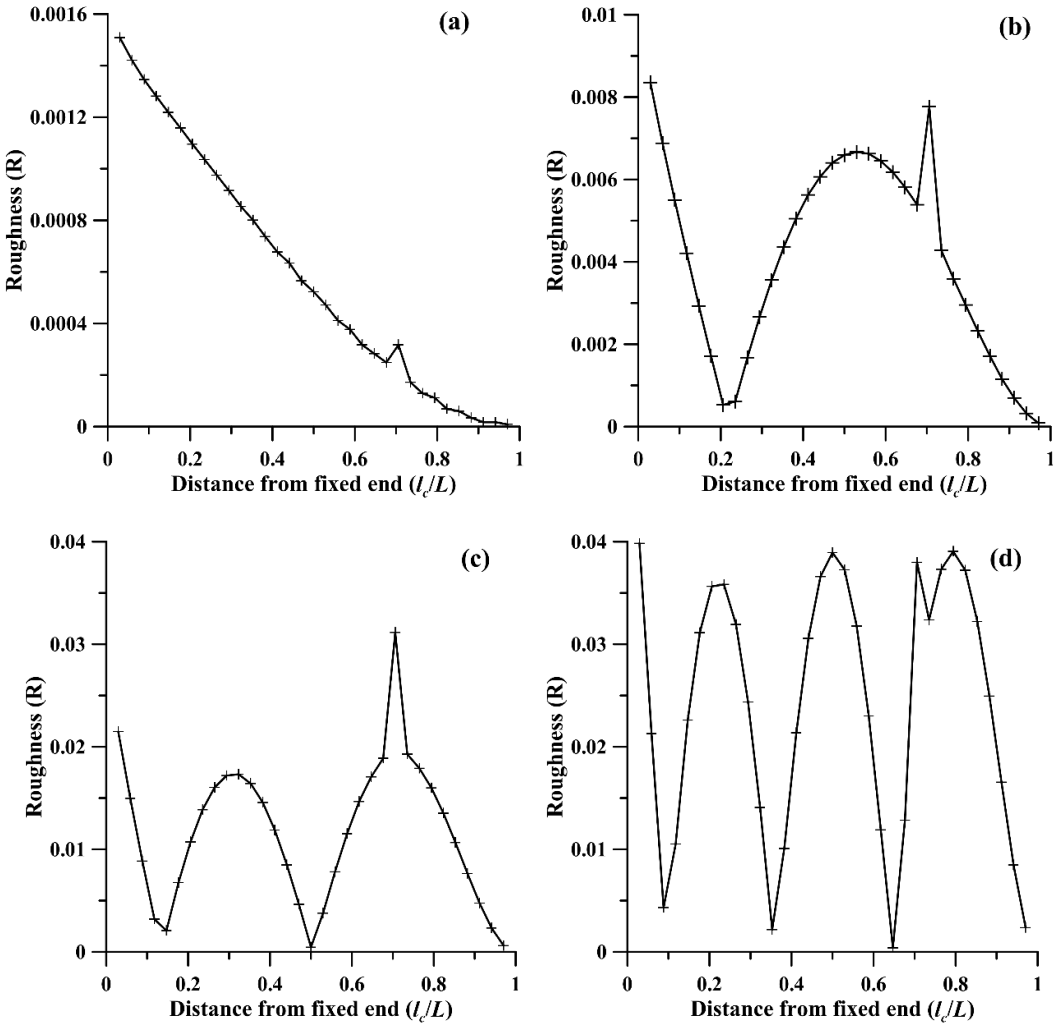

Figure 6.38 Filtration result of the single cracked beam (crack location at l_c/L = 0.7059) based on triangular filtration (a) First mode, (b) Second mode, (c) Third mode, (d) Forth mode.

It is observed that the resolution (sampling point per unit distance) plays an important role in irregularity base damage detection procedure. Filtration analysis is performed on the third mode shape of a cracked beam at crack location at l_c/L= 0.7647 in three different resolutions, namely, r=200, r=40 and r=20 indicating 200 sampling point per meter, 40 sampling point per cm and 20 sampling point per cm. Figure 6.39 shows the results of filtration of mode shape on different resolution. It is clearly observed that higher resolution shows better result.

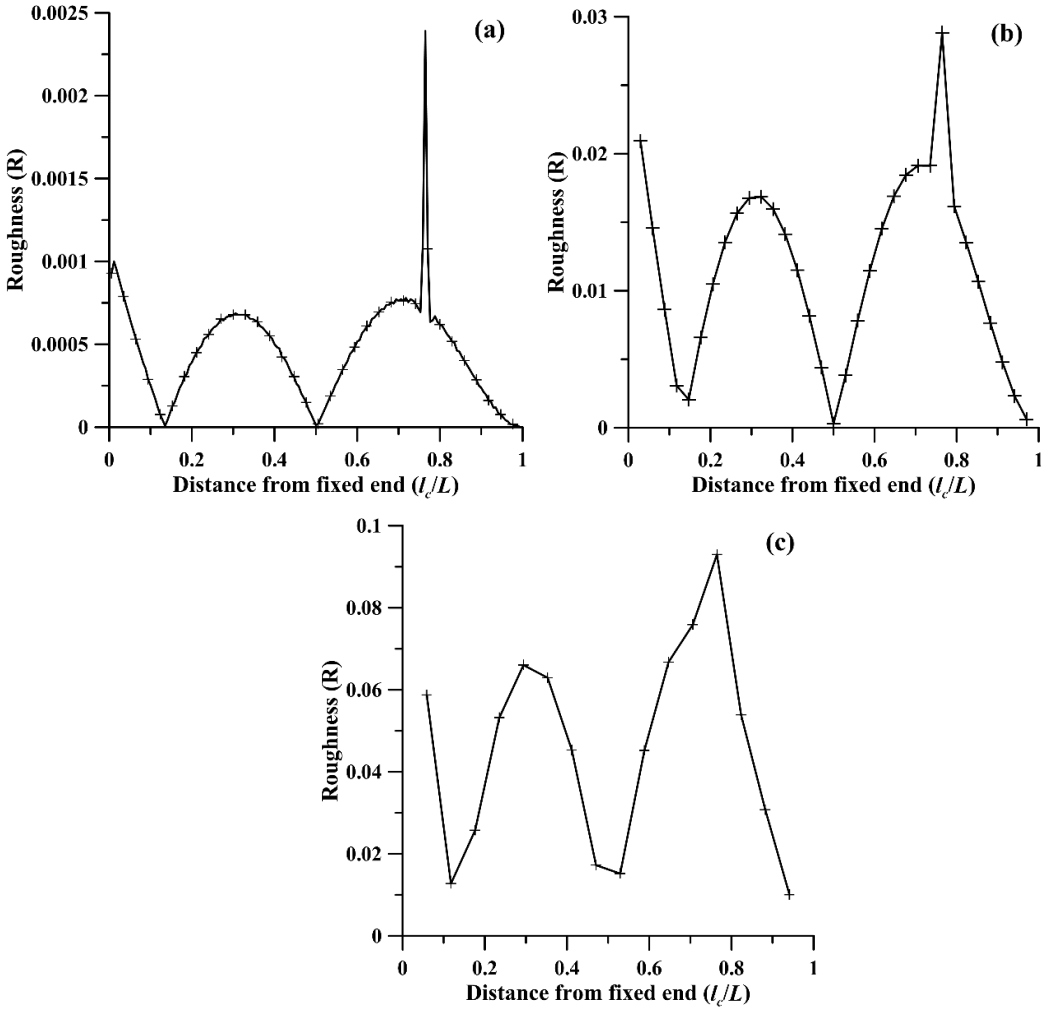

Figure 6.39 Filtration result of third mode of single cracked beam (crack location at l_c/L= 0.7647) based on triangular filtration (a) r=200, (b) r=40, (c) r=20

For structural health monitoring, crack size estimation is also important. Accordingly, five cracked beam are taken having crack sizes (d_c/h) 0.2, 0.3, 0.4, 0.5 and 0.6 at crack location l_c/L= 0.1765. Forth mode shape is taken as input of filtration analysis for subsequent analysis. It is noticeable in filtration plot (Figure 6.40) that roughness peaks are related to the crack depths. When the crack depth is small, roughness peak is small; however, when the crack depth increases, the peaks become more visible. This is because mode shape irregularity produce by a smaller crack is less than that of a larger crack. Roughness differences are measured by comparing roughness value of cracked beam and crack free beam. Roughness differences at crack position with different crack depths are shown Figure 6.41. Therefore, it is possible to determine the crack depth a beam by knowing roughness value of crack location of the beam.

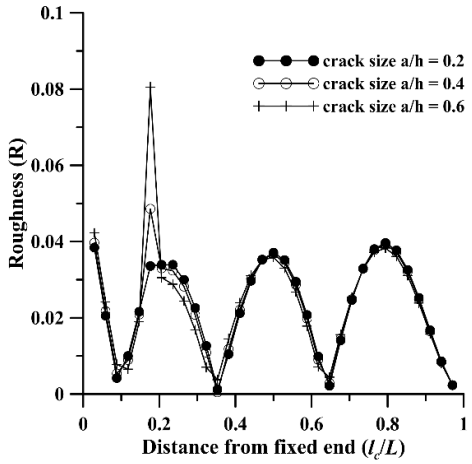

Figure 6.40 Filtration result of forth mode of single cracked beam (crack location at l_c/L= 0.1765) based on triangular filtration with different crack sizes

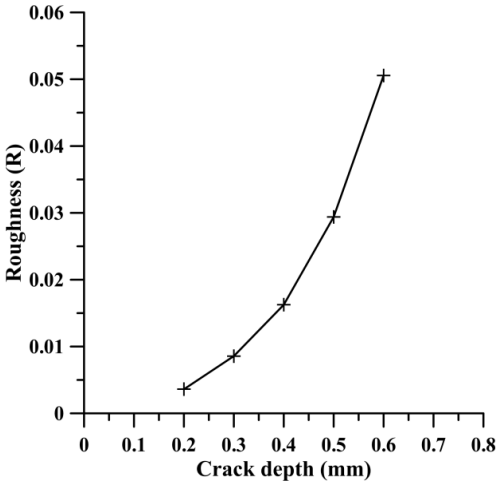

Figure 6.41 Roughness for crack vs. crack size

6.6.5 Identification of Crack on Cantilever Beamfrom Experimental Resultsby Irregularity Extracted Method

Free vibration experiments are carried out for a series of cracked cantilever beams. In order to evaluate mode shape of cracked beam ME'scope VES software is used with Data Acquisition System. Physical and material properties are kept same as mentioned in section 6.6.4. First four mode shape associated with crack beam in transverse direction are collected. Now these mode shapes are used to evaluate crack by means of irregularity extracted technique.

Finite element simulations suggest that the irregularity-based method requires a relatively high measurement resolution. However, during experimentation a very high resolution may be prohibited from the practical view point. In this experiment, mode shape data is obtained by hammering all along the beam maintaining a required distance of 25 mm between consecutive hammering positions. Hence, resolution for experiment is r= 40 i.e. 40 sampling (hammering) point per meter.

Four cracked beams are taken. Two different crack depths (d_c/h =0.2 and d_c/h=0.6) are considered at l_c= 0.1765 L and at l_c=0.765 L of the beam. First four natural frequencies along with corresponding mode shapes are evaluated. The irregularity profile of second, third and fourth mode shapes are considered for the analysis as the first mode shape produced very noisy data. Results are shown in Figures 6.42, 6.43 and 6.44.

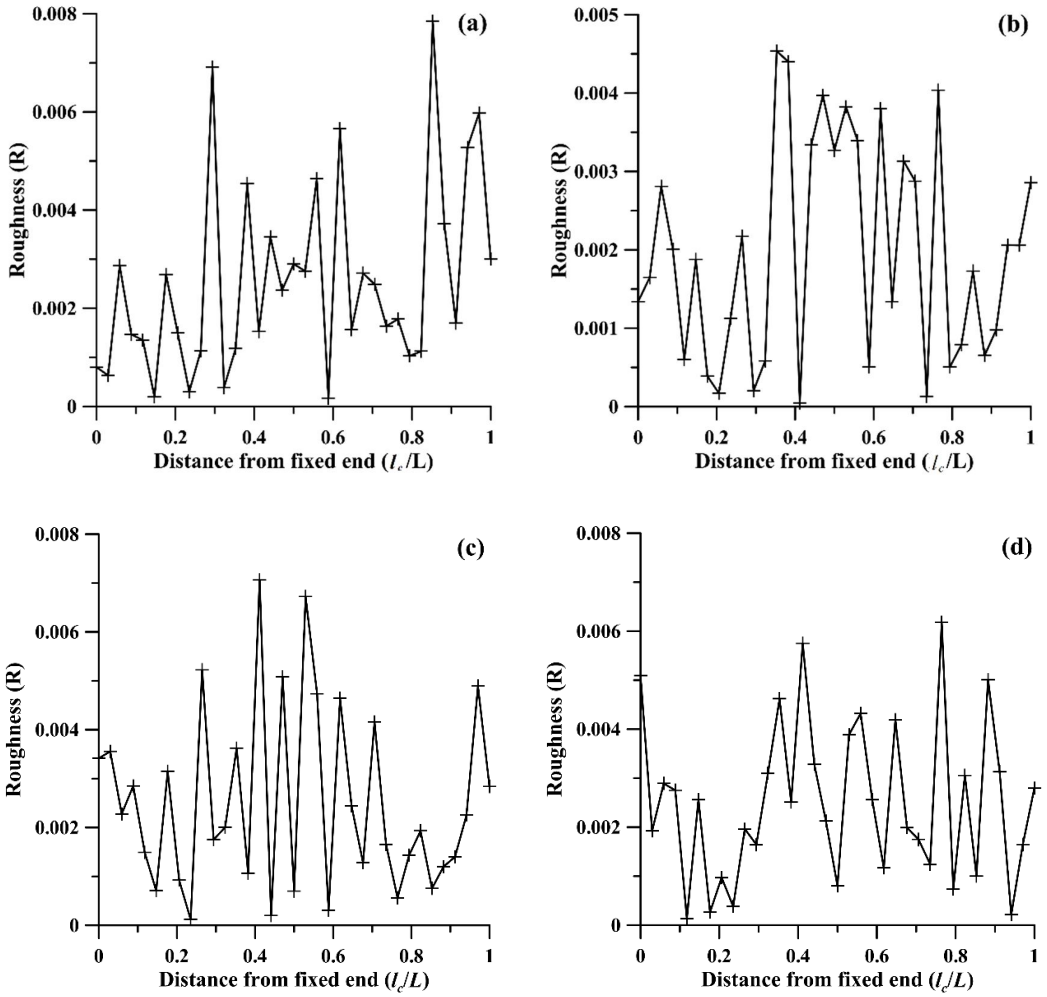

Figure 6.42 Filtration result of second mode shape of single cracked cantilever beam four different crack scenario (a) d_c/h = 0.2 at l_c= 0.412L, (b) d_c/h = 0.2 at l_c = 0.647 L (c) d_c/h = 0.6 at l_c = 0.1765L and (d) d_c/h = 0.6 at l_c = 0.765L based on triangular filtration

Figure 6.42 shows that there is no evidence of crack at location (l_c= 0.1765 L and l_c =0.765 L). In addition a lot of misleading peaks are observed in regularity plot. From Figure 6.43 (a) and (b) it is observed that when crack depth is small (d_c/h= 0.2) a lot of peak appear on the irregularity profile due to the existence of noise. But no peak is detected at the crack location. So it is very difficult to detect the small crack especially when they are located near the nodal point. In case of large crack (d_c/h =0.6) (Figure 6.43(c) and (d)) sharp peaks are visible at crack locations. Further investigation is carried out for third mode shape. Similar type of irregularity profile is observed for roughness measurement of third mode shapes (Figure 6.44). An interesting phenomenon is noted. Sharp peaks are more prominent at crack locations for forth mode shapes than third mode shapes

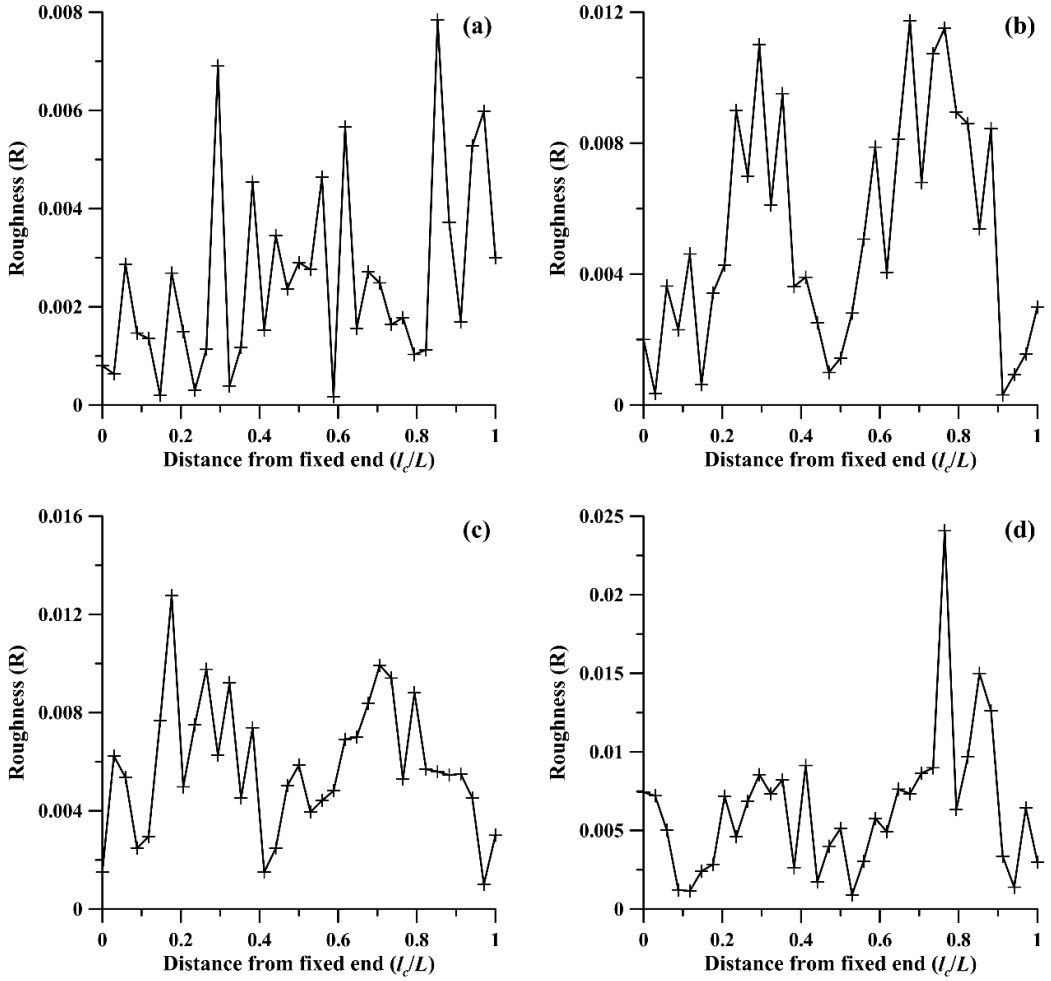

Figure 6.43 Filtration result of third mode shape of single cracked cantilever beam four different crack scenario (a) d_c/h = 0.2 at l_c= 0.412L, (b) d_c/h = 0.2 at l_c = 0.647 L (c) d_c/h = 0.6 at l_c= 0.1765L and (d) d_c/h = 0.6 at l_c = 0.765L based on triangular filtration

Now investigation is carried out for other crack location with medium crack size (d_c/h=0.4). Two cracked beams are taken with crack depth (d_c/h =0.4) at l_c/L = 0.2941and 0.5294. Third and fourth shape are considered for analysis as they are produce better results than second mode shape. Figure 6.45 (a) and (d) shows that there is a sharp peak of irregularity at the crack location. In other cases peak of irregularity are not clearly distinguishable with noisy peak [Figure 6.45 (b) and (c)]. For first two cases cracks are located near anti nodal point of mode shape vibration whereas for last cases cracks are located near nodal point of mode shape of vibration. In order to detect crack, its location should not be near the nodal point. Since it is not known a priori the position of crack, it is advisable to use more than one made shape for prediction of crack using irregularity extracted method.

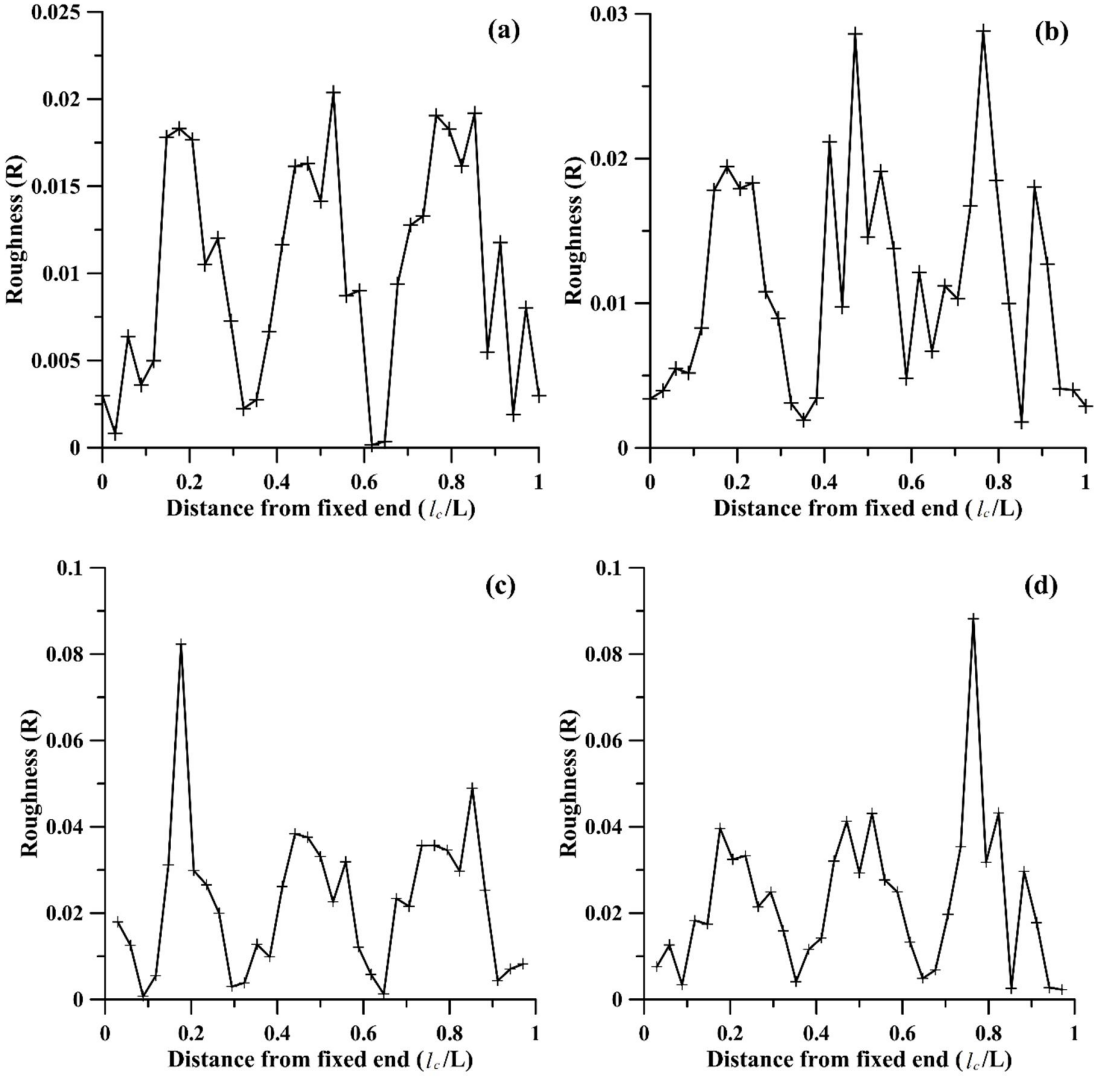

Figure 6.44 Filtration result of forth mode shape of single cracked cantilever beam four different crack scenario (a) d_c/h = 0.2 at l_c = 0.412L, (b) d_c/h = 0.2 at l_c = 0.647 L (c) d_c/h = 0.6 at l_c = 0.1765L and (d) d_c/h = 0.6 at l_c = 0.765L based on triangular filtration

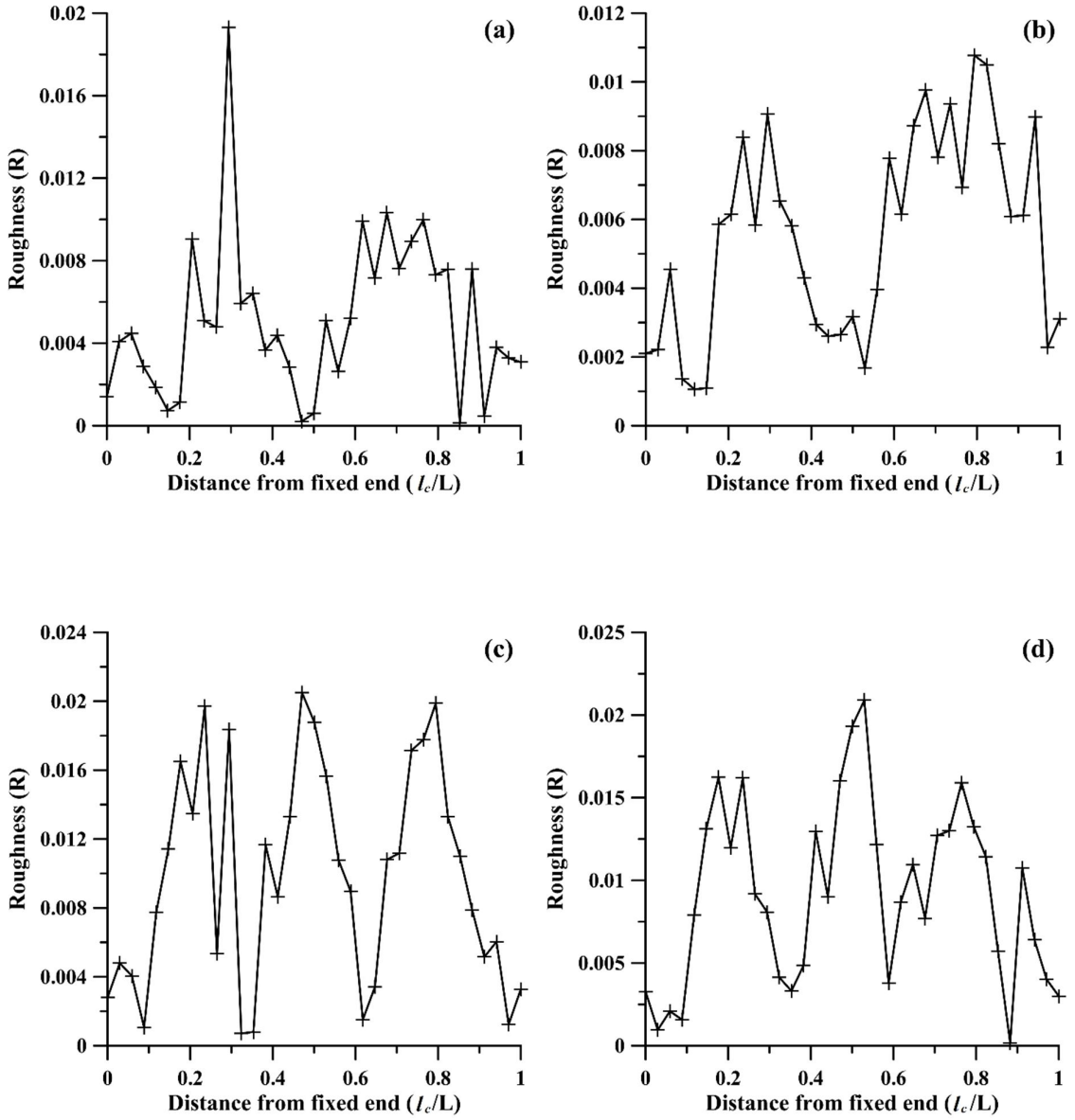

Figure 6.45 Filtration result of third mode shape of single cracked cantilever beam with two different crack scenario (a) d_c/h = 0.4 at l_c = 0.2941L, (b) d_c /h = 0.4 at l_c = 0.5294 L and forth mode shape of single cracked cantilever beam with two different crack scenario (c) d_c/h = 0.4 at l_c= 0.2941L and (d) d_c/h = 0.6 at l_c = 0.5294L based on triangular filtration

Similar investigation is carried out for detection of multiple cracks also. Three beams with double crack are taken for experiment. Since detection of small crack is very difficult from experimental noisy data, medium and large size cracked beams are considered for filtration. First beam has one crack with crack size d_c/h =0.4 (medium size) at l_c/L =0.1765 (near fixed end) and another crack with crack size d_c/h=0.6 (large size) at l_c /L = 0.7647 (near free end). Second beam has one crack with crack size d_c/h =0.6 (large size) at l_c/L =0.1765

(near fixed end) and another crack with crack size d_c/h=0.4 (medium size) at l_c/L = 0.7647 (near free end). Third beam has a large crack (d_c/h=0.6) and a medium crack (d_c/h=0.4) at location l_c/L = 0.2941 and l_c/L = 0.4118 (near the middle portion of beam) respectively. Filtration plot of third mode shape and forth mode shapes of double crack beam are shown in Figures 6.47 and 6.48 respectively. From Figures 6.46 and 6.47, it is clearly shown that large crack can be easily detected for both mode shape filtration plot. But in some case [Figure 6.47(c)] of medium crack, irregularity cannot be distinguished with noisy filtration data.

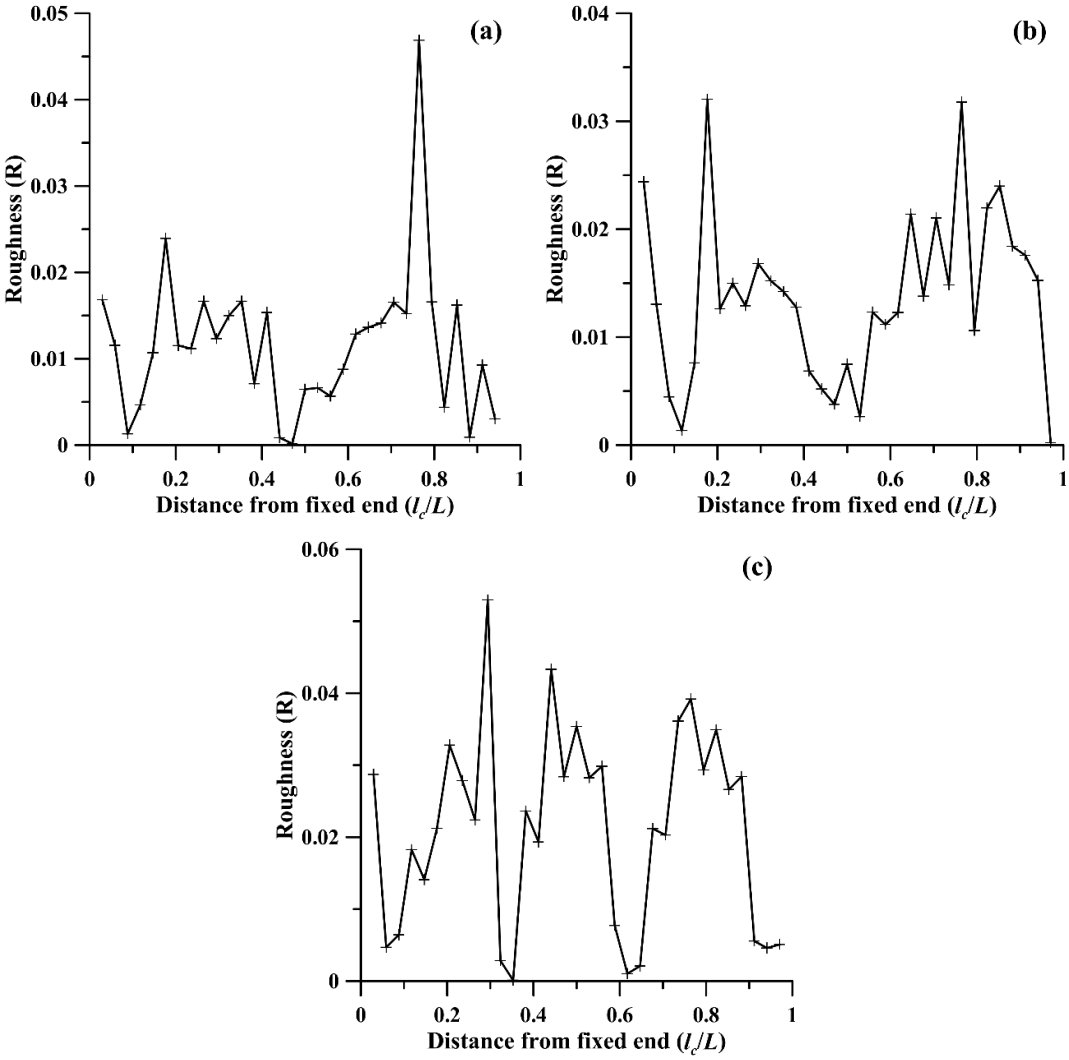

Figure 6.46 Filtration result of third mode shape of double cracked cantilever beam (a) d_c/h =0.4 at l_c/L = 0.1765 and d_c/h =0.6 at $l_c//L$ = 0.7647, (b) d_c/h =0.6 at $l_c//L$ =0.1765 and d_c/h =0.4 at l_c/L = 0.7647, (c) d_c/h=0.6 at l_c/L =0.2941 and d_c /h=0.4 at l_c/L = 0.4118

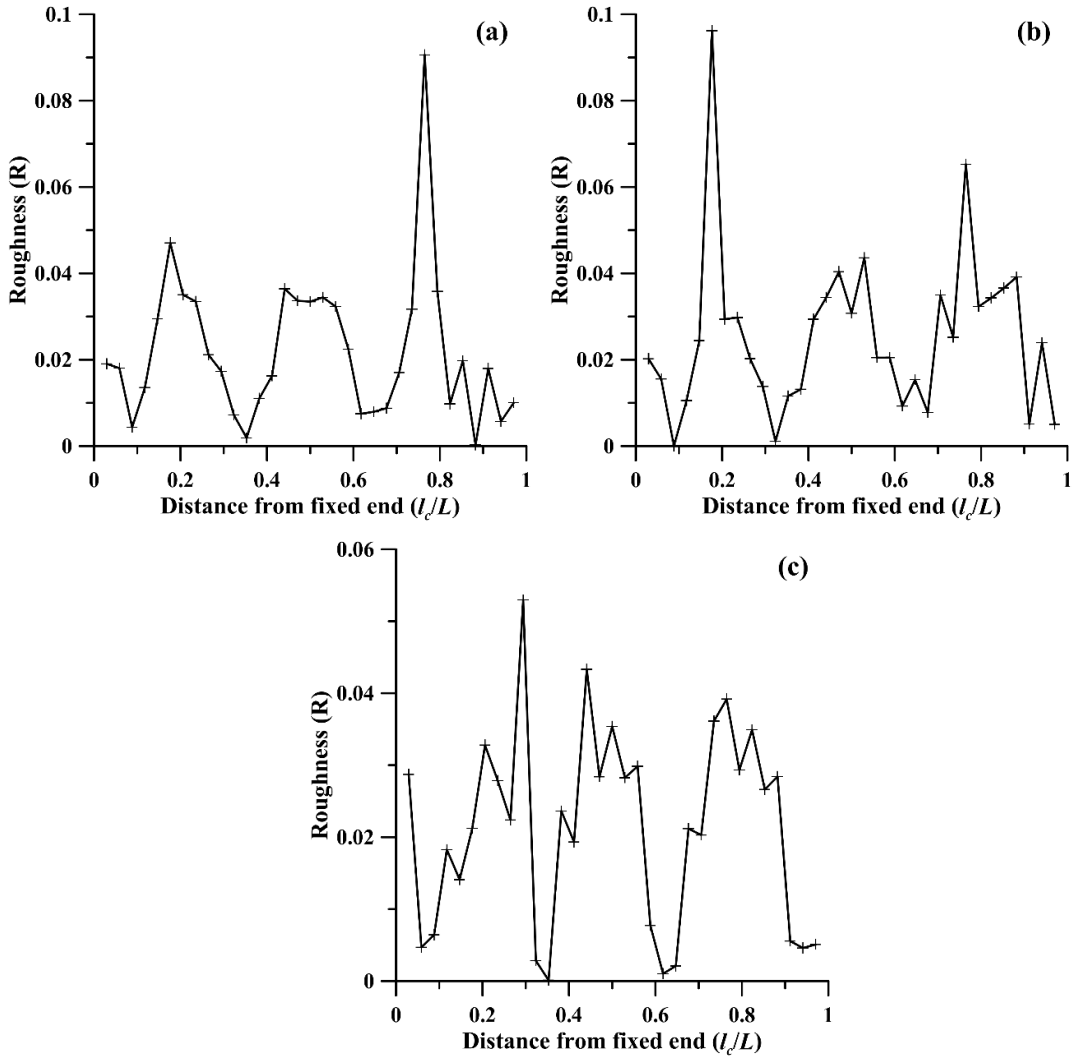

Figure 6.47 Filtration result of forth mode shape of double cracked cantilever beam (a) d_c/h =0.4 at l_c/L = 0.1765 and d_c/h =0.6 at l_c/L = 0.7647, (b) d_c/h =0.6 at l_c/L =0.1765 and d_c/h =0.4 at l_c/L = 0.7647, (c) d_c/h=0.6 at l_c/L =0.2941 and d_c/h=0.4 at x_0/L = 0.4118

6.7 Summary

Different profile analysis techniques in this crack investigation have been implemented in this section. Total four profile analysis techniques for crack investigation are described in this section. Name of those techniques are Wavelet, FD, Curvature method, Irregularity Extracted Method. Those methods are performed with different resolution. Different open transverse crack location and its depth are investigated. Both rotating and non-rotating cracked beams are performed. Overall profile analysis techniques can be used identification of crack parameters from local changes vibration parameters.

CONCLUSION AND FUTURE SCOPE OF WORK

Outline of the Chapter*: 7.1 Introduction, 7.2 Conclusion from crack detection optimization technique, 7.3 Conclusion from profile analysis of mode shapes, 7.4 Future scope of work*

7.1 Introduction

In this section outcomes of the investigations are presented. The dynamic behaviour of beam structure undergoes remarkable changes in presence of crack so far as natural frequencies and mode shapes of the structure are concerned. In the present work, a numerical technique is proposed to capture out the vibrational response of cracked beam followed by commercial finite element programme and experimentation. Two different boundary conditions (clamped-clamped and clamped-free) of the beam are considered under free vibration. Two different materials of the beam are considered, namely aluminium and FGM. An attempt is made to detect crack parameter of rotating beam also.

To prove the authenticity of results obtained from both theoretical and FEA techniques, the experimental setup have been designed. Results obtained from all the three methods are compared. They show good agreement with error percentage within 5%.

Dynamic analyses have been done by varying relative location and relative depth of the crack. From the response analysis, relative frequencies are employed to design different optimization techniques to forecast and quantify the relative crack location and relative crack depth. Mode shape profile of beam structure is changed due to the in presence of crack. Profile analysis is performed to identify the crack parameter from local indiscretion of mode shape.

Finally, a comparison study has been conducted to study the different optimization technique and mode shape profile analysis for different environments. To appreciate the outcomes of the present thesis more clearly, the conclusions from the individual studies are presented in the following sections.

7.2 Conclusion from Crack Detection trough Optimization Technique

Five homogeneous and two hybrid techniques are employed for crack detection. Five homogeneous techniques are cascade artificial neural network, response surface measurement, genetic algorithm, contour plot intersection and adaptive neuro-fuzzy. Two hybrid techniques are Neuro-GA and RSM with GA.

The result obtained from numerical, finite element analysis and experiments are used for CANN techniques. Both forward and inverse problem are performed. Mode shape obtained from finite element analysis and experimentation are applied as input signal of those techniques. Average error is found to be less (less than 0.1%) for all 80 cases for forward problem whereas average error is not very less (less than 5%) for inverse problem. In case of detection of unknown crack parameter (total six crack scenarios) results are also reasonable. Another CANN optimization is performed on experimental data set. First four natural frequencies are used as input data. Average error in this case is this case also moderate. Overall *Cascade* correlation base ANN is found to be an effective tool for crack detection.

Total 80 numbers of data set are performed by ANFIS optimization in forward problem. Better result shows compared to CANN for first and second frequency optimization. In case of third frequencies errors are little on higher (near 0.5 %) side. Same sets of data are use in inverse ANFIS optimization. From the results show that optimization not very accurate (average error 8.9%) especially in case of identification of crack location compared to the results obtained by CANN. In case of detection of unknown crack parameter (total six crack scenarios) results are not good as CANN. It can be concluded that more number of data set required for crack investigation by ANFIS.

Inverse problem is applied for detection of crack parameter by RSM. RSM model developed with total 75 numbers of cracked beam sample with two type of FGM materials (k=2, k=5). Cracks parameters are predicted for of both clamped-clamped and cantilever cracked beam. Predicted results are reasonably good with minimum error (less than 4%) for both boundary conditions.

Crack investigation of clamped-clamped and cantilever FGM beam is also done by contour plot method. Similar types of results are obtained in this method as compare to RSM. In a few cases, contour plot is better than RSM.

GA optimization method is applied for investigation of cracked isotropic beam from experimental data. GA model is developed with 24 cracked beams with different crack scenario. From comparison study it can observed that GA method is better for identification of location than CANN whereas CANN is better in case of crack size determination.

A hybrid technique, combination of CANN and GA are applied form experiment data obtained from cracked cantilever beams. Hybrid technique predicts more accurate results than individual CANN and GA method.

In case of second hybrid technique, a combination of RSM and GA optimization, better results are obtained most in most of the cases compared to RSM techniques.

7.3 Conclusion from Crack Detection Profile Analysis of Mode Shapes

In this thesis four profile analysis methods, namely wavelet, FD, curvature method and irregularity extracted methodhave been employed on mode shape of transverse natural frequencies of cracked beam.

In this thesis a new approach of crack detection based on continuous wavelet analysis with different scale is employed. Overall results show that the proposed method has great potential in the field of crack detection of rotating cantilever beam eliminating boundary effect and can be recommended for applications.

Fractal dimension analysis, has been employed for identification of crack on rotating cantilever beam. From the results, it is evident that FD analysis can be used for detection of crack location and its depth from the deformation profiles of the rotating mode shapes. The inaccuracy in input signal may produce noise during data processing leading to misleading or false reporting of damage in beam. It is shown that higher resolution may be employed as possible measures for noise reduction. In some cases, it is better to apply FD on more than one mode for meaningful detection of multiple cracks in a rotating beam.

Strain energy based curvature method is employed on FEM curvature mode shape data. In order to reduce noise, analysis is undertaken using higher resolution. Overall this profile analysis is acclaimed for crack detection because of its simplicity in application.

Lastly irregularity-based damage detection method is used for crack parameter identification. It is shown that the proposed method can successfully detect not only a single crack, but also multiple cracks in beams. The location and size of a crack in beams are

determined by a peak value at the location of the damage on the irregularity profile of mode shape. Compared with existing damage detection methods such as wavelet transform, this method has a much easier calculation scheme and more straight forward physical understanding. The potential practical application of this method is further confirmed by its low requirement on measurement resolution. The effectiveness and robustness of this method under the influence of noise has been demonstrated by the noise stress tests. The present method is then implemented on the experimentally-measured curvature mode shapes. It can successfully detect the saw-cut crack in the isotropic cantilever beam.

7.4 Future scope of work

The followings are the recommended work that may be carried out in future.

- The optimization technique may be employed for forecasting multi-crack on isometric and composite beam.
- The optimization technique may be designed with novelty for diagnosis of crack in the complex structure other than beam.
- Some new type of hybrid optimization technique may be employed for investigation of crack.
- Breathing crack may be considered for diagnosis.
- Internal crack may be investigated using vibration parameters.
- For accurate measurement of mode shape experiment should be carried out with using scanning laser vibrometer.
- Experiment on rotating and FGM cracked may be employed.

REFERENCES

Abraham, A. (2005), Adaptation of Fuzzy Inference System Using Neural Learning, in Nedjah, Nadia; de Macedo Mourelle, Luiza, Fuzzy Systems Engineering: Theory and Practice, Studies in Fuzziness and Soft Computing, 181, 53–83

Al-Ansari, L. S., (2012), Calculating of Natural Frequency of Stepping Cantilever Beam, International Journal of Mechanical & Mechatronics Engineering, 12(5), 59-68.

Aloulou, W., Yildirim, B., El-Borgi, S. and Zghal, A., (2009), Buckling of an orthotropic graded coating with an embedded crack bonded to a homogeneous substrate, International Journal of Solids and Structures, 46, 1890-1900.

Al-Said, S.M., (2007), Crack identification in a stepped beam carrying a rigid disk, Journal of Sound and Vibration, 300, 863-876.

Andreaus, U, Casini, P and Vestroni, F., (2007), Non-linear dynamics of a cracked cantilever beam under harmonic excitation, International Journal of Non-Linear Mechanics, 42, 566-575.

ANSYS, Released Version.13, User Manual.

Ariaei, A., Ziaei-Rad, S. and Ghayour, M., (2009), Vibration analysis of beams with open and breathing cracks subjected to moving masses, Journal of Sound and Vibration, 326, 709-724.

Attar, M., (2012), A transfer matrix method for free vibration analysis and crack identification of stepped beams with multiple edge cracks and different boundary conditions, International Journal of Mechanical Sciences, 57, 19-33.

Aydogdu, M. and Taskin, V., (2007), Free vibration analysis of functionally graded beams with simply supported edges, Materials and Design, 28, 1651–1656.

Ayhan, A. O., (2007), Stress intensity factors for three-dimensional cracks in functionally graded materials using enriched finite elements, International Journal of Solids and Structures, 44, 8579–8599.

B.Nanda, B., Maity, D.,and Maiti, D.K., (2012), Vibration-Based Structural Damage Detection Technique using Particle Swarm Optimization with Incremental Swarm Size, International Journal Aeronautical and Space Science, 13(3), 322–329.

Bai, R., Cao, M, Su, Z, Ostachowicz, W, and Xu, H., (2012), Fractal Dimension Analysis of Higher-Order Mode Shapes for Damage Identification of Beam Structures, Mathematical Problems in Engineering, 2012 (ID 454568), 1-16.

Bakhary, N., Hao, H and Deeks, A.J., (2007), Damage detection using artificial neural network with consideration of uncertainties, Engineering Structures, 29, 2806–2815.

Barad, K.H., Sharma, D.S. and Vyas, V., (2013), Crack detection in cantilever beam by frequency based method, Procedia Engineering, 51, 770 – 775.

References

Begambre, O. and Laier, J.E., (2009), A hybrid Particle Swarm Optimization - Simplex algorithm (PSOS) for structural damage identification, 40(9), 883-891.

Behzad, M., Meghdari, A. and Ebrahimi, A., (2005), A New Appoach for Vibration Analysis of A Cracked Beam, International Journal of Engineering, 18(4), 319-330.

Behzad M., Ebrahim A.and Meghdari A., (2008), A new continuous model for flexural vibration analysis of a cracked beam, 65 (4), 265-288.

Bikri, K. E., Benamar, R. and Bennouna, M.M., (2006), Geometrically nonlinear free vibration of clamped-clamped beams with an edge crack, Computers and Structures, 84, 485–502.

Binici, B., (2005), Vibration of beams with multiple open cracks subjected to axial force, Journal of Sound and Vibration, 287, 277-295.

Buezas, S. F., Rosales, M. B. and Filipich, C. P., (2008), Damage detection in structural elements taking into account a crack contact model, Asociación Argentina de Mecánica Computacional, 27, 2715-2732.

Buezas, F. S., Rosales, M.B. and Filipich, C.P., (2011), Damage detection with genetic algorithms taking into account a crack contact model, Engineering Fracture Mechanics, 78, 695-712.

Cacciola, P., Impollonia, N. and Muscolino, G., (2003), Crack detection and location in a damaged beam vibrating under white noise, Computers and Structures, 81, 1773-1782.

Cam, E., Orhan, S and Luy, M., (2005), An analysis of cracked beam structure using impact echo method, Nondestructive Testing and Evaluation International, 38, 368-373.

Chang, C. C, and Chen, L. W., (2004), Damage detection of cracked thick rotating blades by a spatial wavelet based approach, Applied Acoustics, 65, 1095-1111.

Chasalevris, A. C. and Papadopoulos, C. A. (2006), Identification of multiple cracks in beams under bending, Journal of Sound and Vibration, 309, 507-528.

Chati, M., Rand, R, and Mukherjee, S., (1997), Modal Analysis of a Cracked Beam, Journal of Sound and Vibration, 207(2), 249-270.

Chatterjee, S., Chatterjee, S. and Doley, B., (2011), Breathing Crack In Beam And Cantilever Using Contact Model Dynamic Analysis, International Journal of Wisdom Based Computing, 1(3), 39-42.

Cheng, Y., Yu, Z., Wu, X, and Yuhua, Y., (2011), Vibration analysis of a cracked rotating tapered beam using the p-version finite element method, Finite Elements in Analysis and Design, 47, 825-834.

Chinchalkar, S., (2001), Determination of crack location in beams using natural frequencies, Journal of Sound and Vibration, 247(3), 417-429.

Chondros T. G. and Dimarogonas A. D., (1980), Identification of cracks in welded joints of complex structures, Journal of. Sound Vibration, 69, 531–538.

Chondros, T. G. and Labeas, G. N., (2007), Torsional vibration of a cracked rod by variational formulation and numerical analysis, Journal of Sound and Vibration, 301, 994-1006.

Chondros, T. G., Dimarogonas, A. D. and Yao, J., (1998), A Continuous Cracked Beam Vibration Theory, Journal of Sound and Vibration, 215(1), 17-34.

Choubey, A., Sehga, D. K. and Tandon, N., (2006), Finite element analysis of vessels to study changes in natural frequencies due to cracks, International Journal of Pressure Vessels and Piping, 83, 181-187.

D.Srinivasarao, D., Rao, K. M. and Raju, G, V., (2010), Crack identification on a beam by vibration measurement and wavelet analysis, International Journal of Engineering Science and Technology, 80, 409-428.

Dado, M. H., (1997), A comprehensive crack identification algorithm for beams, Applied Acoustics, 51(4), 381, 398.

Dharmaraju, N., Tiwari, R. and Talukdar, S., (2004), Identification of an open crack model in a beam based on force–response measurements, Computers and Structures, 82, 167-179.

Dimarogonas, A. D., (1996), Vibration of cracked structures a state of the art review, Engineering Fracture Mechanics, 55(5), 831-857.

Djidrov, M., Gavriloski, V and Jovanova, J, (2014), Vibration analysis of cantilever beam for damage detection, FME Transactions, 42, 311-316.

Doebling, S. W., Farrar, C. R. and Prime, M. B., (1998), A summary review of vibrationbased damage identification methods, Shock and Vibration Digest, 30(2), 91-105.

Douka, E, Loutridis, S and Trochidis, A., (2003), Crack identification in beams using wavelet analysis, International Journal of Solids and Structures, 40, 3557–3569.

Douka, E., Bamnios, G., and Trochidis, A. (2004) A method for determining the location and depth of cracks in double-cracked beams, Applied Acoustics, 65, 997-1008.

Douka, E. and Hadjileontiadis, L. J., (2005), Time–frequency analysis of the free vibration response of a beam with a breathing crack, Nondestructive Testing and Evaluation International, 38, 3-10.

References

Draper, N.R. and Smith, H. (1992). Applied Regression Analysis,Second Edition. John Wiley and sons, Inc. New York.

Eftekhari, M., Javadi, M. and Farsani, R. E., (2011), Free vibration analysis of cracked functionally graded material beam, World Applied Science Journal, 12(8), 1214-1225.

Erdogan, F. and Wu, B. H., (1997), The surface crack problem for a plate with a functionally graded properties, Journal of applied mechanics, 64, 449-456.

Fang, S.E. and Perera, R., (2009), A response surface methodology based damage identification technique, Smart Materials and Structures, 18(6), 1-15

Fayyadh, M., M, and Razak, H.A., (2011), Detection of damage location using mode shape deviation Numerical study, International Journal of the Physical Sciences, 6(24), 5688-5698.

Friswell, R. (1994), Using Vibration Data and Statistical Measures to Locate Damage in Structures, Modal Analysis: The International Journal of Analytical and Experimental Modal Analysis, 9(4), 239-254.

Garg, S., Chawla, R and Singh, B., (2014), Crack detection in cantilever beams using a new hybrid approach, International Journal of Mechanical And Production Engineering, 2(4), 22-27.

Gillich, G. R. and Praisach, Z. I., (2014), Modal identification and damage detection in beam-like structures using the power spectrum and time–frequency analysis, Signal Processing, 96, 29-44.

Goldberg, D. E., (1989), Genetic Algorithms in Search, Optimization and Machine Learning, Addison-Wesley Longman Publishing Co., Inc. Boston

Gounaris, G. D. and Papadopoulos C. A., (2002), Crack identification in rotating shafts by coupled response measurements, Engineering Fracture Mechanics, 69, 339-352

Gounaris, G. D. and Papadopoulos, C. A., (2002), Crack identification in rotating shafts by coupled response measurements, Engineering Fracture Mechanics, 69, 339-352.

Hadjileontiadis, L.J., Douka, E. and Trochidis, A. (2005a), Fractal dimension analysis for crack identification in beam structure, Mechanical Systems and Signal Processing, 19, 659-674.

Hadjileontiadis, L.J., Douka, E. and Trochidis, A. (2005b), Crack detection in beams using kurtosis, Computers and Structures, 83, 909-919.

Hadjileontiadis, L.J. and Douka, E. (2007), Crack detection in plates using fractal dimension, Engineering Structures, 29, 1612-1625.

Hall, S. R., (1999), The effective management and use of structural health data, Structural Health Monitoring 2000, Stanford University, Palo Alto, California,265–275.

Hatch, M.R. (2001) Vibration simulation using MATLAB and ANSYS, Chapman & Hall/CRC

Haykin, S., (2006), Neural Networks, A comprehensive foundation, Pearson Education.

Hecht-Nielsen, R., (1988), Neurocomputing **,** IEEE Spectrum, 5(3), 36-41.

Horibe, T. and Watanabe, K., (2006), Crack identification of plate using genetic algorithm, JSME International Journal, 49(3), 403-410.

Hu. H., Wang. B. T., Lee, C. H., and Su, J. S., (2006), Damage detection of surface cracks in composite laminates using modal analysis and strain energy method, Composite Structures, 74, 399-405.

Jang J-S.R., (1991), Fuzzy modeling using generalized neural networks and Kalman filter algorithm, Proceedings of the ninth National Conference on Artificial Intelligence, AAA1 Press, 2, 762–767.

Jang J-S.R, Sun C.T and Mizutani E (1997) Neuro-fuzzy and soft computing: a computational approach to learning and machine intelligence. Prentice-Hall, Upper Saddle River, NJ

Jiang, X, Ma, Z, J and Ren, W-X, (2012), Crack detection from the slope of the mode shape using complex continuous wavelet transform, Computer-Aided Civil and Infrastructure Engineering, 27, 187-201.

Jose, M., Machorro-Lo, P., Douglas, E. A., JulioC.Go, M. M., and Kamran, A. G., (2009), Identification of damaged shafts using active sensing—Simulation and experimentation, Journal of Sound and Vibration, 327, 368–390.

Juneja, V., Haftka, R. T., and Cudney, H. H., (1997), Damage detection and damage detectability: analysis and experiments, Journal of Aerospace Engineering, 10(4), 135-142.

Karthikeyan, M., Tiwari, R. and Talukdar, S., (2007), Crack localisation and sizing in a beam based on the free and forced response measurements, Mechanical Systems and Signal Processing, 21, 1362-1385.

Karthikeyan, M., Tiwari, R. and Talukdar, S., (2007), Crack localisation and sizing in a beam based on the free and forced response measurements, Mechanical Systems and Signal Processing, 21, 1362-1385.

Katunin, A., (2011), Damage identification in composite plates using two dimensional B-spline wavelets, Mechanical Systems and Signal Processing, 25, 3153-3165.

Katz, M.J., (1988), Fractals and the analysis of waveforms, Computers in Biology and Medicine, 18(3), 145-156.

Khan, A. Z., Stanbridge, A. B., and Ewins, D. J., (2000), Detecting damage in vibrating structures with a scanning LDV. Optics and Lasers in Engineering, 32(6), 583-592.

References

Khan, I.A., Yadao, A. and Parhi, D.R., (2014), Fault diagnosis of cracked cantilever composite beam by vibration measurement and RBFNN, Journal of Mechanical Design and Vibration, 1(1), 1-4.

Kim, J. T., Ryu, Y. S., Cho, H. M. and Stubbs, N., (2003), Damage identification in beam-type structures frequency based method vs. mode shape based method, Engineering Structures, 25, 57-67.

Kisa, M. and Gurel, M. A. (2006), Modal analysis of multi-cracked beams with circular cross section, Engineering Fracture Mechanics, 73, 963-977.

Kitipornchai, S., Kea, L. L., Yang, J. and Xiang, Y., (2009), Nonlinear vibration of edge cracked functionally graded Timoshenko beams, Journal of Sound and Vibration, 324, 962-982.

Krawczuk, M., (1995), Modelling and vibration analysis of a cantilever composite beam with a transverse open crack, Journal of Sound and Vibration, 183(1), 69-89.

Krawczuk, M., (2002), Application of spectral beam finite element with a crack and iterative search technique for damage detection, Finite Elements in Analysis and Design, 38, 537–548

Kumar, D. S., Mahapatra, D. R., Gopalakrishnan, S., (2004), A spectral finite element for wave propagation and structural diagnostic analysis of composite beam with transverse crack, Finite Elements in Analysis and Design, 40, 1729–1751.

L.S. Al-Ansari, L. S, Al-Waily, M and Al-Hajjar, A. M. H.Y., (2012), Experimental and numerical study of crack effect on frequency of simple supported beam, Al-Khwarizmi-Engineering Journal, 8(2), 30-41.

Lee, J., (2009), Identification of multiple cracks in a beam using vibration amplitudes, Journal of Sound and Vibration, 326, 205–212.

Li, B., Chen, X., and He, Z., (2013), Three-steps-meshing based multiple crack identification for structures and its experimental studies, Chinese Journal of Mechanical Engineering, 26(1), 1-7.

Li, H, Huang, Y, Ou, J. and Bao, Y., (2011), Fractal dimension-based damage detection method for beams, Computer-Aided Civil and Infrastructure Engineering, 26, 190-206.

Lin, H. P., (2004), Direct and inverse methods on free vibration analysis of simply supported beams with a crack, Engineering Structures, 26, 427-436.

Liong, R.T. and Proppe, C., (2013), Finite element multi body simulation of a breathing crack in a rotor with a cohesive zone model, ISRN Mechanical Engineering, 2013, 1-10.

Liu, S. W., Huang, J, H, Sung, J, C. and Lee, C, C., (2002), Detection of cracks using neural networks and computational mechanics, Computer Methods in Applied Mechanics and Engineering, 191, 2831-2845.

Liu, Y., Li, Z, and Zhang, W., (2010), Crack detection of fibre reinforced composite beams based on continuous wavelet transform, Nondestructive Testing and Evaluation, 25(1), 25-44.

Lonkar, A, A and Srivastava, R. K., (2011), Crack detection in structure using wavelet transform and higher order differentiated mode, MIT International Journal of Mechanical Engineering, 1(1), 26-34.

Loutridis, S., Douka, E, and Trochidis, A., (2004), Crack identification in double-cracked beams using wavelet analysis, Journal of Sound and Vibration, 277, 1025-1039.

Loutridis, S., Douka, E. and Hadjileontiadis, L .J., (2005), Forced vibration behaviour and crack detection of cracked beams using instantaneous frequency, Nondestructive Testing and Evaluation International, 38, 411-419.

Loya, J.A., Rubio, L. and Fernandez-Saez, J., (2006), Natural frequencies for bending vibration of Timoshenko cracked beams, Journal of Sound and Vibration, 290, 640–653.

M.T. V.Baghmisheh, M.T. V., Sadeghi, M. P. M. H., and Ettefagh, M. M., (2008), Crack detection in beam-like structures using genetic algorithms, Applied Soft Computing, 8, 1150-1160.

Machorro-Lo´ pez, J M., Adams, D. E., Go´ mez-Mancilla, J. C. and Gul, K.A., (2009), Identification of damaged shafts using active sensing—simulation and experimentation, Journal of Sound and Vibration, 327, 368-390.

Majumdar, A, Nanda, B, Maiti, D. K. and Maity, D., (2014), Structural damage detection based on modal parameters using continuous ant colony optimization, Advances in Civil Engineering, 2014, 1-14.

Marur, S. R. and Prathap G., (2005), Non-linear beam vibration problems and simplifications in finite element model, Computer Mechanics, 35, 352-360.

Masoud, S., Jarrah, M. A. and Al-Maamory, M., (1998), Effect of crack depth on the natural frequency of a prestressed fixed-fixed beam, Journal of Sound and Vibration, 214(2), 201-212.

Mazanoglu, K. and Sabuncu, M., (2010), Vibration analysis of non-uniform beams having multiple edge cracks along the beam's height, International Journal of Mechanical Sciences, 52, 515-522.

Mazanoglu, K. and Sabuncu, M., (2012), A frequency based algorithm for identification of single and double cracked beams via a statistical approach used in experiment, Mechanical Systems and Signal Processing, 30, 168-185.

McCulloch, S. W. and Pitts, W. H. (1943), A logical calculus of the ideas immanent in nervous activity, Bulletin of Mathematical Biophysics, 5, 115-133.

Messina, A, (2008), Refinements of damage detection methods based on wavelet analysis of dynamical shapes, International Journal of Solids and Structures, 80, 409-428.

Mohan, S. C., Maiti, D. K. and Maity, D., (2013), Structural damage assessment using FRF employing particle swarm optimization, Applied Mathematics and Computation, 219, 10387-10400.

Moradi, S., Razi, P. and Fatahi, L., (2011), On the application of bees algorithm to the problem of crack detection of beam-type structures, Computers and Structures, 89, 2169–2175.

Nahvi, H. and Jabbari, M., (2005), Crack detection in beams using experimental modal data and finite element model, International Journal of Mechanical Sciences, 47, 1477-1497.

Nanda, B., Maity, D., Maiti, D.K., (2012), Vibration Based Structural Damage Detection Technique using Particle Swarm Optimization with Incremental Swarm Size, International Journal of Aeronautical and Space Sciences, 13(3), 323–331

Nandwana, B. P. and Maiti, S. K., (1997), Detection of the Location and Size of a Crack in Stepped Cantilever Beams Based on Measurements of Natural Frequencies, Journal of Sound and Vibration, 203(3), 435-446.

Narashima Rao, N. V., Chandhu, K, V and Satyanarayana, D. (2012), Fault diagnosis of dynamics cracked structure using fuzzy inference system, International Journal of Emerging trends in Engineering and Development, 5(2), 601-610.

Nazari, F. and Baghalian, S., (2011), A new method for damage detection in symmetric beams using artificial neural network and finite element method, International Journal of Engineering & Applied Sciences, 3(2), 30-36.

Nematollahi, M. A., Farid, M , Hematiyan, M. R. and Safavi, A.A. (2012), Crack detection in beam-like structures using a wavelet-based neural network, Journal of Aerospace Engineering, 226, 1243-1256.

Okafor, A.C. and Dutta, A., (2000), Structural damage detection in beams by wavelet transforms, Smart Materials and Structures, 9, 906-917.

Orhan, S., (2007), Analysis of free and forced vibration of a cracked cantilever beam, Nondestructive Testing and Evaluation International, 40, 443-450.

Ovanesova, A. V, and Suarez, L, E, (2004), Applications of wavelet transforms to damage detection in frame structure, Engineering Structures, 26, 39-49.

Owolabi, G. M., Swamidas, A. S. J. and Seshadri, R., (2003), Crack detection in beams using changes in frequencies and amplitudes of frequency response functions, Journal of Sound and Vibration, 265, 1-22.

Palacz, M., Krawczuk, M., and Ostachowicz, W., (2005), The spectral finite element model for analysis of flexural–shear coupled wave propagation. Part 1: Laminated multilayer composite beam, Composite Structures, 68, 37–44.

Parhi, D. R. and Choudhury, S, (2011), Analysis of smart crack detection methodologies in various structures, Journal of Engineering and Technology Research, 3(5), 139-147.

Parhi, D. R. and Das, H. C., (2008), Structural damage detection by fuzzy-Gaussian technique, Journal of Applied Mathematics and Mechanics, 4(2), 39-59.

Parhi, D. R. and Dash, A. K., (2011), Application of neural networks and finite elements for condition monitoring of structures, Proceedings of the Institution of Mechanical Engineers, Part C: Journal of Mechanical Engineering Science, 225(6), 1329-1339.

Park, J. H., Kim, J. T., Hong, D. S., Ho, D.D. and Yi, J.H., (2009), Sequential damage detection approaches for beams using time-modal features and artificial neural networks, Journal of Sound and Vibration, 323, 451–474.

Patil, D. P. and Maiti, S. K., (2003), Detection of multiple cracks using frequency measurements, Engineering Fracture Mechanics, 70, 1553-1572.

Patil, D. P. and Maiti, S. K., (2005), Experimental verification of a method of detection of multiple cracks in beams based on frequency measurements, Journal of Sound and Vibration, 281, 439-451.

Pohit, G., Mallik A. K. and Venkatesan, C., (1999), Free out-of-plane vibrations of a rotating beam with nonlinear elastomeric constraints, Journal of Sound and Vibration, 220(1), 1-25.

Pugno, N., (2000), Evaluation of the non-linear dynamic response to harmonic excitation of a beam with several breathing cracks, Journal of Sound and Vibration, 235(5), 749-762.

Qiao,P., Lu, K, Lestari, W and Wang, J., (2007), Curvature mode shape-based damage detection in composite laminated plate, Composite Structures, 80, 409-428.

Ramanamurthy, E.V.V. and Chandrasekaran, K., (2008), Damage detection in composite beam using numerical modal analysis, International Journal on Design and Manufacturing Technologies, 2(1), 32-43.

References

Ramanamurthy, E. V. V. and Chandrasekaran, K., (2011), Vibration analysis on a composite beam to identify damage and damage severity using finite element method, International Journal of Engineering Science and Technology, 3(7), 5865-5888.

Ramezani, A., Alasty, A. and Akbari, J., (2006), Effects of rotary inertia and shear deformation on Nonlinear free vibration of micro beams, Journal of Vibration and Acoustics, 128, 611-615.

Rao, N.V.N.L., Chandhu, K.V.P. and Satyanarayana, D., (2012), Fault diagnosis of dynamics cracked structure using Fuzzy Inference system, International Journal of engineering trends in Engineering and Development, 601-610,.

Ratcliffe, C. P., (1997), Damage detection using a modified Laplacian operator on mode shape data, Journal of Sound and Vibration, 204(3), 505-517.

Rezaee, M. and Hassannejad, R., (2010), Free Vibration Analysis of Simply Supported Beam with Breathing Crack Using Perturbation Method, Acta Mechanica Solida Sinica, 23(5), 459-470.

Rosales, M. B., Filipich, C. P. and Buezas, F. S., (2009), Crack detection in beam-like structures, Engineering Structures, 31, 2257-2264.

Rousseau, C. E., and Tippu, H. V., (2000), Compositionally Graded Materials with Cracks Normal to the Elastic Gradient, Acta mater, 48, 4021–4033.

Rytter, A., (1993), Vibration based inspection of civil engineering structures, Ph. D. Dissertation, Department of Building Technology and Structural Engineering, Aalborg University, Denmark.

S. Moradi, S., Razi, P., and Fatahi, L., (2011), On the application of bees algorithm to the problem of crack detection of beam-type structures, Computers and Structures, 89, 2169-2175

Saavedra, P. N. and Quitino, L. A. (2001), Crack detection and vibration behavior of cracked beams, Computers and Structures, 79, 1451-1459.

Saeed, R. A., Galybin, A. N. and Popov, V., (2011), Crack identification in curvilinear beams by using ANN and ANFIS based on natural frequencies and frequency response functions, Neural Computing and Applications, 21,1629–1645.

Sahoo, B and Maity, D., (2007), Damage assessment of structures using hybrid neuro-genetic algorithm, Applied Soft Computing, 7, 89-104.

Salawu, O. S., (1997), Detection of thermal damage to changes in frequency a review, Engineering Structures, 19(9), 718-723.

Saridakis, K. M., Chasalevris, A. C., Papadopoulos, C. A. and Dentsoras, A. J., (2008), Applying neural networks, genetic algorithms and fuzzy logic for the identification of cracks in shafts by using coupled response measurements, Computers and Structures, 86,1318-1338.

Sekhar, A. S. and Prabhu, B. S., (1992), Crack detection and vibration characteristics of cracked shaft, Journal of Sound and Vibration, 157, 375-381.

Sekhar, A. S., (2008), Multiple cracks effects and identification, Mechanical Systems and Signal Processing, 22, 845–878.

Shi, J., Xu, X, Wang, J and Li, G., (2010), Beam damage detection using computer vision technology, Nondestructive Testing and Evaluation, 25(3), 189-204.

Simsek, M., (2010), Vibration analysis of a functionally graded beam under a moving mass by using different beam theory, Composite Structures, 92, 904–917.

Sina, S. A., Navazi, H. M. and Haddadpour, H., (2009), An analytical method for free vibration analysis of functionally graded beams, Materials and Design, 30, 741–747.

Singh, S. K., and Tiwari R., (2010), Identification of multiple crack in a shaft system using transverse frequency response functions, Mechanism and Machine Theory, 45, 1813-1827.

Sinha, J. K. and Friswell, M. I., (2002), Simulation of the dynamic response of a cracked beam, Computers and Structures, 80, 1473-1476.

Srinivasarao, D, Roa, K.M, and Raju, G.V., (2010), Crack identification on a beam by vibration measurement and wavelet analysis, International Journal of Engineering Science and Technology, 2(5), 907-912`

Stojanovic, V., Ribeiro, P and Stoykov, S., (2013), Non-linear vibration of Timoshenko damaged beams by a new p-version finite element method, Computers and Structures, 120, 107-119.

Sugeno, M., (1985), Industrial applications of fuzzy control, Elsevier Science Pub. Co.

Thatoi, D, Choudhury, S and Jena, P. K. J., (2014), Fault diagnosis of beam-like structure using modified fuzzy technique, Advances in Acoustics and Vibration, 2014, 1-18.

Tlaisi, A., Akinturk, A., Swamidas, A. S. J. and Haddara, M. R., (2012), Crack detection in shaft using lateral and torsional vibration measurement and analyses, Mechanical Engineering Research, 2(2), 52-76.

Torabi, K., Afshari, H. and Heidari-Raran, M., (2014), Free vibration analysis of a rotating non-uniform blade with multiple open cracks using DQEM, Universal Journal of Mechanical Engineering, 2(3), 101-111.

Tsai, T.C. and Wang, Y.Z., (1996), Vibration analysis and diagnosis of a cracked shaft, Journal of Sound and Vibration, 192(3), 607-620.

References

Vakil-Baghmisheh, M.T., Peimani, M., Homayoun Sadeghi, M. and Ettefagh M.M., (2008), Crack detection in beam-like structures using genetic algorithms, Applied Soft Computing , **8**(2), 1150-1160.

Vallabhaneni, V. and Maity, D., (2011), Application of radial basis neural network on damage assessment of structures, Procedia Engineering, 14, 3104-3110.

Viola, E., Federisi, L. and Nobile, L. (2001), Detection of crack location using cracked beam element method for structural analysis, 36, 23-35.

Voila, E., Ricci, P. and Aliabadi, M.H. (2007), Free vibration analysis of axially loaded cracked Timoshenko beam structures using the dynamic stiffness method, Journal of Sound and Vibration, 304, 124-153.

Waheed, S.O., Mostafa, N. H., Jawad, D.H., (2011), Nonlinear dynamic characteristics of a simple blade with breathing crack using Ansys software, World Journal of Mechanics, 1, 21-30.

Wang, J., (2006), Damage detection in beams by roughness analysis, Smart Structures and Materials, 6174(1J), 1-12.

Wang, J. and Qiao, P., (2008), On irregularity-based damage detection method for cracked beams, International Journal of Solids and Structures, 45, 688-704.

Wang, Q. and Deng, X., (1999), Damage detection with spatial wavelets, International Journal of Solids and Structures, International Journal of Solids and Structures, 36, 3443-3468.

Wang, Q. and Wu, N., (2011), Detecting the delamination location of a beam with a wavelet transform an experimental study, Smart Materials and Structures, 20, 1-7.

Wang, Y. M., Chen, X, F and He, Z, J, (2011), Daubechies wavelet finite element method and genetic algorithm for detection of pipe crack, Nondestructive Testing and Evaluation, 26(1), 87-99.

Wei, D., Liu, Y., Xiang, Z**.,** (2012), An analytical method for free vibration analysis of functionally graded beams with edge cracks, Journal of Sound and Vibration, 331, 1686–1700.

Wu, N. and Wang, Q., (2011), Experimental studies on damage detection of beam structures with wevelet transform, International Journal of Engineering Science, 49, 253-261.

Xiang, J, Zhong, Y., Chen, X, He, Z., (2008), Crack detection in a shaft by combination of wavelet-based elements and genetic algorithm, International Journal of Solids and Structures, 45, 4782-4795.

Xiang, J.W., Matsumoto, T. and Long, J, Q and Ma, G., (2013), Identification of damage locations based on operating deflection shape, Nondestructive Testing and Evaluation, 28(2), 166-180.

Yan, Y. J., Cheng, L., Wu, Z. and Yam, L.H., (2007), Development in vibration-based structural damage detection technique, Mechanical Systems and Signal Processing, 21, 2198–2211.

Yang, X. F., Swamidas, A. S. J. and Seshadri, R, (2001), Crack identification in vibrating beams using the energy method, Journal of Sound and Vibration, 244(2), 337-357.

Yang, Z., Chen, X., Yu, Y., Liu, R. and Liu, Z., (2013), A damage identification approach for plate structures based on frequency measurements, Nondestructive Testing and Evaluation, 28(4), 321-341.

Yokoyama, T. and Chen, M. C. (1998), Vibration analysis of edge-cracked beams using a line– spring model, Engineering Fracture Mechanics 59, 403–409.

Yoon, H. I., Son, I. S. and Ahn, S. J., (2007), Free vibration analysis of Euler Bernoulli beam with double cracks, Journal of Mechanical Science and Technology, 21, 476-485.

Yu, Z. and Chu, F., (2009), Identification of crack in functionally graded material beams using the p-version of finite element method, Journal of Sound and Vibration, 325, 69-84.

Zheng, D. Y. and Kessissoglou, N. J. (2004), Free vibration analysis of a cracked beam by finite element method, Journal of Sound and Vibration, 273, 457-475.

Zhong, S. and Oyadiji, S. O., (2007), Crack detection in simply supported beams without baseline modal parameters by stationary wavelet transform, Mechanical Systems and Signal Processing, 21, 1853-1884.

Zhong, S. and Oyadiji, S.O., (2011), Detection of cracks in simply-supported beams by continuous wavelet transform of reconstructed modal data, Computers and Structures, 89, 127-148.